University of Alberta

Dynamic Load Models for Industrial Facilities

by

Xiaodong Liang

A thesis submitted to the Faculty of Graduate Studies and Research
in partial fulfillment of the requirements for the degree of

Doctor of Philosophy
in
Energy Systems

Department of Electrical and Computer Engineering

Fall 2013
Edmonton, Alberta

To my parents,

Wenhai Liang and Yunqing Yan

ABSTRACT

Industrial facilities connected to power transmission systems typically draw large amount of power and have complex dynamic responses to system disturbances. Traditional load modeling approaches cannot establish adequate dynamic models especially for future industrial facilities in power systems planning studies.

In this thesis, a new concept, the template-based load modeling technique along with template scaling and model equivalence algorithms, is proposed to address this issue. This method requires minimal user input and can be implemented in a database program for a wide variety of industrial facilities. Oil refinery facilities are used as an example to illustrate the proposed technique.

Variable frequency drives (VFDs) are increasingly used in industrial facilities, however, dynamic models for motor drive systems suitable for power systems dynamic studies are not available. Voltage sags occur when power systems experience short-circuit faults, which is typically the starting point of power systems dynamic simulation. VFDs will trip when they experience a relatively large voltage sag (>20% - 30% voltage drop). As a result, there is no need to include VFDs in dynamic studies. Based on the finding, a simple procedure to determine if a VFD needs to be included for dynamic studies is proposed in this thesis.

When VFDs experience mild voltage disturbances and are able to ride through, the equivalent dynamic model for motor drive systems is proposed. These models are created by the linearization approach, voltage dependence and frequency dependence are both considered. Dynamic models for VSI and cascaded inverter drives and their induction motor loads are developed. Aggregation algorithms for motor drive systems are proposed to achieve load equivalence facility wide.

A generic dynamic load model structure covering all types of commonly used loads including motor drive systems is proposed for industrial facilities. A procedure is provided on how to obtain the final load model, which is tailored from the generic structure based on load types practically involved in an industrial facility of interest.

PREFACE

The research results presented in this thesis have been partly published, accepted for publication, and ready to submit for publications.

1). A version of Chapters 1, 2 and 3 has been published:

Xiaodong Liang, Wilsun Xu, C.Y. Chung, Walmir Freitas, and Kun Xiong, "Dynamic Load Models for Industrial Facilities", IEEE Transactions on Power Systems, Vol. 27, No. 1, February 2012, Page(s): 69-80.

2). A version of Chapter 2 has been published:

Xiaodong Liang, and C.Y. Chung, "Bus Split Algorithm for Aggregation of Induction Motors and Synchronous Motors in Dynamic Load Modeling", Proceedings of 2013 IEEE Industrial and Commercial Power Systems Conference (I&CPS), Stone Mountain, GA, USA, April 30 – May 03, 2013.
(*Note: this paper has been requested modification and resubmission for further review for possible publication in IEEE Transactions on Industry Applications or IEEE Industry Applications Magazine*).

3). A version of Chapter 2 has been accepted for publication:

Xiaodong Liang, Shengqiang Li, and Wilsun Xu, "A New Approach to Creating Dynamic Models for Industrial Facilities", accepted for publication by 2013 CIGRÉ Canadian Conference, Calgary, Alberta, Canada, September 9 – 11, 2013.

4). A version of Chapter 4 has been accepted for publication:

Xiaodong Liang, and Wilsun Xu, "Modeling Variable Frequency Drives and Motor Systems in Power Systems Dynamic Studies", accepted for publication by

2013 IEEE Industry Applications Society (IAS) Annual Meeting, Orlando, Florida, USA, October 6-11, 2013.

5). A version of Chapter 5 is ready to submit:

Xiaodong Liang, and Wilsun Xu, “Aggregation Methods for Variable Frequency Drives and Motor Systems”, to be submitted

ACKNOWLEDGEMENT

I would like to express my deepest gratitude to my supervisor Dr. Wilsun Xu for his professional guidance, continuous encouragement, and financial support during the research work and preparation of the thesis. I learned a lot from Dr. Xu on how to be a successful researcher and how to write papers and reports.

Special thanks are owed to Dr. Yunfei Wang, Jinwei He, Shengqiang Li, Professor Yunwei (Ryan) Li for their suggestions and help during the research work.

It is a great pleasure to know and work with fellow graduate students in Power Disturbance and Signaling (PDS) Research Laboratory at University of Alberta for their friendly smile and heart-warming help.

Finally, I would like to thank my family for their love and support. Their love makes my life more meaningful and pleasant.

TABLE OF CONTENTS

LIST OF TABLES

LIST OF FIGURES

LIST OF SYMBOLS

AC	Alternating current
ADU	Atmospheric distillation unit
AVM	Averaged-value model
C_{dc}	Capacitance of DC link capacitor
CSI	Current source inverter
d	Duty cycle
DC	Direct current
E	RMS phase-to-ground voltage of power source
e_d	DC link voltage before inverter
EP	Equivalent process model
EF	Equivalent facility model
f_g	Power supply frequency at the input of the drive.
H	Combined rotor and load inertia constant
HFO	Heavy fuel oil
HVAC	Heating, ventilation and air conditioning
i_d	DC link current after rectifier
i_I	DC link current entering inverter
IM	Induction motors
i_{dg}	d-axis ac current at drive input
i_{dgcom}	d-axis ac current at drive input during commutation period
i_{dgcond}	d-axis ac current at drive input during conduction period
i_{qg}	q-axis ac current at drive input
i_{qgcom}	q-axis ac current at drive input during commutation period
i_{qgcond}	q-axis ac current at drive input during conduction period
K_{pm}, K_{im}	Proportional and integral gains of the Speed PI controller
l_c	Commutation inductance
L_{dc}	Inductance of DC link reactor
L_s	Total stator inductance, $L_s = l_s + L_m$

l_s	Stator leakage inductance
L_m	Magnetizing inductance
L_r	Total rotor inductance, $L_r = l_r + L_m$
l_r	Rotor leakage inductance
MCC	Motor control center
MVD	Medium voltage drive
P	Real power
PWM	Pulse-width-modulation
P_{IM}	Active power at motor terminal
$P_{Inveter}$	Active power at output of the drive
p	Number of pole pairs
Q	Reactive power
R_s	Stator resistance
R_r	Rotor resistance
r_{dc}	Resistance of DC link
SCR	Silicon controlled rectifier
SPC	Switching power converters
SM	Synchronous motors
TF	Template-based full model
T_e	Electromagnetic torque
T_L	Shaft mechanical torque
u	Commutation angle
V_b	Nominal voltage of the motor per phase
VDU	Vacuum distillation Unit
VFD	Variable frequency drive
VSI	Voltage source inverter
VSS	Variable structure systems
V/f	Voltage per hertz control
v_d	DC link voltage after rectifier
V_{diode}	Diode forward voltage
v_{dg}	d-axis power source voltage

v_{qg}	q-axis power source voltage
v_{ds}	d-axis voltage at inverter output
v_{qs}	q-axis voltage at inverter output
v_{qs}, i_{qs}	q-axis stator voltage and current of the motor
v_{ds}, i_{ds}	d-axis stator voltage and current of the motor
v_{qs}^{e*} , v_{ds}^{e*}	Commanded values of speed controller
Y_0'	Admittances of power source
Y_{c1}	Admittances of cable 1 at the induction motor terminal
Y_{c2}	Admittances of cable 2 at the synchronous motor terminal
Y_{T0}	Admittances of transformer T_0
Y_{T1}	Admittances of transformer T_1
Y_{T2}	Admittances of transformer T_2
ZIP	constant impedance, constant current, and constant power
Ψ_{qs}, Ψ_{ds}	Stator q- and d-axis fluxes
Ψ_{qr}, Ψ_{dr}	Rotor q- and d-axis fluxes
ω_b	Nominal frequency of the motor
ω_r	Electric angular velocity of the rotor
ω_s	Stator field angular velocity in electrical rad/s

CHAPTER 1 INTRODUCTION

1.1 Motivation

It has been recognized for more than two decades that representation of power system loads for dynamic performance analysis can have significant impact on power systems stability. As power systems are designed and operated with less stability margin, adequate load models are of major importance [1, 2].

The decisions made on system reinforcement and performance improvement mostly reply on the results of power flow and stability simulation studies, inadequate load representation could be costly due to under- or over-building of the system or degradation of reliability. The benefits to improve load representation are discussed in detail in IEEE Task Force on Load Representation for Dynamic Performance [1]. If present load representation produces overly-pessimistic results, the benefits of improved load modeling in planning studies will be in deferring or avoiding the expense of system modification and equipment additions; while for operation studies will be in increasing power transfer limits. However, if present load representation is overly optimistic, the benefits of improved load modeling in planning studies will be in avoiding system inadequacies that may result in costly operation limitations; while for operation studies will be in preventing system emergencies resulting from overly-optimistic operating limits [1].

Despite enormous research efforts and acquired knowledge, load modeling remains one of the most uncertain areas in large-scale power system simulations. In today's power industry environment, there are strong incentives to reduce the margin of simulation errors. More detailed load modeling can contribute to this goal, and thus, one option is to model loads at the distribution voltage level, with major load components such as induction motors represented separately. However, it is usually impractical to model the distribution network down to the

point where individual load devices are connected. It is common industry practice to use relatively simple load models for power flow and dynamic simulations. To deal with a reasonable number of discrete load models, the aggregate effects of possibly thousands of individual load components are lumped at the substation voltage level [3].

In this thesis, loads can be classified into two categories based on their ownerships. The first category refers to "aggregate loads", which are the collective load demand of various utility customers and served by the same substation. Examples are power distribution feeders connected to a substation. Load modeling research works are mainly developed for aggregate loads. The second category is the large industrial (and sometimes commercial) facilities owned by a single customer and supplied by a (often dedicated) substation or feeder, which are known as "facility loads". Examples are oil refineries, steel mills, paper mills and large airports. As mentioned in [1], models for some large special loads such as chlorine plants, aluminum reduction plants, smelters, and electric furnaces were provided in EPRI LOADSYN program, and development of special models may be warranted for such large unique loads. These efforts started showing the appreciation of the importance of large loads modeling.

Facility loads constitute major loads in a power system. It is critical to model them properly due to their large power demand and complex responses to system disturbances. Unfortunately, research works on modeling facility loads have been few in numbers. Only a limited number of research works addressed this load modeling gap. Reference [4] presented a method of creating equivalent models for industrial facilities assuming the electrical system structure of the facility is known. Reference [5] proposes an industrial load model that consists of about 76% small and large motors and 24% static load. A few utility companies have adopted similar crude approaches such as the WECC modeling guide [3, 6], this guide suggests that an industry facility can be modeled as 80% static loads and 20% induction motors. If these approaches in [3, 5, 6], which are known as "guideline models" in this thesis, are adopted, an oil refinery will have

dynamic responses similar to a steel mill in power system dynamic studies. This is clearly not acceptable when more and more accurate models are being developed for aggregate loads and other power system components such as generators.

Load models for two existing paper mills (10MVA and 30MVA) were determined by Ontario Hydro using the measured data during disturbances [7]. However, such models were only valid for the two specific facilities. Also, the measurement-based modeling method cannot be used to create load models for future industrial facilities, which do not exist yet.

Developing tools to establish dynamic models for large industry facilities is a project of interest to power industry. One of the challenges is how to model a future industrial facility with limited information in power systems planning studies. A common situation encountered by utilities planers can be described as follows: a manufacturer contacts a utility company and plans to develop a X-type industrial facility in a particular location; the facility needs about Y-MW power and could be in service after a few years. The facilities have poor visibility and the planning-time-frame visibility such as authoritative circuit diagrams, load composition, loading factors etc. is often minimal or non-existent. The utility, however, must include the model of the future facility in its planning study since the load can be large, in hundreds of MWs. Therefore, there are strong requirements to create adequate dynamic load models for industrial facilities.

Another challenge is how to model VFDs and their motor loads in power systems dynamic studies. VFDs can control the speed of an induction or synchronous motor by converting fixed frequency and fixed voltage magnitude to variable frequency and variable voltage magnitude at motor terminals, and provide significantly improved process control, energy saving, and soft motor starting. VFDs are increasingly used in various industrial facilities, for example, the percentage of VFDs in some oil field facilities could be as much as 80% of

total load demand. Therefore, the adequate dynamic model for motor drive systems shall be established with proven accuracy, which is especially important for the facility with large amount of motor drive loads.

Although detailed switching models for motor drive systems are readily available in the simulation software such as Matlab/Simulink, but they are discontinuous due to inherent switching, and hence are not directly suitable for linearization and small-signal frequency-domain characterization, for example obtaining impedance characteristics and input-output transfer functions, which are important in assessing stability of power-electronics-based power systems [8].

This chapter presents literature review on the status of load modeling and dynamic modeling of VFDs. Main objectives and the organization of the thesis are also introduced.

1.2 Literature Review on Load Modeling

1.2.1 Load Definations and Characteristics

There are four categories of the load as defined in [1] as follows: 1) Load device, a device, connected to a power system, that consumes power; 2) System load, the total power (active and/or reactive power) consumed by all devices connected to a power system; 3) Bus load, a portion of the system that is not explicitly represented in a system model, but rather is treated as if it were a single power-consuming device connected to a bus in the system model; 4) Generator or plant load, the power output of a generator or generating plant. In bulk power system studies, a load generally refers to the collective power demand at a substation, which is the “bus load”. Therefore, the bus load, as shown in Figure 1.1, is of main concern for power systems dynamic studies [1].

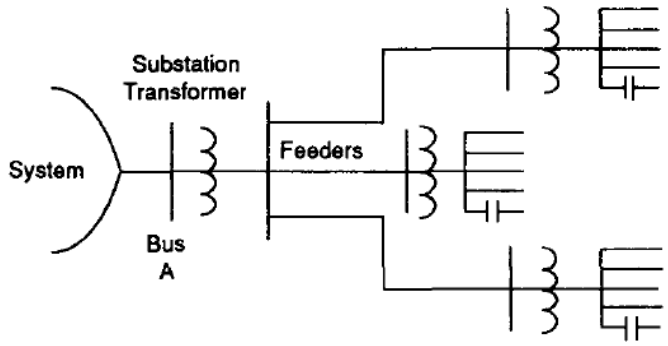

Figure 1.1 Bus load including feeders, transformers, shunt capacitors, and load devices [1]

Major load characteristics are summarized as follows [1]:

1) Loads that exhibit fast dynamic electrical and mechanical characteristics. The primary examples are VFDs.

2) Loads whose response to voltage excursions exhibit significant discontinuities. Example include VFDs that shut down on low voltage (as high as 90% rated voltage); motor contactors that drop open during faults and voltage swings, removing motor loads from the system; motor overload protection that remove stalled motors from the system after about 10 seconds. Motor starter contactors may drop open at 65-75% in the case of 2300V-4000V motors, and 55-65% in the case of motors at 460V and below.

1.2.2 Load Models

The load model is a mathematical representation of the relationship between a bus voltage (magnitude and frequency) and the power (active and reactive power) or current flowing into the bus. The term load model may refer to the equations themselves or the equations plus specific values for the parameters (e.g., coefficients, exponents) of the equations [1].

The static load model is a model expresses the active and reactive power at any instant of time as functions of the bus voltage magnitude and frequency at

the same instant, which involves algebraic equations. Static load models are essentially used for static load components such as resistive and lighting loads. Traditionally, the voltage dependence of load characteristics has been represented by the exponential model [1]:

$$P = P_0\left(\frac{V}{V_0}\right)^a \tag{1.2-1}$$

$$Q = Q_0\left(\frac{V}{V_0}\right)^b \tag{1.2-2}$$

The parameters of this model are the exponents a and b. With these exponents equal to 0, 1, or 2, the model represent constant power, constant current, or constant impedance characteristics, respectively.

An alternative model which has been widely used to represent the voltage dependence of loads is the polynomial model [1]:

$$P = P_0\left[a_1\left(\frac{V}{V_0}\right)^2 + a_2\left(\frac{V}{V_0}\right) + a_3\right] \tag{1.2-3}$$

$$Q = Q_0\left[a_4\left(\frac{V}{V_0}\right)^2 + a_5\left(\frac{V}{V_0}\right) + a_6\right] \tag{1.2-4}$$

This model is also referred to as the "ZIP" model, since it consists of the sum of constant impedance (Z), constant current (I), and constant power (P) terms. If the models are used to represent a specific load device, V_0 should be the rated voltage of the device, P_0 and Q_0 should be the power consumed at rated voltage. However, if the models are used to represent a bus load, V_0, P_0 and Q_0 are normally taken as the values at the initial system operating condition for the study. Polynomials of voltage deviations from rated voltage (ΔV) are sometimes used [1].

The frequency dependence of load characteristics is usually represented by multiplying the exponential model or the polynomial model by a factor

$$\left(1 + K_{pf}\Delta f\right) \qquad (1.2\text{-}5)$$

Where Δf is the frequency deviation ($f\text{-}f_0$) [1].

The dynamic load model is a model that expresses the active and reactive powers at any instant of time as functions of the voltage magnitude and frequency at past instant of time and, usually, including the present instant. Difference or differential equations can be used to represent such models [1]. The dynamic load models are expressed by transfer functions considering voltage and/or frequency dependence in [7, 9, 10]. For large industrial loads, two dynamic models are proposed in [7]: a transfer function model and an induction motor model with a shunt static load.

1.2.3 Load Modeling Approaches

There are two basic approaches to obtain composite load characteristics for bus loads: measurement-based approach and component-based approach. The measurement-based approach is to directly measure the voltage and frequency sensitivity of load active and reactive power at representative substations and feeders. Data of load modeling can be obtained by installing measurement and data acquisition devices at points where bus loads are to be represented. The parameters of a load model are estimated or identified by fitting the measured data to the assumed model [1, 7, 10-19]. The advantage of this method is that the data are obtained directly from the actual system. However, there are several disadvantages, including 1) application of data gathered at one substation to load models for other substations may only be possible if the loads are very similar; 2) determination of characteristics over a wide range of voltage and frequency may be impractical; 3) accounting for variation due to daily, seasonal, weather, and end-use changes requires on-going measurements under these varying conditions [1].

The component-based approach is to develop load models by aggregating models of individual components forming the load [1, 20-25]. Component

characteristics can be determined by theoretical analysis and laboratory measurement. This approach requires typical load composition, i.e., fractions of load consumed by each type of load component. The load modeling can be achieved via several processes: 1) component load modeling, 2) load composition estimation, 3) aggregation of component loads, and 4) aggregation of distribution system [26]. The aggregation of loads especially induction motors are widely discussed in the literature [27, 28].

Les Pereira et al. constructed a dynamic load model with 80% static load and 20% induction motor load, where a sensitivity study is conducted by varying percentages of the induction motor load, parameters of the equivalent induction motor etc. It is found that dynamic responses of overall system vary significantly with percentage and parameters of the induction motor [29], and such assumed load composition and load parameters are critical to the model. However, it is very hard to obtain accurate values for them, and the accuracy of the resultant load models become questionable.

For dynamic load modeling of future industrial facilities in power system planning studies, the measurement-based approach is not possible as the future facilities do not exist yet. If the component-based approach is used, the most challenging part will be how to obtain load composition and parameters of aggregated load devices. Therefore, a new dynamic load modeling method is needed for industrial facilities.

1.3 Literature Review on Dynamic Modeling of VFDs

1.3.1 VFD Characteristics during Disturbances

Power systems dynamic studies investigate system responses after the occurrence of one or multiple disturbances. Typical disturbances are short circuit faults and subsequent line trips. Such disturbances first appear as voltage sags at various buses of the system. It is, therefore, very important to understand how VFDs respond to voltage sags.

Defined by IEEE standard 1159, voltage sag is a decrease to between 0.1 and 0.9 pu in rms voltage at the power frequency for durations of 0.5 cycle to 1 min. Typical voltage sag values are 0.1 to 0.9 pu [30]. Voltage sags are usually associated with system faults but can also be caused by switching of heavy loads or starting of large motors. The common types of short-circuit faults in power systems are single-line-to-ground fault, line-to-line fault, double-line-to-ground fault, and three-phase balanced fault. The first three faults are unbalanced faults. Voltage sags normally do not cause equipment damage but could result in disruption to the operation of sensitive loads such as VFDs.

The voltage sag is characterized by its magnitude and duration. The severity of voltage sag depends on the network structure of the supply system, radial or interconnected for example, and the observation point. The voltage magnitude will depend on the number of phases involved, and the impedance between the observation point and the source of the short circuit. The duration will depend on the speed of the circuit protections, such as fuses, circuit breakers, and differential protections, with a typical clearance time in the range of 100 ms and 500 ms [31].

The common VFD structure comprises of an AC/DC rectifier, a dc link, a DC/AC inverter, additional control and protection circuits. The dominant type of drives is the pulse-width-modulation (PWM)-controlled voltage source inverter (VSI) drives [32].

As complex non-linear power electronics equipment, VFDs are more sensitive to voltage sags than older mechanical systems. The control and protection circuits in VFDs will disconnect the drives to protect their components during large voltage sags [32]. The sensitivity of VFDs to voltage sags are affected by many factors such as voltage sag types, loading and operating condition of the drives, threshold settings in the protection of the drives, and the control method etc [33]. The types of faults have significant

effect on the drive response to voltage sags. The sensitivity of VFDs is highest for voltage sags or short interruptions caused by three-phase balanced faults, and lowest for voltage sags or short interruptions caused by single-line-to-ground faults [32, 33, 34].

The operation mode of VFDs due to the single-line-to-ground fault is significantly different from that of other electrical components. A single-line-to-ground fault at a VFD input is equivalent to operation with a blown fuse in one phase, i.e., the three-phase rectifier is now just like a single-phase rectifier. For a well designed system, the average dc voltage decreases only marginally due to single phasing. For an open-loop V/Hz controlled PWM inverter drive, this means that the fundamental voltage across the machine will remain practically unaltered. Therefore, the average power drawn by the machine and the average DC link current remain constant. In a single-phased operation mode, each diode carries 50% more average current than that of a three-phase mode [35]. The single-phased operation of the three-phase diode rectifier will occur even for 90% voltage sags, and is independent of the voltage sag magnitude [36].

The sensitivity of VFDs to voltage sags can be expressed as a voltage tolerance characteristic curve in terms of voltage sag magnitude/duration values. The two values are denoted as threshold values. If the voltage sag is longer than the specific duration threshold and deeper than the specific voltage magnitude threshold, the VFD will malfunction/trip. In other words, the area below and on the right from the curve represents that voltage sags will cause malfunction/tripping of the VFD, while the area above and on the left from the curve represent that voltage sags will not cause VFD tripping [32, 33].

Based on the published results of equipment testing, the voltage magnitude threshold may vary between 59% and 71% for VFDs, whereas corresponding duration threshold varies between 15ms to 175ms. The probabilistic trip counts may vary over a wide range, from 68 trips per year using a low sensitivity threshold to 152 trips per year using a high sensitivity threshold [37].

1.3.2 Modeling of VFDs

As an important type of loads in industrial facilities, power electronic devices are extensively investigated for modeling [38-59]. Such investigations mostly focused on averaged modeling for power electronics converters/rectifiers at the component level. The dynamic averaged-value model (AVM) of a three phase load commutated converter is proposed in [60], however, such AVM model is just at the converter level, and the DC link, inverter, induction motor and the associated control system are not considered.

The averaged modeling method is explained in [39] in detail. Switching power converters (SPC) belong to a very special class of subjects to be controlled. Due to switching action, which is common to every SPC, the converter's model switches periodically between a set of ordinary differential equations. The whole model is a differential equation system with discontinuous right hand-side functions. Such systems will be simply termed as discontinuous systems. In the control literature, they are also called variable structure systems (VSS). VSS control theory appears to be an immediate choice for control object of SPC, but this was not the widely adopted approach at present. The reasons lie in two aspects: first, many power electronic engineers are not familiar with VSS control theory; second, SPC itself is a special class of VSS, and controller design based on VSS control theory has some limitations. Another logical approach for controlling SPC is to transform the discontinuous system models into continuous ones, so that control methods for continuous systems become applicable, averaging methods are the means for achieving these objectives. With averaging methods, discontinuity of the original discontinuous models is smoothed, and in many cases, the averaged models will be continuous. Recalling the history of power electronics, averaging has been a dominant technique for analysis and control of SPC [39, 40].

IEEE Task Force on Load Representation for Dynamic Performance recommended that a VFD was effectively constant power load if it is able to ride

through voltage sags without tripping [1]. Treating power electronics devices as constant power loads, negative impedance characteristics of such devices are investigated in [61-62]. However, as indicated in [2] using a constant power load to represent a complex non-linear power electronics component is questionable, a more accurate dynamic modeling method for VFDs in industrial facilities is required for power systems dynamic studies.

1.4 Research Objectives

Due to load modeling challenges facing power industry today, this research work is intended to explore proper dynamic load modeling techniques and establish adequate dynamic load models for industry facilities.

Objective 1: Dynamic load modeling technique for industrial facilities

1). Explore a systematic dynamic load modeling technique suitable for various industrial facilities

The current practice by utility companies is to use a guideline model assuming certain percents of static loads and induction motor loads to represent all industrial facilities. However, each type of facilities has its own load compositions and characteristics based on industrial processes, power consumptions and demands. As investigated in [29], dynamic responses of overall system vary significantly when using different percentages and parameters of the equivalent induction motor. Therefore, it is not proper to represent all types of industrial facilities with the same assumed guideline model. To address this issue, a systematic dynamic load modeling technique that can be applied to various industrial facilities will be investigated in this thesis.

2). Determination of the load composition and system configuration for the dynamic load model

Due to the nature of future industrial facilities with very limited information, determination of load compositions and system configuration for different types and sizes of industrial facilities are one of the biggest challenges.

3). Load aggregation techniques for model equivalence

Load aggregation techniques for model equivalence shall be investigated to properly group the loads and simplify the system model into the equivalent model format, which is more suitable for power systems dynamic studies.

Objective 2: The equivalent dynamic model for motor drive systems

1). Investigate the approach creating the equivalent dynamic model for motor drive systems

Although power electronic components are extensively studied and their averaged models are derived, such models cannot serve as dynamic load models for power systems dynamic studies. The converter AVM model does not include the DC link, inverter, the motor and its control system, so it cannot represent dynamic characteristics of the overall motor drive system. The goal is to find an approach to create the equivalent dynamic model for a motor drive system suitable for power systems dynamic studies.

2) Create dynamic models for VSI and cascaded inverter drives and their induction motor loads

To illustrate the approach creating the equivalent dynamic model for motor drive systems, dynamic models are created for two commonly used drive types, low voltage 6-pulse VSI drives and medium voltage cascaded inverter drives, and their induction motor loads.

3) Aggregation of motor drive systems

As part of load modeling task, the motor drive systems are required to be aggregated to achieve the whole facility load equivalence. The aggregation algorithms for motor drive systems need to be investigated.

Objective 3: A generic dynamic load model structure and a procedure on how to determine the final load model for industrial facilities

The ultimate goal of this research work is to create adequate dynamic load models for industrial facilities. It is important that a generic dynamic load model structure is sought to cover all common types of loads, induction motors, synchronous motors, static loads, and/or motor drive systems, in industrial facilities.

On the other hand, load types used in different industrial facilities might be different, for example, some types of facilities have synchronous motors, while others don't. Therefore, after the generic dynamic load model structure is created, a procedure should be established on how to tailor the generic structure into the final load model based on practical load types involved in the facility.

1.5 Thesis Organization

The objectives outlined in Section 1.4 have been accomplished successfully. The main research results are presented in this thesis and organized as follows:

In Chapter 2, a new concept, the template-based load modeling technique for industrial facilities, is proposed to address current load modeling issues faced by power industry. The main ideas including templates, template scaling rules and model equivalence algorithms are presented in this chapter.

In Chapter 3, to illustrate the proposed template-based load modeling technique, oil refinery facilities are used as an example. The template and template scaling rules are established at first, a template-based full model for a

108 MW coking refinery facility is then created based on them. The aggregation algorithms for induction motors, synchronous motors and static loads are applied to the template-based full model to obtain its equivalent models. The accuracy of the template-based full/equivalent models for the sample 108 MW coking oil refinery facility is verified by comparing dynamic responses of the template-based models with that of the real facility and the guideline model under disturbances. Due to limited amount of VFDs in oil refinery facilities, their presence is ignored. ETAP transient stability program is used as simulation tool in this chapter.

In Chapter 4, modeling of motor drive systems is extensively investigated. The research work can be divided into two parts. Part 1: VFDs will trip when they experience a relatively large voltage sag (>20% - 30% voltage drop). As a result, there is no need to include VFDs in dynamic studies. Based on the finding, a simple procedure to determine if a VFD needs to be included for dynamic studies is proposed in this thesis. Part 2: When VFDs experience mild voltage disturbances and are able to ride through, the equivalent dynamic model of motor drive systems is proposed. These models are created by the linearization approach with voltage and frequency dependence considered. Dynamic models for VSI and cascaded inverter drives and their induction motor loads are developed. These dynamic models are verified to be accurate by comparing their dynamic responses with that of the detailed switching model under disturbances. Sensitivity studies are also conducted to evaluate effects of parameters on the developed dynamic models. Matlab/Simulink is used as simulation tool in this chapter.

In Chapter 5, aggregation algorithms for motor drive systems are proposed by considering two cases: 1) VFDs connected to the same bus; 2) VFDs connected with upstream series impedance and transformers. The proposed algorithms are verified to be accurate by comparing dynamic responses of the aggregated equivalent dynamic model for VSI motor drive systems with that of

the detailed switching models. Matlab/Simulink is used as simulation tool in this chapter.

In Chapter 6, a generic dynamic load model structure for industrial facilities is proposed including all common loads. A procedure is recommended on how to tailor the generic structure into the final model based on loads practically involved in an industrial facility of interest. Conclusions are drawn and future works are presented in this chapter.

CHAPTER 2 TEMPLATE-BASED LOAD MODELING TECHNIQUE FOR INDUSTRIAL FACILITIES

In this thesis, a new concept, the template-based load modeling technique, is proposed to establish dynamic load models for industrial facilities. The main ideas of the technique include templates, template scaling rules and the model equivalence method.

2.1 Main Ideas

The basic idea is derived from the consideration that each type of facilities has a most common electrical system configuration, called a facility template. The template includes, but is not limited to, industry processes and their electric circuits, the number of circuit branches and voltage levels, load types and load composition, common motor sizes for different processes, motor voltage levels, and distribution lines/cables etc.

The facility templates are created mainly through a) facility design manuals, and b) extracting common characteristics of sample facilities. Facilities of same type share many common characteristics including characteristics of their respective electric systems. Such characteristics are often documented in industry specific design codes or manuals so that similar facilities can be designed and constructed by engineering companies. For example, design manuals and books are available for airports including their electric systems [63], [64]. Template electric systems can thus be created based on these design manuals. One can create a template database for different types of facilities.

The template needs to be scaled up or down to match the size of a specific facility to be modeled. For example, if a template represents a 100 MW facility and a model of 75 MW facility of the same type is to be created, template scaling will be used to achieve this goal. Template scaling is a process to modify

template circuits and loads automatically so that the scaled facility consumes approximately the expected amount of power. Scaling is based on a set of criteria that are developed according to different manufacturing processes.

The third aspect of the proposed technique is the model equivalence. The size-specific template-based full (TF) model created from the template and template scaling rules often contains hundreds of buses and motors, which is still large and complex. To further simplify the model to be suitable for power systems dynamic studies, equivalent models are obtained by aggregating the TF model.

Industrial facilities are constructed according to production processes and there are usually several processes involved in one facility. If all loads in one process are reduced into one equivalent load, the template-based equivalent model known as the "Equivalent Process (EP) model" is obtained. In subsequent steps, several or all processes can be aggregated into one load and lead to the simplest equivalent model known as the "Equivalent Facility (EF) model".

It is recommended in [2] that each individual load type (static loads, induction motors, and synchronous motors) may have multiple representations for load modeling. For example, a bus load may consist of one or more static load models, one or more induction motors, and a synchronous motor. Such statements support the proposed EP and EF load model formats in this thesis.

Among the above three components (electrical templates, template scaling rules and model equivalence method), the creation of facility templates and template scaling rules are facility dependent, while the model equivalence method is generally applicable to many facility types. A database tool can be developed to store the information of the three components. The process of using the database to establish dynamic load models for industrial facilities can be summarized as follows (Figure 2.1):

- Step 1: User input. The basic information needed from the user are: a) Facility type, defined based on the standard industry classifications for manufacturing facilities. For example, oil refineries, steel mills, coal mines and oil fields are facility types. b) Power demand of the facility, normally expressed as nominal or rated MW of the facility. c) Format of the output data. The user may input the preferred model type so that a case-specific model can be derived from the database.

- Step 2: Creation of size-specific template-based full facility model. The database is first searched to extract the template for the specific type of industrial facility of interest. Utilizing the template scaling rules stored in the database, the template is then scaled up or down to match the power demand level specific by the user. This process leads to a full model, which is denoted as the "template-based full (TF) model" in this thesis, tailored to the power demand of the user. Such model may contain hundreds of buses.

- Step 3: Model equivalence using aggregation algorithms. In this step, a set of aggregation algorithms can be used to conduct model equivalence for the TF model from Step 2). It will reduce the size of the TF model but preserve its key electrical response characteristics as viewed from the utility-facility interface point. The model equivalence will provide a much smaller template-based equivalent model, EP or EF model, say with 2 to 30 buses.

- Step 4: Model output. Based on the user information, the database tool will output the resultant template-based equivalent model in a format that can be directly incorporated in simulation of the power systems without editing. The database tool can also output a comparison of dynamic responses between the full model and the equivalent model.

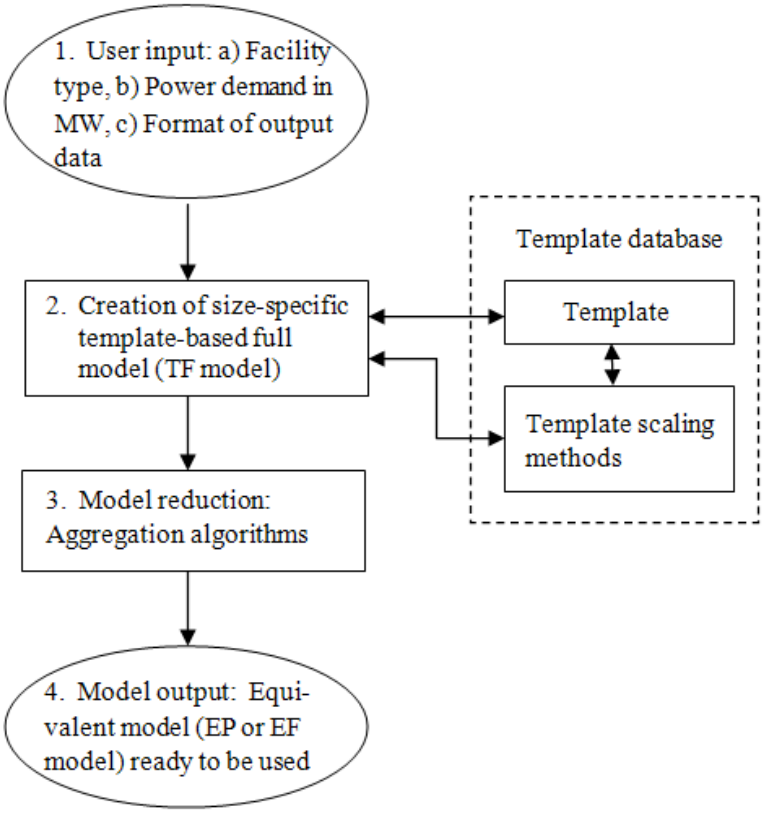

Figure 2.1 Process using the template-based load modeling technique for industrial facilities

For some types of industrial facilities such as oil refineries, VFDs are used in very small amount, therefore, only three types of loads, induction motors, synchronous motors, and static loads, are considered in the template-based load modeling. In other types of industrial facilities such as oil field, however, VFDs are widely used and must be included. The equivalent dynamic model and aggregation algorithms for motor drive systems need extensive investigations and will be discussed in detail in Chapters 4 and 5.

2.2 Model Equivalence

It is recognized that load aggregation is an effective way and also a critical part in load modeling, which directly affects accuracy of load models. There are two load aggregation methods available, theoretical and identification aggregation. The theoretical aggregation lumps similar loads analytically using

pre-defined parameter values of the loads based on the load type. Only similar loads will be grouped, for example, induction motors are aggregated with induction motors, and synchronous motors are aggregated with synchronous motors. The identification aggregation method is to create aggregated load model through identification based on field measurements [65].

Induction and synchronous motors form significant portion of loads in industrial facilities, and dynamic response of these motors plays a key role in transient behavior of the entire system. Techniques for aggregating a group of induction motors were investigated in [66-78]. Franklin et al proposed a dynamic aggregation method for induction motors with improved accuracy comparing to other existing aggregation methods, a group of induction motors connected to a common bus can be aggregated into a single equivalent induction motor model [66]. Similarly, the aggregation method for synchronous machines is extensively studied in [79-93].

Electric systems of the majority of industrial facilities have radial (tree) configurations as shown in Figure 2.2. At the tip of the systems are multiple motors and/or other types of loads connected to same buses. Several such branches are often connected to a higher voltage bus through transformers and cables/lines. The group of branches forms one of the production processes of the facility.

Aggregation algorithms for common types of loads need to be determined to achieve the model equivalence for the template-based full model and obtain the simplified template-based EP or EF models.

The aggregation methods for static loads, induction motors, and synchronous motors are discussed in this chapter. The dynamic modeling and aggregation methods for motor drive systems will be discussed in Chapters 4 and 5.

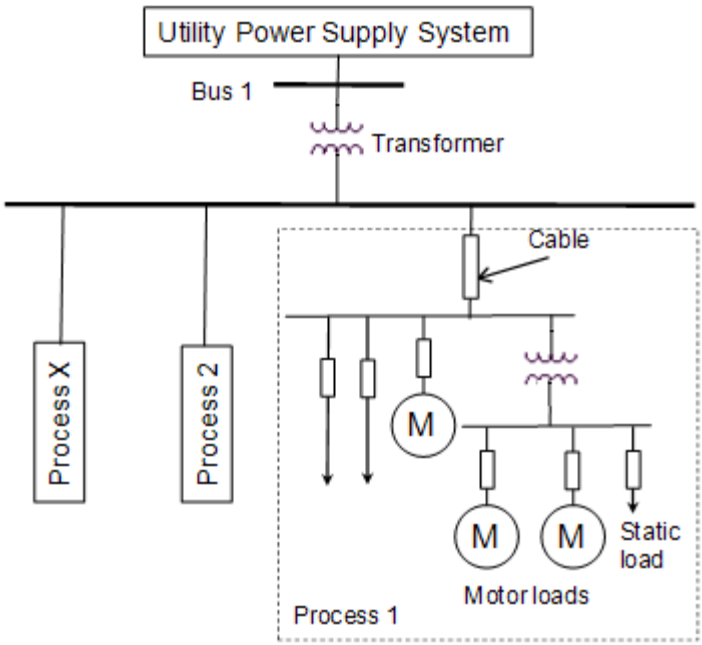

Figure 2.2 Electrical system configuration of a typical industrial facility

The first step of load aggregation for the template-based full model is to group static loads. The rated static loads measured in MW for individual processes are added together to form an equivalent static load of the whole facility. The lumped equivalent static load is modeled as a constant impedance load and usually connected to utility-customer interface bus. The static load model was proposed in [94] as a single admittance connected from bus to ground. The equivalent static load parameters can be calculated as follows [94]:

$$G_{SL} = \frac{\sum_{i=1}^{n\ loads} P_{SLi}}{V^2} \tag{2.2-1}$$

$$B_{SL} = \frac{\sum_{i=1}^{n\ loads} Q_{SLi}}{V^2} \tag{2.2-2}$$

where P_{SLi} and Q_{SLi} are active and reactive power drawn by individual static load in the system, V is the voltage of the bus that the equivalent static load is

connected to. After grouping static loads, the template-based full model contains only motor loads at downstream buses.

A bottom-up aggregation scheme for radial network configuration is proposed in this thesis to group various electric machines. This method includes three key steps: 1) Aggregate induction motors (IM) connected to the same bus into one equivalent induction motor. 2) Aggregate synchronous machines (SM) connected to the same bus into one equivalent synchronous machine. 3). Split a bus into two for the cases where both (equivalent) induction motor and (equivalent) synchronous machine are connected to the same bus through a common transformer and/or series impedance in the upstream circuit. This procedure is repeated from the buses with the lowest voltage levels upward to the substation bus, which eventually leads to an equivalent model for the entire facility.

For Steps 1) and 2), the techniques proposed in [66] for aggregating a group of induction machines and in [81, 82] for aggregating a group of synchronous machines have been adopted by this work. For Step 3), a new machine equivalence method, a bus split algorithm, is proposed. Therefore, the major contribution for this part of the research work is Step 3) with the bus split algorithm.

Figure 2.3 illustrates the proposed bottom-up aggregation scheme for a simple radial network with induction and synchronous motors:

1) A group of three induction motors, IM3, IM4, IM5, and their feeding transformer TX-3 in Figure 3 (a) is aggregated to be an equivalent induction motor IM-TX3-eq in Figure 3 (b); Similarly, a group of three induction motors, IM8, IM9, IM10, and their feeding transformer TX-5 in Figure 3 (a) is aggregated to be an equivalent induction motor IM-TX5-eq in Figure 3 (b).
2) A group of three induction motors, IM1, IM2, IM-TX3-eq, and their feeding transformer TX-1 in Figure 3 (b) is aggregated to be an

equivalent induction motor IM-TX1-eq in Figure 3 (c); Similarly, a group of two induction motors, IM7, IM-TX5-eq, in Figure 3 (b) is aggregated to be an equivalent induction motor IM-7-TX5eq in Figure 3 (c).

3) One induction motor and one synchronous motor, IM-7-TX5eq, SM1, fed by their common transformer TX-4 in Figure 3 (c) are converted to the new system structure using the bus-split algorithm, fed by two new transformers TX-6 and TX-7, respectively, in Figure 3 (d).

4) A group of two induction motors, IM6, IM-7-TX5eq and its new transformer TX-6, in Figure 3 (d) is aggregated to be an equivalent induction motor IM6-TX6-eq in Figure 3 (e).

5) One induction motor and one synchronous motor, IM6-TX6-eq, SM1 and its new transformer TX-9, with a upstream transformer TX-2 in Figure 3 (e) are converted to the new system structure using the bus-split algorithm, fed by two new transformers TX-8 and TX-9, respectively, in Figure 3 (f).

6) A group of two induction motors, IM-TX1-eq, IM6-TX6-eq and its new transformer TX-8, in Figure 3 (f) is aggregated to be an equivalent induction motor IM-TX1-TX8-eq in Figure 3 (g). At this step, the whole system becomes a simplified format consisting of an equivalent induction motor and an equivalent synchronous motor.

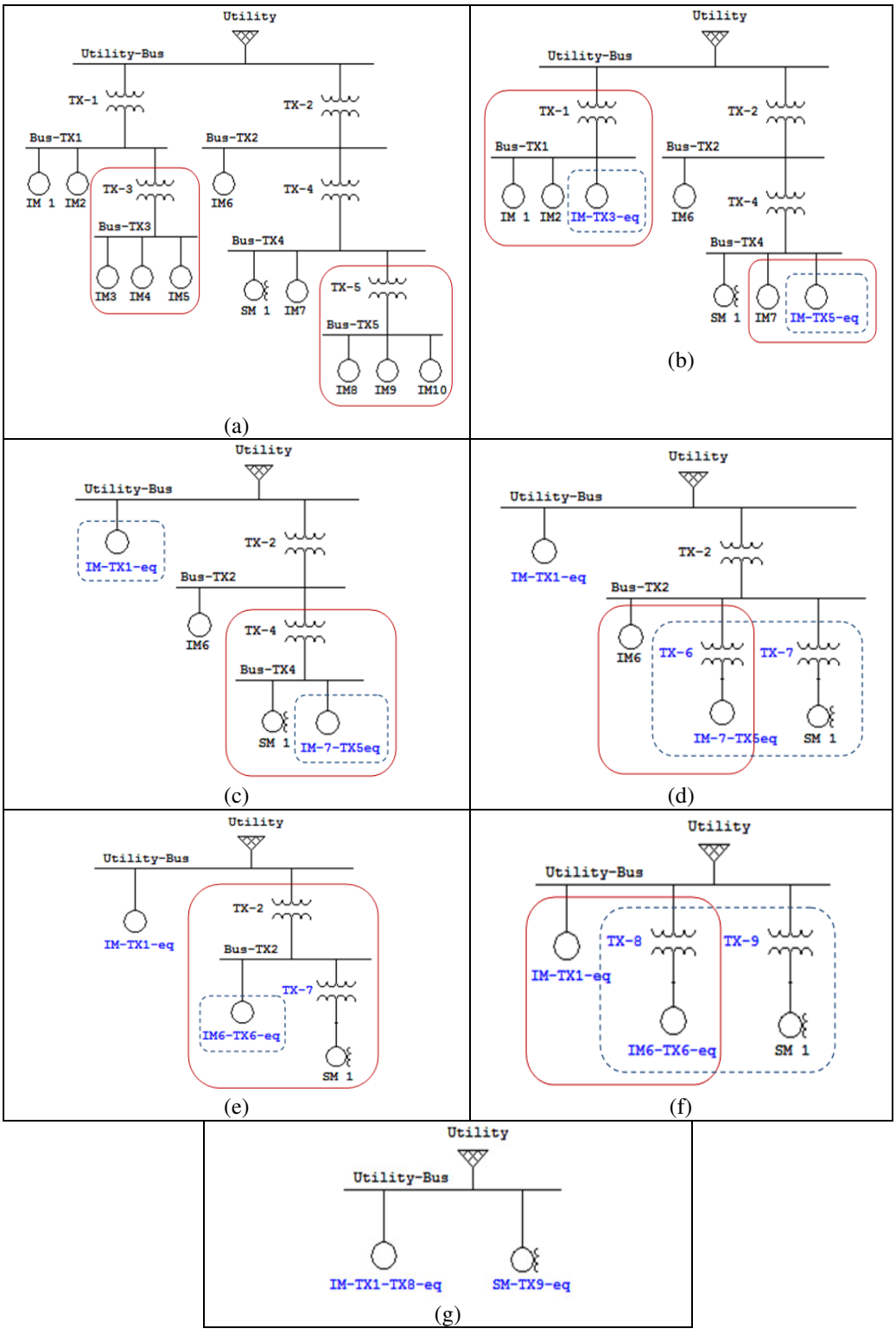

Figure 2.3 Bottom-up aggregation scheme for radial networks

2.3 Bus Split Algorithm

Rogers et al [4] recommended an aggregated induction motor model for industry plants, but did not conduct work considering synchronous motors aggregation; it simply mentioned that large synchronous motors should be modeled in detail in any transient stability study in which plant dynamics are important and thus are not considered to be part of the aggregated load. In real life, however, synchronous motors may be present at the downstream motor control center (MCC) bus mixed with many induction motors, and usually a transformer and/or series impedance such as a cable is used to connect between the downstream MCC bus and upstream circuits. In this case, how to aggregate upstream motors with induction and synchronous motors connected to the downstream MCC bus remains unsolved, i.e., presently the aggregation process for induction and synchronous motors is stuck when such condition occurs. Therefore, it is critical to develop an algorithm that is able to separate synchronous motors from induction motors connected to a common bus through a transformer and/or series impedance to continue motor loads aggregation toward upstream. A bus split algorithm with detailed mathematical derivation is proposed to address this issue.

For large industrial facilities, synchronous motors, if present, are normally connected to the MCC with induction motors. A typical system configuration of a MCC connected with i induction motors, j synchronous motors, and an upstream transformer T_0 is shown in Figure 2.4 (a). Using the aggregation method for induction motors connected to a common bus [66], the i induction motors can be aggregated into a single equivalent induction motor. Similarly, using the aggregation method for synchronous motors connected to a common bus [81, 82], the j synchronous motors can be aggregated into a single equivalent synchronous motor. After such aggregations, the MCC bus configuration is simplified to be Figure 2.4 (b) with only one aggregated induction motor and one

aggregated synchronous motor. This simplified system is known as "Original system" in this thesis.

At this stage, the two different types of equivalent motors are still connected through a common transformer T_0, so they cannot be directly aggregated with upstream motors. To achieve further load aggregation, an equivalent system is desired with the induction and synchronous motor connected by two separate branches through two new transformers (T_1 and T_2). The proposed bus split algorithm can achieve such equivalence, and the new system shown in Figure 2.4 (c) is known as "Equivalent system" in this thesis. Note: the proposed algorithm is also valid for upstream series impedance instead of a transformer.

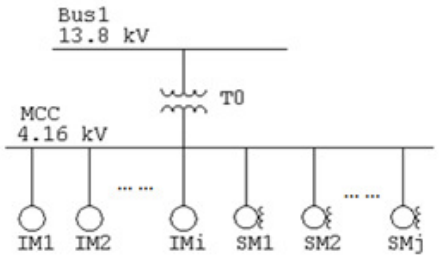

(a) Typical MCC bus in an industrial facility (before motor aggregation)

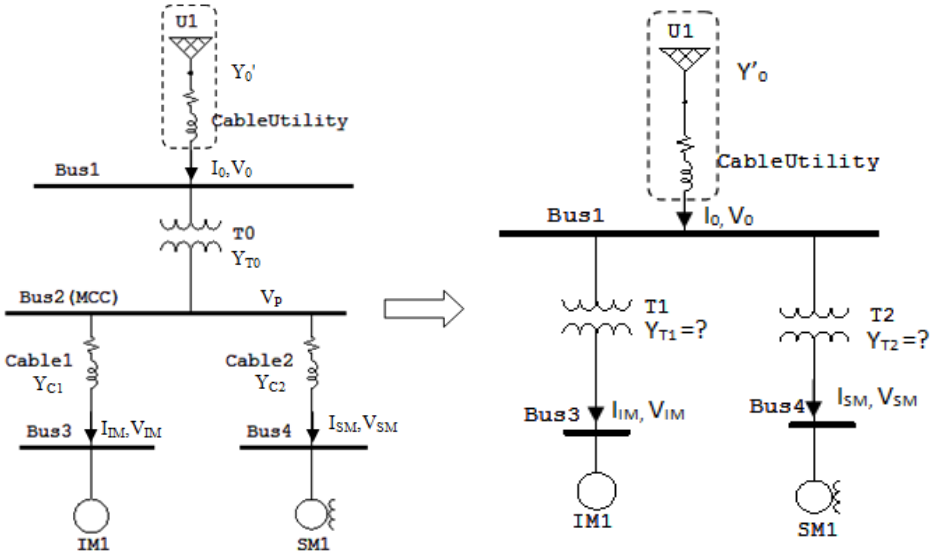

(b) Original system (before bus split algorithm)

(c) Equivalent system (after bus split algorithm)

Figure 2.4 The bus split algorithm at a motor control center bus

The state space equations and network equations in terms of the nodal admittance matrix Y (I = YV) for the original and equivalent systems are used to accomplish such equivalence. To summarize, the following steps are needed for getting ready to use the bus split algorithm:

1) Choose the MCC bus with induction and synchronous motors.
2) Aggregate induction motors using the induction motors aggregation method proposed in [66] and obtain the aggregated induction motor IM_1 (Note if only one induction motor is present, then no aggregation is required).
3) Aggregate synchronous motors using the synchronous motors aggregation method proposed in [81, 82] and obtain the aggregated synchronous motor SM_1 (Note if only one synchronous motor is present, then no aggregation is required).
4) To this point, the bus split algorithm is ready to be used for further load aggregation.

2.3.1 State Space Equations

2.3.1.1 Induction Motors

The per unit voltage and flux linkage equations for a single rotor winding induction motors in d-q coordinates can be expressed as follows [4, 83]:

$$v_{ds} = R_s i_{ds} - \omega_s \Psi_{qs} + \dot{\Psi}_{ds} \tag{2.3-1}$$

$$v_{qs} = R_s i_{qs} + \omega_s \Psi_{ds} + \dot{\Psi}_{qs} \tag{2.3-2}$$

$$v_{dr} = R_r i_{dr} - \omega_s S \Psi_{qr} + \dot{\Psi}_{dr} \tag{2.3-3}$$

$$v_{qr} = R_r i_{qr} + \omega_s S \Psi_{dr} + \dot{\Psi}_{qr} \tag{2.3-4}$$

$$\Psi_{ds} = L_s i_{ds} + L_m i_{dr} \tag{2.3-5}$$

$$\Psi_{qs} = L_s i_{qs} + L_m i_{qr} \tag{2.3-6}$$

$$\Psi_{dr} = L_m i_{ds} + L_r i_{dr} \tag{2.3-7}$$

$$\Psi_{qr} = L_m i_{qs} + L_r i_{qr} \tag{2.3-8}$$

Where

Ψ_{ds}, Ψ_{qs} – stator flux linkages in terms of direct- and quadrature-axis components

Ψ_{dr}, Ψ_{qr} – rotor flux linkages in terms of direct- and quadrature-axis components

v_{ds}, v_{qs} – stator voltages in terms of direct- and quadrature-axis components

i_{ds}, i_{qs} – stator phase currents in terms of direct- and quadrature-axis components

v_{dr}, v_{qr} – rotor voltages in terms of direct- and quadrature-axis components

i_{dr}, i_{qr} – rotor currents in terms of direct- and quadrature-axis components

R_s, R_r – stator voltages in terms of direct- and quadrature-axis components

ω_s – angular velocity of the stator field in electrical rad/s

L_m – magnetizing inductance

l_s – stator leakage inductance

l_r – rotor leakage inductance

L_s – total stator inductance, $L_s = l_s + L_m$

L_r – total rotor inductance, $L_r = l_r + L_m$

S – constant slip

The following assumptions are made:

1) The stator transient is negligible:

$$\dot{\Psi}_{ds} = 0 \tag{2.3-9}$$

$$\dot{\Psi}_{qs} = 0 \tag{2.3-10}$$

2) The rotor is shorted:

$$v_{dr} = 0 \tag{2.3-11}$$

$$v_{qr} = 0 \tag{2.3-12}$$

3) Define the new variable, the internal voltage for induction motor, as follows:

$$V_d' = \left(-\frac{X_m}{L_r} \right) \Psi_{qr} \tag{2.3-13}$$

$$V_q' = \left(\frac{X_m}{L_r} \right) \Psi_{dr} \tag{2.3-14}$$

4) Define normal transient impedance:

$$X_s' = X_s - \frac{X_m^2}{X_r} \tag{2.3-15}$$

$$X_s = X_{ls} + X_m \tag{2.3-16}$$

$$X_r = X_{lr} + X_m \tag{2.3-17}$$

Where X_{ls} is the stator leakage reactance, X_{lr} is the rotor leakage reactance, and X_m is the magnetizing reactance.

Substitute Equations (2.3-9) and (2.3-10) in Equations (2.3-1) and (2.3-2), the following equations are obtained:

$$v_{ds} = R_s i_{ds} - \omega_s \Psi_{qs} \tag{2.3-18}$$

$$v_{qs} = R_s i_{qs} + \omega_s \Psi_{ds} \tag{2.3-19}$$

Substitute Equations (2.3-5) and (2.3-6) in Equations (2.3-18) and (2.3-19), we have

$$v_{ds} = R_s i_{ds} - \omega_s \left(L_s i_{qs} + L_m i_{qr} \right) \tag{2.3-20}$$

$$v_{qs} = R_s i_{qs} + \omega_s \left(L_s i_{ds} + L_m i_{dr} \right) \tag{2.3-21}$$

By rearranging, Equations (2.3-7) and (2.3-8), the following equations are obtained:

$$i_{dr} = \left(\frac{1}{L_r} \right) \Psi_{dr} - \left(\frac{L_m}{L_r} \right) i_{ds} \tag{2.3-22}$$

$$i_{qr} = \left(\frac{1}{L_r} \right) \Psi_{qr} - \left(\frac{L_m}{L_r} \right) i_{qs} \tag{2.3-23}$$

By rearranging, Equations (2.3-13) and (2.3-14) can be expressed as follows:

$$\Psi_{dr} = \left(\frac{L_r}{X_m}\right)V_q' \tag{2.3-24}$$

$$\Psi_{qr} = \left(-\frac{L_r}{X_m}\right)V_d' \tag{2.3-25}$$

Substitute Equations (2.3-24) and (2.3-25) in Equations (2.3-22) and (2.3-23):

$$i_{dr} = \left(\frac{1}{X_m}\right)V_q' - \left(\frac{L_m}{L_r}\right)i_{ds} \tag{2.3-26}$$

$$i_{qr} = \left(-\frac{1}{X_m}\right)V_d' - \left(\frac{L_m}{L_r}\right)i_{qs} \tag{2.3-27}$$

Substitute Equations (2.3-26) and (2.3-27) in Equations (2.3-20) and (2.3-21):

$$v_{ds} = R_s i_{ds} + \left(\frac{\omega_s L_m^2}{L_r} - \omega_s L_s\right) i_{qs} + \frac{\omega_s L_m}{X_m} V_d' \tag{2.3-28}$$

$$v_{qs} = R_s i_{qs} + \left(\omega_s L_s - \frac{\omega_s L_m^2}{L_r}\right) i_{ds} + \frac{\omega_s L_m}{X_m} V_q' \tag{2.3-29}$$

$$X_s = \omega_s L_s \tag{2.3-30}$$

$$X_m = \omega_s L_m \tag{2.3-31}$$

$$X_r = \omega_s L_r \tag{2.3-32}$$

Based on Equations (2.3-15), (2.3-30), (2.3-31), and (2.3-32), Equations (2.3-28) and (2.3-29) can be rewritten as follows:

$$v_{ds} = R_s i_{ds} - X_s' i_{qs} + V_d' \tag{2.3-33}$$

$$v_{qs} = X_s' i_{ds} + R_s i_{qs} + V_q' \tag{2.3-34}$$

In the phasor form, Equations (2.3-33) and (2.3-34) can be expressed by

$$V_{IM} = (R_s + jX_s')I_s + E_m' \tag{2.3-35}$$

Substitute Equations (2.3-11) and (2.3-12) in Equations (2.3-3) and (2.3-4), the following can be determined:

$$0 = R_r i_{dr} - S\omega_s \Psi_{qr} + \dot{\Psi}_{dr} \tag{2.3-36}$$

$$0 = R_r i_{qr} + S\omega_s \Psi_{dr} + \dot{\Psi}_{qr} \tag{2.3-37}$$

Based on Equations (2.3-24) and (2.3-25), we have:

$$\dot{\Psi}_{dr} = \left(\frac{L_r}{X_m}\right)\dot{V}'_q \tag{2.3-38}$$

$$\dot{\Psi}_{qr} = \left(-\frac{L_r}{X_m}\right)\dot{V}'_d \tag{2.3-39}$$

Substitute Equations (2.3-24), (2.3-25), (2.3-26), (2.3-27), (2.3-38), (2.3-39) in Equations (2.3-36) and (2.3-37), the differential equations expressed by the motor internal voltage and the stator current can then be determined as follows:

$$\dot{V}'_d = \left(-\frac{R_r}{L_r}\right)V'_d + \omega_s S V'_q - \frac{L_m X_m R_r}{L_r^2} i_{qs} \tag{2.3-40}$$

$$\dot{V}'_q = -\omega_s S V'_d - \frac{R_r}{L_r} V'_q + \frac{L_m X_m R_r}{L_r^2} i_{ds} \tag{2.3-41}$$

The equation of the motion in per unit for the induction motor is expressed as follows:

$$\frac{2H\dot{\omega}_r}{\omega_s} = P_e - P_L \tag{2.3-42}$$

$$\omega_r = \omega_s(1 - S) \tag{2.3-43}$$

$$P_e = V'_d i_{ds} + V'_q i_{qs} \tag{2.3-44}$$

Rearranging Equations (2.3-42)-(2.3-44), the following equation can be determined:

$$2H\dot{S} = P_L - \left(V'_d i_{ds} + V'_q i_{qs}\right) \tag{2.3-45}$$

Linearizing Equations (2.3-40), (2.3-41) and (2.3-45), the following are obtained:

$$\Delta \dot{V}_d' = \left(-\omega_s \frac{R_r}{X_r}\right)\Delta V_d' + S_0\omega_s \Delta V_q' + \omega_s V_{q0}' \Delta S - \left(\omega_s \frac{R_r}{X_r}\right)(X_s - X_s')\Delta i_{qs} \tag{2.3-46}$$

$$\Delta \dot{V}_q' = (-S_0\omega_s)\Delta V_d' - \left(\omega_s \frac{R_r}{X_r}\right) S_0\omega_s \Delta V_q' - \omega_s V_{d0}' \Delta S + \left(\omega_s \frac{R_r}{X_r}\right)(X_s - X_s')\Delta i_{ds} \tag{2.3-47}$$

$$2H\Delta \dot{S} = -\left(i_{d0}\Delta V_d' + i_{q0}\Delta V_q' + V_{d0}'\Delta i_{ds} + V_{q0}'\Delta i_{qs}\right) \tag{2.3-48}$$

If written in the matrix format, Equations (2.3-46), (2.3-47) and (2.3-48) can be expressed as follows:

$$\begin{bmatrix} \Delta \dot{V}_d' \\ \Delta \dot{V}_q' \\ \Delta \dot{S} \end{bmatrix} = \begin{bmatrix} \left(-\omega_s \frac{R_r}{X_r}\right) & (S_0\omega_s) & (\omega_s V_{q0}') \\ (-S_0\omega_s) & \left(-\omega_s \frac{R_r}{X_r}\right) & (-\omega_s V_{d0}') \\ \left(-\frac{i_{d0}}{2H}\right) & \left(-\frac{i_{q0}}{2H}\right) & 0 \end{bmatrix} \begin{bmatrix} \Delta V_d' \\ \Delta V_q' \\ \Delta S \end{bmatrix} + \begin{bmatrix} 0 & \left(-\omega_s \frac{R_r}{X_r}\right)(X_s - X_s') \\ \left(\omega_s \frac{R_r}{X_r}\right)(X_s - X_s') & 0 \\ \left(-\frac{V_{d0}'}{2H}\right) & \left(-\frac{V_{q0}'}{2H}\right) \end{bmatrix} \begin{bmatrix} \Delta i_{ds} \\ \Delta i_{qs} \end{bmatrix} \tag{2.3-49}$$

In the partitioned form, the state space equation for the induction motor can be rewritten as follows [4]:

$$\begin{bmatrix} \Delta \dot{E}_m' \\ \Delta \dot{S} \end{bmatrix} = \begin{bmatrix} E_1 & E_2 \\ E_3 & 0 \end{bmatrix} \begin{bmatrix} \Delta E_m' \\ \Delta S \end{bmatrix} + \begin{bmatrix} F_1 \\ F_2 \end{bmatrix} [\Delta I_{IM}] \tag{2.3-50}$$

Where,

$$E_1 = \begin{bmatrix} \left(-\omega_s \frac{R_r}{X_r}\right) & (S_0\omega_s) \\ (-S_0\omega_s) & \left(-\omega_s \frac{R_r}{X_r}\right) \end{bmatrix} \tag{2.3-51}$$

$$E_2 = \begin{bmatrix} \omega_s V_{q0}' \\ -\omega_s V_{d0}' \end{bmatrix} \tag{2.3-52}$$

$$E_3 = \begin{bmatrix} \left(-\frac{i_{d0}}{2H}\right) & \left(-\frac{i_{q0}}{2H}\right) \end{bmatrix} \tag{2.3-53}$$

$$F_1 = \begin{bmatrix} 0 & \left(-\omega_s \frac{R_r}{X_r}\right)(X_s - X_s') \\ \left(\omega_s \frac{R_r}{X_r}\right)(X_s - X_s') & 0 \end{bmatrix} \tag{2.3-54}$$

$$F_2 = \begin{bmatrix} \left(-\frac{V_{d0}'}{2H}\right) & \left(-\frac{V_{q0}'}{2H}\right) \end{bmatrix} \tag{2.3-55}$$

The state variables for the induction motor are as follows:

$$\Delta X = \begin{bmatrix} \Delta E_m' \\ \Delta S \end{bmatrix} \tag{2.3-56}$$

2.3.1.2 Synchronous Motors

By neglecting amortisseur windings, per unit voltages and flux linkage equations for synchronous motors are given as follows [83]:

$$e_d = -\Psi_q - R_a i_d \tag{2.3-57}$$

$$e_q = \Psi_d - R_a i_q \tag{2.3-58}$$

$$e_{fd} = \dot{\Psi}_{fd} + R_{fd} i_{fd} \tag{2.3-59}$$

$$\Psi_d = -L_d i_d + L_{ad} i_{fd} \tag{2.3-60}$$

$$\Psi_q = -L_q i_q \tag{2.3-61}$$

$$\Psi_{fd} = -L_{ad} i_d + L_{ffd} i_{fd} \tag{2.3-62}$$

where

e_d , e_q – stator voltage in terms of direct- and quadrature-axis components

i_d , i_q – stator current in terms of direct- and quadrature-axis components

Ψ_d , Ψ_q – stator flux linkage in terms of direct- and quadrature-axis components

e_{fd} – rotor voltage

i_{fd} – rotor current

Ψ_{fd} – rotor flux linkage

$L_d = L_l + L_{ad}$

$L_q = L_l + L_{aq}$

$L_{ffd} = L_{fd} + L_{ad}$

L_d, L_q – d-axis and q-axis synchronous inductance

L_{ad}, L_{aq} – mutual inductance

L_l – the leakage inductance

R_a – armature resistance per phase

R_{fd} – rotor circuit resistance

L_{fd} – rotor leakage inductance

In above equations, the stator transients are neglected and the per unit value of the rotor speed ω_r is assumed to be equal to 1 in the stator voltage equation. The assumption of per unit $\omega_r = 1$ in the stator voltage equations does not contribute to computational simplicity in itself, the primary reason for making this assumption is that it counterbalances the effect of neglecting stator transients ($\dot{\Psi}_d, \dot{\Psi}_q$) so far as the low frequency rotor oscillations are concerned [83].

Define the following new parameters:

$$E'_q = \frac{L_{ad}}{L_{ffd}} \Psi_{fd} \tag{2.3-63}$$

$$X'_d = L_d - \frac{L^2_{ad}}{L_{ffd}} \tag{2.3-64}$$

$$E_{fd} = \left(\frac{L_{ad}}{R_{fd}} \right) e_{fd} \tag{2.3-65}$$

$$L_d - L'_d = \left(\frac{L^2_{ad}}{L_{ffd}} \right) \tag{2.3-66}$$

$$T'_{d0} = \left(\frac{L_{ffd}}{R_{fd}} \right) \tag{2.3-67}$$

Note in per unit $X_d = L_d$, and $X_d' = L_d'$. Equations (2.3-64) and (2.3-66) are the same equation but write separately for convenience.

Substitute Equations (2.3-60) and (2.3-61) in Equations (2.3-57) and (2.3-58), we have

$$e_d = -R_a i_d + L_q i_q \tag{2.3-68}$$

$$e_q = -L_d i_d - R_a i_q + L_{ad} i_{fd} \tag{2.3-69}$$

Rearrange Equation (2.3-62) as follows:

$$i_{fd} = \frac{1}{L_{ffd}} \left(\Psi_{fd} + L_{ad} i_d \right) \tag{2.3-70}$$

Substitute Equation (2.3-70) in Equation (2.3-69), the following equation is determined:

$$e_q = \left(\frac{L_{ad}^2}{L_{ffd}} - L_d \right) i_d - R_a i_q + \left(\frac{L_{ad}}{L_{ffd}} \right) \Psi_{fd} \tag{2.3-71}$$

Rewrite Equation (2.3-71) based on Equations (2.3-63) and (2.3-64) as follows:

$$e_q = \left(- X'_d \right) i_d - R_a i_q + E'_q \tag{2.3-72}$$

In the phasor form, Equations (2.3-68) and (2.3-72) can be rewritten as follows:

$$V_{SM} = \left[- \left(R_a + jX'_d \right) \right] I_{SM} + E'_q \tag{2.3-73}$$

Rearrange Equation (2.3-63) and find its derivative as follows:

$$\Psi_{fd} = \left(\frac{L_{ffd}}{L_{ad}} \right) E'_q \tag{2.3-74}$$

$$\dot{\Psi}_{fd} = \left(\frac{L_{ffd}}{L_{ad}} \right) \dot{E}'_q \tag{2.3-75}$$

Substitute Equations (2.3-74) in Equation (2.3-70) as follows:

$$i_{fd} = \left(\frac{1}{L_{ad}}\right)E'_q + \left(\frac{L_{ad}}{L_{ffd}}\right)i_d \tag{2.3-76}$$

Substitute Equations (2.3-75) and (2.3-76) in Equation (2.3-59), the following equation is determined:

$$e_{fd} = \left(\frac{L_{ffd}}{L_{ad}}\right)\dot{E}'_q + \left(\frac{R_{fd}}{L_{ad}}\right)E'_q + \left(\frac{R_{fd}L_{ad}}{L_{ffd}}\right)i_d \tag{2.3-77}$$

Rearrange Equation (2.3-77) based on Equation (2.3-65) as follows:

$$\dot{E}'_q = \left(\frac{R_{fd}}{L_{ffd}}\right)\left[E_{fd} - E'_q - \left(\frac{L_{ad}^2}{L_{ffd}}\right)i_d\right] \tag{2.3-78}$$

The following relationship is obtained for the internal voltage for synchronous motors by substituting Equations (2.3-66) and (2.3-67) in Equation (2.3-78):

$$\dot{E}'_q = \frac{1}{T'_{d0}}\left[E_{fd} - E'_q - (L_d - L'_d)i_d\right] \tag{2.3-79}$$

The equation for the motion is

$$\frac{d\omega_r}{dt} = \frac{1}{2H}(T_e - T_L - D\omega_r) \tag{2.3-80}$$

$$T_e = E'_q i_q \tag{2.3-81}$$

Where H is the combined inertia constant of the motor and loads, D is the Damping factor. Substitute Equation (2.3-81) in Equation (2.3-80), we have

$$\dot{\omega}_r = \frac{1}{2H}\left(E'_q i_q - T_L - D\omega_r\right) \tag{2.3-82}$$

Assuming E_{fd} = constant, the linearized forms for Equations (2.3-79) and (2.3-82) are derived as follows:

$$\Delta\dot{E}'_q = \left(-\frac{1}{T'_{d0}}\right)\Delta E'_q - \left(\frac{L_d - L'_d}{T'_{d0}}\right)\Delta i_d \tag{2.3-83}$$

$$\Delta\dot{\omega}_r = \left(\frac{i_{q0}}{2H}\right)\Delta E'_q - \left(\frac{D}{2H}\right)\Delta\omega_r + \left(\frac{E'_{q0}}{2H}\right)\Delta i_q \tag{2.3-84}$$

In the matrix format, Equations (2.3-83) and (2.3-84) can be expressed by

$$\begin{bmatrix}\Delta\dot{E}'_q \\ \Delta\dot{\omega}_r\end{bmatrix} = \begin{bmatrix}\left(-\frac{1}{T'_{d0}}\right) & 0 \\ \left(\frac{i_{q0}}{2H}\right) & \left(-\frac{D}{2H}\right)\end{bmatrix}\begin{bmatrix}\Delta E'_q \\ \Delta\omega_r\end{bmatrix} + \begin{bmatrix}\left(-\frac{(L_d - L'_d)}{T'_{d0}}\right) & 0 \\ 0 & \left(\frac{E'_{q0}}{2H}\right)\end{bmatrix}\begin{bmatrix}\Delta i_d \\ \Delta i_q\end{bmatrix} \tag{2.3-85}$$

Equation (2.3-85) is rewritten as follows

$$\begin{bmatrix}\Delta\dot{E}'_q \\ \Delta\dot{\omega}_r\end{bmatrix} = \begin{bmatrix}E_4 & 0 \\ E_5 & E_6\end{bmatrix}\begin{bmatrix}\Delta E'_q \\ \Delta\omega_r\end{bmatrix} + \begin{bmatrix}F_3 \\ F_4\end{bmatrix}[\Delta I_{SM}] \tag{2.3-86}$$

Where,

$$E_4 = \left(-\frac{1}{T'_{d0}}\right) \tag{2.3-87}$$

$$E_5 = \left(\frac{i_{q0}}{2H}\right) \tag{2.3-88}$$

$$E_6 = \left(-\frac{D}{2H}\right) \tag{2.3-89}$$

$$F_3 = \begin{bmatrix}\left(-\frac{(L_d - L'_d)}{T'_{d0}}\right) & 0\end{bmatrix} \tag{2.3-90}$$

$$F_4 = \begin{bmatrix}0 & \left(\frac{E'_{q0}}{2H}\right)\end{bmatrix} \tag{2.3-91}$$

The state variables for the synchronous motor:

$$\Delta X = \begin{bmatrix}\Delta E'_q \\ \Delta\omega_r\end{bmatrix} \tag{2.3-92}$$

2.3.1.3 Induction and Synchronous Motors

If both induction and the synchronous motors are included in the state space equation as requested in Figure 2.4 (b), the state variables in this case can be chosen as follows:

$$\Delta X = \begin{bmatrix} \Delta E'_m \\ \Delta S \\ \Delta E'_q \\ \Delta \omega_r \end{bmatrix} \tag{2.3-93}$$

The state space equations can be obtained based on Equations (2.3-50) and (2.3-86) as follows:

$$\begin{bmatrix} \Delta \dot{E}'_m \\ \Delta \dot{S} \\ \Delta \dot{E}'_q \\ \Delta \dot{\omega}_r \end{bmatrix} = \begin{bmatrix} E_1 & E_2 & 0 & 0 \\ E_3 & 0 & 0 & 0 \\ 0 & 0 & E_4 & 0 \\ 0 & 0 & E_5 & E_6 \end{bmatrix} \begin{bmatrix} \Delta E'_m \\ \Delta S \\ \Delta E'_q \\ \Delta \omega_r \end{bmatrix} + \begin{bmatrix} F_1 & 0 \\ F_2 & 0 \\ 0 & F_3 \\ 0 & F_4 \end{bmatrix} \begin{bmatrix} \Delta I_{IM} \\ \Delta I_{SM} \end{bmatrix} \tag{2.3-94}$$

2.3.2 Original Network Equations before Bus Spliting

The transformer and the cables for the original system (Figure 2.4 (b)) can be represented by an admittance matrix Y. Total 4 buses (Bus1, Bus2 (MCC), Bus3, and Bus4) are involved including two terminal buses for the induction and synchronous motors. The network equation (I=YV) of the original system can be written as follows:

$$\begin{bmatrix} \Delta I_0 \\ 0 \\ \Delta I_{IM} \\ \Delta I_{SM} \end{bmatrix} = \begin{bmatrix} (Y'_0 + Y_{T0}) & (-Y_{T0}) & 0 & 0 \\ (-Y_{T0}) & (Y_{T0} + Y_{c1} + Y_{c2}) & (-Y_{c1}) & (-Y_{c2}) \\ 0 & (-Y_{c1}) & (Y_{c1}) & 0 \\ 0 & (-Y_{c2}) & 0 & (Y_{c2}) \end{bmatrix} \begin{bmatrix} \Delta V_0 \\ \Delta V_p \\ \Delta V_{IM} \\ \Delta V_{SM} \end{bmatrix} \tag{2.3-95}$$

Rearrange Equation (2.3-95) in equations format as follows:

$$\Delta I_0 = (Y'_0 + Y_{T0})\Delta V_0 - Y_{T0}\Delta V_p \tag{2.3-96}$$

$$0 = (-Y_{T0})\Delta V_0 + (Y_{T0} + Y_{c1} + Y_{c2})\Delta V_p - Y_{c1}\Delta V_{IM} - Y_{c2}\Delta V_{SM} \tag{2.3-97}$$

$$\Delta I_{IM} = \left(-Y_{c1}\right)\Delta V_p + Y_{c1}\Delta V_{IM} \tag{2.3-98}$$

$$\Delta I_{SM} = \left(-Y_{c2}\right)\Delta V_p + Y_{c2}\Delta V_{SM} \tag{2.3-99}$$

Where $Y_0', Y_{T0}, Y_{c1}, Y_{c2}$ are admittances for power source, transformer T_0, cable 1 connected to the induction motor terminal, cable 2 connected to the synchronous motor terminal, which are given data for the original system; $\Delta I_0, \Delta V_0$ are current and voltage for Bus 1; $\Delta I_p, \Delta V_p$ are current and voltage for Bus2 (MCC); $\Delta I_{IM}, \Delta V_{IM}$ are current and voltage for the induction motor terminal bus (Bus 3); $\Delta I_{SM}, \Delta V_{SM}$ are current and voltage for the synchronous motor terminal bus (Bus 4).

Linearize Equation (2.3-35), the terminal voltage of the induction motor can be expressed by its internal voltage as follows:

$$\Delta V_{IM} = \left(R_s + jX_s'\right)\Delta I_{IM} + \Delta E_m' \tag{2.3-100}$$

Similarly, linearize Equation (2.3-73), the terminal voltage of the synchronous motor can be expressed by its internal voltage as follows:

$$\Delta V_{SM} = \left[-\left(R_a + jX_d'\right)\right]\Delta I_{SM} + \Delta E_q' \tag{2.3-101}$$

Substitute Equations (2.3-100) and (2.3-101) in Equations (2.3-96) - (2.3-99), the following equations can be determined:

$$\Delta I_0 = Y_{00}''\Delta V_0 + Y_{01}''\Delta E_m' + Y_{02}''\Delta E_q' \tag{2.3-102}$$

$$\Delta I_{IM} = Y_{10}''\Delta V_0 + Y_{11}''\Delta E_m' + Y_{12}''\Delta E_q' \tag{2.3-103}$$

$$\Delta I_{SM} = Y_{20}''\Delta V_0 + Y_{21}''\Delta E_m' + Y_{22}''\Delta E_q' \tag{2.3-104}$$

Where,

$$Y_{20}'' = \frac{Y_{20}' + \dfrac{Y_{21}'Y_{10}'}{\left(Y_{IM} - Y_{11}'\right)}}{1 - \dfrac{Y_{21}'Y_{12}'}{Y_{SM}\left(Y_{IM} - Y_{11}'\right)} - \dfrac{Y_{22}'}{Y_{SM}}} \tag{2.3-105}$$

$$Y''_{21} = \frac{Y'_{21} + \frac{Y'_{21}Y'_{11}}{(Y_{IM} - Y'_{11})}}{1 - \frac{Y'_{21}Y'_{12}}{Y_{SM}(Y_{IM} - Y'_{11})} - \frac{Y'_{22}}{Y_{SM}}} \tag{2.3-106}$$

$$Y''_{22} = \frac{Y'_{22} + \frac{Y'_{21}Y'_{12}}{(Y_{IM} - Y'_{11})}}{1 - \frac{Y'_{21}Y'_{12}}{Y_{SM}(Y_{IM} - Y'_{11})} - \frac{Y'_{22}}{Y_{SM}}} \tag{2.3-107}$$

$$Y''_{10} = \frac{Y'_{10}Y_{IM}}{(Y_{IM} - Y'_{11})} + \frac{Y'_{12}Y_{IM}Y''_{20}}{Y_{SM}(Y_{IM} - Y'_{11})} \tag{2.3-108}$$

$$Y''_{11} = \frac{Y'_{11}Y_{IM}}{(Y_{IM} - Y'_{11})} + \frac{Y'_{12}Y_{IM}Y''_{21}}{Y_{SM}(Y_{IM} - Y'_{11})} \tag{2.3-109}$$

$$Y''_{12} = \frac{Y'_{12}Y_{IM}}{(Y_{IM} - Y'_{11})} + \frac{Y'_{12}Y_{IM}Y''_{22}}{Y_{SM}(Y_{IM} - Y'_{11})} \tag{2.3-110}$$

$$Y''_{00} = Y'_{00} + \frac{Y'_{01}Y''_{10}}{Y_{IM}} + \frac{Y'_{02}Y''_{20}}{Y_{SM}} \tag{2.3-111}$$

$$Y''_{01} = Y'_{01} + \frac{Y'_{01}Y''_{11}}{Y_{IM}} + \frac{Y'_{02}Y''_{21}}{Y_{SM}} \tag{2.3-112}$$

$$Y''_{02} = Y'_{02} + \frac{Y'_{01}Y''_{12}}{Y_{IM}} + \frac{Y'_{02}Y''_{22}}{Y_{SM}} \tag{2.3-113}$$

$$Y'_{00} = \frac{Y'_0 Y_{T0} + (Y'_0 + Y_{T0})(Y_{c1} + Y_{c2})}{Y_{T0} + Y_{c1} + Y_{c2}} \tag{2.3-114}$$

$$Y'_{01} = \frac{-Y_{c1}Y_{T0}}{Y_{T0} + Y_{c1} + Y_{c2}} \tag{2.3-115}$$

$$Y'_{02} = \frac{-Y_{c2}Y_{T0}}{Y_{T0} + Y_{c1} + Y_{c2}} \tag{2.3-116}$$

$$Y'_{10} = \frac{Y_{c1}[Y'_{00} - (Y'_0 + Y_{T0})]}{Y_{T0}} \tag{2.3-117}$$

$$Y'_{11} = \frac{Y_{c1}}{Y_{T0}} Y'_{01} + Y_{c1} \tag{2.3-118}$$

$$Y'_{12} = \frac{Y_{c1}}{Y_{T0}} Y'_{02} \tag{2.3-119}$$

$$Y'_{20} = \frac{Y_{c2}\left[Y'_{00} - \left(Y'_0 + Y_{T0}\right)\right]}{Y_{T0}} \tag{2.3-120}$$

$$Y'_{21} = \frac{Y_{c2}}{Y_{T0}} Y'_{01} \tag{2.3-121}$$

$$Y'_{22} = \frac{Y_{c2}}{Y_{T0}} Y'_{02} + Y_{c2} \tag{2.3-122}$$

$$Y_{IM} = \frac{1}{Z_{IM}} = \frac{1}{\left(R_s + jX'_s\right)} \tag{2.3-123}$$

$$Y_{SM} = \frac{1}{Z_{SM}} = \frac{1}{-\left(R_a + jX'_d\right)} \tag{2.3-124}$$

The state space equation for the system can be obtained by substituting Equations (2.3-103) and (2.3-104) in Equation (2.3-94):

$$\begin{bmatrix} \Delta\dot{E}'_m \\ \Delta\dot{S} \\ \Delta\dot{E}'_q \\ \Delta\dot{\omega}_r \end{bmatrix} = \begin{bmatrix} \left(E_1 + F_1 Y''_{11}\right) & E_2 & \left(F_1 Y''_{12}\right) & 0 \\ \left(E_3 + F_2 Y''_{11}\right) & 0 & \left(F_2 Y''_{12}\right) & 0 \\ \left(F_3 Y''_{21}\right) & 0 & \left(E_4 + F_3 Y''_{22}\right) & 0 \\ \left(F_4 Y''_{21}\right) & 0 & \left(E_5 + F_4 Y''_{22}\right) & E_6 \end{bmatrix} \begin{bmatrix} \Delta E'_m \\ \Delta S \\ \Delta E'_q \\ \Delta\omega_r \end{bmatrix} + \begin{bmatrix} F_1 Y''_{10} \\ F_2 Y''_{10} \\ F_3 Y''_{20} \\ F_4 Y''_{20} \end{bmatrix} \left[\Delta V_0\right] \tag{2.3-125}$$

In the general state space equation format, Equation (2.3-125) is rewritten as follows

$$\Delta\dot{X} = A\Delta X + B\Delta u \tag{2.3-126}$$

Where,

$$X = \begin{bmatrix} E'_m \\ S \\ E'_q \\ \omega_r \end{bmatrix} \tag{2.3-127}$$

$$u = \begin{bmatrix} V_{d0} \\ V_{q0} \end{bmatrix} \tag{2.3-128}$$

$$A=\left[\begin{array}{cc:cc} (E_1+F_1Y''_{11}) & E_2 & (F_1Y''_{12}) & 0 \\ (E_3+F_2Y''_{11}) & 0 & (F_2Y''_{12}) & 0 \\ \hdashline (F_3Y''_{21}) & 0 & (E_4+F_3Y''_{22}) & 0 \\ (F_4Y''_{21}) & 0 & (E_5+F_4Y''_{22}) & E_6 \end{array}\right]$$, i.e.,

$$A=\begin{bmatrix} A_{11} & A_{12} \\ A_{21} & A_{22} \end{bmatrix} \tag{2.3-129}$$

$$B=\begin{bmatrix} F_1Y''_{10} \\ F_2Y''_{10} \\ F_3Y''_{20} \\ F_4Y''_{20} \end{bmatrix} \tag{2.3-130}$$

Based on the control theory, in order to have two sub-systems in the parallel connection, A_{12} and A_{21} should be 0, i.e., $Y''_{12}=Y''_{21}=0$ in Equation (2.3-129). To successfully equivalent the original system (Figure 2.4 (b)) into its equivalent system (Figure 2.4 (c)), our objective is to satisfy the following relationship in the matrix A:

$$F_1Y''_{12} << E_1+F_1Y''_{11} \tag{2.3-131}$$

$$F_2Y''_{12} << E_3+F_2Y''_{11} \tag{2.3-132}$$

$$F_3Y''_{21} << E_4+F_3Y''_{22} \tag{2.3-133}$$

$$F_4Y''_{21} << E_5+F_4Y''_{22} \tag{2.3-134}$$

Or simply $Y''_{12}=Y''_{21}\approx 0$

The injected power at the connecting bus (Bus1) can be determined by

$$\begin{bmatrix} \Delta P_0 \\ \Delta Q_0 \end{bmatrix}=\begin{bmatrix} I_d & I_q \\ -I_q & I_d \end{bmatrix}\begin{bmatrix} \Delta V_d \\ \Delta V_q \end{bmatrix}+\begin{bmatrix} V_d & V_q \\ V_q & -V_d \end{bmatrix}\begin{bmatrix} \Delta I_d \\ \Delta I_q \end{bmatrix}=G_I\Delta V_0+G_V\Delta I_0 \tag{2.3-135}$$

Substitute Equation (2.3-102) in Equation (2.3-135), we have

$$\begin{bmatrix}\Delta P_0\\ \Delta Q_0\end{bmatrix} = (G_V Y''_{01})\Delta E'_m + (G_V Y''_{02})\Delta E'_q + (G_I + G_V Y''_{00})\Delta V_0$$

$$= \begin{bmatrix}(G_V Y''_{01}) & 0 & (G_V Y''_{02}) & 0\end{bmatrix}\begin{bmatrix}\Delta E'_m\\ \Delta S\\ \Delta E'_q\\ \Delta \omega_r\end{bmatrix} + \begin{bmatrix}(G_I + G_V Y''_{00})\end{bmatrix}\begin{bmatrix}\Delta V_0\end{bmatrix} \quad (2.3\text{-}136)$$

In the general state space equation format, Equation (2.3-136) is rewritten as follows

$$\Delta y = C\Delta X + D\Delta u \quad (2.3\text{-}137)$$

Where,

$$y = \begin{bmatrix}P_0\\ Q_0\end{bmatrix} \quad (2.3\text{-}138)$$

$$C = \begin{bmatrix}(G_V Y''_{01}) & 0 & (G_V Y''_{02}) & 0\end{bmatrix} \quad (2.3\text{-}139)$$

$$D = \begin{bmatrix}(G_I + G_V Y''_{00})\end{bmatrix} \quad (2.3\text{-}140)$$

2.3.3 Equivalent Network Equations after Bus Spliting

For the equivalent system, total 3 buses (Bus1, Bus3, and Bus4) are involved including two terminal buses for the induction and synchronous motors. The network equation (I=YV) of the equivalent system (Figure 2.4 (c)) can be written as follows:

$$\begin{bmatrix}\Delta I_0\\ \Delta I_{IM}\\ \Delta I_{SM}\end{bmatrix} = \begin{bmatrix}(Y'_0 + Y_{T1} + Y_{T2}) & (-Y_{T1}) & (-Y_{T2})\\ (-Y_{T1}) & (Y_{T1}) & 0\\ (-Y_{T2}) & 0 & (Y_{T2})\end{bmatrix}\begin{bmatrix}\Delta V_0\\ \Delta V_{IM}\\ \Delta V_{SM}\end{bmatrix} \quad (2.3\text{-}141)$$

where Y'_0 is the admittances for power source, which is the given data the same as that in the original system. Note: the value of the power source admittance will not affect the final calculation results. Y_{T1} and Y_{T2} are admittances for the two transformers T_1 and T_2 in the equivalent system, respectively, which are unknown data and need to be determined. ΔI_0 and ΔV_0 are current and voltage for Bus1. ΔI_{IM} and ΔV_{IM} are current and voltage for the terminal bus for the

induction motor (Bus3). ΔI_{SM} and ΔV_{SM} are current and voltage for the terminal bus for the synchronous motor (Bus4).

Rearrange Equation (2.3-141) in the equation format as follows:

$$\Delta I_0 = (Y_0' + Y_{T1} + Y_{T2})\Delta V_0 - Y_{T1}\Delta V_{IM} - Y_{T2}\Delta V_{SM} \tag{2.3-142}$$

$$\Delta I_{IM} = -Y_{T1}\Delta V_0 + Y_{T1}\Delta V_{IM} \tag{2.3-143}$$

$$\Delta I_{SM} = -Y_{T2}\Delta V_0 + Y_{T2}\Delta V_{SM} \tag{2.3-144}$$

Substitute Equations (2.3-100) and (2.3-101) in Equations (2.3-142) - (2.3-144), similar to the original system, the currents at the three buses can be expressed as follows:

$$\Delta I_0 = Y'_{00eq}\Delta V_0 + Y'_{01eq}\Delta E'_m + Y'_{02eq}\Delta E'_q \tag{2.3-145}$$

$$\Delta I_{IM} = Y'_{10eq}\Delta V_0 + Y'_{11eq}\Delta E'_m \tag{2.3-146}$$

$$\Delta I_{SM} = Y'_{20eq}\Delta V_0 + Y'_{22eq}\Delta E'_q \tag{2.3-147}$$

Where,

$$Y'_{20eq} = \frac{Y_{T2}Y_{SM}}{Y_{T2} - Y_{SM}} \tag{2.3-148}$$

$$Y'_{22eq} = -Y'_{20eq} = -\frac{Y_{T2}Y_{SM}}{Y_{T2} - Y_{SM}} \tag{2.3-149}$$

$$Y'_{10eq} = \frac{Y_{T1}Y_{IM}}{Y_{T1} - Y_{IM}} \tag{2.3-150}$$

$$Y'_{11eq} = -Y'_{10eq} = -\frac{Y_{T1}Y_{IM}}{Y_{T1} - Y_{IM}} \tag{2.3-151}$$

$$Y'_{00eq} = (Y_0' + Y_{T1} + Y_{T2}) - \frac{Y_{T1}Y'_{10}}{Y_{IM}} - \frac{Y_{T2}Y'_{20}}{Y_{SM}} \tag{2.3-152}$$

$$Y'_{01eq} = Y'_{10eq} = -\left(Y_{T1} + \frac{Y_{T1}Y'_{11}}{Y_{IM}}\right) \tag{2.3-153}$$

$$Y'_{02eq} = Y'_{20eq} = -\left(Y_{T2} + \frac{Y_{T2} Y'_{22}}{Y_{SM}} \right) \tag{2.3-154}$$

Substitute Equations (2.3-146) and (2.3-147) in Equation (2.3-94), the state space equation for the equivalent system can be calculated as follows:

$$\begin{bmatrix} \Delta\dot{E}'_m \\ \Delta\dot{S} \\ \Delta\dot{E}'_q \\ \Delta\dot{\omega}_r \end{bmatrix} = \begin{bmatrix} \left(E_1 + F_1 Y'_{11eq}\right) & E_2 & 0 & 0 \\ \left(E_3 + F_2 Y'_{11eq}\right) & 0 & 0 & 0 \\ 0 & 0 & \left(E_4 + F_3 Y'_{22eq}\right) & 0 \\ 0 & 0 & \left(E_5 + F_4 Y'_{22eq}\right) & E_6 \end{bmatrix} \begin{bmatrix} \Delta E'_m \\ \Delta S \\ \Delta E'_q \\ \Delta\omega_r \end{bmatrix} + \begin{bmatrix} F_1 Y'_{10eq} \\ F_2 Y'_{10eq} \\ F_3 Y'_{20eq} \\ F_4 Y'_{20eq} \end{bmatrix} [\Delta V_0] \tag{2.3-155}$$

Substitute Equation (2.3-142) in Equation (2.3-135), the injected power at the connecting bus (Bus-1) for the equivalent system can be written as follows:

$$\begin{aligned} \begin{bmatrix} \Delta P_0 \\ \Delta Q_0 \end{bmatrix} &= G_V Y'_{01eq} \Delta E'_m + G_V Y'_{02eq} \Delta E'_q + \left(G_I + G_V Y'_{00eq}\right) \Delta V_0 \\ &= \begin{bmatrix} \left(G_V Y'_{01eq}\right) & 0 & \left(G_V Y'_{02eq}\right) & 0 \end{bmatrix} \begin{bmatrix} \Delta E'_m \\ \Delta S \\ \Delta E'_q \\ \Delta\omega_r \end{bmatrix} + \left[\left(G_I + G_V Y'_{00eq}\right)\right] [\Delta V_0] \end{aligned} \tag{2.3-156}$$

In the general state space equation format, Equations (2.3-155) and (2.3-156) can be rewritten as follows for the equivalent system:

$$\Delta\dot{X} = A_{eq} \Delta X + B_{eq} \Delta u \tag{2.3-157}$$

$$\Delta y = C_{eq} \Delta X + D_{eq} \Delta u \tag{2.3-158}$$

Where,

$$X = \begin{bmatrix} E'_m \\ S \\ E'_q \\ \omega_r \end{bmatrix} \tag{2.3-159}$$

$$u = \begin{bmatrix} V_{d0} \\ V_{q0} \end{bmatrix} \tag{2.3-160}$$

$$y = \begin{bmatrix} P_0 \\ Q_0 \end{bmatrix} \tag{2.3-161}$$

$$A_{eq} = \begin{bmatrix} \left(E_1 + F_1 Y'_{11eq}\right) & E_2 & 0 & 0 \\ \left(E_3 + F_2 Y'_{11eq}\right) & 0 & 0 & 0 \\ 0 & 0 & \left(E_4 + F_3 Y'_{22eq}\right) & 0 \\ 0 & 0 & \left(E_5 + F_4 Y'_{22eq}\right) & E_6 \end{bmatrix} \tag{2.3-162}$$

$$B_{eq} = \begin{bmatrix} F_1 Y'_{10eq} \\ F_2 Y'_{10eq} \\ F_3 Y'_{20eq} \\ F_4 Y'_{20eq} \end{bmatrix} \tag{2.3-163}$$

$$C_{eq} = \begin{bmatrix} \left(G_V Y'_{01eq}\right) & 0 & \left(G_V Y'_{02eq}\right) & 0 \end{bmatrix} \tag{2.3-164}$$

$$D_{eq} = \begin{bmatrix} \left(G_I + G_V Y'_{00eq}\right) \end{bmatrix} \tag{2.3-165}$$

To make the two systems equivalent, the output functions (the injected power at Bus 1) for both systems, Equations (2.3-136) and (2.3-156), are considered to be the same, i.e.,

$$Y'_{01eq} = Y''_{01} \tag{2.3-166}$$

$$Y'_{02eq} = Y''_{02} \tag{2.3-167}$$

$$Y'_{00eq} = Y''_{00} \tag{2.3-168}$$

The admittances of the two unknown transformers, Y_{T1} and Y_{T2}, in the equivalent system can then be determined from Equations (2.3-166) and (2.3-167) as follows:

$$Y_{T1} = \frac{Y''_{01} Y_{IM}}{Y''_{01} - Y_{IM}} \tag{2.3-169}$$

$$Y_{T2} = \frac{Y''_{02} Y_{SM}}{Y''_{02} - Y_{SM}} \tag{2.3-170}$$

By substituting the calculated Y_{T1} and Y_{T2} from Equations (2.3-169) and (2.3-170) in Equation (2.3-168), it is verified that Equation (2.3-168) is true.

The calculation indicates that the parameters in Equations (2.3-125) and (2.3-155) make the following equations satisfied:

$$Y'_{10eq} = Y''_{10} \tag{2.3-171}$$

$$Y'_{20eq} = Y''_{20} \tag{2.3-172}$$

$$Y'_{11eq} \approx Y''_{11} \tag{2.3-173}$$

$$Y'_{22eq} \approx Y''_{22} \tag{2.3-174}$$

$$Y''_{12} = Y''_{21} \approx 0 \tag{2.3-175}$$

Equation (2.3-175) is one of the objectives for the two system equivalence, which is verified to be met. Based on these equations, the state space equations for both systems are considered approximately the same with similar dynamic response characteristics. As a result, the equivalent model can be successfully obtained.

In summary, the following procedure is proposed to split a bus with both induction and synchronous motors connected to:

1) Obtain the impedances of the induction and synchronous motors (Y_{IM} and Y_{SM}). These data are known for a given machine or an aggregated equivalent machine.

2) Obtain the branch impedance for the transformer T_0, the cable c_1 for the induction motor, the cable c_2 for the synchronous motor (Y_{T0}, Y_{c1} and Y_{c2}) for the original system. These are also known data.

3) Calculate the impedances of the two equivalent transformers T_1 and T_2 (Y_{T1} and Y_{T2}) using Equations (2.3-169) and (2.3-170). The circuit impedances of the new equivalent circuit are thus determined.

Note: The motor parameters remain the same in the above calculation. The impedance of the two new transformers, Y_{T1} and Y_{T2}, are affected by the machine parameters, so the bus-split algorithm is not a simple Y-Δ transform.

2.3.4 Case Study of the Bus Split Algorithm

To verify the accuracy of the proposed bus split algorithm, a case study is conducted using a sample system. The system configurations for the original and equivalent sample systems are shown in Figure 2.5.

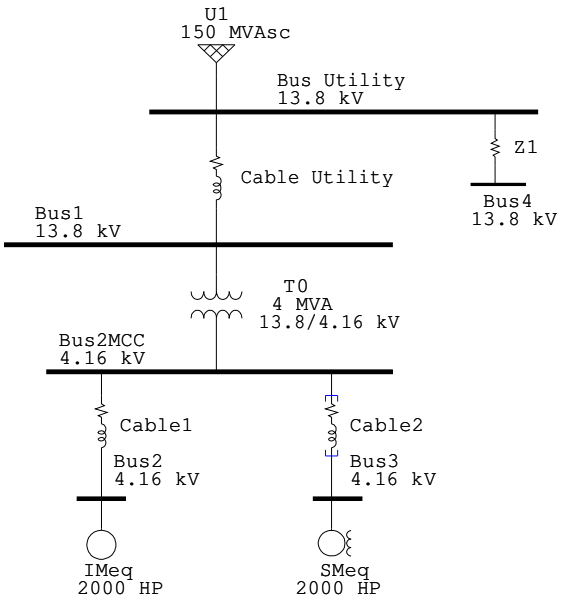

(a) Original system

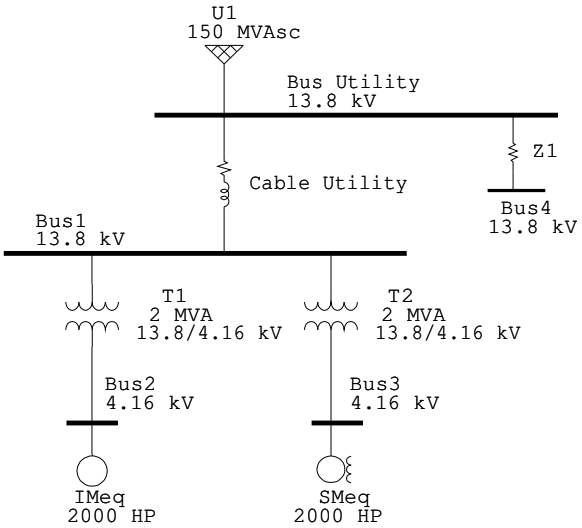

(b) Equivalent system

Figure 2.5 A case study to verify the bus split algorithm

In the case study, both induction and synchronous motors are rated at 4.16 kV and 2000 HP. The transformer T_0 is rated at 4 MVA, 13.8/4.16kV, the impedance Z_{T0} = 5.5% and X/R=10.67. The cables connecting the induction and synchronous motors are 500AWG in size and 50 feet long each. The cable impedance per 1000 ft is R + jX = 0.0284 + j0.0351 ohms. The impedance of the utility at the 100 MVA and 13.8 kV base is assumed to be Z_0' = 0.02562 + j0.66617 p.u. (Note: the impedance of the utility will be cancelled during the calculation, so this value will not affect final results). The equivalent circuit parameters for the induction motor at machine base are R_s = 0.0194 p.u., X_{ls} = 0.1261 p.u., X_m = 3.1333 p.u., X_{lr}=0.1026 p.u., and R_r = 0.0179 p.u. The parameters for the synchronous motor at machine base are R_a = 0.005 p.u., X_d'=0.28 p.u.

The calculated impedance for the two new transformers T_1 and T_2 in the equivalent system (rated at 2MVA each, 13.8/4.16kV) at transformer base using Equations (2.3-169) and (2.3-170) are:

1). For T_1 (connected with IM): Z_{T1} = 1.66%, X/R = 17.57 ($Z_{T1} = 1/Y_{T1}$)

2). For T_2 (connected with SM): Z_{T2} = 4.05%, X/R = 41.88 ($Z_{T2} = 1/Y_{T2}$)

Three types of faults are applied to the original and equivalent sample systems in Figure 2.5 using ETAP. The faults are applied to the specified faulted bus at 1.00 second, and cleared at 1.15 second. The total simulation time is 5 second.

Fault 1 refers to a local three-phase fault occurred at “Bus Utility” in the original and equivalent systems with the voltage at “Bus1” in the original and equivalent systems equal to 0% of nominal voltage during the fault. The dynamic response characteristics of the bus voltage at “Bus1”, the real power P and the reactive power Q through “Cable Utility” in the original and equivalent systems during Fault 1 are shown in Figure 2.6.

Fault 2 refers to a remote three phase fault occurred at “Bus4” in the original and equivalent systems with the voltage at “Bus1” in the original and equivalent systems equal to 50% of nominal voltage during the fault. The dynamic response characteristics of the bus voltage at “Bus1”, the real power P and the reactive power Q through “Cable Utility” in the original and equivalent systems during Fault 2 are shown in Figure 2.7.

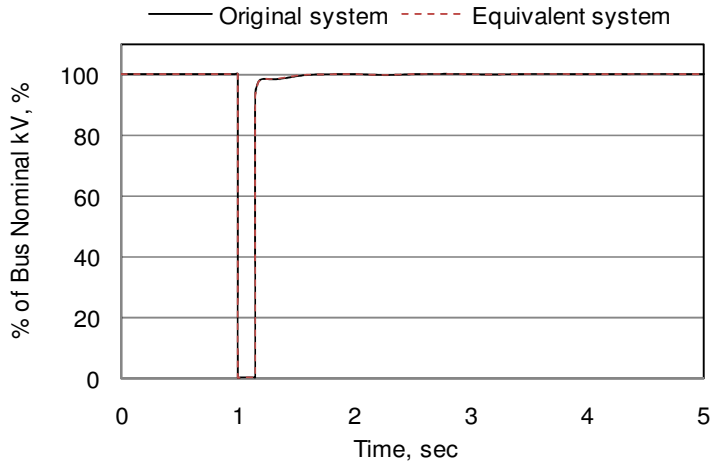

(a) Voltage at “Bus1” (Fault 1)

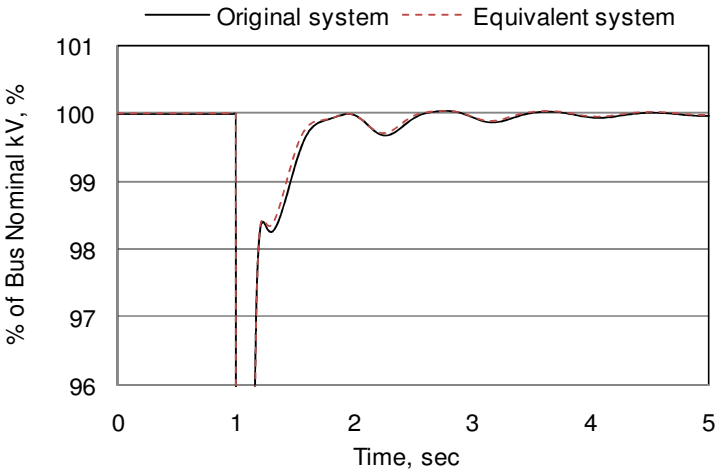

(b) Zoomed-in view for voltage at “Bus1” (Fault 1)

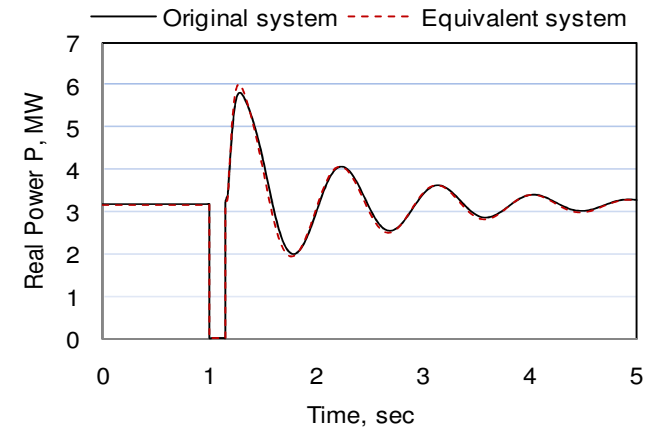

(c) Real Power through "Cable Utility" (Fault 1)

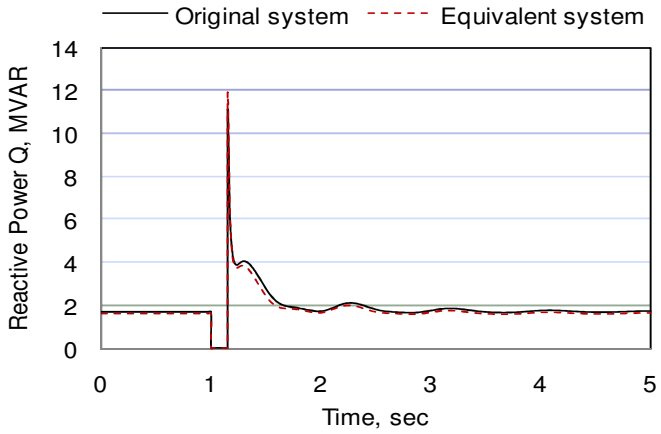

(d) Reactive Power through "Cable Utility" (Fault 1)

Figure 2.6 Dynamic responses of the original and equivalent systems (Fault 1)

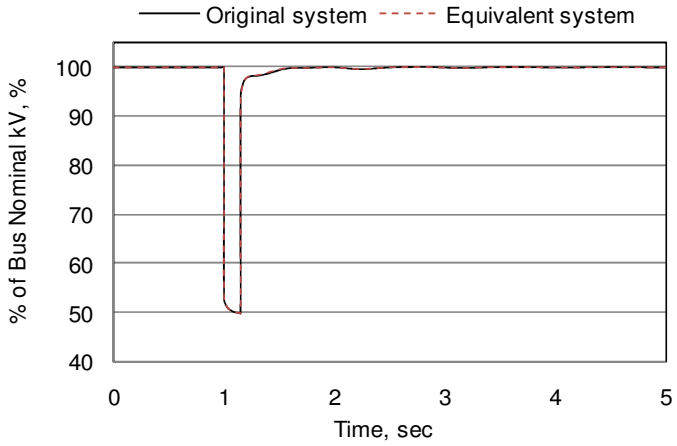

(a) Voltage at "Bus1" (Fault 2)

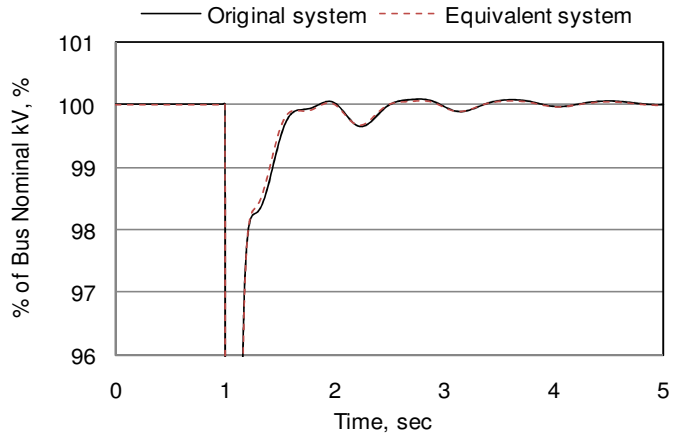

(b) Zoomed-in view for voltage at "Bus1" (Fault 2)

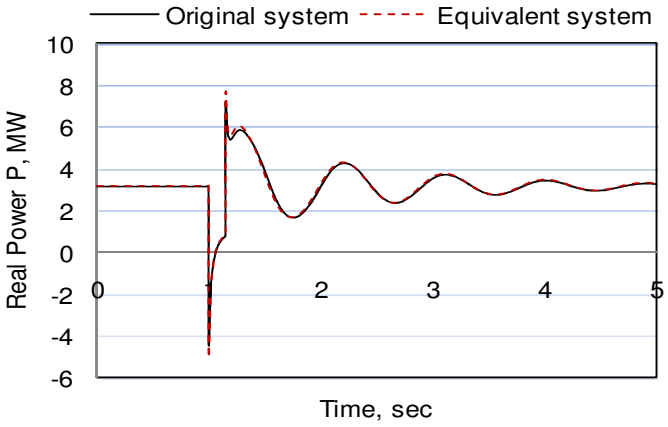

(c) Real Power through "Cable Utility" (Fault 2)

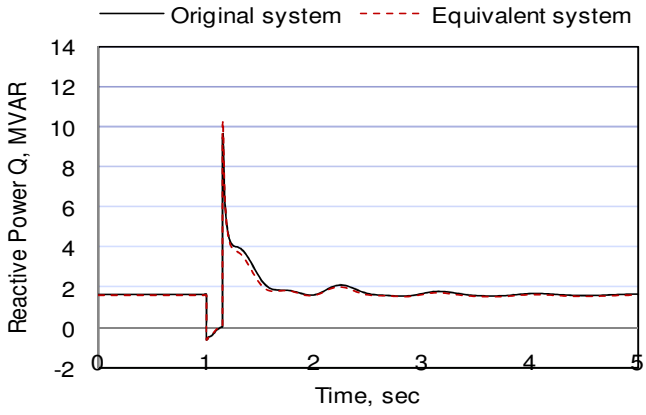

(d) Reactive Power through "Cable Utility" (Fault 2)

Figure 2.7 Dynamic responses of the original and equivalent systems (Fault 2)

Fault 3 refers to a remote three phase fault occurred at "Bus 4" in the original and equivalent systems with the voltage at "Bus1" in the original and equivalent systems equal to 75% of nominal voltage during the fault. The dynamic response characteristics of the bus voltage at "Bus1", the real power P and the reactive power Q through "Cable Utility" in the original and equivalent systems during Fault 3 are shown in Figure 2.8.

It is found that dynamic responses match very well between the original and equivalent sample systems in the case study, which verifies the accuracy of the proposed bus split algorithm.

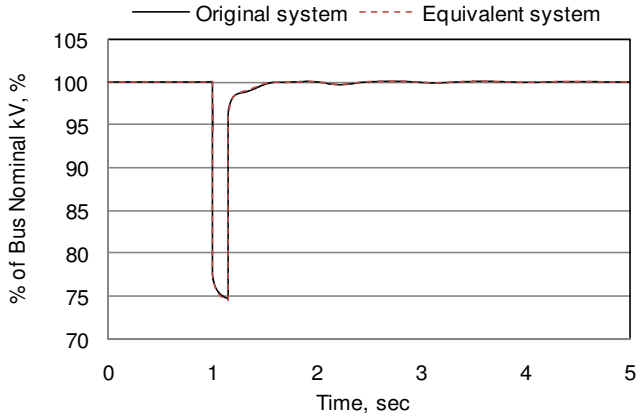

(a) Voltage at "Bus1" (Fault 3)

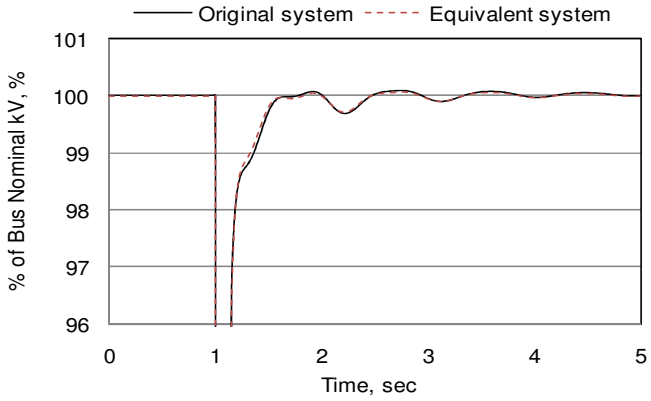

(b) Zoomed-in view for voltage at "Bus1" (Fault 3)

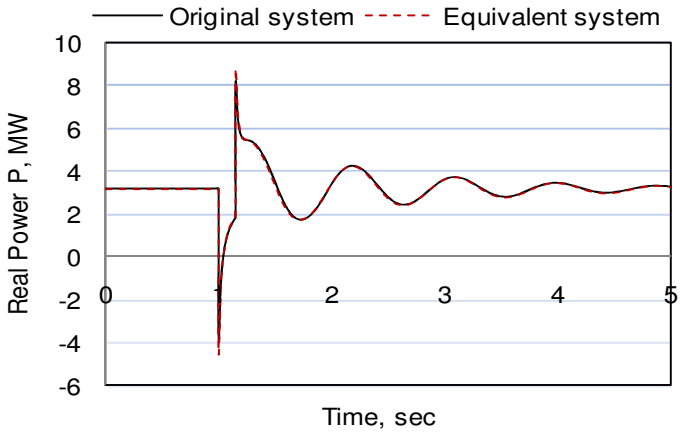

(c) Real Power through "Cable Utility" (Fault 3)

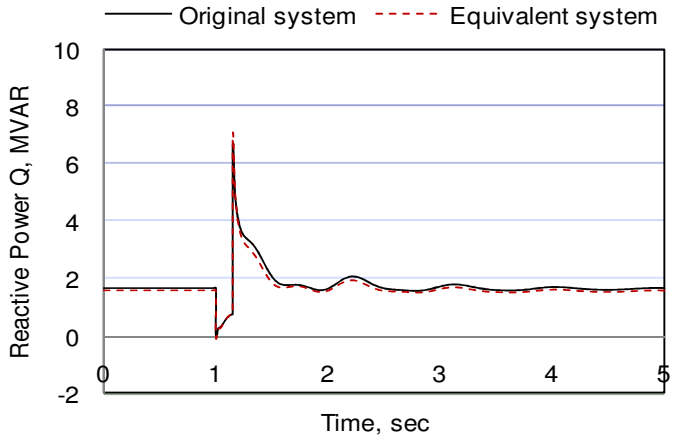

(d) Reactive Power through "Cable Utility" (Fault 3)

Figure 2.8 Dynamic responses of the original and equivalent systems (Fault 3)

Please note: The linearization method is used to develop the model reduction technique, the bus split algorithm. The following three facts support the validity of the proposed method: 1) The linear approach has been verified to be effective for facility modeling by Reference [4], 2) Case studies presented in the thesis have shown that the equivalent model derived from the proposed method produces quite acceptable responses even for large disturbances, 3) The facility modeling task does not require accurate duplication of specific machine response inside the facility. It is only concerned with the collective machine responses seen at the facility-utility interface point.

2.4 Summary and Conclusions

In this chapter, a new concept, the template-based load modeling technique for industrial facilities, is proposed and the main ideas of this technique are introduced.

There are three major components for this technique: templates, template scaling rules, and the model equivalence method. Each type of industrial facilities has its own unique templates and associated template scaling rules, which are the basis for the creation of the template-based full model. The established template-based full model shall represent all loads inside the facility and capture major system dynamic characteristics during disturbances. The model equivalence for the template-based full model can be achieved by using the proposed aggregation algorithms for static loads and electric machines.

The proposed aggregation algorithms for electric machines are known as "the bottom-up aggregation scheme" in this thesis, which is dedicated to group various electric machines. As one of the essential steps for the bottom-up aggregation scheme, a bus split algorithm is developed to deal with the case that induction and synchronous motors are connected to a downstream MCC bus through a transformer and/or series impedance at the upstream circuit. The bus split algorithm makes aggregation of upstream motors with the induction and synchronous motors connected to the downstream MCC bus feasible. This algorithm is verified to be accurate by a simple case study in this chapter.

The proposed bus-split algorithm is based on linearization of differential equations of electrical machines and the network, so it is suitable for small signal stability analysis. Although case studies have verified that this method works for large disturbance such as three-phase faults, more "bullet proven" equivalence method is desirable. Future research will be conducted to address this issue.

For some types of industrial facilities such as oil refineries, VFDs are used in very small amount, therefore, only three types of loads, induction motors, synchronous motors, and static loads, are considered in the template-based load modeling. In other types of industrial facilities such as oil field, however, VFDs are widely used and motor drive systems must be included in the template-based load modeling. The equivalent dynamic model and aggregation algorithms for motor drive system will be provided in Chapters 4 and 5.

CHAPTER 3 TEMPLATE-BASED LOAD MODELING FOR OIL REFINERY FACILITIES

To illustrate the template-based load modeling technique for industrial facilities, oil refinery facilities are chosen as an example. The dynamic load model for the specific type of facilities is established using the proposed technique. The following are major parts to work on:

- Establish templates for oil refinery facilities,
- Create template scaling rules,
- Determine the template-based full model (including electrical single-line diagrams, ratings and parameters for individual components) based on the template and template scaling rules,
- Obtain the template-based equivalent model(s) by conducting model equivalence for the template-based full model using aggregation algorithms,
- Verify the model equivalent method by comparing dynamic responses of the template-based equivalent model(s) with that of the template-based full model, and
- Verify the accuracy of the template-based load modeling technique for industrial facilities by comparing dynamic responses of the template-based full/equivalent models with that of the real facility and guideline models.

3.1 Process of Template-Based Load Modeling

3.1.1 Survey on Oil Refinery Facilities

The templates and template scaling rules for oil refinery facilities are created based on extensive literature review [95-102] and the information from real facilities. Three general categories of oil refinery facilities are found in the

literature as follows [103] (the schematic flow chart of a typical oil refinery facility can be found in Figure 3.1 [104]):

1) Topping refinery. This refinery separates the crude oil into its constituent products by Atmospheric Distillation unit (ADU). It consists only of an ADU and probably a catalytic reformer to provide octane (blue circle in Figure 3.1). Typically only condensates or light sweet crude would be processed at this type of facility unless markets for heavy fuel oil (HFO) are readily and economically available. Asphalt plants are topping refineries that run heavy crude oil because they are only interested in producing asphalt.
2) Cracking refinery. This refinery is equipped with Vacuum Distillation Unit (VDU) and catalytic cracking in addition to equipment in a topping refinery (green rectangle in Figure 3.1). The cracking refinery reduces fuel oil by conversion to light distillates and middle distillates. It takes the gas oil portion from the VDU (a stream heavier than diesel fuel, but lighter than HFO) and breaks it down further into gasoline and distillate components using catalysts, high temperature and/or pressure.
3) Coking refinery. This refinery processes vacuum residual fuel, the heaviest material from the VDU and thermally cracks it into lighter product using Delayed Coking process. The coking refinery adds more complexity to the cracking refinery (pink oval in Figure 3.1).

Topping refinery plants are not common type of refinery facilities, only small amount of topping plants are found in Canada. Primary refinery facilities are Cracking Refinery in Canada. Therefore, only cracking refinery facilities and coking refinery facilities are considered to construct the template and dynamic load models.

Compared to Canadian refinery facilities, the US refineries are configured to process a large percentage of heavy, high sulphur crude and to produce large quantities of gasoline, and low amounts of heavy fuel oil. U.S. refiners have

invested in more complex refinery configurations, which allow them to use cheaper feedstock and have a higher processing capability. Canadian refineries do not have the high conversion capability of the US refineries, because, on average, they process a lighter, sweeter crude slate. Canadian refineries also face a higher distillate demand, as a percent of crude, than those found in the U.S. so gasoline yields are not as high as those in the US, but are still significantly higher than European yields [103].

Research is conducted on electricity consumption for each process in oil refinery facilities. Reference [105] provides electrical consumption for each process based on estimated 2001 energy balance for the U.S. petroleum refining industry. Electrical consumptions for an individual refinery, however, will be different due to different process configurations. The estimate is based on combination of data from different sources and assumptions on process throughput and process energy intensities. Reference [106] summarizes total electricity demand in Hypothetical California Refinery. The three process units that consume most electricity are catalytic hydrocracker, alkylation unit and coker in this case. The published data in [105, 106] are summarized in Table 3.1. Electricity consumption for an existing Canadian coking oil refinery facility is also summarized in this table for comparison purpose.

Table 3.1 indicates that the first three columns for refineries in U.S. and California show large electricity consumptions on the hydrotreater process. The general data for U.S. Refineries in the first column shows 33.395% electricity consumption, and for California refineries in the second and third columns show 18.072% electricity consumption only from the hydrotreater process. Hydrotreating is a process used to remove sulphur from finished products. As the requirement to produce ultra low sulphur products increases, additional hydrotreating capability is being added to refineries. Refineries that currently have large hydrotreating capability are able to process crude oil with higher sulphur content. For comparison, the 4^{th} column in Table 3.1 for a Canadian coking refinery facility shows that the hydrotreater process only consumes

2.14% electricity. Therefore, U.S. coking refineries process high sulphur crude oil, while Canadian coking refineries process low sulfur crude oil.

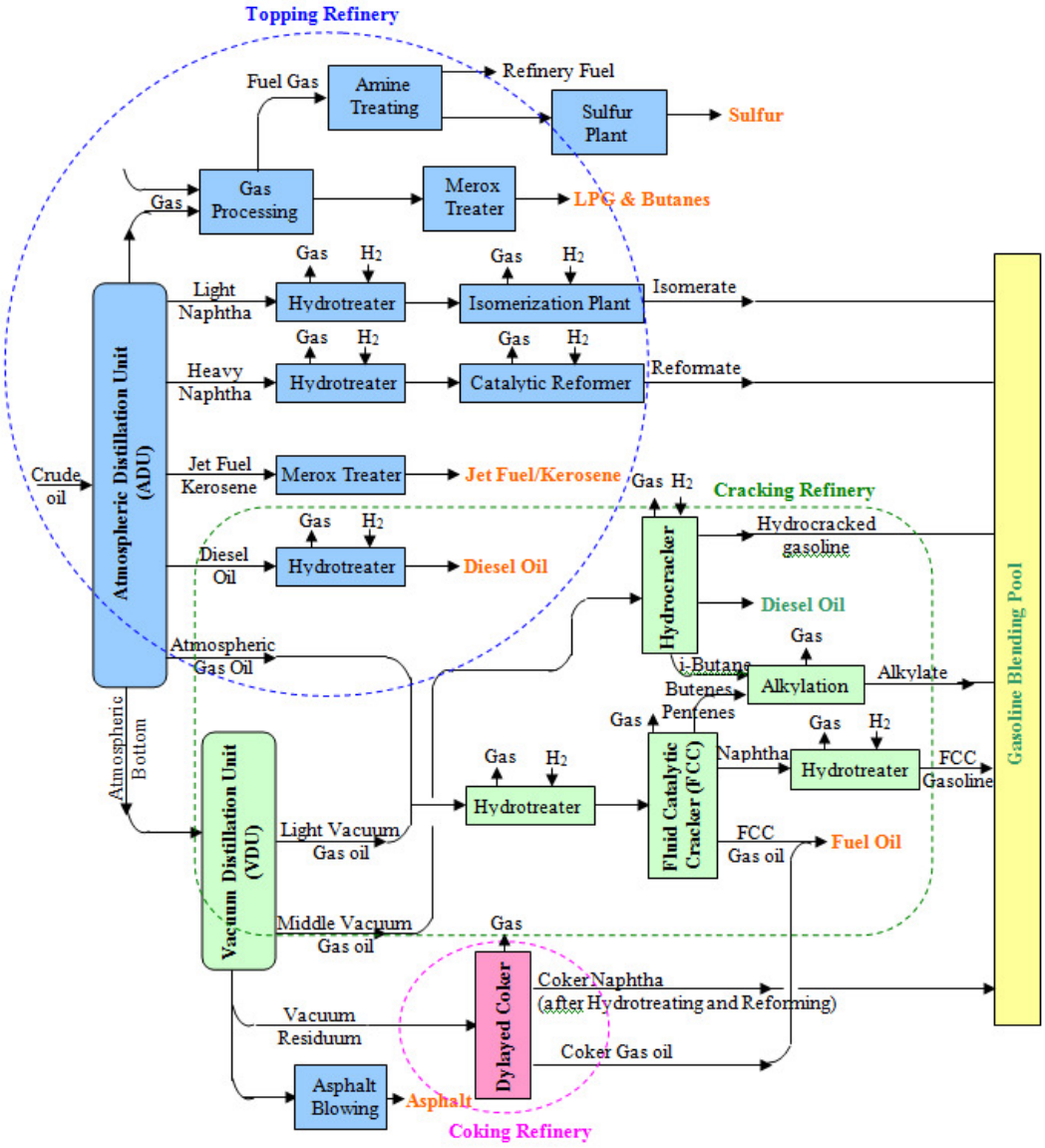

Figure 3.1 Schematic flow chart of a typical oil refinery [104]

Table 3.1 Electrical consumptions of each process [105, 106]

Petroleum refinery process	Electrical consumptions of each process in percent of total electrical consumption for coking refinery in US and Canada			
	U.S. Refineries %	California Refineries %	Hypothetical California Refinery, %	A Canadian Coking Refinery, %
Desalter	0.561	0.451	--	--
CDU(Crude Distillation Unit)	7.625	4.539	6.827	2.68
VDU(Vacuum Distillation Unit)	1.785	1.861	2.289	9.86
Hydrotreater	33.395	18.072	17.884	2.14
Coking/Thermal Cracking	9.772	7.697	18.028	8.57
FCC(Fluid Catalytic Cracker)	14.803	11.094	4.413	2.97
Hydrocracker	12.396	25.289	32.731	30.02
Reforming	7.210	5.498	2.778	0.67
Deasphalting	0.451	0.423	0.656	--
Alkylates	5.852	3.186	11.785	1.26
Aromatics	0.615	0.014	0.008	--
Asphalt	1.563	0.874	0.733	--
Isomers	0.841	0.733	0.630	5.97
Lubes	2.632	2.270	0.17	--
Sulfur	0.229	0.226	1.052	2.30
Hydrogen	0.189	4.412	--	3.60
Gas Plant	--	--	--	3.09
Other	0.081	13.361	0.016	26.87
Total process use	100	100	100	100

3.1.2 Create Templates and Template Scaling Rules

Due to significant differences in crude oil sulphur content processed by U.S. and Canadian oil refinery facilities, oil refineries are classified into four types as follows:

1) Type 1: coking refinery processing high sulphur crude;
2) Type 2: coking refinery processing low sulphur crude;
3) Type 3: cracking refinery processing high sulphur crude;
4) Type 4: cracking refinery processing low sulphur crude

Total electrical consumption of an oil refinery facility is the sum of power consumed by each process. Typical processes in facilities of Types 2 and 4 and corresponding electrical consumption as percent of total consumption are

presented in Table 3.2. The electrical consumption of Type 2 facilities is based on a Canadian coking refinery while the electrical consumption of Type 1 facilities is taken as the average mean of corresponding values for different US refineries [105, 106]. The electrical consumption for each process in Types 3 and 4 can be easily calculated from Types 1 and 2, respectively, by assuming zero consumption for coking process.

A survey on actual facilities and literature review indicate that major motor voltage levels used in oil refinery facilities are 480V/600V, 2.4 kV and 4.16 kV. Although 13.2 kV motors are used in some facilities, they are not very common. Therefore, the final motor data used to create templates (as shown in Table 3.3) do not include 13.2 kV motors.

Based on the survey on a 108 MW actual oil refinery facility, it is found that only four VFDs are used in this large facility and supply power to two 250 HP rated induction motors and two 150 HP rated induction motors. The power consumption of these drives is only 0.55% of the whole facility's power consumption. Therefore, the presence of the VFDs can be ignored in the load modeling without introducing errors. Induction motors, synchronous motors and static loads are common loads in oil refinery facilities, therefore, only these three types of loads need to be included in the templates and the template-based load models.

Using the data listed in Tables 3.2 and 3.3, the template and template scaling rules for Types 2 and 4 oil refinery facilities are established as shown in Table 3.4. The template and template scaling rules for Types 1 and 3 can be established in a similar manner.

The proposed templates are suitable for modeling any sized oil refinery. Based on the user input power demand (in MW) for a size-specific facility, loads contained in each process can be determined using templates and template scaling rules.

Table 3.2 Template for Types 2 and 4: electrical consumptions of each process

Petroleum refinery process	Electrical consumptions of each process in percent of total facility electrical consumption, %	
	Type 2	Type 4
CDU (Crude Distillation Unit)	2.68	2.93
VDU (Vacuum Distillation Unit)	9.86	10.78
Hydrotreater	2.14	2.34
Coking	8.57	3.25
FCC (Fluid Catalytic Cracker)	2.97	32.83
Hydrocracker	30.02	0.73
Reforming	0.67	1.38
Alkylates	1.26	6.53
Isomers	5.97	2.52
Sulfur	2.30	3.94
Hydrogen	3.60	3.38
Gas plant	3.09	29.39
Other	26.87	100
Total process use	100	2.93

Table 3.3 Template: horsepower distribution vs. voltage levels for induction motors

Individual motor HP in percent of total induction motor HP in the facility, %						
Voltage level	Reference [13]	Reference [8]	Real facility 1	Real facility 2	Calculated average	Template data
480/600V	40.85	44.29	16.67	29.66	33	35
2.4 kV	15.33	7.65	29.1	0	13	15
4.16 kV	43.82	48.06	54.23	60.08	51.5	50
13.2kV	0	0	0	10.26	2.5	0

Table 3.4 Templates and scaling rules for Types 2 and 4

Scaling Criteria		CDU	VDU	Hydro-treater	Cok-ing	FCC	Hydro-cracker	Refor-ming	Alkyl-Ates	Iso-mers	Sul-phur	Hydro-gen	Gas Plant	Other
1. Rated loads as % of total loads	Type 2	2.68	9.86	2.14	8.57	2.97	30.02	0.67	1.26	5.97	2.30	3.60	3.09	26.87
	Type 4	2.93	10.78	2.34	--	3.25	32.83	0.73	1.38	6.53	2.52	3.94	3.38	29.39
2. Rated Static loads as % of total loads	Type 2	1.23	4.68	0	2.74	1.35	4.92	0.49	0.91	0.95	1.27	0	1.37	9.09
	Type 4	1.42	4.79	0.17	--	1.41	6.04	0.51	1.00	1.05	1.28	0.24	1.47	9.75
3. Rated synchronous motor MW as % of total loads	Type 2	0	0	1.21	0	0	11.74	0	0	0	0	2.76	0	0
	Type 4	0	0	1.21	--	0	11.74	0	0	0	0	2.76	0	0
4. Rated induction motor MW as % of total loads	Type 2	1.45	5.18	0.93	5.83	1.62	13.36	0.18	0.35	5.02	1.03	0.84	1.72	17.78
	Type 4	1.51	5.99	0.96	--	1.84	15.05	0.22	0.38	5.48	1.24	0.94	1.91	19.64
5. 460V induction motor MW as % of total loads	Type 2	0.14	2.11	0.04	1.714	0.68	1.468	0.18	0.105	0.17	0.95	0.057	0.51	1.35
	Type 4	0.17	2.58	0.05	--	0.83	1.79	0.22	0.13	0.21	1.16	0.07	0.62	1.65
6. 2.3kV induction motor MW as % of total loads	Type 2	1.31	0.24	0.89	0.173	0.42	0	0	0.245	0	0.08	0	0.66	3.59
	Type 4	1.34	0.25	0.91	--	0.43	0	0	0.25	0	0.08	0	0.68	3.67
7. 4kV induction motor MW as % of total loads	Type 2	0	2.83	0	3.943	0.52	11.892	0	0	4.85	0	0.783	0.55	12.84
	Type 4	0	3.16	0	--	0.58	13.26	0	0	5.27	0	0.87	0.61	14.32
8. 460V induction motor capacities in HP	Type 2	200	200 1200 1500	200	200 800	200	200 350 800 1000	200	200	200	1000 1500	200	200	200
	Type 4	200	200 1200 1500	200	--	200	200 350 800 1000	200	200	200	1000 1500	200	200	200
9. 2.3kV induction motor capacities in HP	Type 2	350 800	350	350 800	350	350	N/A	N/A	350	N/A	N/A	N/A	350	350 800
	Type 4	350 800	350	350 800	--	350	N/A	N/A	350	N/A	N/A	N/A	350	350 800
10. 4kV induction motor capacities in HP	Type 2	N/A	350 1000	N/A	350 1500 3000	350	350 2000 3000 4000	N/A	N/A	1500 5500	N/A	350	800	350 800 1000 1500
	Type 4	N/A	350 1000	N/A	--	350	350 2000 3000 4000	N/A	N/A	1500 5500	N/A	350	800	350 800 1000 1500

3.1.3 Establish the Template-Based Full Model

In developing the template-based full models, it is assumed that the connected load does not change during the observed disturbances, i.e., none of the load is tripped by protective equipment. This is a reasonable assumption for the model development due to the following reasons:

1) Voltage variations at the interface bus between the industrial facility and the power grid are usually small in real life. A measurement had been conducted at a 230 kV bus for three years in [12], there were 2768 snap shots of voltage perturbations recorded, most perturbations are between 1% and 4%, and only 22 perturbations with voltage variations exceeding 20%.

2) As the worst case scenario, a short circuit analysis is conducted for a 108 MW coking oil refinery facility currently in operation in Canada. If a three-phase fault is applied at the 138kV utility interface bus of the facility which will cause 0% voltage at this bus during the fault, the motor control centers and switchgears where all motors are connected to will obtain 45%-65% nominal voltages during this fault. Based on Reference [1], motor starter contactors may drop open at 65-75% in the case of 2300V-4000V motors, and 55-65% in the case of motors at 460V and below. Therefore, if the duration of the applied three phase fault is long enough in this case, the motors might trip out of line. Although such condition is very rare, in most cases the motors should remain on line, considering the possible motor tripping in the template could serve as the future work.

Based on the survey of oil refinery facilities, it is found that network configurations for this type of facilities are radial configurations, and the most common characteristics are the processes involved, which are almost the same for each category of oil refinery facilities. The electrical consumptions of the processes in refinery facilities were also investigated [105, 106]. Therefore, as

part of the template creation work, the electrical single-line diagrams for oil refinery facilities are established by showing particular industrial processes as substations.

The electrical single-line diagrams for coking refinery facilities (Types 1 and 2) and cracking oil refinery facilities (Types 3 and 4) are shown in Figures 3.2 and 3.3, respectively. Each substation in the two figures represents a refinery process. Thus, coking refinery facilities are represented by 13 substations, while cracking refinery facilities are represented by 12 substations without the coking process. Note: some facilities may or may not have co-generation, which can be in or out of service according to the practical facility plan.

Internal structures of the electrical single-line diagrams for coking and cracking refinery facilities in Figures 3.2 and 3.3 are created as follows based on extensive survey:

1) The utility power supply is 138 kV.

2) Two main transformers deliver power from the 138 kV UtilityBus to the 13.8 kV system main bus (Bus 1).

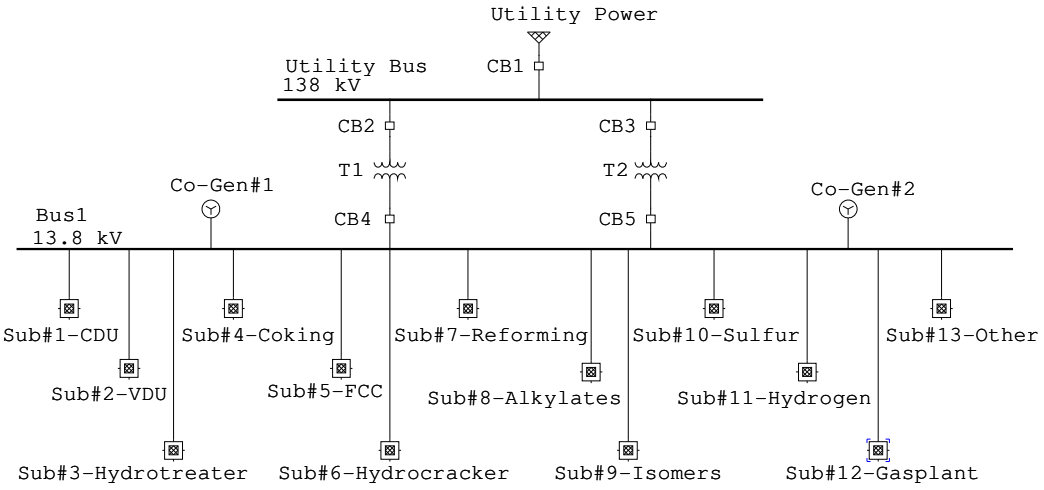

Figure 3.2 Template: electrical single-line diagram for Types 1 and 2

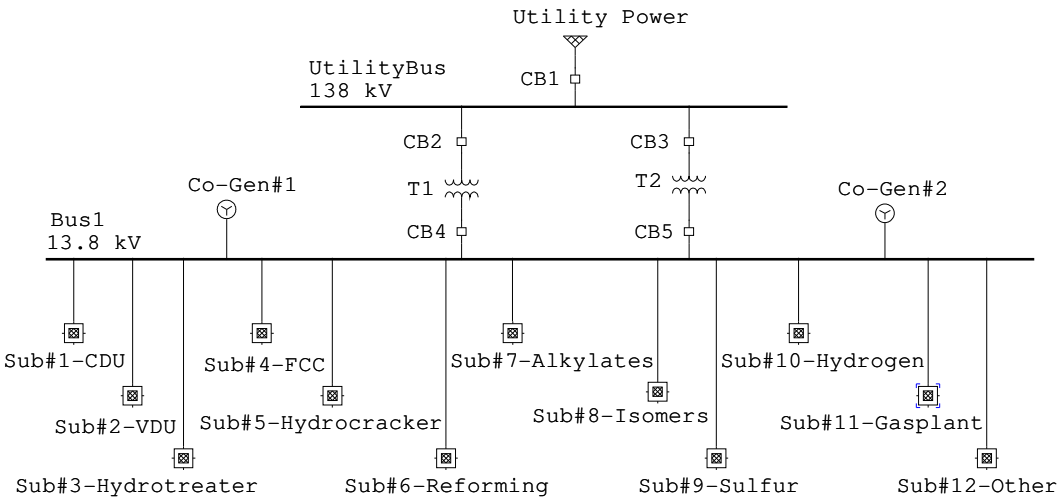

Figure 3.3 Template: electrical single-line diagram for Types 3 and 4

3) Each refinery process is modeled as a substation connected to Bus 1.

4) A 2000 ft main cable connects 13.8 kV Bus 1 to the 13.8 kV process main bus for each process.

5) Within individual processes, motors and static loads are determined based on the templates. Induction motors are further divided into three groups, 0.46 kV, 2.3 kV and 4 kV.

6) The step-down transformers convert the voltages from 13.8 kV process main bus to 0.48 kV, 2.4 kV and 4.16 kV, for the three induction motor groups.

7) A 100 ft cable connects the 13.8 kV process main bus to the primary side of each step-down transformer.

8) For refinery facilities, usually only three processes have synchronous motors: Hydroteater, Hydrocracker and Hydrogen. Synchronous motors, if present in the process, are connected to the same MCC bus (which is the secondary of one of the step-down transformers) as the 4 kV group of the induction motors for Hydrocraker and Hydrogen or as the 2.3 kV group of induction motors for Hydrotreater. That is to say, the induction and synchronous motors are connected to the same bus in a configuration

similar to Figure 2.4 (a).

9) To simplify the model, static loads of each process are added together to form a single lumped static load for the whole facility, which is modeled as constant impedance connected to Bus 1.

Using the electrical single-line diagram templates proposed in Figure 3.2 or Figure 3.3, and assigning loads inside each process/substation based on templates and template scaling rules provided in Table 3.4, the template-based full model for a size-specific oil refinery facility can be developed.

The detailed data for induction motors, synchronous motors, transformers, and cables used in the model creation can be found in Appendix A. As examples, load assignments inside each process/substation for a 108 MW Type 2 coking refinery facility are provided in Appendix B.

3.2 Template-Based Models for a 108MW Coking Refinery Facility

The template-based full (TF) model for a 108 MW Type 2 coking refinery facility is created and shown in Figure 3.4 based on load assignments in Appendix B.

By applying the model equivalence methods proposed in Chapter 2 to the TF model, two template-based equivalent models, the EP and EF models, are obtained and shown in Figures 3.5 and 3.6.

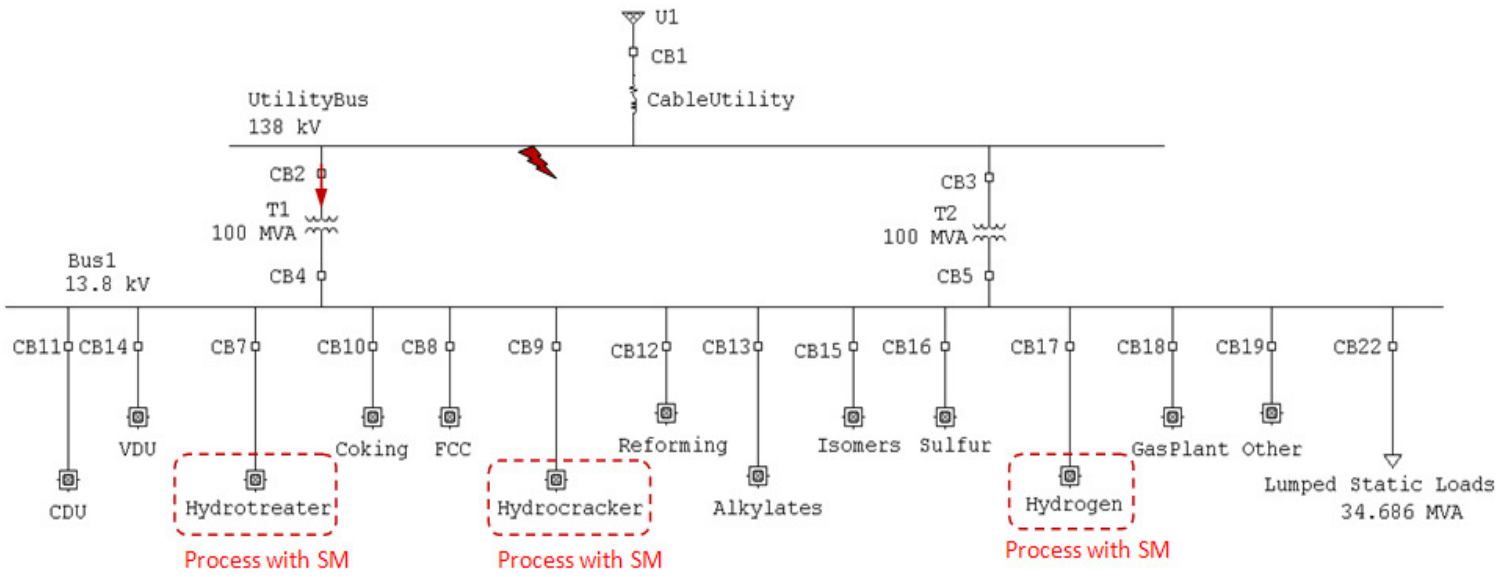

Figure 3.4 The TF model for the 108 MW coking refinery facility

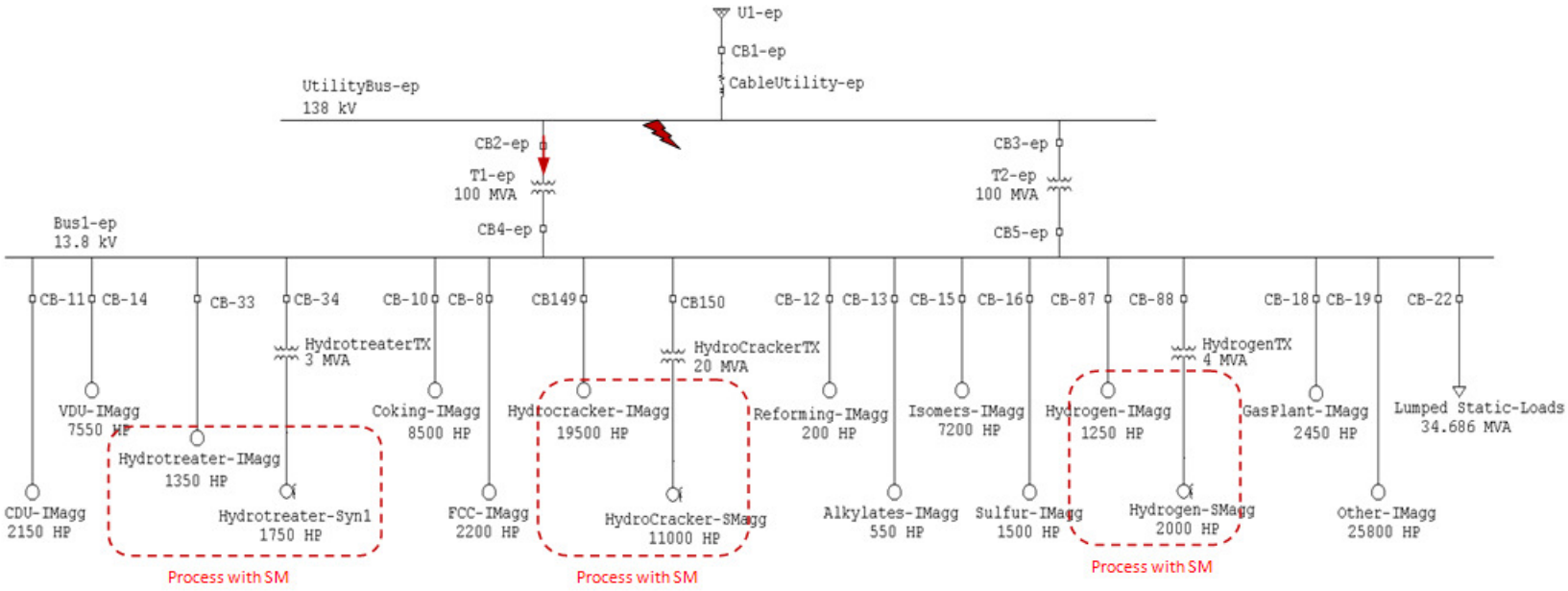

Figure 3.5 The EP model for the 108 MW coking refinery facility

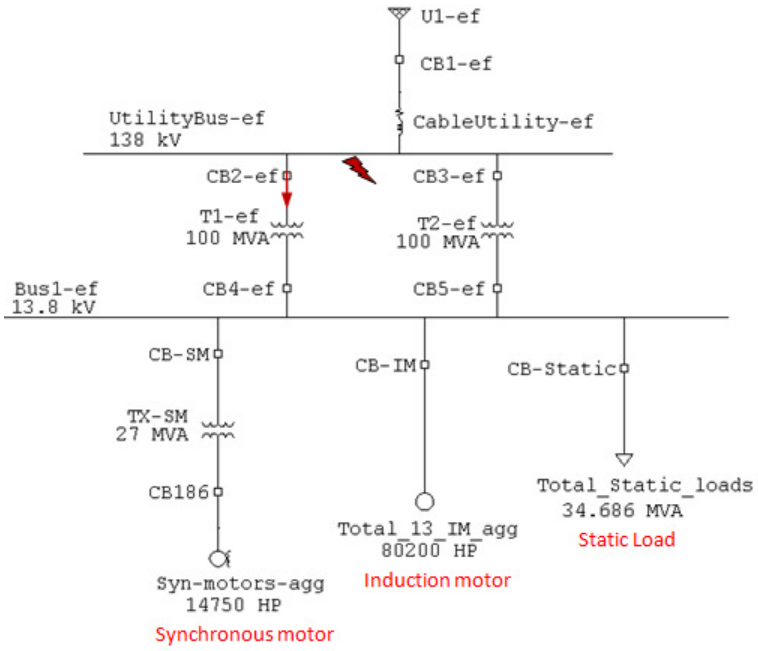

Figure 3.6 The EF model for the 108 MW coking refinery facility

3.3 Model Verification for the 108MW Coking Refinery Facility

3.3.1 Three Template-Based Models

Three template-based models (a full model and two equivalent models) for the 108MW coking oil refinery facility are obtained in previous section, however, only the equivalent models can be used for power systems dynamic studies because of their acceptable small size. However, to use the equivalent models, the equivalence between the template-based full model and its equivalent models, i.e., the accuracy of the proposed model equivalence method, must be verified.

A 3-phase fault is applied at the 138 kV UtilityBus of the three template-based models as shown in Figures 3.4-3.6. The fault starts at 1.0 second and ends at 1.15 seconds with total simulation time equal to 5 seconds. The simulation tool is ETAP. Dynamic responses of the three template-based models for the event are shown in Figure 3.7.

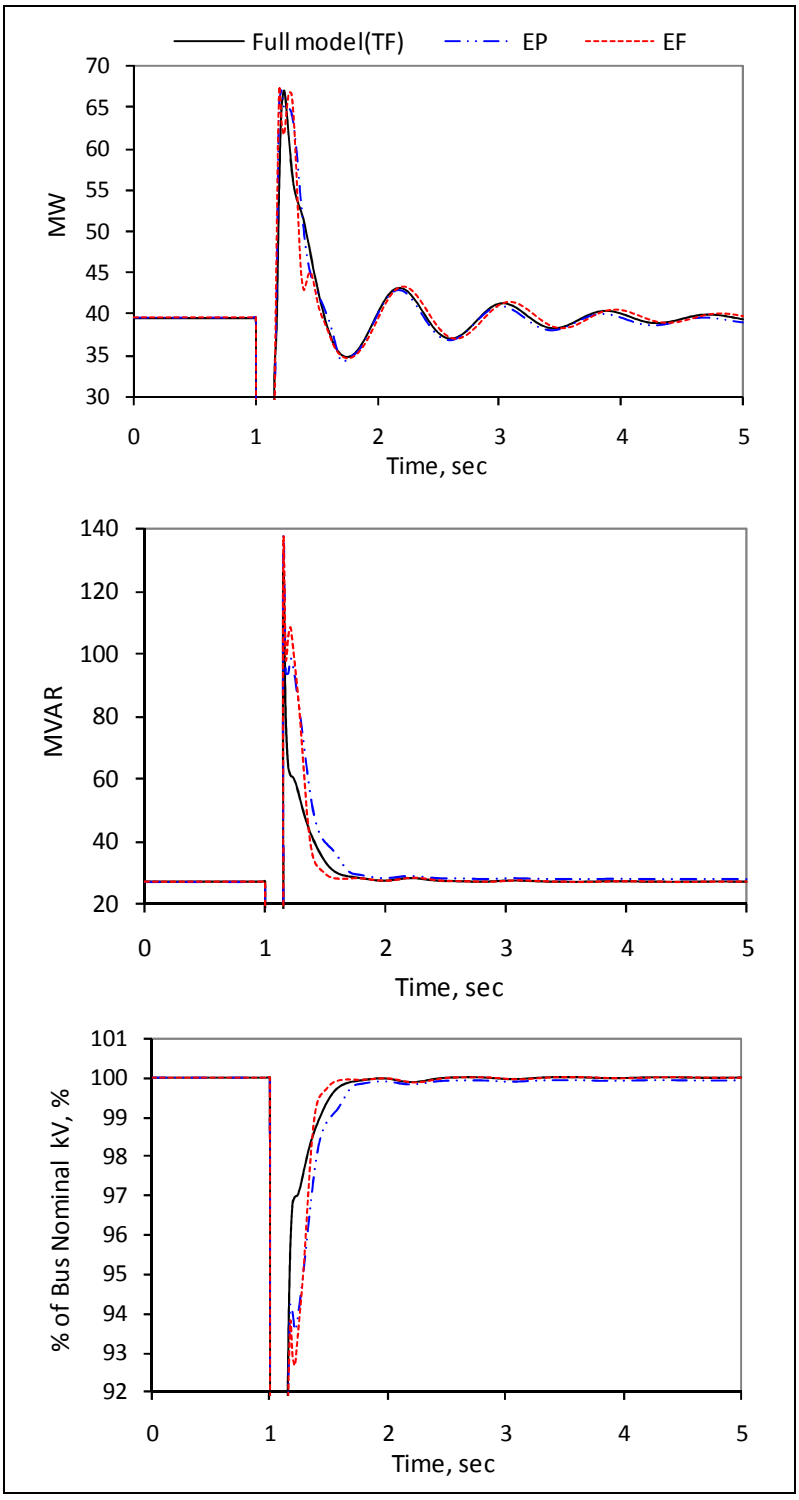

Figure 3.7 Dynamic responses at the transformer T1 and Utility main bus for the three template-based models

There are good agreements among the three models, which verify the accuracy of the proposed model equivalence methods. The two template-based equivalent models appear to have similar accuracies. The EP model has more physical meaning as each branch of the circuit represents a refinery process, while the EF model has the simplest form. The users can choose the equivalent model based on practical needs.

3.3.2 Template-Based Full Model and Guideline Model

To demonstrate advantages of the proposed template-based load modeling technique over the guideline modeling method, which is current practice for some utility companies, a guideline model is built using 30% static loads and 70% induction motors for the 108 MW coking oil refinery facility. The electrical single-line diagram of the guideline model is shown in Figure 3.8.

One issue faced by utility companies is that parameters such as the equivalent circuit parameters and inertia of the large motor in the guideline model are not available. Some utility companies simply use the default data provided by software tools such as the PSS/E, which may lead to serious errors in system modeling. In comparison, the template-based load modeling does not have such concerns as induction and synchronous motors used in the template-based full model are small motors, the equivalent circuit parameters and inertia of these small motors are readily available either from manufacturer published data or typical data such as listed in Tables A.1 and E.2 and Figure A.1 in Appendices A and E. By applying the model equivalence method, the aggregated equivalent circuit parameters and inertia of the lumped large motors in the template-based equivalent models are calculated based on equivalent circuit parameters and inertia of each individual small motor in the template-based full model, and thus, major dynamic response characteristics of each individual small motor are kept in the lumped large motor.

The following three sets of equivalent circuit parameters and inertia of the 101340 HP induction motor in the guideline model are used to investigate effects of these parameters on dynamic responses of the system during disturbances:

1) IM1: The equivalent circuit parameters proposed in [2] for large induction motors are used for the 101340 HP induction motor in the guideline model. The inertia constant H of the motor is assumed to be 10 based on the default data from ETAP.

2) IM2: The default equivalent circuit parameters of a 100 MVA induction motor provided in PSS/E are used for the 101340 HP induction motor in the guideline model. The inertia constant H is assumed to be 10.

3) IM3: The equivalent circuit parameters of IM3 are the same as IM1, but the inertia constant H is assumed to be 2. The purpose is to show the impact of the inertia on the results.

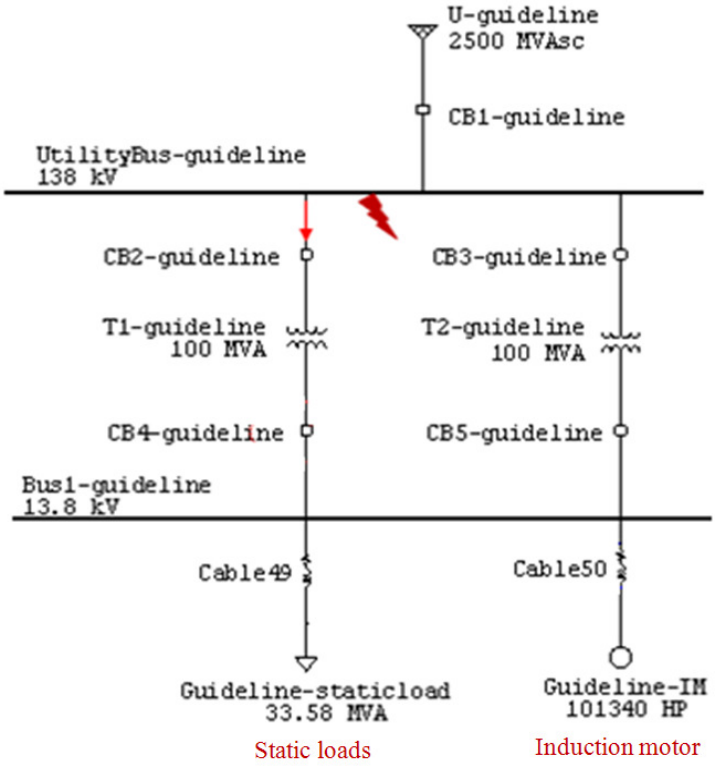

Figure 3.8 The guideline model for the 108 MW coking refinery facility

A 3-phase fault is applied at the 138 kV UtilityBus for the TF model (Figure 3.4) as well as the guideline model (Figure 3.8). Dynamic responses for the two models are compared in Figure 3.9. It is found that dynamic responses of the guideline models are much different when using different equivalent circuit parameters and inertia for the 101340 HP induction motor. Furthermore, the guideline model's response will be the same for different types of industrial facilities with similar MW size. As a result, the template-based models have clear advantages over the guideline model to provide adequate representation of an industry facility.

3.3.3 Template-Based Full Model and Real Facility Model

To validate the proposed template-based load modeling technique, dynamic responses of the detailed ETAP model for a real 108 MW coking refinery facility are simulated using the transient stability program. This real facility is very large and complex with 35 plants on site. The simulated dynamic responses of the real facility are compared with that of the template-based full model under the same disturbance event.

A three-phase fault is applied at the UtilityBus at 1.0 second and cleared at 1.15 seconds for the TF model (Figure 3.4) and the detailed ETAP model of the real facility. To ensure consistency, a Utility Bus and two main transformers with MVA sizes identical to the TF model are added to the ETAP model of the real facility. Dynamic responses at the transformer T1 and 138 kV Utility main bus for both models are shown in Figure 3.9.

It is found that dynamic responses of the template-based full model are very close to that of the real facility, while dynamic responses of the three guideline models drift away dramatically compared to that of the real facility. This proves that the template-based full/equivalent models can adequately represent industrial facilities.

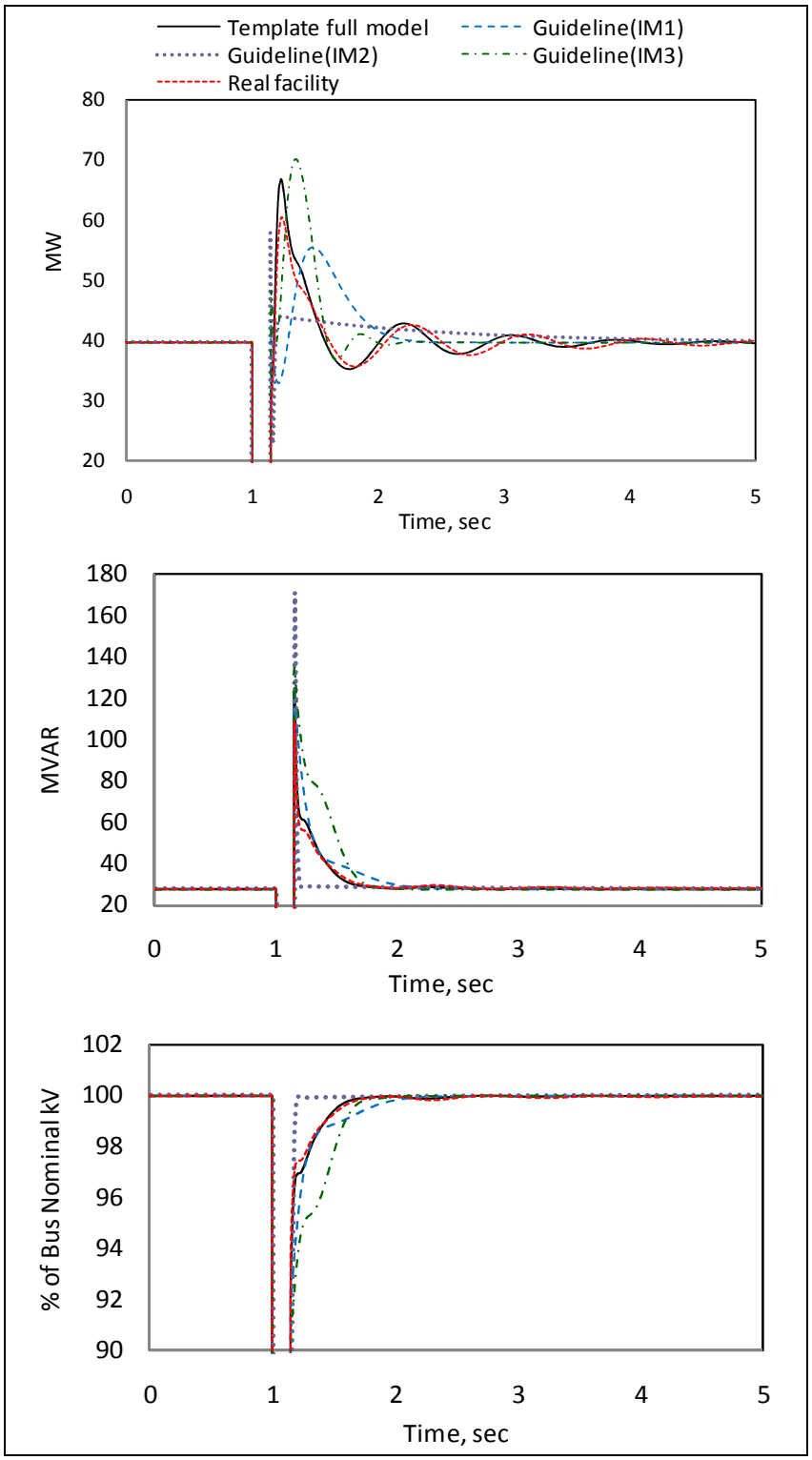

Figure 3.9 Dynamic responses at the transformer T1 and 138 kV Utility main bus for the TF, guideline and real facility models

3.3.4 Effects of Configuration Change in Refinery Processes

The templates for oil refinery facilities shown in Table 3.4 could be different from real refinery facilities. Therefore, effects of configuration change in refinery processes are studied to evaluate the robustness of the proposed templates. The following three cases are investigated for the 108 MW coking refinery facility:

1) Case 1: The base case using the template provided in Table 3.4.
2) Case 2: Compared to Case 1, remove 7000 HP induction motors (5% power consumption of the facility) in the process Hydrocracker and add 7000 HP induction motors in the process FCC.
3) Case 3: Compared to Case 1, remove 7000 HP induction motors in the process Hydrocracker and add 7000 HP synchronous motors in the process FCC.

The established template-based full models for Cases 2 and 3 are different from that of Case 1 due to the variations of the template. A 3-phase fault is applied at the 138 kV UtilityBus for the three different template-based full models corresponding to the three cases, and their dynamic responses are compared in Figure 3.10.

It is found that although modifying the template and the circuit by adding synchronous motors in Case 3 shows more influence on dynamic responses than only adding or removing induction motors in Case 2, dynamic models are in general insensitive to 5% changes in power consumption in the two processes. Since the system does not react greatly to a change in parameter values, it reduces uncertainty of the model behavior.

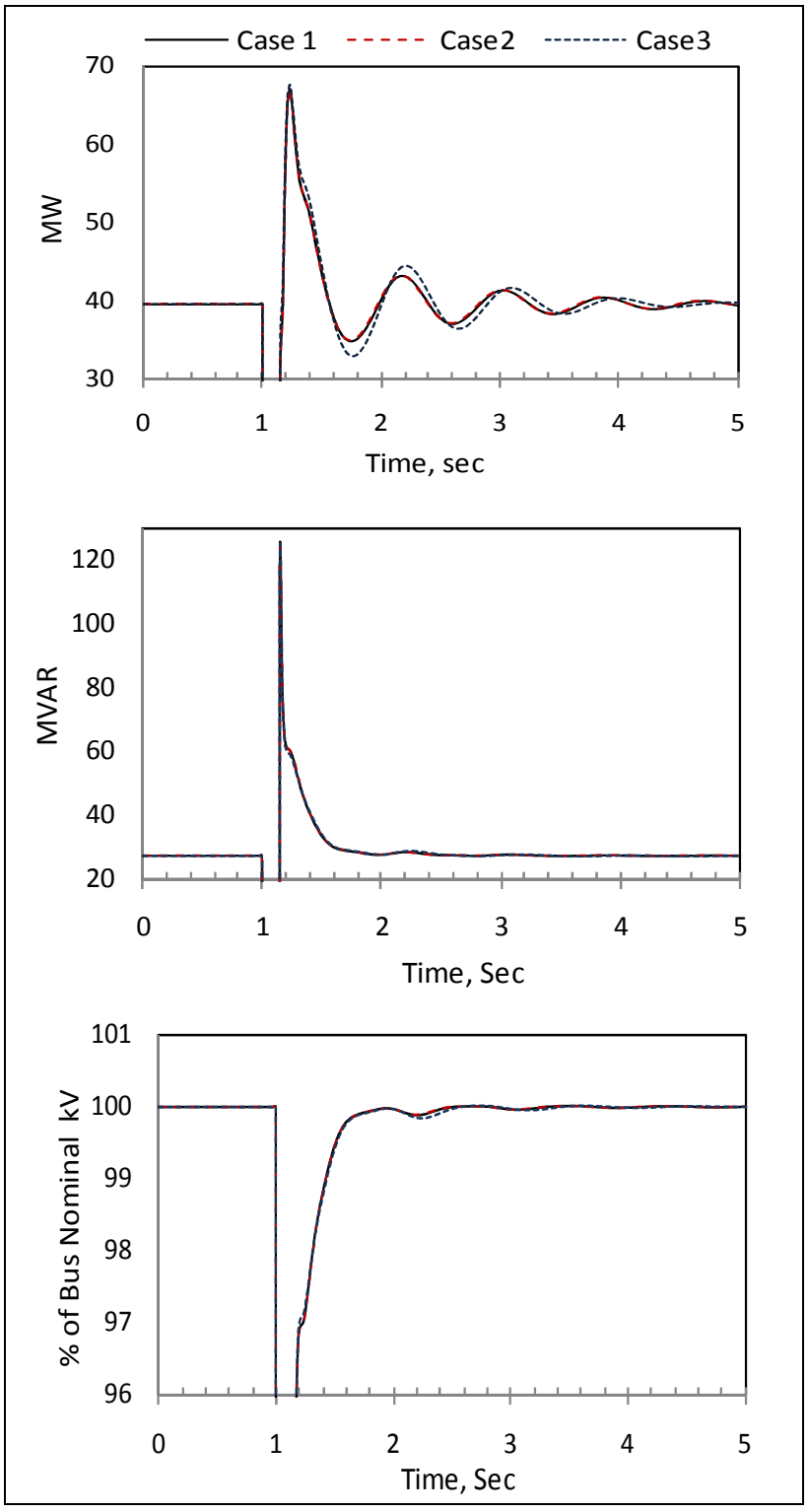

Figure 3.10 Dynamic responses at the transformer T1 and 138 kV Utility main bus for three template-based full models (Cases 1, 2 and 3)

3.4 Summary and Conclusions

To illustrate the proposed template-based load modeling technique, the template-based full model and equivalent models are established for oil refinery facilities.

The process of utilizing template-based load modeling for oil refinery facilities is explained in detail: step 1, create templates and template scaling rules according to extensive survey; step 2, establish the template-based full model based on the templates and template scaling rules; step 3, perform the model equivalence to the template-based full model to determined two template-based equivalent models, EP and/or EF models, which can be readily used for power systems dynamic studies.

To verify the accuracy of the model equivalence method, dynamic responses of the template-based full model are compared to that of the two template-based equivalent models, it is found that there are good agreements among the three models, and thus, the accuracy of the model equivalence methods is verified. The two equivalent models appear to have similar accuracies. The EP model has more physical meaning as each branch of the circuit represents a process, while the EF model has the simplest form. The users can choose the equivalent model based on practical needs.

To demonstrate that the developed template-based full/equivalent models are adequate dynamic models for oil refinery facilities, dynamic responses of the template-based full model are compared with that of a real facility and the guideline model. There are good agreements between the template-based full model and the real facility, while the guideline model using three different sets of parameters for the induction motor drifts away dramatically from the real facility model. Therefore, it is verified that the template-based full/equivalent models can adequately represent practical industrial facilities.

The robustness of the created templates is also verified using a sensitivity study by conducting load changes in different refinery processes. It is found that the system does not react greatly to a 5% load change in the template, so it reduces uncertainty of the model behavior.

CHAPTER 4 DYNAMIC MODELS FOR MOTOR DRIVE SYSTEMS

Two sets of research results on developing models of motor drive systems for power systems dynamic studies are presented in this chapter. The first set of research results clarifies how a VFD responds to voltage sags. Voltage sags occur when power systems experience short-circuit faults, which is typically the starting point of power systems dynamic simulation. This research shows that VFDs will trip when they experience a relatively large voltage sag (>20% - 30% voltage drop). As a result, there is no need to include VFDs in dynamic studies. Based on the finding, a simple procedure to determine if a VFD needs to be included for dynamic studies is proposed in this chapter.

The second set of research results presents how to model VFDs when they experience mild voltage disturbances and are able to ride through. The equivalent dynamic models for motor drive systems dedicated under such conditions are proposed. These models are created using the linearization approach and include effects of the drive, the motor, and the control system. Since major work is focused on the second set, it will be introduced first in this chapter in Sections 4.1 – 4.5. The first set regarding the VFD tripping will be discussed in Section 4.6.

4.1 Modeling Methodology for Ride-Through Variable Frequency Drives

VFDs can be categorized into four most commonly used types based on their inverter topologies (Figure 4.1): 1) low voltage VSI drives, 2) low voltage CSI drives, 3) medium voltage neutral point clamped (NPC) inverter drives, and 4) medium voltage cascaded inverter drives. Due to significant different topologies for the four types of drives, their mathematical models are different.

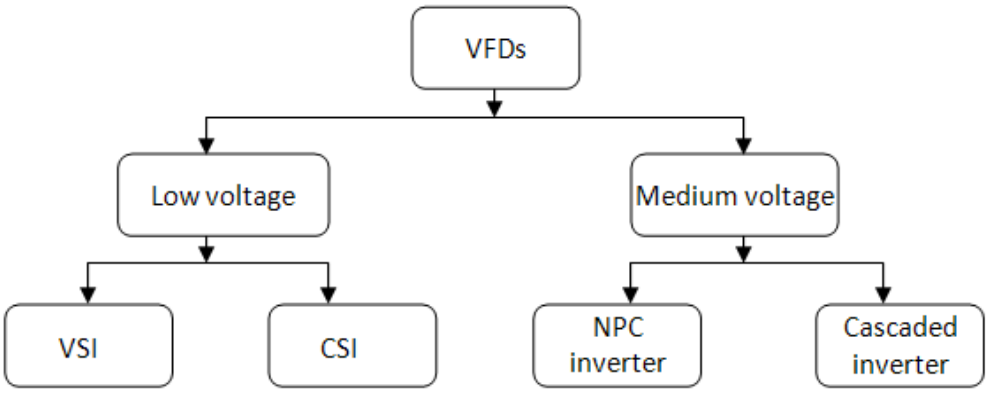

Figure 4.1 Common types based on inverter topologies of drives

VSI drives require a simple diode bridge as a front-end converter featuring minimum costs, high efficiency, and high reliability for the rectifying stage [108]. This type of VFDs is most widely used in industrial facilities. Both scalar (voltage per Hz control) and vector control are used in VSIs. The energy storage is more practical and efficient in capacitors than in inductors. The main disadvantage of VSIs is the high dv/dt transient of the PWM-controlled inverter output voltage, which could cause harmful effect on the motor insulation, but such effect can be significantly lowered by adding a sine wave/load filter at the output of the inverter, which have been successfully practiced in real life [108, 109].

Although not as widely used as VSI drives, CSI drives are also used in industrial facilities. The CSIs offer a number of advantages including: 1) short circuit protection, the output current being limited by the regulated DC bus current; 2) low output voltage dv/dt due to the filtering effect of the output capacitors at the output of inverter; 3) instantaneous and continuous regenerative capabilities. These features in addition to the availability of large reverse blocking devices make the CSI-based drive attractive in medium to high power applications. Despite the advantages, CSI drives based on a thyristor front-end rectifier presents a poor and variable overall input power factor, and losses at dc-link inductor for low voltage applications [109].

Two common multilevel inverter structures widely used for high power applications are the NPC inverter and the cascaded inverter. The NPC inverter uses one DC link subdivided into a number of voltage levels by a series string of capacitors [158-161]. The configuration of a three-level NPC inverter motor drive system is shown in Figure 4.2 [160].

The cascaded inverter is made up from series connected single phase full bridge inverters, each with their own isolated DC bus [161, 118]. Figure 4.3 shows a configuration for an 18-pulse cascaded inverter motor drive system [118]. The detailed descriptions for cascaded inverter drives can be found in Section 4.4.1. Both NPC and cascaded inverter drives have similar front-end, multiple 6-pulse rectifiers with phase-shifting transformers forming 18-pulse or 24-pulse front-end, but their DC link and inverter configurations are completely different.

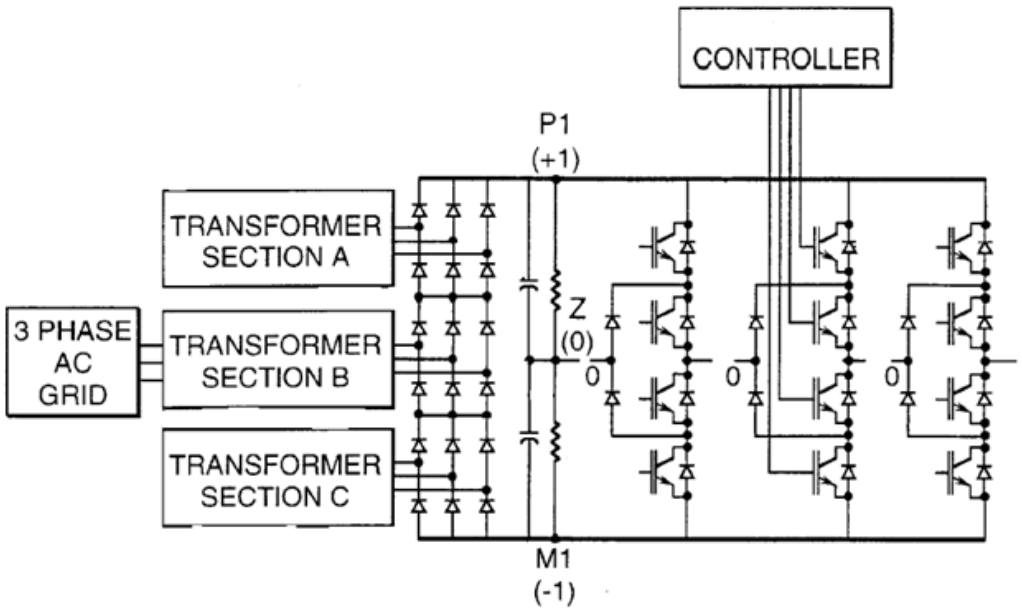

Figure 4.2 Configuration for a three-level NPC motor drive system [160]

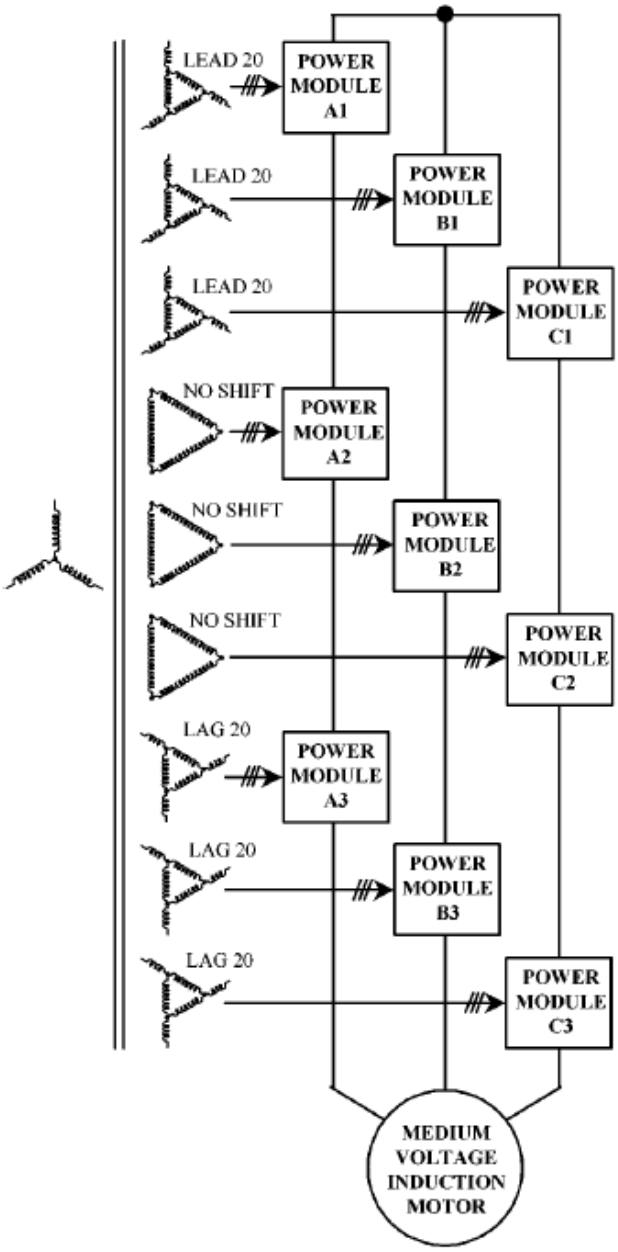

Figure 4.3 Topology of a nine-module 18-pulse cascaded inverter drive [118]

Regardless how many differences the system configurations have, a motor drive system usually consists of three main components: 1) the drive, 2) the motor, and 3) the control system. The mathematical models of these components can be expressed by differential equations. Induction motors are workhorse in industry, and are also major loads for VFDs. Three common control methods for

induction motors are: 1) voltage per Hz control, 2) field oriented control, and 3) direct torque control.

During mild disturbances, drives can ride through and remain in service. The drives, their motor loads and the control systems all play a role in the overall dynamic response. Therefore, mathematical models for the drive, the motor and the control scheme shall be included in the development of the equivalent dynamic model.

In this thesis, a linearization approach to create the equivalent dynamic model for motor drive systems when VFDs can ride through during disturbances is proposed as follows (illustrated in Figure 4.4):

1) Find differential equations for the drive, the motor and the control system[1],
2) Combine all equations to establish the relationship among them,
3) Linearize the combined differential equations to obtain the dynamic model for the motor drive system.

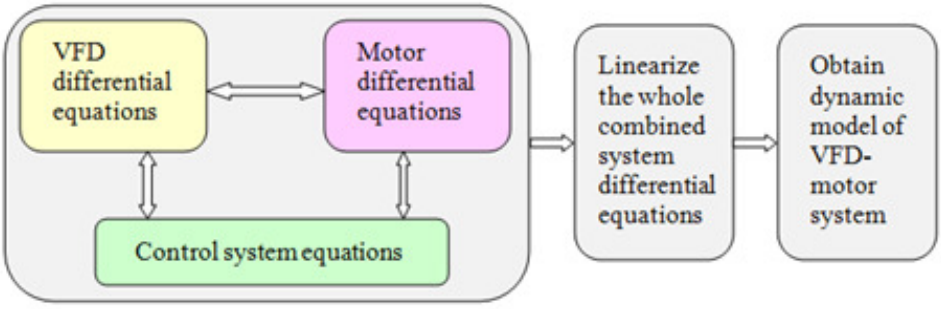

Figure 4.4 The linearization approach to create equivalent dynamic models

By applying the proposed approach, the equivalent dynamic model of a motor drive system can be established as shown in Figure 4.5. This model includes influences of the drive, the motor and their control system on the

[1] Note: the control system considered in this thesis is the normal control such as the voltage per Hz control. Special designed control feature such as control for drives riding-through under faulted conditions are not included.

overall contribution to the power grid during disturbances, and thus accurately represents its dynamic characteristics. Both voltage dependence and frequency dependence are considered. The input variables for the model are the rms voltage per phase (E^2) and the frequency (f_g) of the drive power supply. The output variables are active power (P) and reactive power (Q) at the drive AC input connected to the power grid.

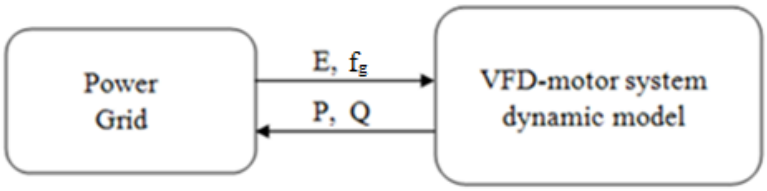

Figure 4.5 Equivalent dynamic model for motor drive systems

Sabir et al. summarize in [7] that the loads are usually subjected to two kinds of changes in stability studies: the first is the sudden voltage change caused by application and removal of faults; the other type is the change in voltage and frequency due to inter-area swings. Therefore, it is important that both voltage dependence and frequency dependence are included in the dynamic load model to cover all possible cases.

The voltage variations are also known as voltage sags/dips, which are extensively discussed in the literature [31-37]. Andrew et al provide detailed explanations on the frequency variation in power grid [107]. The frequency deviations of a transient nature may result from increased or decreased consumption and/or removal or addition of power generation systems. Increased consumption and removal of power generation systems tend to cause a decrease of the grid frequency. Decreased consumption and addition of the power generation systems tend to cause an increase of the grid frequency. Power consumption and generation are time-dependent variables which may cause frequency variations in a range of approximately ±0.5 Hz. The frequency

[2] Note: E is the symbol for the bus terminal voltage V here in the drive modeling sections

transients are usually of the duration measured in seconds or minutes. The magnitude of a frequency transient is typically influenced by a ratio of magnitude of a power variation to the total power level within the grid and associated interconnected grids throughout the duration of the variation. Larger frequency transients outside the range ±0.5 Hz could be a result of an immediate loss of one or more power generators [107].

The proposed equivalent dynamic model is based on linearization of differential equations for motor drive systems, and it is suitable for small signal stability studies. On the other hand, VFDs will trip out of lines during large disturbances, and the motor drive systems are only considered in dynamic modeling for small voltage sags, so the equivalent dynamic model will serve well for power systems dynamic studies.

In this chapter, dynamic models for VSI and cascaded inverter drives with their induction motor loads are created. Development of dynamic models for CSI ([132-151]) and NPC inverter [158-161] motor drive systems will be part of the future work.

4.2 Dynamic Models of VSI Motor drive Systems

4.2.1 Overview of the Motor Drive Systems

The low voltage 6-pulse PWM-controlled VSI based drives with diode front-ends (Figure 4.6) are most commonly used in various industrial facilities supplying power to induction motors. The equivalent dynamic model for this type of motor drive systems is developed. The control method considered is the voltage per Hz control.

A group of differential equations representing dynamic average-value model for a load-commuted converter/rectifier proposed in [60] is adopted in this work. The DC link and voltage source inverter are also represented by differential equations. The average DC voltage and the average direct (d)- and

quadrature (q) -axis components of the AC source currents at the input of the drive can be predicted by differential equations of the rectifier. The d- and q-axis AC source currents are used to calculate real and reactive power supplied to motor drive systems. It is assumed that the cable between the drive and the motor is short, and thus, the impedance of the cable can be ignored. In this case, the inverter output voltage is considered to be directly applied to the motor stator, the relationship between parameters of the VFD and the motor are simplified and linked together easily. The control system applies more constraints on the VFD and the motor parameters and forms a complete picture of the whole system.

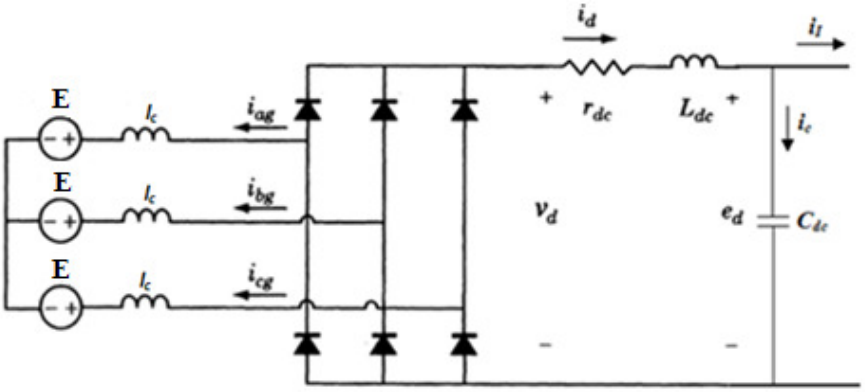

(a) Rectifier and DC link

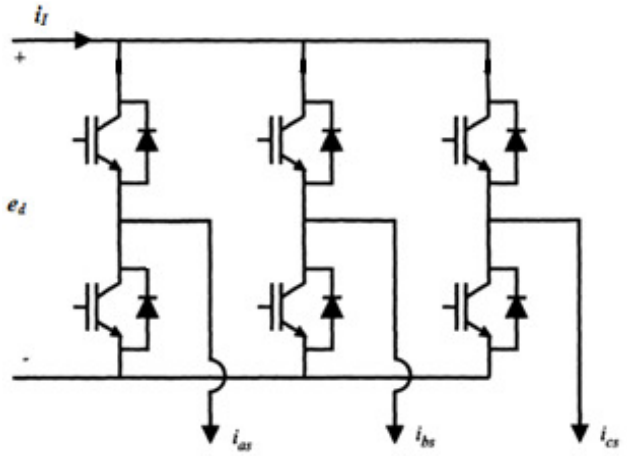

(b) Inverter

Figure 4.6 Configuration of a low voltage 6-pulse VSI drive [60]

The voltage per Hz control method is designed to accommodate variable speed commends by using the inverter to apply a voltage of correct magnitude and frequency so as to achieve the commended speed [60].

The constant voltage per hertz (V/f) control is an effective method for AC motor drive speed regulation. In this method, the inverter output voltage is varied proportionally to the reference frequency such that constant stator flux is maintained. Particularly in an induction motor drive, this operating mode results in shunt speed-torque characteristics (linear portion of the torque-speed curve), yielding low slip frequency, high energy efficiency and good speed regulation. Therefore, the method gained wide acceptance in many industrial and residential induction motor drive speed regulation applications. However, the V/f method is seldom implemented in its naive form, additional algorithms and control loops are included in the control algorithm to enhance its performance. Slip frequency compensation methods to improve the load overhaul characteristics, voltage boost methods to compensate for the resistive voltage drop at low speed, and frequency skipping techniques to avoid the unstable operating regions are widely established and utilized. State of the art V/f inverter drives perform satisfactorily in a wide speed range with 5% or better speed accuracy and higher resolution can be obtained with shaft encoder feedback. Typical application areas of V/f drives are pumps, ventilation systems etc., which have passive torque-speed characteristics (with inherent damping) and no precise speed regulation requirement [110].

There are two types of voltage per Hz control methods available for induction motors: open-loop and closed-loop. The open-loop speed control is used when the accuracy in speed response is not a concern such as in HVAC (heating, ventilation and air conditioning), fan or blower applications. In this case, the supply frequency is determined based on the desired speed and the assumption that the motor will roughly follow its synchronous speed. The error in speed resulted from slip of the motor is considered acceptable. When the accuracy in speed response is a concern, the closed-loop speed control can be

implemented with the constant V/f principle through regulation of slip speed, where a PI controller is employed to regulate the slip speed of the motor to keep the motor speed at its set value [111-116]. The open-loop and closed-loop voltage per Hz control can be found in Figures 4.7 (a) and 4.7(b), respectively.

In this thesis, a closed-loop voltage per Hz control method is chosen for the dynamic model development. The voltage per Hz control scheme provided in Matlab/Simulink (Figure 4.8) is adopted and will be used in the detailed switching models [117]. The open-loop voltage per Hz control method can be treated as a simplified case of the close-loop control by removing the speed feedback and the PI speed controller.

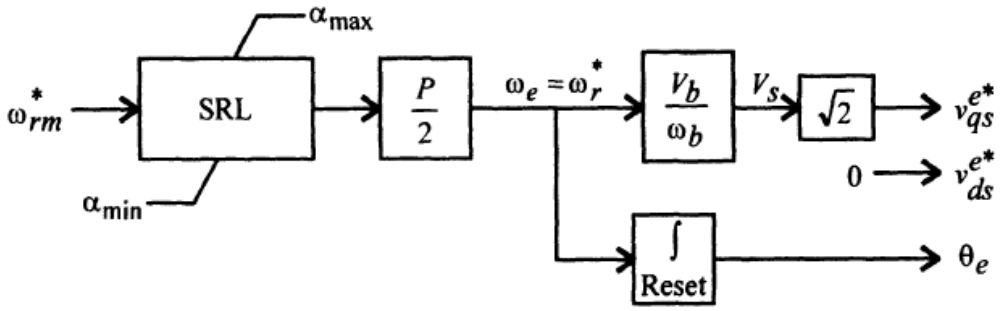

(a) Open-loop voltage per Hz control [60]

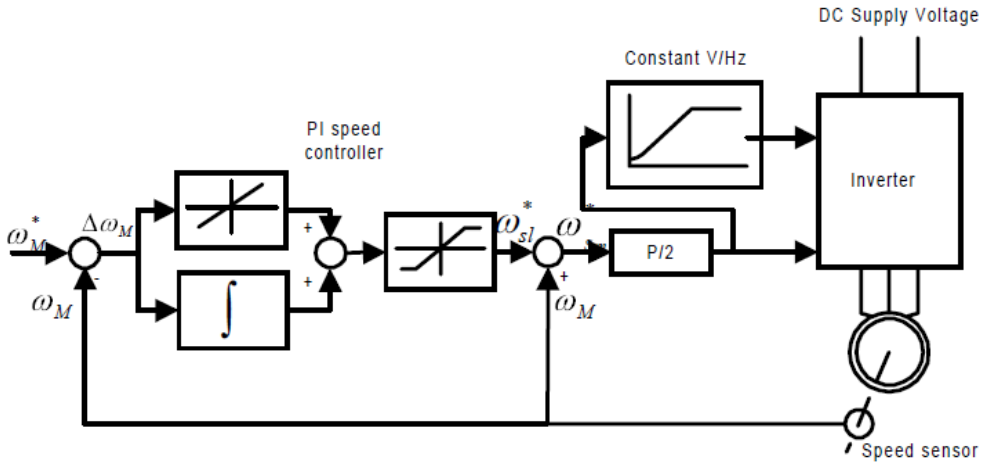

(b) Closed-loop voltage per Hz control [111]

Figure 4.7 Voltage per Hz control schemes

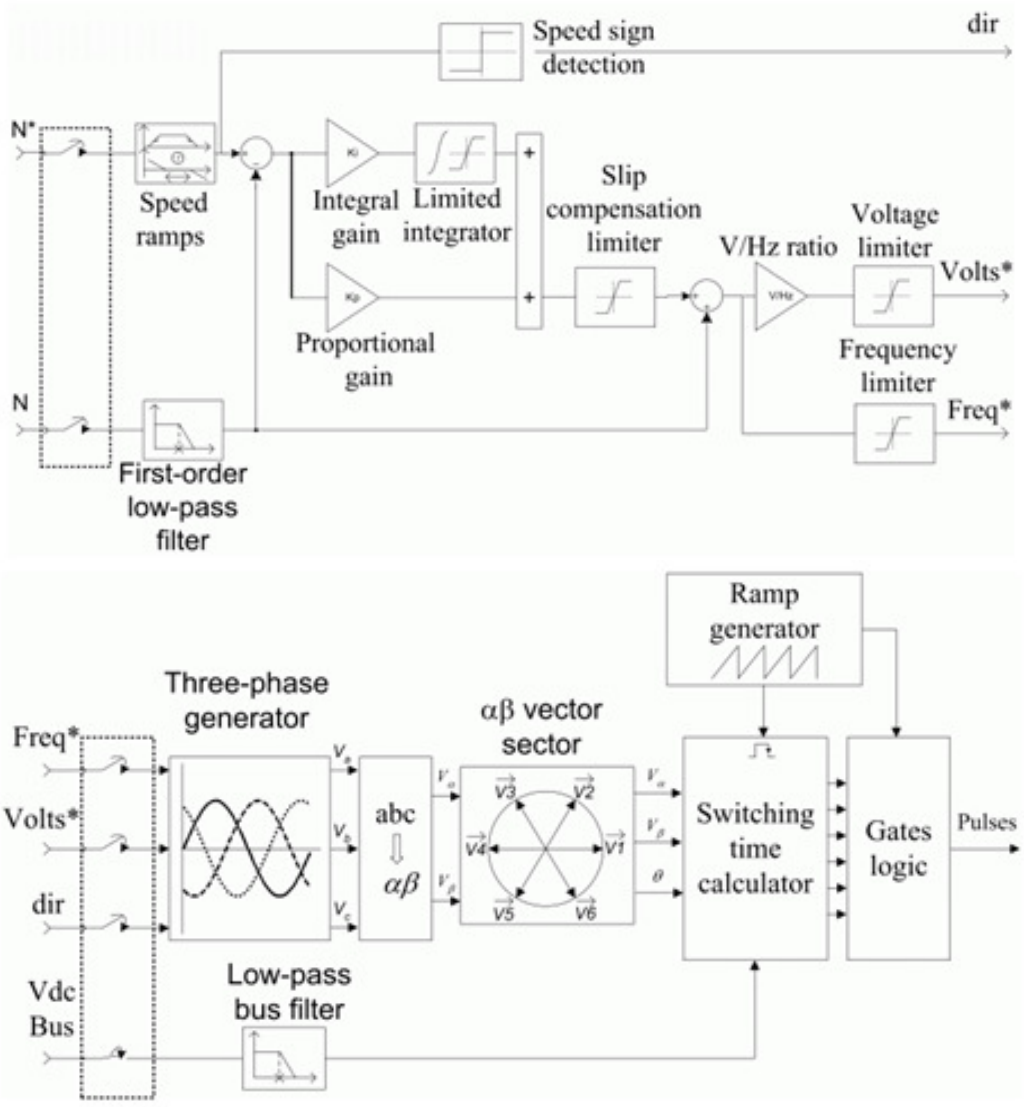

Figure 4.8 The closed-loop voltage per Hz controller schematic from Matlab/Simulink [117]

4.2.2 Mathematical Model of VSI Drives

The differential equations for the PWM-controlled VSI drives with diode front end in the three phase mode can be written in Equations (4.2-1)-(4.2-19). The effect of the commutation inductance l_c in front of the VFD is included in these equations [60].

$$v_d = \frac{3\sqrt{6}}{\pi} E - \frac{3}{\pi} l_c (2\pi f_g) i_d - 2l_c \frac{di_d}{dt} - 2V_{diode} \tag{4.2-1}$$

$$v_d = r_{dc} i_d + L_{dc} \frac{di_d}{dt} + e_d \tag{4.2-2}$$

$$i_I = i_d - C_{dc} \frac{de_d}{dt} \tag{4.2-3}$$

$$P = \frac{3}{2}\left(v_{dg} i_{dg} + v_{qg} i_{qg}\right) \tag{4.2-4}$$

$$Q = \frac{3}{2}\left(v_{qg} i_{dg} - v_{dg} i_{qg}\right) \tag{4.2-5}$$

$$v_{qg} = \sqrt{2}E \tag{4.2-6}$$

$$v_{dg} = 0 \tag{4.2-7}$$

$$i_{dg} = i_{dgcom} + i_{dgcond} \tag{4.2-8}$$

$$i_{dgcom} = \frac{2\sqrt{3}}{\pi} i_d \left[-\cos\left(u - \frac{5\pi}{6}\right) + \cos\left(-\frac{5\pi}{6}\right) \right] + \frac{3\sqrt{2}E}{\pi l_c (2\pi f_g)} \sin u - \frac{3\sqrt{2}E}{4\pi l_c (2\pi f_g)} \sin 2u - \frac{3\sqrt{2}E}{2\pi l_c (2\pi f_g)} u \tag{4.2-9}$$

$$i_{dgcond} = \frac{2\sqrt{3}}{\pi} i_d \left[-\cos\left(\frac{7\pi}{6}\right) + \cos\left(u + \frac{5\pi}{6}\right) \right] \tag{4.2-10}$$

$$i_{qg} = i_{qgcom} + i_{qgcond} \tag{4.2-11}$$

$$i_{qgcom} = \frac{2\sqrt{3}}{\pi} i_d \left[\sin\left(u - \frac{5\pi}{6}\right) - \sin\left(-\frac{5\pi}{6}\right) \right] + \frac{3\sqrt{2}E}{\pi l_c (2\pi f_g)} (\cos u - 1) + \frac{3\sqrt{2}E}{4\pi l_c (2\pi f_g)} (1 - \cos 2u) \tag{4.2-12}$$

$$i_{qgcond} = \frac{2\sqrt{3}}{\pi} i_d \left[\sin\left(\frac{7\pi}{6}\right) - \sin\left(u + \frac{5\pi}{6}\right) \right] \quad (4.2\text{-}13)$$

$$u = \arccos\left[1 - \frac{2l_c (2\pi f_g) i_d}{\sqrt{6}E} \right] \quad (4.2\text{-}14)$$

$$v_{qs} = \frac{1}{2} de_d \quad (4.2\text{-}15)$$

$$v_{ds} = 0 \quad (4.2\text{-}16)$$

$$P_{IM} = \frac{3}{2} \left(v_{ds} i_{ds} + v_{qs} i_{ds} \right) \quad (4.2\text{-}17)$$

$$P_{Inverter} = e_d i_I \quad (4.2\text{-}18)$$

$$P_{Inverter} = P_{IM} \quad (4.2\text{-}19)$$

where,

P and Q – active and reactive power at the input of the VFD in front of the commutation inductor,

l_c – the commutation inductance, which is the sum of the power source inductance and the inductance of the ac line reactor if any

E – the rms phase-to-ground voltage of power source,

f_g – the power supply frequency at the input of the drive.

v_d – the DC link voltage after rectifier

e_d – the DC link voltage before inverter

i_d – the DC link current after rectifier

i_I – the DC link current entering inverter

V_{diode} – the diode forward voltage

C_{dc} – the capacitance of DC link capacitor

r_{dc} – the resistance of DC link

L_{dc} – the inductance of DC link reactor

v_{qg} – q-axis power source voltage

v_{dg} – d-axis power source voltage

i_{qg} – q-axis ac current at drive input

i_{qgcom} – q-axis ac current at drive input during commutation period

i_{qgcond} – q-axis ac current at drive input during conduction period

i_{dg} – d-axis ac current at drive input

i_{dgcom} – d-axis ac current at drive input during commutation period

i_{dgcond} – d-axis ac current at drive input during conduction period

u – commutation angle

v_{qs} – q-axis voltage at inverter output

v_{ds} – d-axis voltage at inverter output

d – duty cycle

P_{IM} – active power at motor terminal (assuming there is only a short cable between the drive and the induction motor)

$P_{Inveter}$ – active power at output of the drive

4.2.3 Mathematical Model of Induction Motors

The differential equations representing the 5th order induction motor model are given as follows [4, 83]:

$$v_{ds} = R_s i_{ds} - \omega_s \Psi_{qs} + \frac{d\Psi_{ds}}{dt} \tag{4.2-20}$$

$$v_{qs} = R_s i_{qs} + \omega_s \Psi_{ds} + \frac{d\Psi_{qs}}{dt} \tag{4.2-21}$$

$$v_{dr} = R_r i_{dr} - (\omega_s - \omega_r)\Psi_{qr} + \frac{d\Psi_{dr}}{dt} \tag{4.2-22}$$

$$v_{qr} = R_r i_{qr} + (\omega_s - \omega_r)\Psi_{dr} + \frac{d\Psi_{qr}}{dt} \tag{4.2-23}$$

$$\Psi_{ds} = L_s i_{ds} + L_m i_{dr} \tag{4.2-24}$$

$$\Psi_{qs} = L_s i_{qs} + L_m i_{qr} \tag{4.2-25}$$

$$\Psi_{dr} = L_m i_{ds} + L_r i_{dr} \tag{4.2-26}$$

$$\Psi_{qr} = L_m i_{qs} + L_r i_{qr} \tag{4.2-27}$$

$$T_e = 1.5\, p(\Psi_{ds} i_{qs} - \Psi_{qs} i_{ds}) \tag{4.2-28}$$

$$\frac{d\omega_r}{dt} = \frac{p}{2H}(T_e - T_L) \tag{4.2-29}$$

Assuming the stator transients can be negligible, the induction motor model becomes the 3rd order:

$$\frac{d\Psi_{ds}}{dt} = 0 \tag{4.2-30}$$

$$\frac{d\Psi_{qs}}{dt} = 0 \tag{4.2-31}$$

For induction motors, the rotor is shorted, and thus, we have

$$v_{dr} = 0 \tag{4.2-32}$$

$$v_{qr} = 0 \tag{4.2-33}$$

where,

R_s – Stator resistance

L_s – Total stator inductance, $L_s = l_s + L_m$

l_s – Stator leakage inductance

L_m – Magnetizing inductance

R_r – Rotor resistance

L_r – Total rotor inductance, $L_r = l_r + L_m$

l_r – Rotor leakage inductance

v_{qs}, i_{qs} – q-axis stator voltage and current

v_{ds}, i_{ds} – d-axis stator voltage and current

Ψ_{qs}, Ψ_{ds} – stator q and d axis fluxes

Ψ_{qr}, Ψ_{dr} – rotor q and d axis fluxes

ω_r – Electric angular velocity of the rotor

ω_s – Stator field angular velocity in electrical rad/s

p – number of pole pairs

T_e – electromagnetic torque

T_L – shaft mechanical torque

H – Combined rotor and load inertia constant

4.2.4 Modeling of Motor Drive System Control Scheme

The principle of the closed-loop voltage per Hz controller is investigated in this research. Reference [60] provides information on the voltage control method for duty-cycle modulator, which is a critical part in addition to the voltage per Hz control schemes shown in Figures 4.7 (a) and 4.7 (b). The goal is to obtain the appropriate duty cycle(s) and the converter reference frame position in order to achieve a desired fast average synchronous reference frame direct- and quadrature-axis voltage. The voltage control of a duty-cycle modulator for the pulse-width modulation is shown in Figure 4.9 [60].

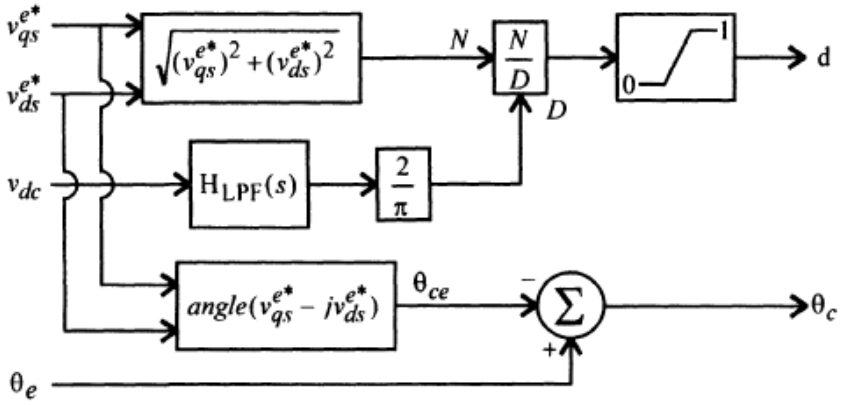

Figure 4.9 Voltage control of a duty-cycle modulator for PWM [60]

The voltage command related to the duty-cycle modulation can be expressed as follows [60]:

$$\begin{bmatrix} v_{qs}^{e} \\ v_{ds}^{e} \end{bmatrix} = \begin{bmatrix} \cos\theta_{ce} & \sin\theta_{ce} \\ -\sin\theta_{ce} & \cos\theta_{ce} \end{bmatrix} \begin{bmatrix} v_{qs}^{c} \\ v_{ds}^{c} \end{bmatrix} \tag{4.2-34}$$

where θ_{ce} is angular displacement of the converter reference frame from the synchronous reference frame, that is

$$\theta_{ce} = \theta_c - \theta_e \tag{4.2-35}$$

In this research work, the sine-triangle PWM is considered. In this case, replacing v_{qs}^{e} with the commanded value v_{qs}^{e*}, v_{ds}^{e} with the commanded value

v_{ds}^{e*}, v_{qs}^{c} and v_{ds}^{c} with the average values expression by Equations (4.2-15) and (4.2-16) yield

$$\begin{bmatrix} v_{qs}^{e*} \\ v_{ds}^{e*} \end{bmatrix} = \begin{bmatrix} \cos\theta_{ce} & \sin\theta_{ce} \\ -\sin\theta_{ce} & \cos\theta_{ce} \end{bmatrix} \begin{bmatrix} \frac{1}{2} de_d \\ 0 \end{bmatrix} \tag{4.2-36}$$

From Equation (4.2-36), the following relationships are obtained:

$$d = \frac{\sqrt{\left(v_{qs}^{e*}\right)^2 + \left(v_{ds}^{e*}\right)^2}}{\frac{1}{2} e_d} \tag{4.2-37}$$

$$\theta_{ce} = angle\left(v_{qs}^{e*} - v_{ds}^{e*}\right) \tag{4.2-38}$$

The developed block diagram for the closed-loop voltage per Hz control scheme used for the formula derivation is shown in Figure 4.10.

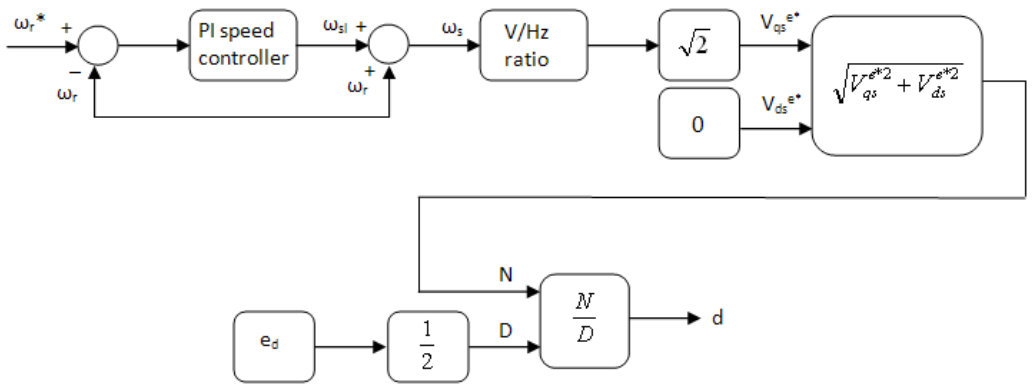

Figure 4.10 Voltage per Hz control scheme for VSI motor drive systems

The equations for the closed-loop voltage per Hz control are given as follows:

$$\omega_{SL} = K_{pm}\left(\omega_r^* - \omega_r\right) + \int_0^t K_{im}\left(\omega_r^* - \omega_r\right)dt + \left(\omega_{s0} - \omega_{r0}\right) \tag{4.2-39}$$

$$\omega_{SL} + \omega_r = \omega_s \tag{4.2-40}$$

$$d = \frac{\omega_s \left(\frac{V_b}{\omega_b} \right) \sqrt{2}}{\frac{1}{2} e_d} \tag{4.2-41}$$

where K_{pm} is speed PI controller proportional gain, and K_{im} is speed PI controller integral gain.

Dynamic models of the VSI motor drive systems with the open-loop voltage per Hz control can be easily obtained by simplifying the derived dynamic model using the closed-loop voltage per Hz control.

4.2.5 The Equivalent Dynamic Model

By combining Equations (4.2-1)-(4.2-41) and conducting linearization for the whole set of differential equations of the overall system, the dynamic model of the PWM controlled VSI based drive and induction motor system can be determined by Equations (4.2-42) and (4.2-43).

$$P = P_0 + G_{P1}\Delta E + G_{P2}\Delta E^2 + \left(G_{P3} + G_{P4}\Delta E\right)\Delta f_g \tag{4.2-42}$$

$$Q = Q_0 + G_{Q1}\Delta E + G_{Q2}\Delta E^2 + \left(G_{Q3} + G_{Q4}\Delta E\right)\Delta f_g \tag{4.2-43}$$

The developed dynamic model includes both voltage dependence and frequency dependence for real and reactive power, and the coefficients, G_{P1}, G_{P2}, G_{P3}, G_{P4}, G_{Q1}, G_{Q2}, G_{Q3}, and G_{Q4}, in Equations (4.2-42) and (4.2-43) are expressed by 7^{th} order transfer functions. The Simulink models for the dynamic model are shown in Figure 4.11.

The 7^{th} order transfer function represents seven first order differential equations in the overall motor drive system. The induction motor is 3^{rd} order after ignoring stator transients, which represents three differential equations. The drive and the control system together have four differential equations. When the topology of the drive is changed, the order of the transfer functions could

change. For example, for CSI motor drive systems, it will be 10th order transfer functions in the dynamic model as more control is added.

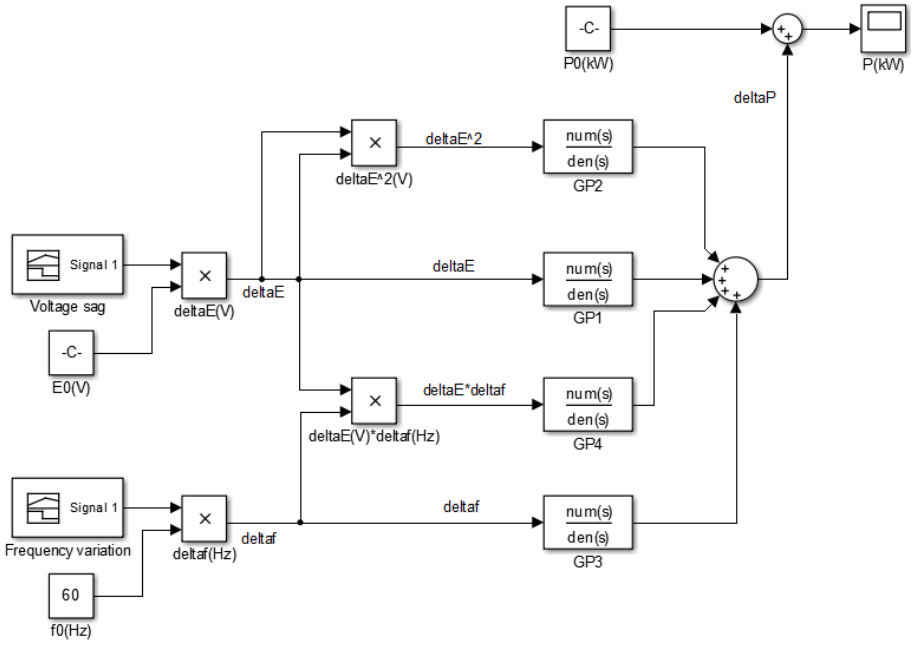

(a) Real power P

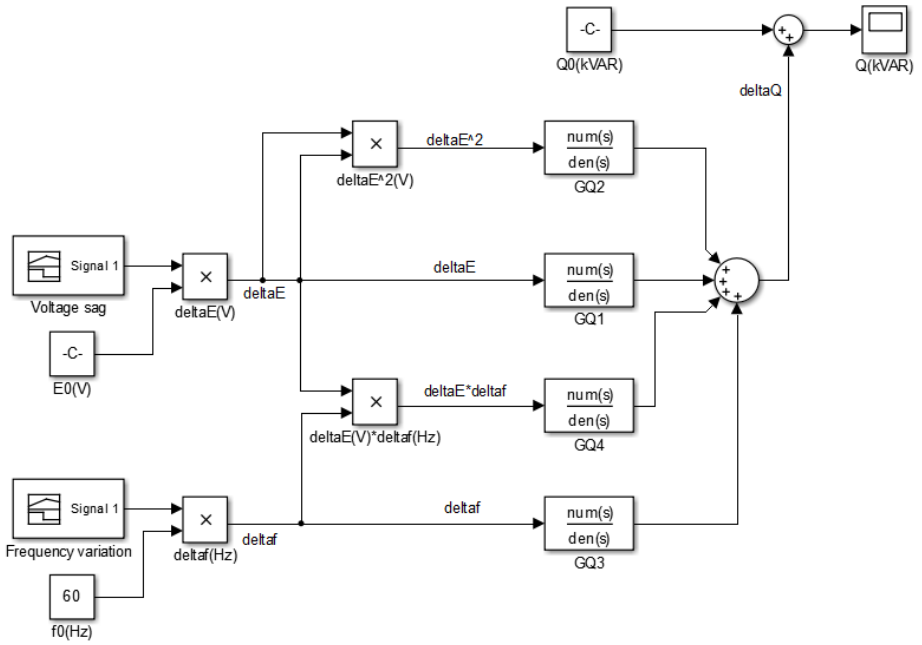

(b) Reactive power Q

Figure 4.11 Simulink models for the equivalent dynamic model

The AC current at the drive input can be determined by Equations (4.2-44) and (4.2-45). Both voltage and frequency dependence are also considered. The coefficients, G_{Iqg1}, G_{Iqg2}, G_{Idg1}, and G_{Idg2}, in the AC current calculations are expressed by 7th order transfer functions.

$$i_{qg} = i_{qg0} + G_{Iqg1}\Delta E + G_{Iqg2}\Delta f_g \tag{4.2-44}$$

$$i_{dg} = i_{dg0} + G_{Idg1}\Delta E + G_{Idg2}\Delta f_g \tag{4.2-45}$$

All coefficients appear in the dynamic model and AC currents calculation can be determined by Equations (4.2-46)-(4.2-59).

$$G_{P1} = \frac{G_{P1\_1}S^7 + G_{P1\_2}S^6 + G_{P1\_3}S^5 + G_{P1\_4}S^4 + G_{P1\_5}S^3 + G_{P1\_6}S^2 + G_{P1\_7}S + G_{P1\_8}}{P_{b1}S^7 + P_{b2}S^6 + P_{b3}S^5 + P_{b4}S^4 + P_{b5}S^3 + P_{b6}S^2 + P_{b7}S + P_{b8}} \tag{4.2-46}$$

$$G_{P2} = \frac{G_{P2\_1}S^7 + G_{P2\_2}S^6 + G_{P2\_3}S^5 + G_{P2\_4}S^4 + G_{P2\_5}S^3 + G_{P2\_6}S^2 + G_{P2\_7}S + G_{P2\_8}}{P_{b1}S^7 + P_{b2}S^6 + P_{b3}S^5 + P_{b4}S^4 + P_{b5}S^3 + P_{b6}S^2 + P_{b7}S + P_{b8}} \tag{4.2-47}$$

$$G_{P3} = \frac{G_{P3\_1}S^7 + G_{P3\_2}S^6 + G_{P3\_3}S^5 + G_{P3\_4}S^4 + G_{P3\_5}S^3 + G_{P3\_6}S^2 + G_{P3\_7}S + G_{P3\_8}}{P_{b1}S^7 + P_{b2}S^6 + P_{b3}S^5 + P_{b4}S^4 + P_{b5}S^3 + P_{b6}S^2 + P_{b7}S + P_{b8}} \tag{4.2-48}$$

$$G_{P4} = \frac{G_{P4\_1}S^7 + G_{P4\_2}S^6 + G_{P4\_3}S^5 + G_{P4\_4}S^4 + G_{P4\_5}S^3 + G_{P4\_6}S^2 + G_{P4\_7}S + G_{P4\_8}}{P_{b1}S^7 + P_{b2}S^6 + P_{b3}S^5 + P_{b4}S^4 + P_{b5}S^3 + P_{b6}S^2 + P_{b7}S + P_{b8}} \tag{4.2-49}$$

$$G_{Q1} = \frac{G_{Q1\_1}S^7 + G_{Q1\_2}S^6 + G_{Q1\_3}S^5 + G_{Q1\_4}S^4 + G_{Q1\_5}S^3 + G_{Q1\_6}S^2 + G_{Q1\_7}S + G_{Q1\_8}}{P_{b1}S^7 + P_{b2}S^6 + P_{b3}S^5 + P_{b4}S^4 + P_{b5}S^3 + P_{b6}S^2 + P_{b7}S + P_{b8}} \tag{4.2-50}$$

$$G_{Q2} = \frac{G_{Q2\_1}S^7 + G_{Q2\_2}S^6 + G_{Q2\_3}S^5 + G_{Q2\_4}S^4 + G_{Q2\_5}S^3 + G_{Q2\_6}S^2 + G_{Q2\_7}S + G_{Q2\_8}}{P_{b1}S^7 + P_{b2}S^6 + P_{b3}S^5 + P_{b4}S^4 + P_{b5}S^3 + P_{b6}S^2 + P_{b7}S + P_{b8}} \tag{4.2-51}$$

$$G_{Q3} = \frac{G_{Q3\_1}S^7 + G_{Q3\_2}S^6 + G_{Q3\_3}S^5 + G_{Q3\_4}S^4 + G_{Q3\_5}S^3 + G_{Q3\_6}S^2 + G_{Q3\_7}S + G_{Q3\_8}}{P_{b1}S^7 + P_{b2}S^6 + P_{b3}S^5 + P_{b4}S^4 + P_{b5}S^3 + P_{b6}S^2 + P_{b7}S + P_{b8}}$$

(4.2-52)

$$G_{Q4} = \frac{G_{Q4\_1}S^7 + G_{Q4\_2}S^6 + G_{Q4\_3}S^5 + G_{Q4\_4}S^4 + G_{Q4\_5}S^3 + G_{Q4\_6}S^2 + G_{Q4\_7}S + G_{Q4\_8}}{P_{b1}S^7 + P_{b2}S^6 + P_{b3}S^5 + P_{b4}S^4 + P_{b5}S^3 + P_{b6}S^2 + P_{b7}S + P_{b8}}$$

(4.2-53)

$$\Delta E = E - E_0 \tag{4.2-54}$$

$$\Delta f_g = f_g - f_{g0} \tag{4.2-55}$$

$$G_{Iqg1} = \frac{G_{Iqg11}S^7 + G_{Iqg12}S^6 + G_{Iqg13}S^5 + G_{Iqg14}S^4 + G_{Iqg15}S^3 + G_{Iqg16}S^2 + G_{Iqg17}S + G_{Iqg18}}{P_{b1}S^7 + P_{b2}S^6 + P_{b3}S^5 + P_{b4}S^4 + P_{b5}S^3 + P_{b6}S^2 + P_{b7}S + P_{b8}}$$

(4.2-56)

$$G_{Iqg2} = \frac{G_{Iqg21}S^7 + G_{Iqg22}S^6 + G_{Iqg23}S^5 + G_{Iqg24}S^4 + G_{Iqg25}S^3 + G_{Iqg26}S^2 + G_{Iqg27}S + G_{Iqg28}}{P_{b1}S^7 + P_{b2}S^6 + P_{b3}S^5 + P_{b4}S^4 + P_{b5}S^3 + P_{b6}S^2 + P_{b7}S + P_{b8}}$$

(4.2-57)

$$G_{Idg1} = \frac{G_{Idg11}S^7 + G_{Idg12}S^6 + G_{Idg13}S^5 + G_{Idg14}S^4 + G_{Idg15}S^3 + G_{Idg16}S^2 + G_{Idg17}S + G_{Idg18}}{P_{b1}S^7 + P_{b2}S^6 + P_{b3}S^5 + P_{b4}S^4 + P_{b5}S^3 + P_{b6}S^2 + P_{b7}S + P_{b8}}$$

(4.2-58)

$$G_{Idg2} = \frac{G_{Idg21}S^7 + G_{Idg22}S^6 + G_{Idg23}S^5 + G_{Idg24}S^4 + G_{Idg25}S^3 + G_{Idg26}S^2 + G_{Idg27}S + G_{Idg28}}{P_{b1}S^7 + P_{b2}S^6 + P_{b3}S^5 + P_{b4}S^4 + P_{b5}S^3 + P_{b6}S^2 + P_{b7}S + P_{b8}}$$

(4.2-59)

P_0, Q_0, E_0, f_{g0} are steady-state values for real and reactive power, phase-to-ground voltage, and frequency at drive input connecting to the power grid. G_{P11}–G_{P18}, …, G_{Q41}–G_{Q48}, and G_{Iqg11}–G_{Iqg18}, …, G_{Idg21}–G_{Idg28}, P_{b1}–P_{b8} are characteristic parameters in the form of real constant numbers for a given system. S is the Laplace transform variable. For a given motor drive system, the denominators of the transfer functions for all coefficients (G_{P1}, G_{P2}, G_{P3}, G_{P4}, G_{Q1}, G_{Q2}, G_{Q3}, G_{Q4}, G_{Iqg1}, G_{Iqg2}, G_{Idg1}, and G_{Idg2}) are the same and determined by P_{b1}–P_{b8}. The Detailed model derivation can be found in Appendix C.

Using the transfer function format representing active and reactive power in dynamic models for power systems is introduced in [9] as follows:

$$\frac{\Delta L(S)}{L_0} = \frac{b_n S^n + \cdots + b_1 S + b_0}{a_n S^n + \cdots + a_1 S + a_0} \frac{\Delta V(S)}{V_0} \tag{4.2-60}$$

Since the transfer function format for dynamic load models has been well accepted, therefore, 7^{th} order transfer functions are used for the equivalent dynamic models of VSI motor drive systems.

To verify the accuracy of the dynamic model in Equations (4.2-42) and (4.2-43), a case study is conducted in next section.

The equivalent dynamic model for the low voltage 6-pulse VSI motor drive systems is suitable for normal operating and three-phase balanced fault conditions, when three phases of the rectifier remain in operation. VFDs are most sensitive for balanced three phase faults [32, 33, 34], if the drive is able to ride through a balanced three phase fault, three phases of the rectifier will get involved just as the three phase normal operation mode. The equivalent dynamic models of VSI motor drive systems for unbalanced faults will serve as the future work.

4.3 Verification and Sensitivity Case Studies for VSI Motor drive Systems

4.3.1 Case Study 1

To verify the developed dynamic model for the low voltage 6-pulse PWM-controlled VSI based drive and induction motor systems, a sample system is used as a case study with its parameters listed in Table 4.1.

Table 4.1 Electrical parameters of the motor drive system for Case Study 1

Induction Motor Parameters	Converter, inverter, DC parameters, controller
Nominal Power = 3 HP	Diode forward voltage V_{diode} = 1.3V
Nominal voltage V_b = 220 V (rms)	DC bus capacitor C_{dc} = 3400e-6 F
Nominal frequency f_{rated} = 60 Hz	DC bus resistance r_{dc} = 0 Ω
R_s = 0.435 Ω	DC bus inductance L_{dc} = 0 H
l_s = 0.002 H	Output frequency f_{out} = 59.8 Hz
R_r = 0.816 Ω	PI speed controller Proportional gain K_{pm} = 9
l_r = 0.002 H	PI speed controller Integral gain K_{im} = 10
L_m = 69.31e-3 H	Power Source
Inertia J = 0.089 Kg* m^2	Rated voltage 230V (rms)
Nominal speed n_{rated} = 1705 rpm	Rated frequency f_g = 60Hz
Pole pairs P = 2	Commutation inductance l_c = 10mH
Load torque T_L = 11 NM	
Target speed n_r = 1700 rpm	

The detailed switching model and the dynamic model for the sample system are created using the parameters in Table 4.1 and simulated by Matlab/Simulink. The detailed switching model utilizing the library component, "Space Vector PWM VSI induction motor drive", readily available in Matlab/Simulink. This library component consists of a low voltage 6-pulse VFD with a diode rectifier and a PWM controlled VSI, an induction motor, and the voltage per Hz controller. Its PWM control method is the space vector PWM. The high level schematic and Simulink schematic for this library component are shown in Figure 4.12. The dynamic model is created based on Equations (4.2-42) and (4.2-43).

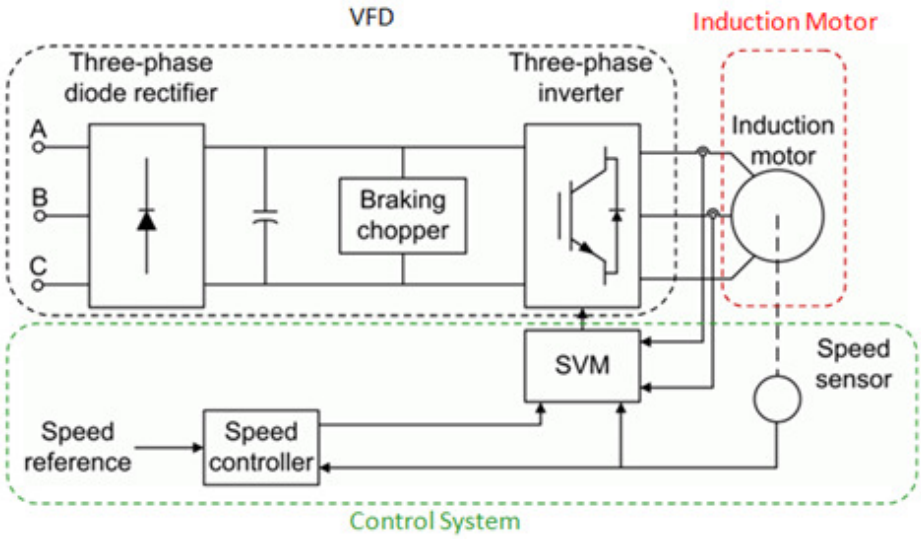

(a) The high level schematic

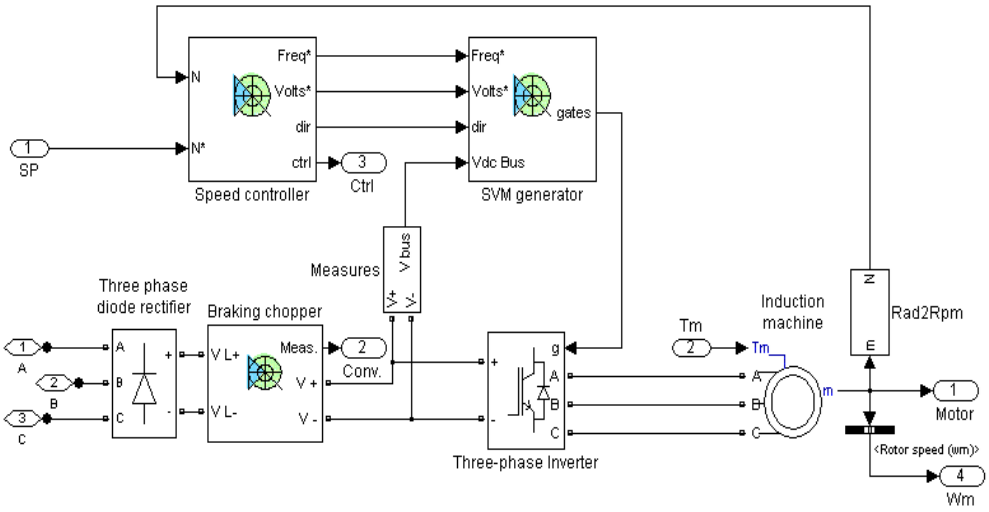

(b) The Simulink schematic

Figure 4.12 “Space Vector PWM VSI induction motor drive” from Matlab/Simulink library [117]

4.3.1.1 Voltage Dependence

The verification of the dynamic model considering voltage dependence is conducted. The power source frequency remains constant in this case. The detailed switching model for the sample system is shown in Figure 4.13.

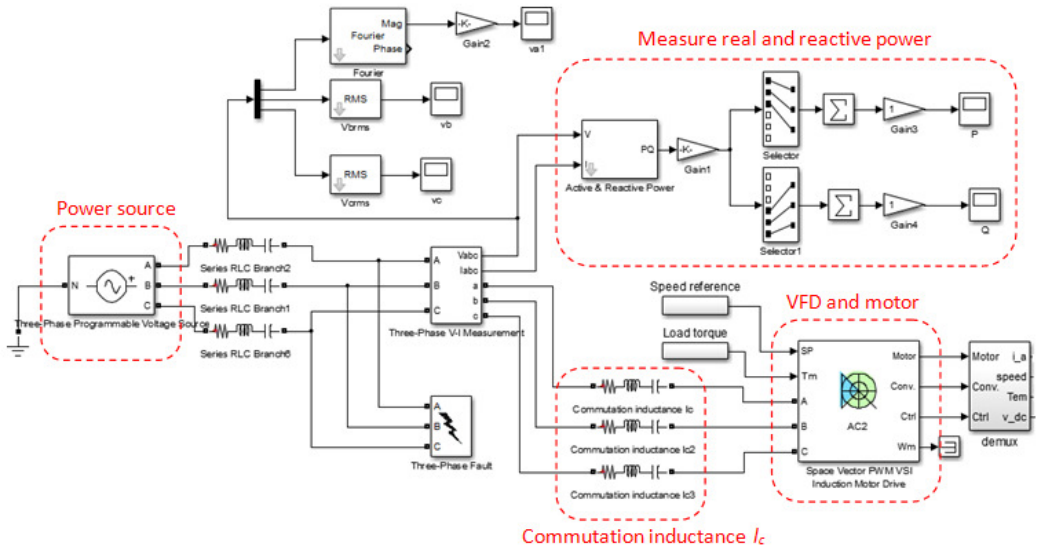

Figure 4.13 The detailed switching model for Case Study 1 (voltage sag)

A three phase fault is applied near the power source in front of the commutation inductance l_c in the detailed model. The fault is applied at 1.4 s and cleared at 1.65 s. The total simulation time is 2 seconds. The applied three phase fault will result in the 90% and 80% voltage sags at the fault location in the detailed switching model to represent real life events.

The dynamic model for the sample system in this case is given in Table 4.2 showing the detailed 7^{th} order transfer functions as coefficients of the dynamic model. The resultant 90% and 80% voltage sags from the detailed switching model are applied directly to the dynamic model. Dynamic responses of the dynamic model are compared with that of the detailed switching model as shown in Figures 4.14 and 4.15. Note: the measured real and reactive power values from the detailed switching model are fundamental components. This applies to all drive simulation cases in this thesis.

Table 4.2 The dynamic model for Case Study 1 (Loading 1)

	Calculated transfer functions for the dynamic model
Derived Dynamic Model	$P = P_0 + G_{P1}\Delta E + G_{P2}\Delta E^2 + (G_{P3} + G_{P4}\Delta E)\Delta f_g$ $Q = Q_0 + G_{Q1}\Delta E + G_{Q2}\Delta E^2 + (G_{Q3} + G_{Q4}\Delta E)\Delta f_g$
P_0, Q_0	2.163kW, 0.916kVAR
G_{P1}	$G_{P1} = \frac{(2.1635\times10^{-5}S^7 + 0.052S^6 + 24.9266S^5 + 5.0718\times10^3 S^4 + 4.7484\times10^5 S^3 + 1.6125\times10^7 S^2 + 1.9576\times10^7 S + 1.4459\times10^6)}{(-1.2103\times10^{-6}S^7 - 8.8511\times10^{-4}S^6 - 0.2787S^5 - 48.3385S^4 - 4.8821\times10^3 S^3 - 2.7531\times10^5 S^2 - 6.8740\times10^6 S - 7.4598\times10^6)}$
G_{P2}	$G_{P2} = \frac{(2.1646\times10^{-8}S^7 + 2.8828\times10^{-4}S^6 + 0.1552S^5 + 32.5514S^4 + 3.006\times10^3 S^3 + 8.9298\times10^4 S^2 - 6.5497\times10^5 S - 8.5988\times10^5)}{(-1.2103\times10^{-6}S^7 - 8.8511\times10^{-4}S^6 - 0.2787S^5 - 48.3385S^4 - 4.8821\times10^3 S^3 - 2.7531\times10^5 S^2 - 6.8740\times10^6 S - 7.4598\times10^6)}$
G_{P3}	$G_{P3} = \frac{(-4.2410\times10^{-6}S^7 - 0.0102S^6 - 4.8862S^5 - 994.1934S^4 - 9.308\times10^4 S^3 - 3.161\times10^6 S^2 - 3.8373\times10^6 S - 2.8343\times10^5)}{(-1.2103\times10^{-6}S^7 - 8.8511\times10^{-4}S^6 - 0.2787S^5 - 48.3385S^4 - 4.8821\times10^3 S^3 - 2.7531\times10^5 S^2 - 6.8740\times10^6 S - 7.4598\times10^6)}$
G_{P4}	$G_{P4} = \frac{(-3.1938\times10^{-8}S^7 - 7.6763\times10^{-5}S^6 - 0.0368S^5 - 7.4869S^4 - 700.9526S^3 - 2.3804\times10^4 S^2 - 2.8898\times10^4 S - 2.1344\times10^3)}{(-1.2103\times10^{-6}S^7 - 8.8511\times10^{-4}S^6 - 0.2787S^5 - 48.3385S^4 - 4.8821\times10^3 S^3 - 2.7531\times10^5 S^2 - 6.8740\times10^6 S - 7.4598\times10^6)}$
G_{Q1}	$G_{Q1} = \frac{(4.4123\times10^{-6}S^7 + 0.0282S^6 + 14.7898S^5 + 3.0820\times10^3 S^4 + 2.8545\times10^5 S^3 + 8.7410\times10^6 S^2 - 4.6276\times10^7 S - 6.3892\times10^7)}{(-1.2103\times10^{-6}S^7 - 8.8511\times10^{-4}S^6 - 0.2787S^5 - 48.3385S^4 - 4.8821\times10^3 S^3 - 2.7531\times10^5 S^2 - 6.8740\times10^6 S - 7.4598\times10^6)}$
G_{Q2}	$G_{Q2} = \frac{(-4.4516\times10^{-8}S^7 + 1.556\times10^{-4}S^6 + 0.0935S^5 + 20.1044S^4 + 1.836\times10^3 S^3 + 4.8141\times10^4 S^2 - 7.9003\times10^5 S - 9.6032\times10^5)}{(-1.2103\times10^{-6}S^7 - 8.8511\times10^{-4}S^6 - 0.2787S^5 - 48.3385S^4 - 4.8821\times10^3 S^3 - 2.7531\times10^5 S^2 - 6.8740\times10^6 S - 7.4598\times10^6)}$
G_{Q3}	$G_{Q3} = \frac{(8.7219\times10^{-6}S^7 + 0.0015S^6 - 0.6919S^5 - 221.2662S^4 - 1.7284\times10^4 S^3 + 4.6725\times10^5 S^2 + 6.3518\times10^7 S + 7.1612\times10^7)}{(-1.2103\times10^{-6}S^7 - 8.8511\times10^{-4}S^6 - 0.2787S^5 - 48.3385S^4 - 4.8821\times10^3 S^3 - 2.7531\times10^5 S^2 - 6.8740\times10^6 S - 7.4598\times10^6)}$
G_{Q4}	$G_{Q4} = \frac{(6.5681\times10^{-8}S^7 + 1.115\times10^{-5}S^6 - 0.0052S^5 - 1.6663S^4 - 130.1592S^3 + 3.5187\times10^3 S^2 + 4.7834\times10^5 S + 5.3928\times10^5)}{(-1.2103\times10^{-6}S^7 - 8.8511\times10^{-4}S^6 - 0.2787S^5 - 48.3385S^4 - 4.8821\times10^3 S^3 - 2.7531\times10^5 S^2 - 6.8740\times10^6 S - 7.4598\times10^6)}$

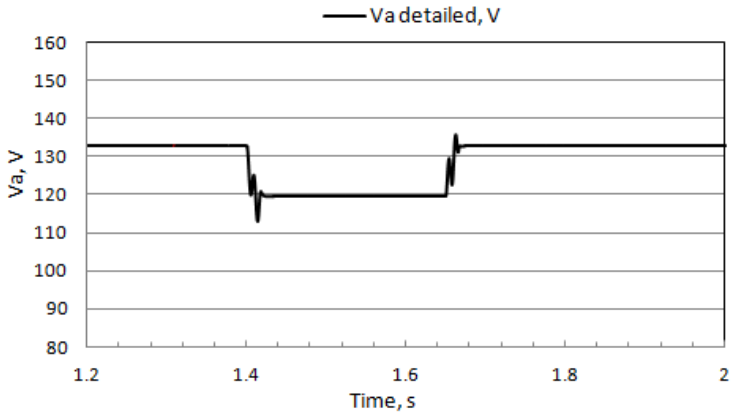

(a) Voltage Sag

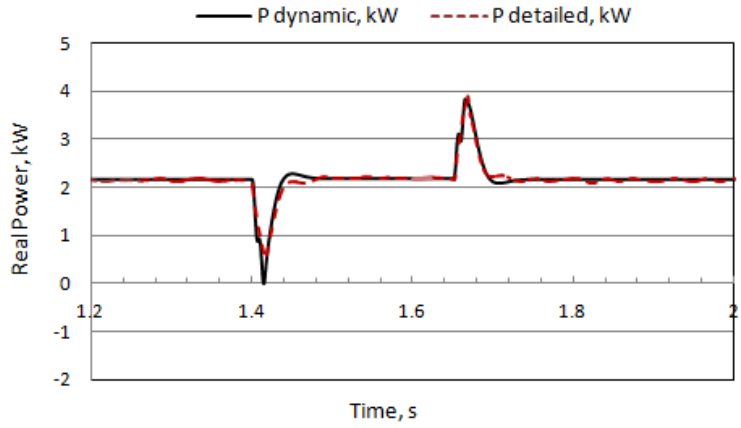

(b) Real Power P

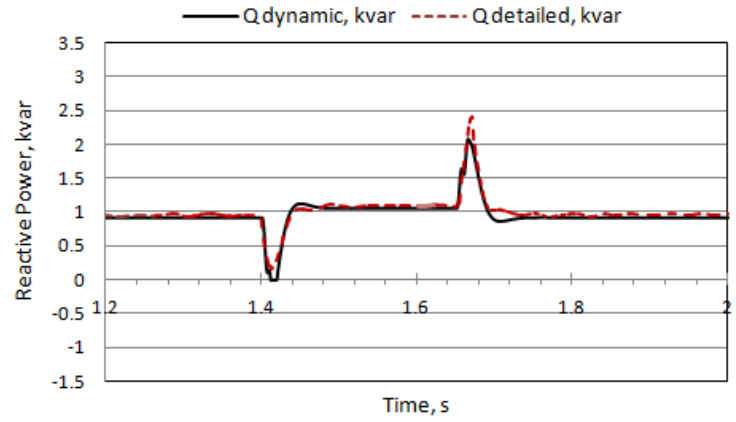

(c) Reactive Power Q

Figure 4.14 Dynamic responses of the dynamic and detailed switching models for Case Study 1, 90% voltage sag

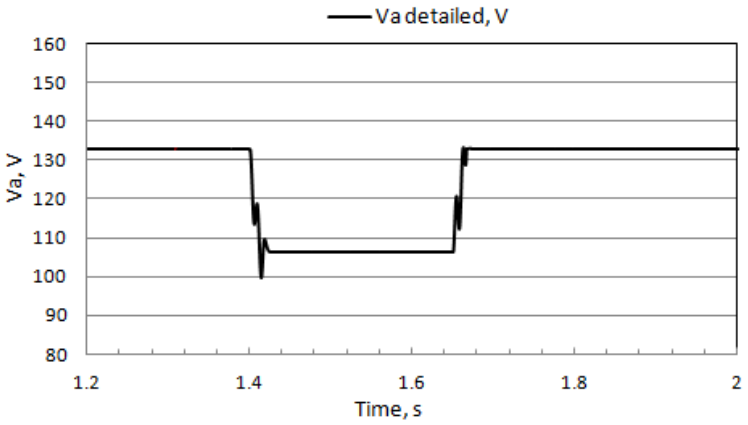

(a) Voltage Sag

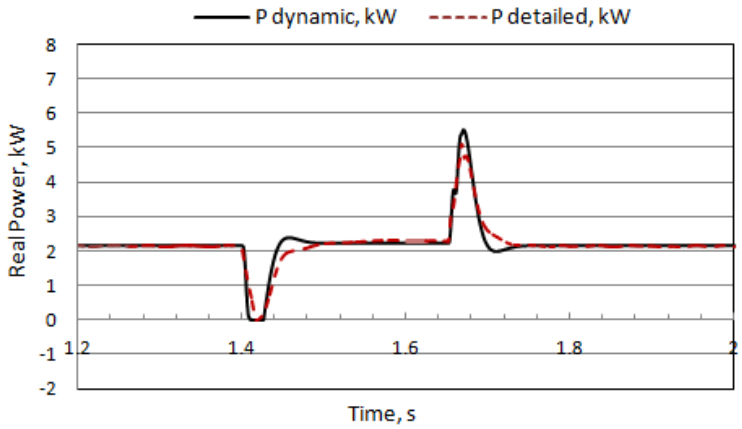

(b) Real Power P

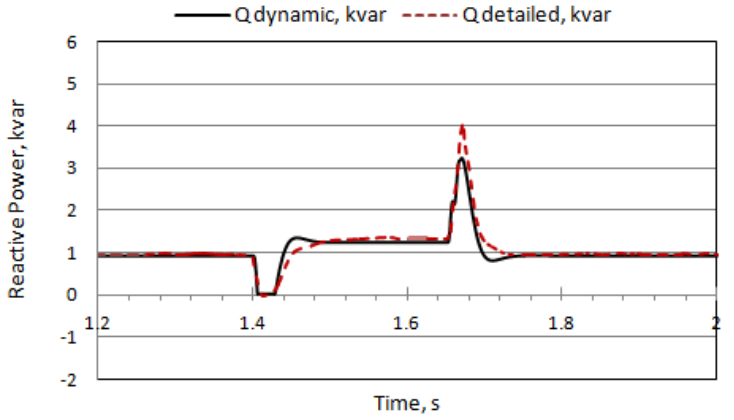

(c) Reactive Power Q

Figure 4.15 Dynamic responses of the dynamic and detailed switching models for Case Study 1, 80% voltage sag

It is found that dynamic responses of the dynamic model have good agreements with that of the detailed switching model under 90% and 80% voltage sag conditions. Therefore, it is verified that the dynamic model considering voltage dependence is accurate.

4.3.1.2 Frequency Dependence

The equivalent dynamic model of VSI motor drive systems considering frequency dependence is verified. The parameters used in the simulation are the same as Table 4.1 except the following slight loading and speed changes of the induction motor: Load torque T_L= 12 NM, and Target speed n_r = 1705 rpm.

The detailed switching model is shown in Figure 4.16. The dynamic model in this case can be found in Table 4.3.

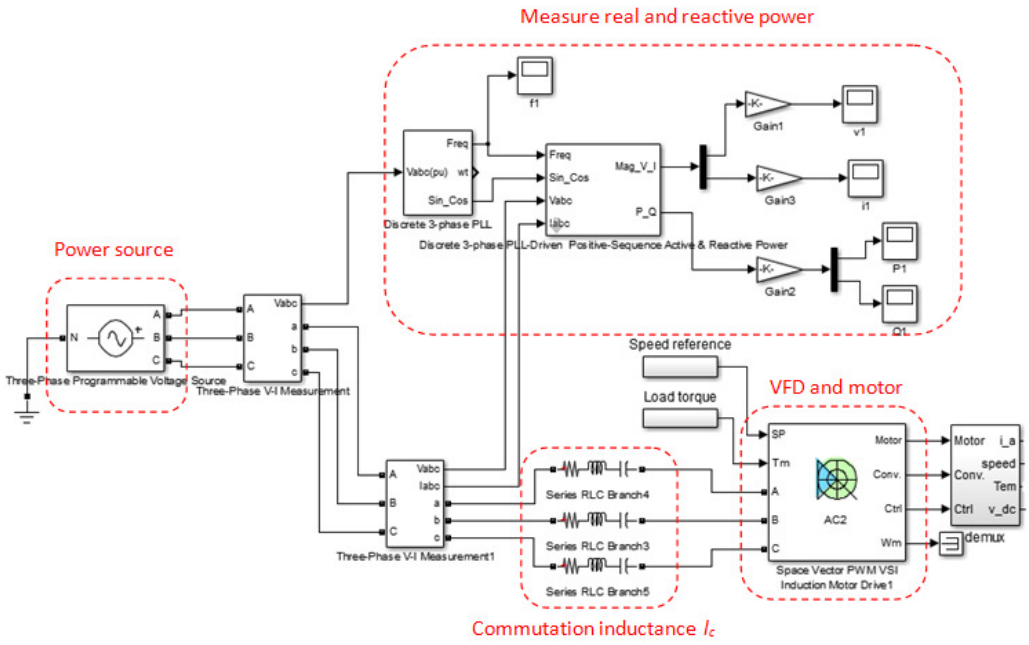

Figure 4.16 The detailed switching model for Case Study 1 (frequency variation)

Table 4.3 The dynamic model for Case Study 1 (Loading 2)

	Calculated transfer functions for the dynamic model
Derived Dynamic Model	$P = P_0 + G_{P1}\Delta E + G_{P2}\Delta E^2 + (G_{P3} + G_{P4}\Delta E)\Delta f_g$ $Q = Q_0 + G_{Q1}\Delta E + G_{Q2}\Delta E^2 + (G_{Q3} + G_{Q4}\Delta E)\Delta f_g$
P_0, Q_0	2.390kW, 1.079kVAR
G_{P1}	$G_{P1} = \frac{\left(2.5104\times10^{-5}S^7 + 0.055S^6 + 25.9075S^5 + 5.2246\times10^3 S^4 + 4.8122\times10^5 S^3 + 1.5598\times10^7 S^2 + 2.0327\times10^7 S + 2.728\times10^6\right)}{\left(-1.257\times10^{-6}S^7 - 9.1785\times10^{-4}S^6 - 0.2882S^5 - 49.6932S^4 - 4.966\times10^3 S^3 - 2.76\times10^5 S^2 - 6.7504\times10^6 S - 7.3298\times10^6\right)}$
G_{P2}	$G_{P2} = \frac{\left(2.8061\times10^{-8}S^7 + 2.9631\times10^{-4}S^6 + 0.1582S^5 + 32.9807S^4 + 2.9879\times10^3 S^3 + 8.2116\times10^4 S^2 - 7.1147\times10^5 S - 9.182\times10^5\right)}{\left(-1.257\times10^{-6}S^7 - 9.1785\times10^{-4}S^6 - 0.2882S^5 - 49.6932S^4 - 4.966\times10^3 S^3 - 2.76\times10^5 S^2 - 6.7504\times10^6 S - 7.3298\times10^6\right)}$
G_{P3}	$G_{P3} = \frac{\left(-5.4979\times10^{-6}S^7 - 0.012S^6 - 5.674S^5 - 1144.2S^4 - 1.0539\times10^5 S^3 - 3.4161\times10^6 S^2 - 4.4519\times10^6 S - 5.9746\times10^5\right)}{\left(-1.257\times10^{-6}S^7 - 9.1785\times10^{-4}S^6 - 0.2882S^5 - 49.6932S^4 - 4.966\times10^3 S^3 - 2.76\times10^5 S^2 - 6.7504\times10^6 S - 7.3298\times10^6\right)}$
G_{P4}	$G_{P4} = \frac{\left(-4.1403\times10^{-8}S^7 - 9.0638\times10^{-5}S^6 - 0.0427S^5 - 8.6169S^4 - 793.6598S^3 - 2.5726\times10^4 S^2 - 3.3526\times10^4 S - 4.4993\times10^3\right)}{\left(-1.257\times10^{-6}S^7 - 9.1785\times10^{-4}S^6 - 0.2882S^5 - 49.6932S^4 - 4.966\times10^3 S^3 - 2.76\times10^5 S^2 - 6.7504\times10^6 S - 7.3298\times10^6\right)}$
G_{Q1}	$G_{Q1} = \frac{\left(5.4298\times10^{-6}S^7 + 0.0312S^6 + 16.2491S^5 + 3.3658\times10^3 S^4 + 3.0591\times10^5 S^3 + 8.702\times10^6 S^2 - 5.6084\times10^7 S - 7.53\times10^7\right)}{\left(-1.257\times10^{-6}S^7 - 9.1785\times10^{-4}S^6 - 0.2882S^5 - 49.6932S^4 - 4.966\times10^3 S^3 - 2.76\times10^5 S^2 - 6.7504\times10^6 S - 7.3298\times10^6\right)}$
G_{Q2}	$G_{Q2} = \frac{\left(-5.4008\times10^{-8}S^7 + 1.6593\times10^{-4}S^6 + 0.1006S^5 + 21.5953S^4 + 1.9288\times10^3 S^3 + 4.4695\times10^4 S^2 - 9.3198\times10^5 S - 1.1204\times10^6\right)}{\left(-1.257\times10^{-6}S^7 - 9.1785\times10^{-4}S^6 - 0.2882S^5 - 49.6932S^4 - 4.966\times10^3 S^3 - 2.76\times10^5 S^2 - 6.7504\times10^6 S - 7.3298\times10^6\right)}$
G_{Q3}	$G_{Q3} = \frac{\left(1.0582\times10^{-5}S^7 + 0.0018S^6 - 0.8597S^5 - 271.8093S^4 - 2.0493\times10^4 S^3 + 6.7872\times10^5 S^2 + 7.5495\times10^7 S + 8.5129\times10^7\right)}{\left(-1.257\times10^{-6}S^7 - 9.1785\times10^{-4}S^6 - 0.2882S^5 - 49.6932S^4 - 4.966\times10^3 S^3 - 2.76\times10^5 S^2 - 6.7504\times10^6 S - 7.3298\times10^6\right)}$
G_{Q4}	$G_{Q4} = \frac{\left(7.9686\times10^{-8}S^7 + 1.321\times10^{-5}S^6 - 0.0065S^5 - 2.0469S^4 - 154.3265S^3 + 5.1112\times10^3 S^2 + 5.6853\times10^5 S + 6.4108\times10^5\right)}{\left(-1.257\times10^{-6}S^7 - 9.1785\times10^{-4}S^6 - 0.2882S^5 - 49.6932S^4 - 4.966\times10^3 S^3 - 2.76\times10^5 S^2 - 6.7504\times10^6 S - 7.3298\times10^6\right)}$

The disturbance in this case is a step decrease of the power source frequency from 60Hz to 52Hz. The frequency variation is applied at 1.4 s and cleared at 1.65 s at the power source in the detailed switching model. The total simulation time is 2 seconds. It is interesting to notice when the power source frequency is changed, the voltage will vary slightly, i.e., the frequency variation causes a frequency sag and corresponding small voltage variation in the detailed switching model. The resultant frequency sag and voltage variation are applied directly to the developed dynamic model for model verification purpose.

The dynamic responses of the dynamic model and the detailed switching model at the drive AC input during the frequency disturbance are simulated by Matlab/Simulink and compared in Figure 4.17.

It is found that dynamic responses of the dynamic model have good agreements with that of the detailed switching model. Therefore, it is verified that the dynamic model considering frequency dependence is accurate.

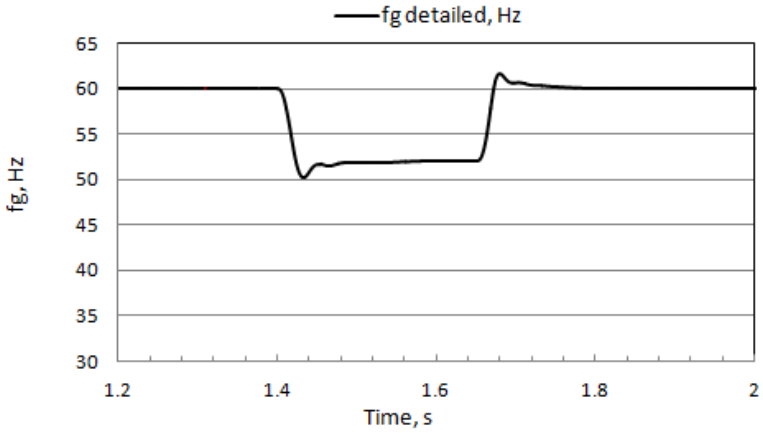

(a) Frequency variation

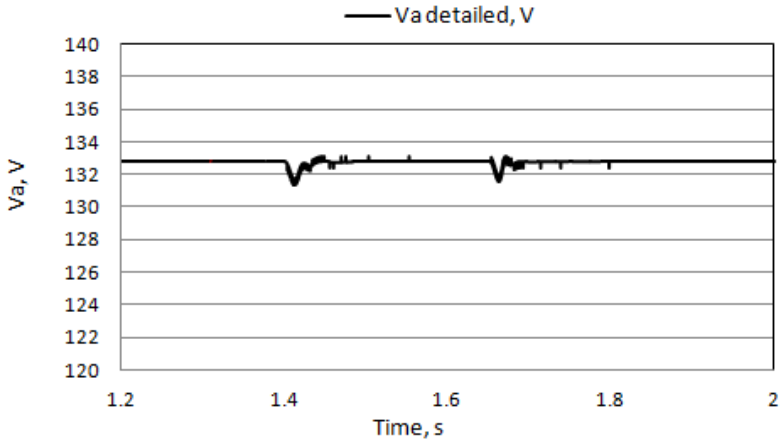

(b) Voltage variation caused by frequency variation

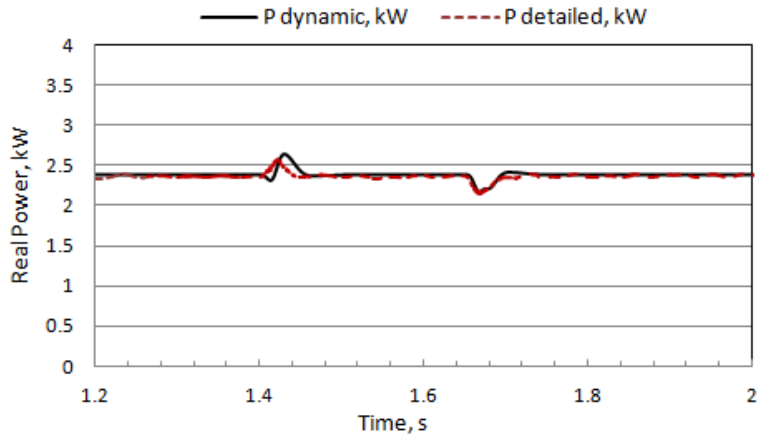

(c) Real Power P

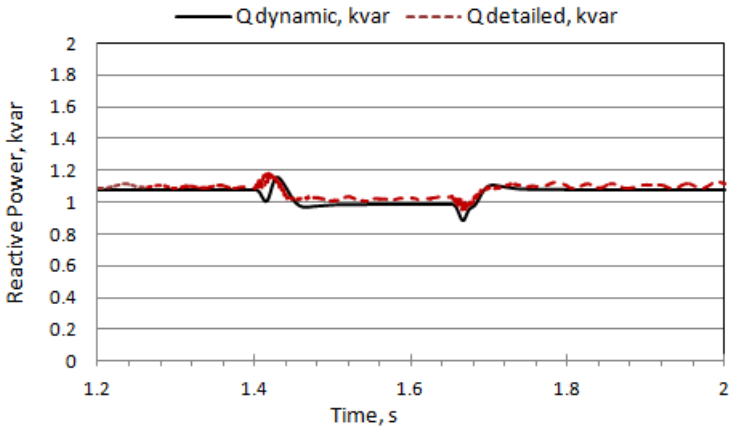

(d) Reactive Power Q

Figure 4.17 Dynamic responses of the dynamic and detailed switching models for Case Study 1, frequency variation

4.3.1.3 Voltage Sag and Frequency Variation

In this scenario, it is assumed that the voltage sag and the frequency variation happen at the same time in the system. To simulate such a condition, the detailed switching model of the system has a three-phase fault applied in front of the commutation inductance l_c, which causes the 92.2% voltage sag. In the mean while, the power source frequency decreases from 60 Hz to 52 Hz. Both voltage sag and frequency variation are applied to the detailed switching model at 1.4 s and cleared at 1.65 s with total simulation time equal to 2 seconds.

The detailed switching model is shown in Figure 4.18 with a frequency step variation applied at the power source and a three-phase fault applied at the upstream of the commutation inductance. The simulation parameters are the same as that used for the frequency dependence verification in Section 4.3.2. The developed dynamic model is the same as Table 4.3.

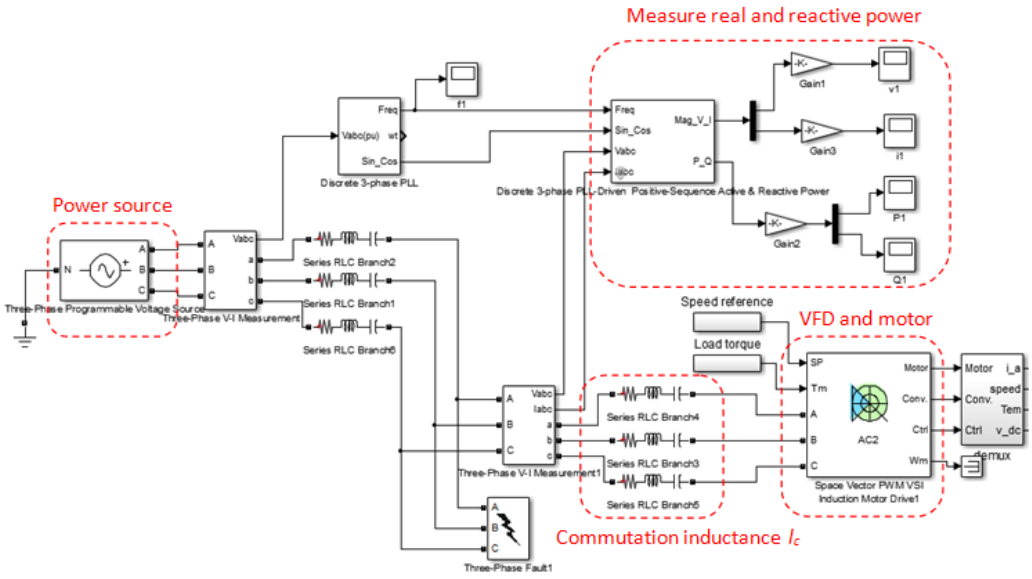

Figure 4.18 The detailed switching model for Case Study 1 (voltage sag and frequency variation)

The dynamic responses of the dynamic model and the detailed switching model for this scenario are shown in Figure 4.19. There are good agreements

between the two models, which provide further verification of the accuracy of the dynamic model.

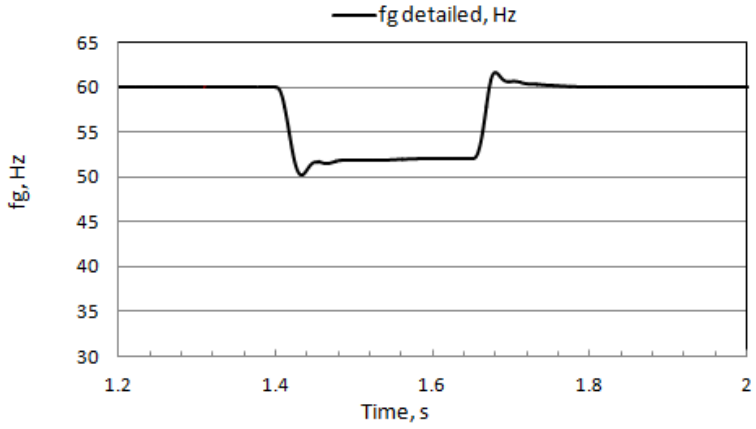

(a) Frequency variation

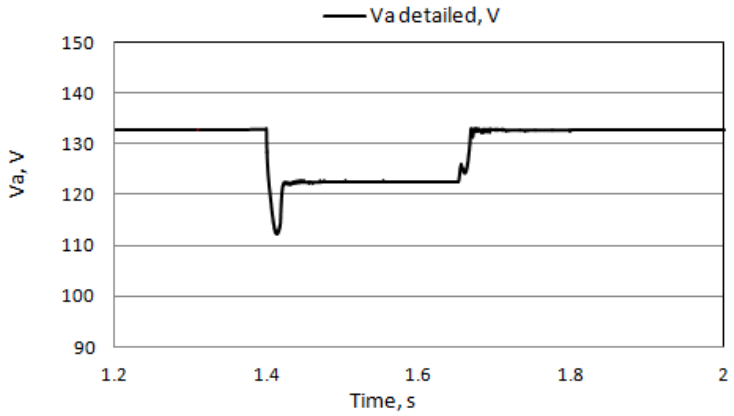

(b) Voltage variation

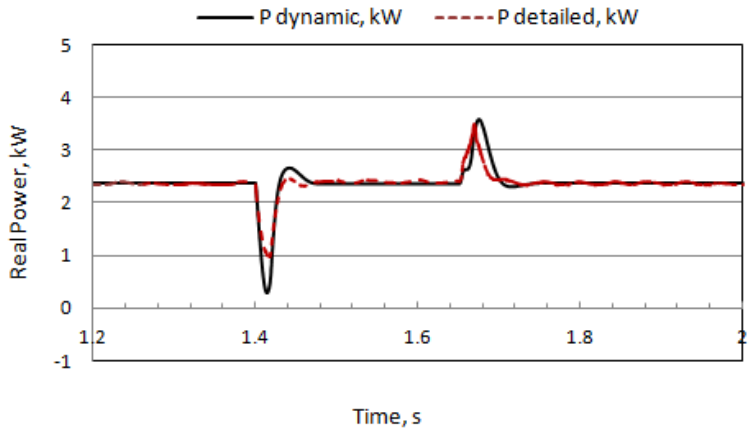

(c) Real power

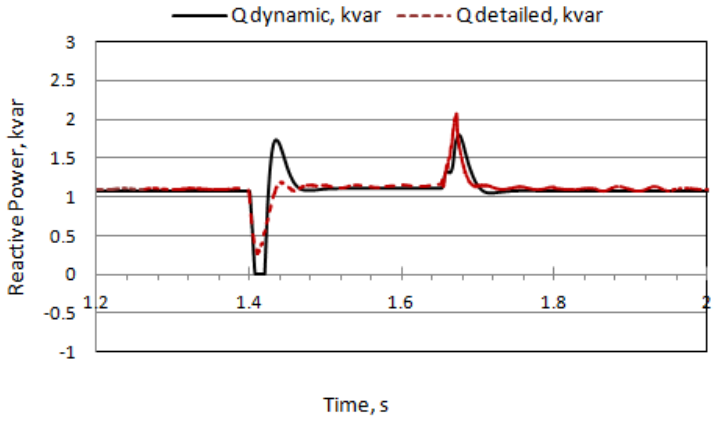

(d) Reactive power

Figure 4.19 Dynamic responses of the dynamic and detailed switching models for Case Study 1, voltage sag and frequency variation

4.3.2 Case Study 2

To further verify the dynamic model for low voltage 6-pulse VSI drives and induction motor systems, the second case study is conducted. The detailed switching model and the equivalent dynamic model for Case Study 2 are created using the parameters listed in Table 4.4. The data of the 25 HP induction motor are from Table E.2 in Appendix E.

Table 4.4 Electrical parameters of the motor drive system for Case Study 2

Induction Motor Parameters	Converter, inverter, DC parameters, controller
Nominal Power = 25 HP	Diode forward voltage V_{diode} = 1.3V
Nominal voltage V_b = 460 V (rms)	DC bus capacitor C_{dc} = 4500e-6 F
Nominal frequency f_{rated} = 60 Hz	DC bus resistance r_{dc} = 0 Ω
R_s = 0.249 Ω	DC bus inductance L_{dc} = 0 H
l_s = 0.0015 H	Output frequency f_{out} = 60 Hz
R_r = 0.536 Ω	PI speed controller Proportional gain K_{pm} = 9
l_r = 0.0015 H	PI speed controller Integral gain K_{im} = 10
L_m = 58.7e-3 H	**Power Source**
Inertia J = 0.554 Kg* m^2	Rated voltage 480V (rms)
Nominal speed n_{rated} = 1695 rpm	Rated frequency f_g = 60Hz
Pole pairs P = 2	Commutation inductance l_c = 4mH
Load torque T_L = 87.5 NM	
Target speed n_r = 1695 rpm	

4.3.2.1 Voltage Dependence

The system configuration of the detailed switching model for Case Study 2 is similar to Figure 4.13. The power source frequency remains constant in this case.

A three phase fault is applied near the power source in front of the commutation inductance l_c in the detailed switching model. The fault is applied at 4.4 s and cleared at 4.65 s. The total simulation time is 5 seconds. The applied three-phase fault will result in the 90% and 80% voltage sags.

The dynamic model for Case Study 2 is provided in Table 4.5. The resultant 90% and 80% voltage sags from the detailed switching model are applied directly to the developed dynamic model.

The dynamic responses at the fault location for the dynamic model are compared with that for the detailed switching model in Case Study 2 as shown in Figures 4.20 and 4.21. Good agreements between the two models are obtained. Therefore, it is verified by Case Study 2 that the dynamic model considering the voltage dependence is accurate.

Table 4.5 The dynamic model for Case Study 2

	Calculated transfer functions for the dynamic model
Derived Dynamic Model	$P = P_0 + G_{P1}\Delta E + G_{P2}\Delta E^2 + (G_{P3} + G_{P4}\Delta E)\Delta f_g$ $Q = Q_0 + G_{Q1}\Delta E + G_{Q2}\Delta E^2 + (G_{Q3} + G_{Q4}\Delta E)\Delta f_g$
P_0, Q_0	17.114kW, 6.436kVAR
G_{P1}	$G_{P1} = \frac{\left(\begin{array}{l}6.7595\times10^{-5}S^7 + 0.217S^6 + 102.1273S^5 + 1.9886\times10^4 S^4 + \\ 1.8184\times10^6 S^3 + 6.409\times10^7 S^2 + 8.2785\times10^7 S + 1.1622\times10^7\end{array}\right)}{\left(\begin{array}{l}-1.0261\times10^{-6}S^7 - 7.1073\times10^{-4}S^6 - 0.2262S^5 - 42.5586S^4 \\ -4.9247\times10^3 S^3 - 3.2899\times10^5 S^2 - 9.8519\times10^6 S - 1.0757\times10^6\end{array}\right)}$
G_{P2}	$G_{P2} = \frac{\left(\begin{array}{l}2.2889\times10^{-8}S^7 + 6.2982\times10^{-4}S^6 + 0.3198S^5 + 62.5897S^4 + \\ 5.5009\times10^3 S^3 + 1.604\times10^5 S^2 - 1.8234\times10^6 S - 2.2752\times10^6\end{array}\right)}{\left(\begin{array}{l}-1.0261\times10^{-6}S^7 - 7.1073\times10^{-4}S^6 - 0.2262S^5 - 42.5586S^4 \\ -4.9247\times10^3 S^3 - 3.2899\times10^5 S^2 - 9.8519\times10^6 S - 1.0757\times10^6\end{array}\right)}$
G_{P3}	$G_{P3} = \frac{\left(\begin{array}{l}-1.9532\times10^{-5}S^7 - 0.0627S^6 - 29.5108S^5 - 5.7462\times10^3 S^4 - \\ 5.2545\times10^5 S^3 - 1.8519\times10^7 S^2 - 2.3922\times10^7 S - 3.3583\times10^6\end{array}\right)}{\left(\begin{array}{l}-1.0261\times10^{-6}S^7 - 7.1073\times10^{-4}S^6 - 0.2262S^5 - 42.5586S^4 \\ -4.9247\times10^3 S^3 - 3.2899\times10^5 S^2 - 9.8519\times10^6 S - 1.0757\times10^6\end{array}\right)}$
G_{P4}	$G_{P4} = \frac{\left(\begin{array}{l}-7.0481\times10^{-8}S^7 - 2.2623\times10^{-4}S^6 - 0.1065S^5 - 20.7349S^4 - \\ 1.8961\times10^3 S^3 - 6.6826\times10^4 S^2 - 8.6319\times10^4 S - 1.2118\times10^4\end{array}\right)}{\left(\begin{array}{l}-1.0261\times10^{-6}S^7 - 7.1073\times10^{-4}S^6 - 0.2262S^5 - 42.5586S^4 \\ -4.9247\times10^3 S^3 - 3.2899\times10^5 S^2 - 9.8519\times10^6 S - 1.0757\times10^6\end{array}\right)}$
G_{Q1}	$G_{Q1} = \frac{\left(\begin{array}{l}1.149\times10^{-5}S^7 + 0.1022S^6 + 50.8228S^5 + 9.9336\times10^3 S^4 + \\ 8.8225\times10^5 S^3 + 2.7167\times10^7 S^2 - 2.0314\times10^8 S - 2.6542\times10^8\end{array}\right)}{\left(\begin{array}{l}-1.0261\times10^{-6}S^7 - 7.1073\times10^{-4}S^6 - 0.2262S^5 - 42.5586S^4 \\ -4.9247\times10^3 S^3 - 3.2899\times10^5 S^2 - 9.8519\times10^6 S - 1.0757\times10^6\end{array}\right)}$
G_{Q2}	$G_{Q2} = \frac{\left(\begin{array}{l}-5.7507\times10^{-8}S^7 + 3.0007\times10^{-4}S^6 + 0.1616S^5 + 31.74S^4 + \\ 2.7085\times10^3 S^3 + 6.6299\times10^4 S^2 - 1.6833\times10^6 S - 1.9953\times10^6\end{array}\right)}{\left(\begin{array}{l}-1.0261\times10^{-6}S^7 - 7.1073\times10^{-4}S^6 - 0.2262S^5 - 42.5586S^4 \\ -4.9247\times10^3 S^3 - 3.2899\times10^5 S^2 - 9.8519\times10^6 S - 1.0757\times10^6\end{array}\right)}$
G_{Q3}	$G_{Q3} = \frac{\left(\begin{array}{l}4.9073\times10^{-5}S^7 + 0.0068S^6 - 3.1357S^5 - 697.3895S^4 - \\ 3.4788\times10^3 S^3 + 8.9479\times10^6 S^2 + 5.6174\times10^8 S + 6.2596\times10^8\end{array}\right)}{\left(\begin{array}{l}-1.0261\times10^{-6}S^7 - 7.1073\times10^{-4}S^6 - 0.2262S^5 - 42.5586S^4 \\ -4.9247\times10^3 S^3 - 3.2899\times10^5 S^2 - 9.8519\times10^6 S - 1.0757\times10^6\end{array}\right)}$
G_{Q4}	$G_{Q4} = \frac{\left(\begin{array}{l}1.7708\times10^{-7}S^7 + 2.4433\times10^{-5}S^6 - 0.0113S^5 - 2.5165S^4 - \\ 12.5532S^3 + 3.2288\times10^4 S^2 + 2.027\times10^6 S + 2.2587\times10^6\end{array}\right)}{\left(\begin{array}{l}-1.0261\times10^{-6}S^7 - 7.1073\times10^{-4}S^6 - 0.2262S^5 - 42.5586S^4 \\ -4.9247\times10^3 S^3 - 3.2899\times10^5 S^2 - 9.8519\times10^6 S - 1.0757\times10^6\end{array}\right)}$

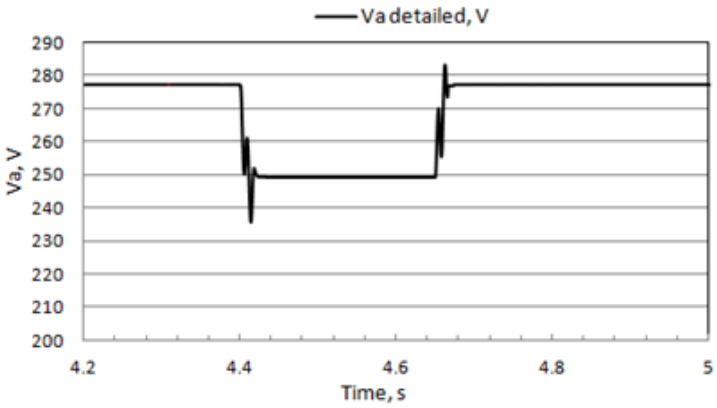

(a) Voltage Sag

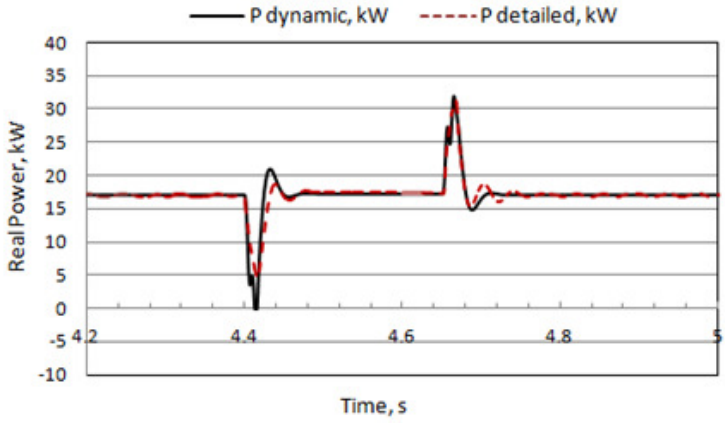

(b) Real Power P

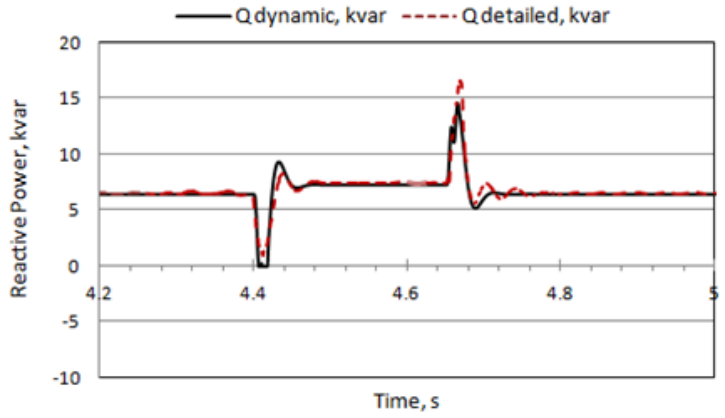

(c) Reactive Power Q

Figure 4.20 Dynamic responses of the dynamic and detailed switching models for Case Study 2, 90% voltage sag

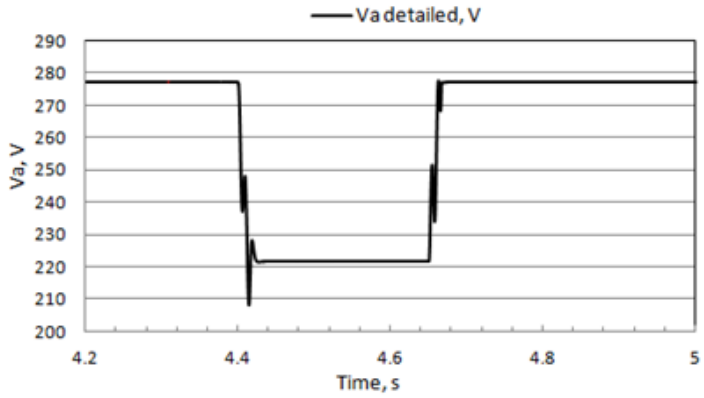

(a) Voltage Sag

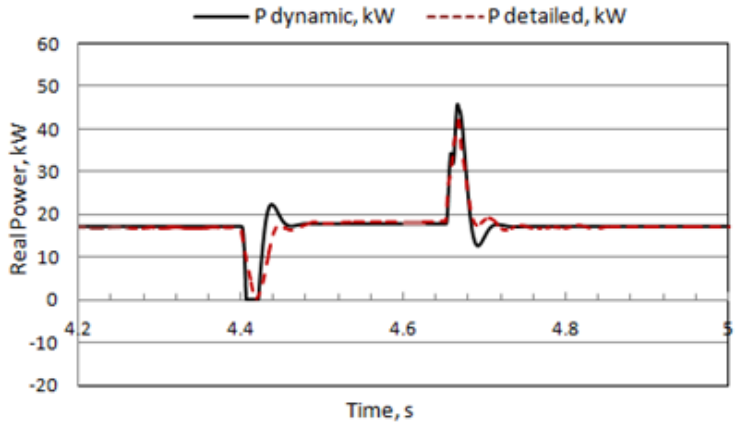

(b) Real Power P

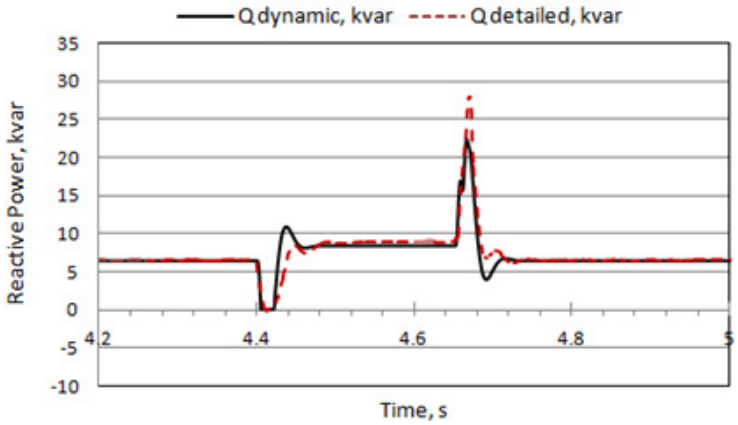

(c) Reactive Power Q

Figure 4.21 Dynamic responses of the dynamic and detailed switching models for Case Study 2, 80% voltage sag

4.3.2.2 Frequency Dependence

The disturbance in this case is the frequency step decrease at the power source from 60 Hz to 52 Hz. The frequency variation is applied at 4.4 s and cleared at 4.65 s in the detailed switching model. The total simulation time is 5 seconds. It is interesting to notice when the power source frequency is changed, the voltage will vary slightly, i.e., the frequency variation causes a frequency sag and corresponding small voltage variation in the detailed switching model. The resultant frequency sag and voltage variation are applied directly to the dynamic model.

The dynamic responses of the dynamic model and the detailed switching model during the frequency disturbance are simulated by Matlab/Simulink and shown in Figure 4.22. Good agreements are obtained between the two models. Therefore, it is verified that the dynamic model considering the frequency dependence is accurate for Case Study 2.

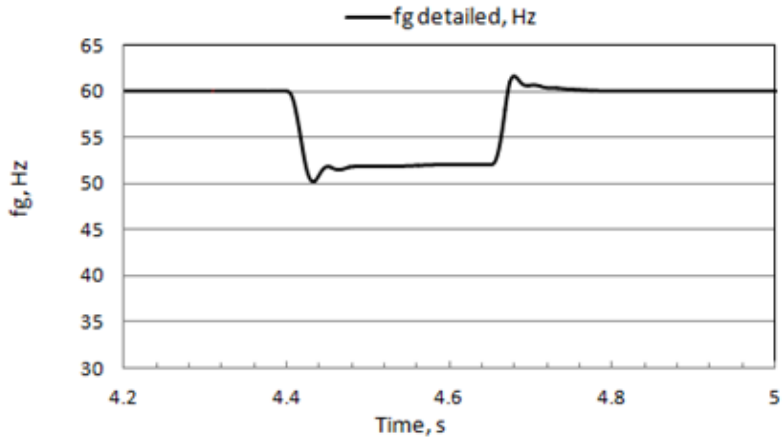

(a) Frequency Sag

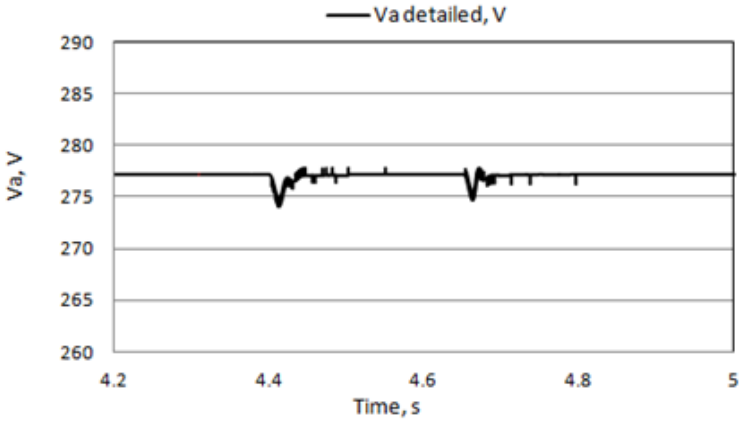

(b) Voltage variation during the frequency sag

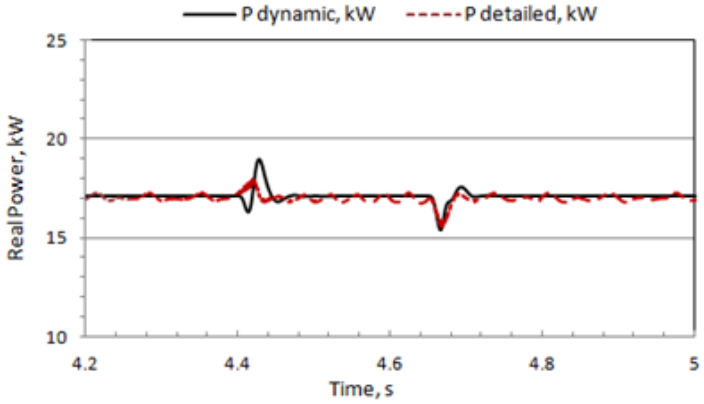

(c) Real Power P

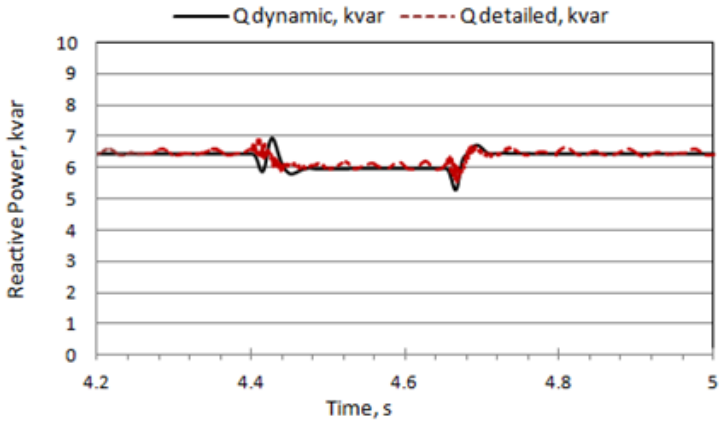

(d) Reactive Power Q

Figure 4.22 Dynamic responses of the dynamic and detailed switching models for Case Study 2, frequency variation

4.3.2.3 Voltage Sag and Frequency Variation

In this scenario, it is assumed that the voltage sag and the frequency variation happen at the same time in the system. To simulate such a condition, the detailed switching model has a three-phase fault applied in front of the commutation inductance l_c, which causes the 92.2% voltage sag, and the power source frequency decreases from 60 Hz to 52 Hz. Both voltage sag and frequency variation are applied to the detailed switching model at 4.4 s and cleared at 4.65 s with total simulation time equal to 5 seconds. The simulation parameters are the same as Table 4.4. The derived dynamic model is the same as Table 4.5.

The dynamic responses of the dynamic model and the detailed switching model for this scenario in Case Study 2 are shown in Figure 4.23. There are good agreements between the two models, which provide further verification of the accuracy for the dynamic model.

Based on the model verification using Case Studies 1 and 2, it is concluded that the equivalent dynamic model is able to capture major dynamic characteristics of the system and accurately determine its contribution to the power grid during disturbances. Therefore, it is an adequate load model for VSI motor drive systems for power systems dynamic studies.

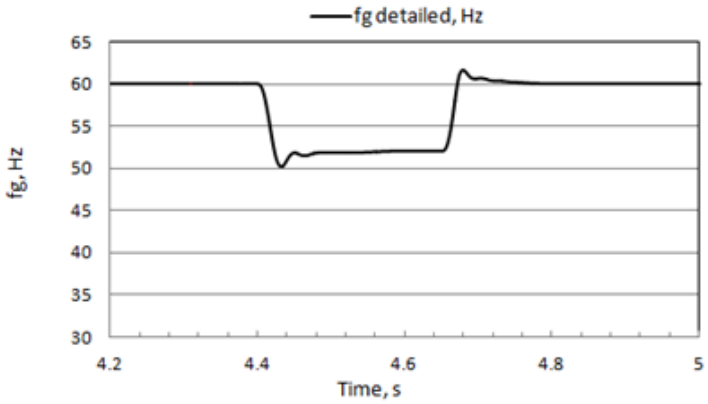

(a) Frequency variation

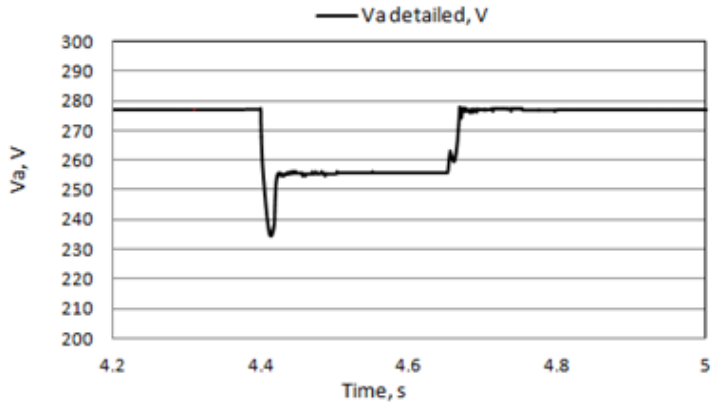

(b) Voltage variation

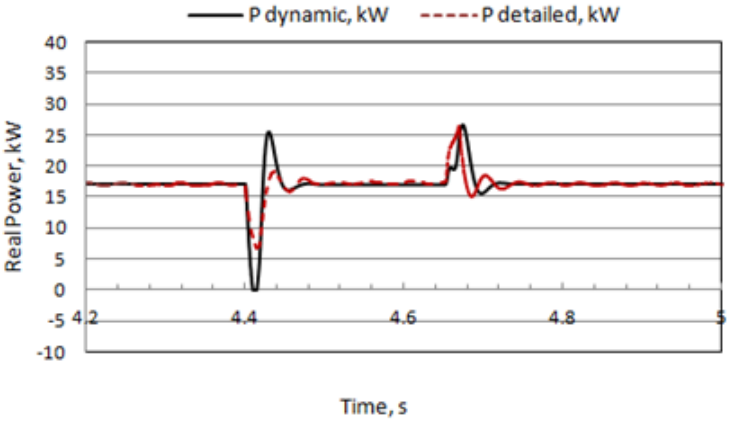

(c) Real power

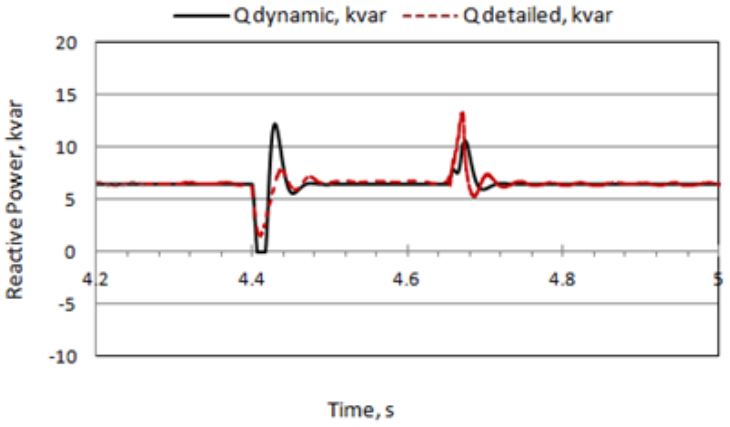

(d) Reactive power

Figure 4.23 Dynamic responses of the dynamic and detailed switching models for Case Study 2, voltage sag and frequency variation

4.3.3 Sensitivity Study

All parameters play a role on overall dynamic responses of motor drive systems, it is important to know their individual influence on the equivalent dynamic model. A sensitivity study is conducted for Case Study 1 evaluating the impact of the following three parameters on dynamic responses of the developed dynamic model: 1) the commutation inductance l_c, 2) the DC link capacitance C_{dc}, and 3) Load torque T_L of the induction motor.

Figure 4.24 shows the dynamic responses of the dynamic model for 90% voltage sag with the commutation inductance l_c varies, the l_c values considered in the simulation are 12 mH, 10 mH, and 5 mH. Other parameters are the same as that in Table 4.1. It is found that the commutation inductance has more influence on dynamic transients on real power than that on reactive power but almost no effect on the steady-state value of the real power. On the other hand, the commutation inductance has significant effect on the steady-state value of the reactive power.

The dynamic responses of the developed dynamic model for 90% voltage sag are shown in Figure 4.25 with the DC link capacitance C_{dc} varies, the C_{dc} values considered in the simulation are 2500 μF, 3400 μF and 4500 μF. Other parameters are the same as that in Table 4.1. It is found that increasing the DC link capacitance tends to increase the magnitude of the dynamic transient for real and reactive power. The DC link capacitance has no effect on the steady-state values for the real and reactive power.

The following three different load torques T_L applied to the induction motor for Case Study 1 for 90% voltage sag: 5 NM, 8 NM, and 11 NM, which correspond to 42%, 67%, and 92% loading of the motor, respectively. Other parameters are the same as Table 4.1. The simulated dynamic responses of the developed dynamic model in this case are shown in Figure 4.26. It is found that

the load torque/loading factor of the motor has significant effect on both steady-state and dynamic transient responses for real and reactive power.

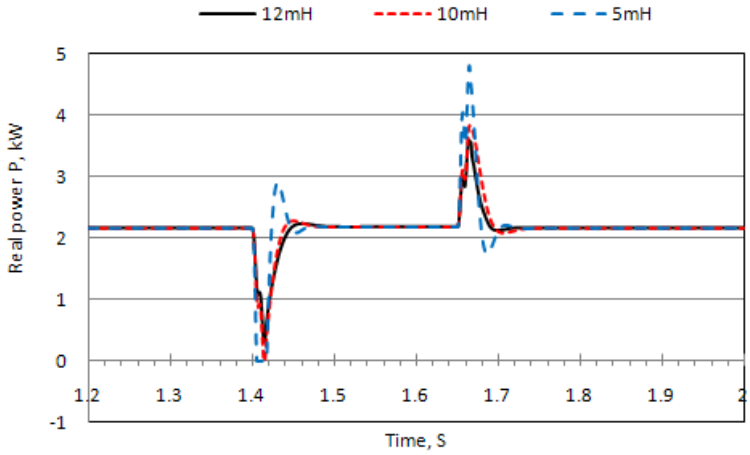

(a) Real power P

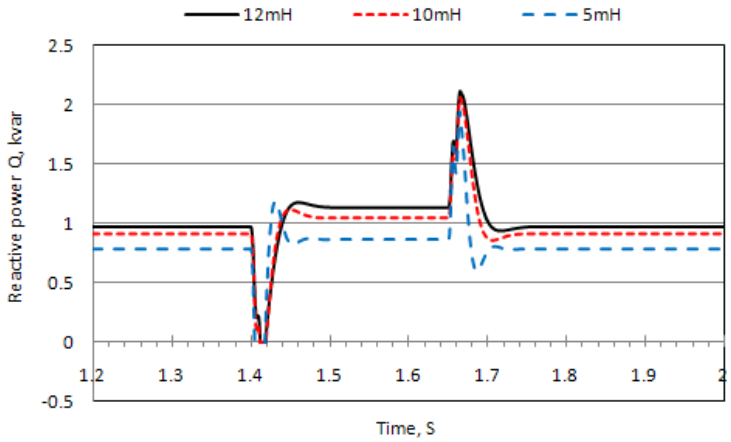

(b) Reactive power Q

Figure 4.24 Commutation inductance l_c

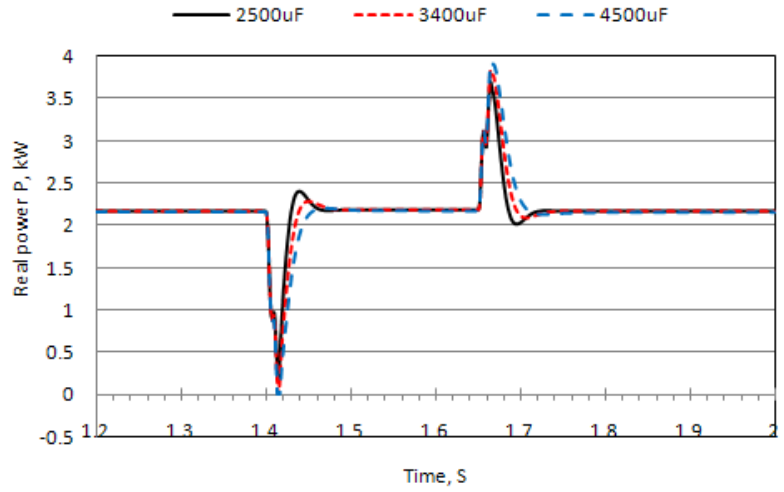

(a) Real power P

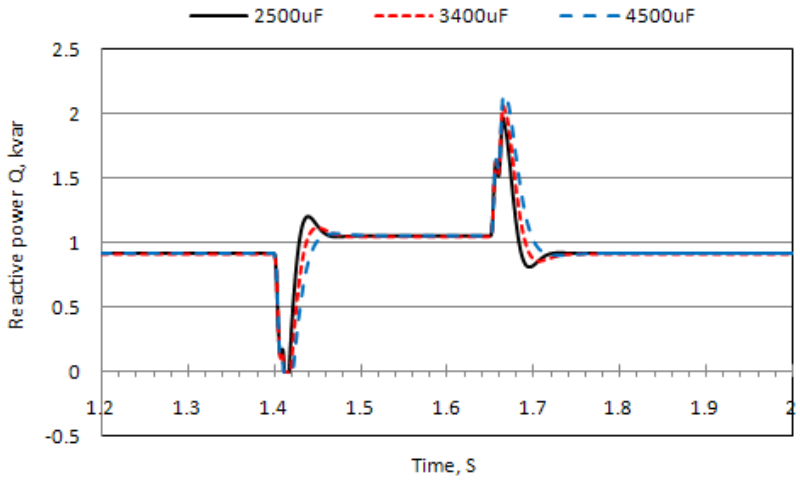

(b) Reactive power Q

Figure 4.25 DC link capacitance C_{dc}

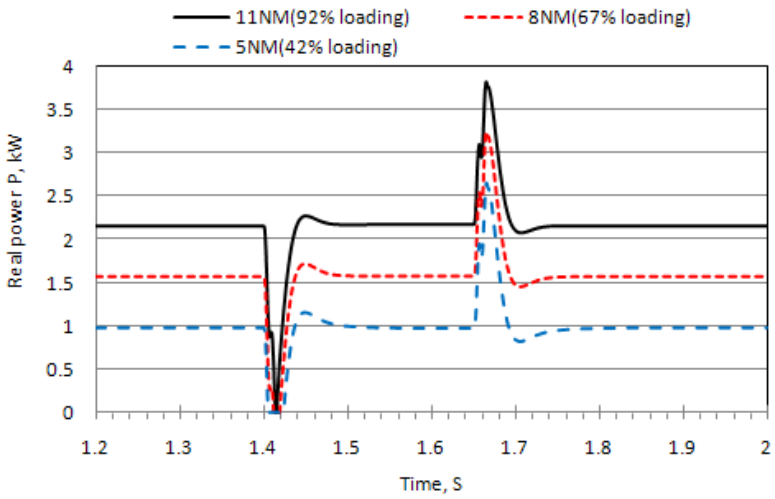

(a) Real power P

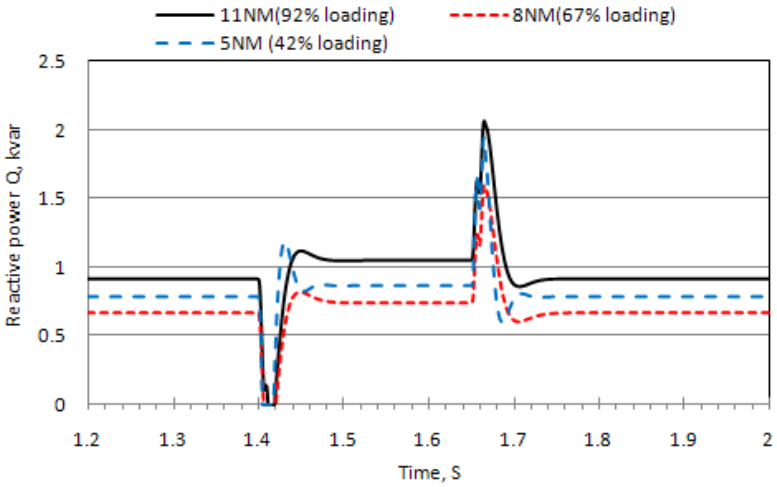

(b) Reactive power Q

Figure 4.26 Load torque of the motor T_L

4.4 Dynamic Model for Cascaded Inverter Motor Drive Systems

4.4.1 Overview of Motor Drive Systems

The cascaded H-bridge multi-level inverter type medium voltage drives are one of topologies for very high power applications [118-122]. This type of medium voltage drive and induction motor systems is modeled in the thesis. The drive is constructed using a series of low voltage power module. Usually, nine power modules will form an 18-pulse, and twelve power modules will form a 24-pulse system at the drive input.

The topology of a nine-module 18-pulse medium voltage drive is shown in Figure 4.3 [118]. With three power modules in series per phase, the drive can produce as much as 1440Vac line-to-neutral, or 2494Vac line-to-line at the output. The voltage waveforms consist of seven distinct line-to-neutral voltage levels (±1800, ±1200, ±600, or 0 volts). Similarly, for a twelve-module 24-pulse medium voltage drive, it can produce line-to-neutral voltage up to 1920Vac (line-to-line voltage up to 3325V). At the drive input, there is a phase-shifting transformer, and the phase-shift angle differs by multiple of 20º for 2400Vac 18-pulse drives and by multiple of 15º for 3300Vac 24-pulse drives [118].

The configuration of each power module is shown in Figure 4.27 [118, 120]. Each power module is a static PWM power converter, there is a three phase full bridge diode converter exactly the same as the low voltage 6-pulse drive, which is capable of receiving input power from one of the phase-shifting transformer secondary's at 480Vac, 50/60Hz, charges a DC link capacitor to about 600Vdc. The DC voltage feeds a single-phase full bridge inverter, which is delivered to a single-phase load at any voltage up to 480Vac [118]. The output of multiple single-phase inverters will be connected in series feeding one phase of an induction motor as shown in Figure 4.28 [121].

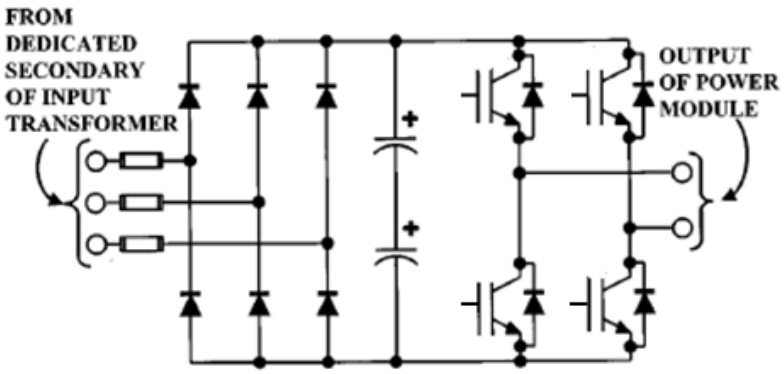

Figure 4.27 A typical power module [118, 120]

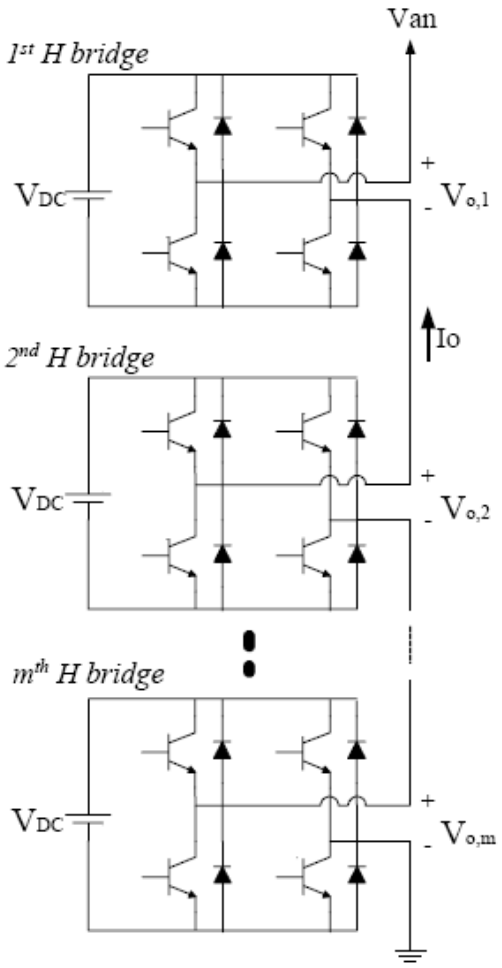

Figure 4.28 One phase of H bridge cascaded multi-level inverter connecting to Phase a of an induction motor [121]

4.4.2 Mathematical Model of Each Power Module

The dynamic model derivation of the medium voltage cascaded H-bridge multi-level inverter drives starts from the low voltage power module. For each low voltage power module connected to the transformer secondary windings without phase-shifting (phase-shifting angles equal to 0º), the dc link voltage from the diode converter can be calculated as follows:

$$v_d = \frac{3\sqrt{6}}{\pi} E - \frac{3}{\pi} l_c (2\pi f_g) i_d - 2l_c \frac{di_d}{dt} - 2V_{diode} \tag{4.6-1}$$

$$v_d = r_{dc} i_d + L_{dc} \frac{di_d}{dt} + e_d \tag{4.6-2}$$

$$i_I = i_d - C_{dc} \frac{de_d}{dt} \tag{4.6-3}$$

$$P_{ea} = \frac{3}{2}\left(v_{dg} i_{dg} + v_{qg} i_{qg}\right) \tag{4.6-4}$$

$$Q_{ea} = \frac{3}{2}\left(v_{qg} i_{dg} - v_{dg} i_{qg}\right) \tag{4.6-5}$$

$$v_{qg} = \sqrt{2}E \tag{4.6-6}$$

$$v_{dg} = 0 \tag{4.6-7}$$

$$i_{dg} = i_{dgcom} + i_{dgcond} \tag{4.6-8}$$

$$i_{dgcom} = \frac{2\sqrt{3}}{\pi} i_d \left[-\cos\left(u - \frac{5\pi}{6}\right) + \cos\left(-\frac{5\pi}{6}\right) \right] + \frac{3\sqrt{2}E}{\pi l_c (2\pi f_g)} \sin u - \frac{3\sqrt{2}E}{4\pi l_c (2\pi f_g)} \sin 2u - \frac{3\sqrt{2}E}{2\pi l_c (2\pi f_g)} u \tag{4.6-9}$$

$$i_{dgcond} = \frac{2\sqrt{3}}{\pi} i_d \left[-\cos\left(\frac{7\pi}{6}\right) + \cos\left(u + \frac{5\pi}{6}\right) \right] \tag{4.6-10}$$

$$i_{qg} = i_{qgcom} + i_{qgcond} \tag{4.6-11}$$

$$i_{qgcom} = \frac{2\sqrt{3}}{\pi} i_d \left[\sin\left(u - \frac{5\pi}{6}\right) - \sin\left(-\frac{5\pi}{6}\right) \right] + \frac{3\sqrt{2}E}{\pi l_c (2\pi f_g)} (\cos u - 1) + \frac{3\sqrt{2}E}{4\pi l_c (2\pi f_g)} (1 - \cos 2u)$$

(4.6-12)

$$i_{qgcond} = \frac{2\sqrt{3}}{\pi} i_d \left[\sin\left(\frac{7\pi}{6}\right) - \sin\left(u + \frac{5\pi}{6}\right) \right] \quad (4.6\text{-}13)$$

$$u = \arccos\left[1 - \frac{2l_c (2\pi f_g) i_d}{\sqrt{6}E} \right] \quad (4.6\text{-}14)$$

where,

P_{ea} and Q_{ea} – active and reactive power at the input of each power module,

l_c – the commutation inductance, which is the sum of the power source inductance and the inductance of the phase-shifting transformer

E – the rms phase-to-ground voltage supplied to the power module,

f_g – the power supply frequency at the input of the drive.

v_d – the DC link voltage after rectifier

e_d – the DC link voltage before inverter

i_d – the DC link current after rectifier

i_I – the DC link current entering inverter

V_{diode} – the diode forward voltage

C_{dc} – the capacitance of DC link capacitor

r_{dc} – the resistance of DC link

L_{dc} – the inductance of DC link reactor

v_{qg} – q-axis power source voltage at the input of each power module

v_{dg} – d-axis power source voltage at the input of each power module

i_{qg} – q-axis ac current at the input of each power module

i_{qgcom} – q-axis ac current at the input of each power module during commutation period

i_{qgcond} – q-axis ac current at the input of each power module during conduction period

i_{dg} – d-axis ac current at the input of each power module

i_{dgcom} – d-axis ac current at the input of each power module during commutation period

i_{dgcond} – d-axis ac current at the input of each power module during conduction period

u – commutation angle

It is verified in this study that the dc link voltages from the diode converters connected to the transformer secondary windings with phase-shifting angles not equal to 0º are exactly the same as Equation (4.6.1).

The output voltage from the single-phase full bridge inverter for each power module can be determined as follows:

$$V_0 = de_d \tag{4.6-15}$$

where V_0 is the output voltage from each power module, d is duty cycle.

For an 18-pulse system with three power modules each phase connected to the induction motors, the phase a voltage of the induction motor can be determined as follows:

$$n_{pulse} = 18$$

$$V_{an} = \left(\frac{n_{pulse}}{6} \right) de_d \cos\theta \tag{4.6-16}$$

where n_{pulse} is the pulse number of the MVD, V_{an} is the voltage at phase a of the induction motor.

The voltages at phases b and c can be determined similarly as follows:

$$V_{bn} = \left(\frac{n_{pulse}}{6} \right) de_d \cos\left(\theta - \frac{2\pi}{3} \right)$$

$$V_{cn} = \left(\frac{n_{pulse}}{6} \right) de_d \cos\left(\theta + \frac{2\pi}{3} \right)$$

The three phase voltages of the induction motor in *abc* frame are converted to *dq0* frame as follows:

$$V_{qs} = \left(\frac{n_{pulse}}{6}\right) de_d \tag{4.6-17}$$

$$V_{ds} = 0 \tag{4.6-18}$$

where,

v_{qs} – q-axis voltage at the terminal of induction motor

v_{ds} – d-axis voltage at the terminal of induction motor

The differential equations for induction motors are the same as Equations (4.2-20)-(4.2-29), so they will not be repeated here.

4.4.3 Modeling of Motor Drive System Control Scheme

The real power supplying to the induction motor for an 18-pulse MVD P_{ac_IM} is:

$$P_{ac\_IM} = \frac{3}{2}\left(V_{ds} i_{qs} + V_{qs} i_{qs}\right) = \frac{3}{2} V_{qs} i_{qs} = \frac{3}{2} \times \left(\frac{n_{pulse}}{6} de_d\right) i_{qs} = \left(\frac{n_{pulse}}{4}\right) de_d i_{qs} \tag{4.6-19}$$

The total DC power at DC links for all power modules corresponding to real power supplying to the induction motor for the 18-pulse MVD is:

$$P_{dc} = \left(\frac{n_{pulse}}{2}\right) P_{dc\_per\,module} = \left(\frac{n_{pulse}}{2}\right) e_d i_I \tag{4.6-20}$$

Ignoring the losses at the inverters at the power modules, the following equation is satisfied:

$$P_{ac\_IM} = P_{dc} \tag{4.6-21}$$

Substitute Equations (4.6-19) and (4.6-20) in Equation (4.6-21):

$$\left(\frac{n_{pulse}}{4}\right) de_d i_{qs} = \left(\frac{n_{pulse}}{2}\right) e_d i_I \tag{4.6-22}$$

Substitute Equation (4.6-3) in Equation (4.6-22), we have

$$\frac{1}{2}de_d i_{qs} = e_d\left(i_d - C_{dc}\frac{de_d}{dt}\right) \tag{4.6-23}$$

The q-axis component of the motor stator current can be determined from Equation (4.6-23) as follows:

$$i_{qs} = \frac{2i_d}{d} - 2C_{dc}\left(\frac{de_d}{dt}\frac{1}{d}\right) \tag{4.6-24}$$

Linearize Equation (4.6-24):

$$\Delta i_{qs} = \frac{2}{d_0}\Delta i_d - \frac{i_{qs0}}{d_0}\Delta d - \frac{2C_{dc}}{d_0}S\Delta e_d \tag{4.6-25}$$

Substitute Equations (4.6-17) and (4.6-18) in Equation (4.2-34) yield:

$$\begin{bmatrix} v_{qs}^{e*} \\ v_{ds}^{e*} \end{bmatrix} = \begin{bmatrix} \cos\theta_{ce} & \sin\theta_{ce} \\ -\sin\theta_{ce} & \cos\theta_{ce} \end{bmatrix}\begin{bmatrix} v_{qs} \\ v_{ds} \end{bmatrix} = \begin{bmatrix} \cos\theta_{ce} & \sin\theta_{ce} \\ -\sin\theta_{ce} & \cos\theta_{ce} \end{bmatrix}\begin{bmatrix} \frac{n_{pulse}}{6}de_d \\ 0 \end{bmatrix} \tag{4.6-26}$$

From Equation (4.2-36), the following relationships are obtained:

$$d = \frac{\sqrt{\left(v_{qs}^{e*}\right)^2 + \left(v_{ds}^{e*}\right)^2}}{\left(\frac{n_{pulse}}{6}\right)e_d} \tag{4.6-27}$$

The developed block diagram for the closed-loop voltage per Hz control scheme used for the formula derivation for the 18-pulse MVD-induction motor system is shown in Figure 4.29. The equations for the closed-loop voltage per Hz control are given as follows:

$$\omega_{SL} = K_{pm}\left(\omega_r^* - \omega_r\right) + \int_0^t K_{im}\left(\omega_r^* - \omega_r\right)dt + \left(\omega_{s0} - \omega_{r0}\right) \tag{4.6-28}$$

$$\omega_{SL} + \omega_r = \omega_s \tag{4.6-29}$$

$$d = \frac{\omega_s\left(\frac{V_b}{\omega_b}\right)\sqrt{2}}{\left(\frac{n_{pulse}}{6}\right)e_d} \tag{4.6-30}$$

$$V_{qs}^{e*} = \omega_s \left(\frac{V_b}{\omega_b} \right) \sqrt{2} \tag{4.6-31}$$

$$V_{ds}^{e*} = 0 \tag{4.6-32}$$

where K_{pm} is speed PI controller proportional gain, and K_{im} is speed PI controller integral gain.

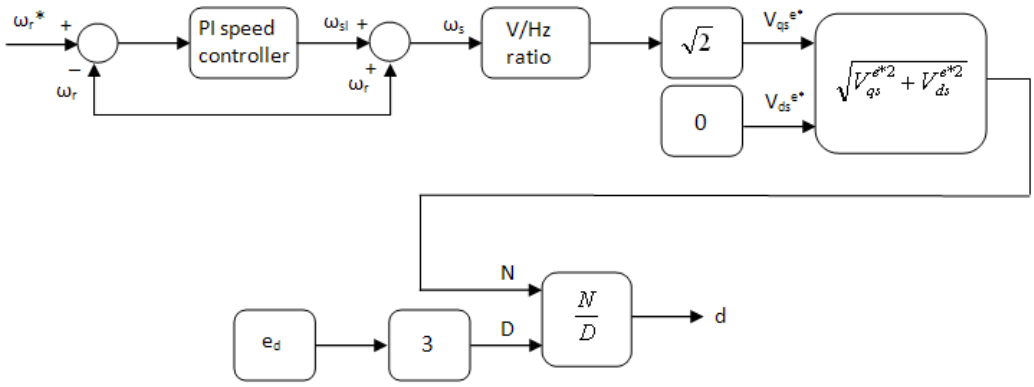

Figure 4.29 Voltage per Hz control scheme for the 18-pulse cascaded inverter motor drive system

Linearize Equations (4.6-28) and (4.6-29), the relationship between ω_s and ω_r can be determined as follows:

$$\Delta\omega_s = \frac{A_{11}S + A_{12}}{S} \Delta\omega_r \tag{4.6-33}$$

Linearize Equation (4.6-30):

$$\Delta d = \left(-\frac{\sqrt{2}V_b \omega_{s0}}{\frac{n_{pulse}}{6} \omega_b e_{d0}^2} \right) \Delta e_d + \left(\frac{\sqrt{2}V_b}{\frac{n_{pulse}}{6} \omega_b e_{d0}} \right) \Delta\omega_s \tag{4.6-34}$$

Substitute Equation (4.6-34) in Equation (4.6-25):

$$\Delta i_{qs} = A_{21}\Delta i_d + A_{22}\Delta\omega_s + (A_{231}S + A_{232})\Delta e_d \tag{4.6-35}$$

$$A_{21} = \frac{2}{d_0} \tag{4.6-36}$$

$$A_{22} = -\frac{\sqrt{2} i_{qs0} V_b}{\frac{n_{pulse}}{6} d_0 \omega_b e_{d0}} \tag{4.6-37}$$

$$A_{231} = -\frac{2C_{dc}}{d_0} \tag{4.6-38}$$

$$A_{232} = \frac{\sqrt{2} i_{qs0} V_b \omega_{s0}}{\frac{n_{pulse}}{6} d_0 \omega_b e_{d0}^2} \tag{4.6-39}$$

Linearize Equation (4.6-17):

$$\Delta V_{qs} = \left(\frac{n_{pulse}}{6} \right) d_0 \Delta e_d + \left(\frac{n_{pulse}}{6} \right) e_{d0} \Delta d \tag{4.6-40}$$

Substitute Equation (4.6-34) in Equation (4.6-40), we have

$$\Delta V_{qs} = \left(\frac{n_{pulse}}{6} \right) d_0 \Delta e_d + \left(\frac{n_{pulse}}{6} e_{d0} \right) \left(- \frac{\sqrt{2} V_b \omega_{s0}}{\frac{n_{pulse}}{6} \omega_b e_{d0}^2} \Delta e_d + \frac{\sqrt{2} V_b}{\frac{n_{pulse}}{6} \omega_b e_{d0}} \Delta \omega_s \right) \tag{4.6-41}$$

$$= A_{31} \Delta \omega_s + A_{32} \Delta e_d$$

$$A_{31} = \frac{\sqrt{2} V_b}{\omega_b} \tag{4.6-42}$$

$$A_{32} = \frac{n_{pulse}}{6} d_0 - \frac{\sqrt{2} V_b \omega_{s0}}{\omega_b e_{d0}} \tag{4.6-43}$$

4.4.4 The Equivalent Dynamic Model

At the input of the MVD, the real and reactive power at each power module are the same, and thus, the total real and reactive power of the 18-pulse MVD can be expressed by the power module number, which is 9 for 18-pulse MVD, multiplied by the real ad reactive power for each power module as follows:

$$P_{ac} = \left(\frac{n_{pulse}}{2} \right) P_{ac\_per\,module} \tag{4.6-44}$$

$$Q_{ac} = \left(\frac{n_{pulse}}{2} \right) Q_{ac\_per\,module} \tag{4.6-45}$$

$$P_{ac\_per\,module} = \frac{3}{2}\left(V_{dg} i_{dg} + V_{qg} i_{qg} \right) \tag{4.6-46}$$

$$Q_{ac\_per\,module} = \frac{3}{2}\left(-V_{dg} i_{qg} + V_{qg} i_{dg} \right) \tag{4.6-47}$$

$$V_{qg} = \sqrt{2}E \tag{4.6-48}$$

$$V_{dg} = 0 \tag{4.6-49}$$

The method for deriving the dynamic model for the 18-pulse cascaded inverter motor drive systems are similar to the 6-pulse VSI motor drive systems, and the detailed derivation can be found in Appendix F.

The derived dynamic model for the cascaded inverter motor drive systems is given as follows, which has the same format as that for VSI motor drive systems:

$$P = P_0 + G_{P1}\Delta E + G_{P2}\Delta E^2 + \left(G_{P3} + G_{P4}\Delta E \right)\Delta f_g \tag{4.6-50}$$

$$Q = Q_0 + G_{Q1}\Delta E + G_{Q2}\Delta E^2 + \left(G_{Q3} + G_{Q4}\Delta E \right)\Delta f_g \tag{4.6-51}$$

where the formula of all coefficients G_{P1}-G_{P4} and G_{Q1}-G_{Q4} are the same as Equations (4.2-46) – (4.2-53).

4.5 Verification and Sensitivity Case Studies for Cascaded Inverter Motor Drive Systems

4.5.1 Case Study

To verify the dynamic model for the cascaded inverter motor drive systems, a case study is conducted. The system consists an 18-pulse MVD with cascaded H-bridge inverter, a 2300V 1500HP rated induction motor with voltage per Hz control. The detailed switching model and the dynamic models for this case study are created using the parameters listed in Table 4.6. The data of the motor are from Table E.2 in Appendix E. The derived dynamic mathematical model for the given system is provided in Table 4.7.

Table 4.6 Electrical parameters of the cascaded inverter motor drive system

Induction Motor Parameters	Converter, inverter, DC parameters, controller
Nominal Power = 1500 HP Nominal voltage V_b = 2300 V (rms) Nominal frequency f_{rated} = 60 Hz R_s = 0.056 Ω l_s = 0.001 H R_r = 0.037 Ω l_r = 0.001 H L_m = 0.0527 H Inertia J = 44.548 Kg* m^2 Nominal speed n_{rated} = 1783 rpm Pole pairs P = 2 Load torque T_L = 1500 NM Target speed n_r = 1771 rpm	Diode forward voltage V_{diode} = 1.3V DC bus capacitor C_{dc} = 10000e-6 F DC bus resistance r_{dc} = 0 Ω DC bus inductance L_{dc} = 0 H Output frequency f_{out} = 60 Hz PI speed controller Proportional gain K_{pm} = 9 PI speed controller Integral gain K_{im} = 10 **Power Source** Rated voltage 480V (rms) Rated frequency f_g = 60Hz Commutation inductance l_c including the phase-shifting transformer impedance = 1.2mH

4.5.1.1 Voltage Dependence

The detailed switching model used in the simulation for voltage dependence verification is shown in Figure 4.30. The 90% and 80% voltage sags are applied at the power source in the dynamic model and the detailed switching model at 14.4 s and cleared at 14.65 s. The total simulation time is 15 seconds.

Table 4.7 The dynamic model for the cascaded inverter motor drive system

	The derived dynamic model for the sample MVD-induction motor system
Derived Dynamic Model	$P = P_0 + G_{P1}\Delta E + G_{P2}\Delta E^2 + (G_{P3} + G_{P4}\Delta E)\Delta f_g$ $Q = Q_0 + G_{Q1}\Delta E + G_{Q2}\Delta E^2 + (G_{Q3} + G_{Q4}\Delta E)\Delta f_g$
P_0, Q_0	291kW, 73kVAR
G_{P1}	$G_{P1} = \frac{\left(\begin{array}{l}0.0388S^7 + 203.1771S^6 + 3.9584\times10^4 S^5 + 9.4318\times10^5 S^4 + \\ 3.2896\times10^7 S^3 + 2.6099\times10^8 S^2 + 1.3533\times10^9 S + 8.0349\times10^8\end{array}\right)}{\left(\begin{array}{l}-3.5641\times10^{-5} S^7 - 0.0133S^6 - 2.8328S^5 - 347.3130S^4 \\ -1.2962\times10^4 S^3 - 3.8931\times10^5 S^2 - 4.6363\times10^6 S - 4.819\times10^6\end{array}\right)}$
G_{P2}	$G_{P2} = \frac{\left(\begin{array}{l}7.2285\times10^{-6} S^7 + 0.6836S^6 + 132.2883S^5 + 2.1104\times10^3 S^4 + \\ 7.0446\times10^4 S^3 - 5.0765\times10^5 S^2 - 1.2378\times10^7 S - 1.5042\times10^7\end{array}\right)}{\left(\begin{array}{l}-3.5641\times10^{-5} S^7 - 0.0133S^6 - 2.8328S^5 - 347.3130S^4 \\ -1.2962\times10^4 S^3 - 3.8931\times10^5 S^2 - 4.6363\times10^6 S - 4.819\times10^6\end{array}\right)}$
G_{P3}	$G_{P3} = \frac{\left(\begin{array}{l}-0.0062S^7 - 32.3206S^6 - 6.2968\times10^3 S^5 - 1.5004\times10^5 S^4 - \\ 5.2329\times10^6 S^3 - 4.1517\times10^7 S^2 - 2.1528\times10^8 S - 1.2782\times10^8\end{array}\right)}{\left(\begin{array}{l}-3.5641\times10^{-5} S^7 - 0.0133S^6 - 2.8328S^5 - 347.3130S^4 \\ -1.2962\times10^4 S^3 - 3.8931\times10^5 S^2 - 4.6363\times10^6 S - 4.819\times10^6\end{array}\right)}$
G_{P4}	$G_{P4} = \frac{\left(\begin{array}{l}-2.2258\times10^{-5} S^7 - 0.1166S^6 - 22.7216S^5 - 541.3991S^4 - \\ 1.8883\times10^4 S^3 - 1.4981\times10^5 S^2 - 7.7682\times10^5 S - 4.6122\times10^5\end{array}\right)}{\left(\begin{array}{l}-3.5641\times10^{-5} S^7 - 0.0133S^6 - 2.8328S^5 - 347.3130S^4 \\ -1.2962\times10^4 S^3 - 3.8931\times10^5 S^2 - 4.6363\times10^6 S - 4.819\times10^6\end{array}\right)}$
G_{Q1}	$G_{Q1} = \frac{\left(\begin{array}{l}0.0048S^7 + 75.7226S^6 + 1.4683\times10^4 S^5 + 2.6868\times10^5 S^4 + \\ 9.1246\times10^6 S^3 - 1.0722\times10^7 S^2 - 8.1504\times10^8 S - 1.0834\times10^9\end{array}\right)}{\left(\begin{array}{l}-3.5641\times10^{-5} S^7 - 0.0133S^6 - 2.8328S^5 - 347.3130S^4 \\ -1.2962\times10^4 S^3 - 3.8931\times10^5 S^2 - 4.6363\times10^6 S - 4.819\times10^6\end{array}\right)}$
G_{Q2}	$G_{Q2} = \frac{\left(\begin{array}{l}-2.5154\times10^{-5} S^7 + 0.2573S^6 + 49.5929S^5 + 553.9201S^4 + \\ 1.7416\times10^4 S^3 - 5.0453\times10^5 S^2 - 8.4886\times10^6 S - 9.6756\times10^6\end{array}\right)}{\left(\begin{array}{l}-3.5641\times10^{-5} S^7 - 0.0133S^6 - 2.8328S^5 - 347.3130S^4 \\ -1.2962\times10^4 S^3 - 3.8931\times10^5 S^2 - 4.6363\times10^6 S - 4.819\times10^6\end{array}\right)}$
G_{Q3}	$G_{Q3} = \frac{\left(\begin{array}{l}0.0215S^7 - 3.7420S^6 - 568.3827S^5 + 1.7394\times10^5 S^4 + \\ 6.6348\times10^6 S^3 + 2.4459\times10^8 S^2 + 3.0221\times10^9 S + 3.1788\times10^9\end{array}\right)}{\left(\begin{array}{l}-3.5641\times10^{-5} S^7 - 0.0133S^6 - 2.8328S^5 - 347.3130S^4 \\ -1.2962\times10^4 S^3 - 3.8931\times10^5 S^2 - 4.6363\times10^6 S - 4.819\times10^6\end{array}\right)}$
G_{Q4}	$G_{Q4} = \frac{\left(\begin{array}{l}7.7453\times10^{-5} S^7 - 0.0135S^6 - 2.0510S^5 + 627.6462S^4 + \\ 2.3941\times10^4 S^3 + 8.8257\times10^5 S^2 + 1.0905\times10^7 S + 1.1470\times10^7\end{array}\right)}{\left(\begin{array}{l}-3.5641\times10^{-5} S^7 - 0.0133S^6 - 2.8328S^5 - 347.3130S^4 \\ -1.2962\times10^4 S^3 - 3.8931\times10^5 S^2 - 4.6363\times10^6 S - 4.819\times10^6\end{array}\right)}$

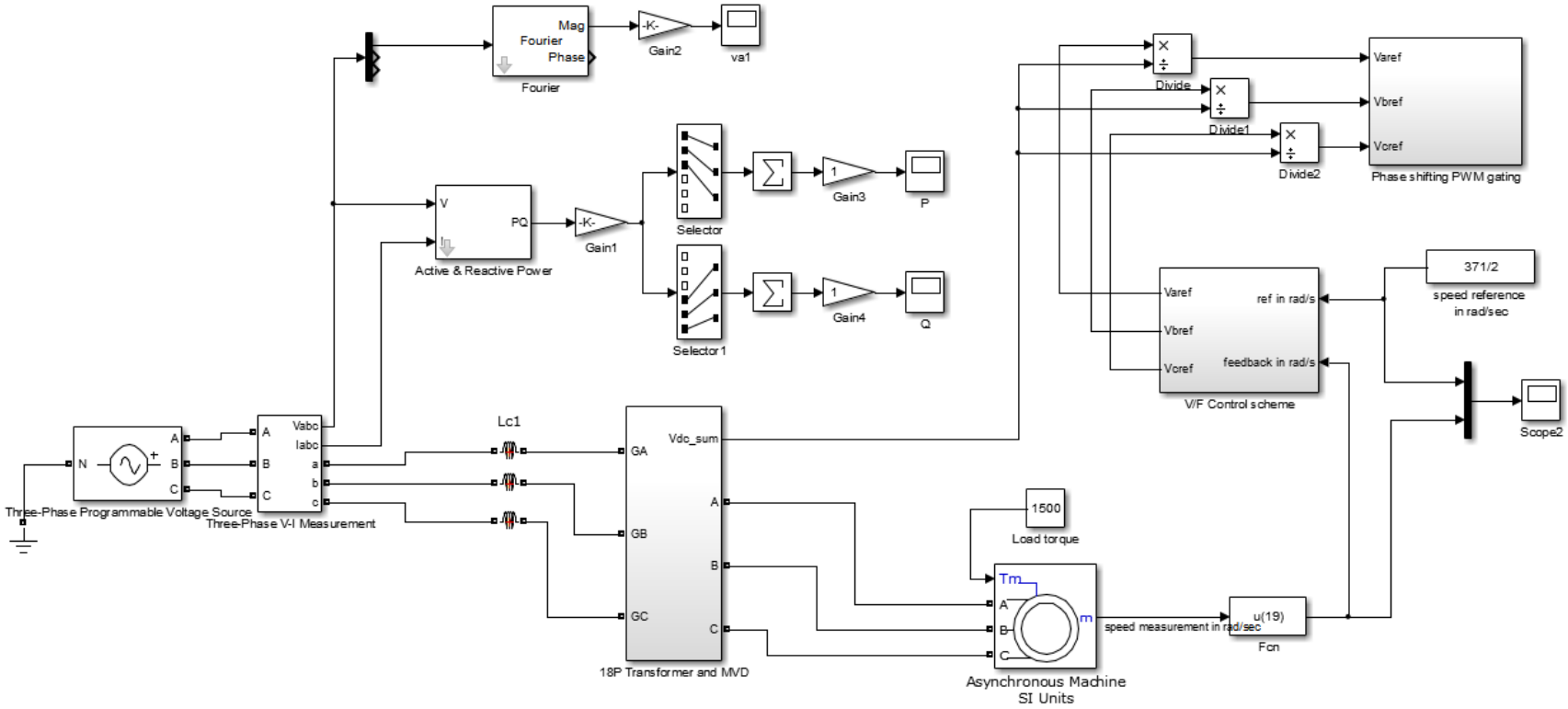

Figure 4.30 The detailed switching model for the 18-pulse cascaded inverter motor drive system (Voltage dependence)

The dynamic responses of the dynamic model and the detailed switching model for 90% and 80% voltage sags are shown in Figures 4.31 and 4.32, respectively. It is found there are good agreements between the two models, which verify the adequacy of the derived dynamic model.

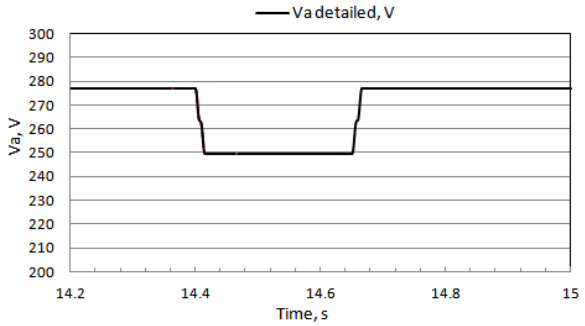

(a) Voltage Sag

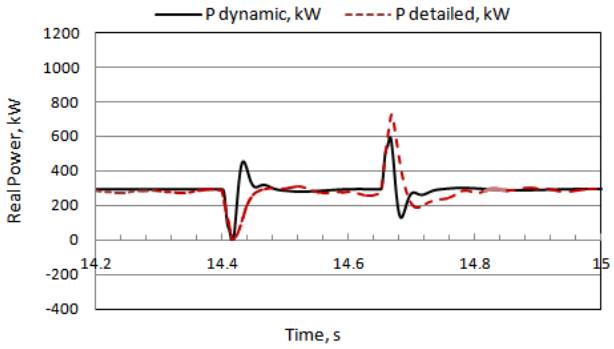

(b) Real Power P

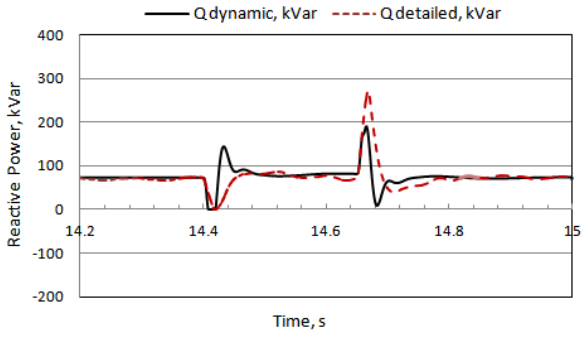

(c) Reactive Power Q

Figure 4.31 Dynamic responses of the dynamic and detailed switching models for the cascaded inverter motor drive system, 90% voltage sag

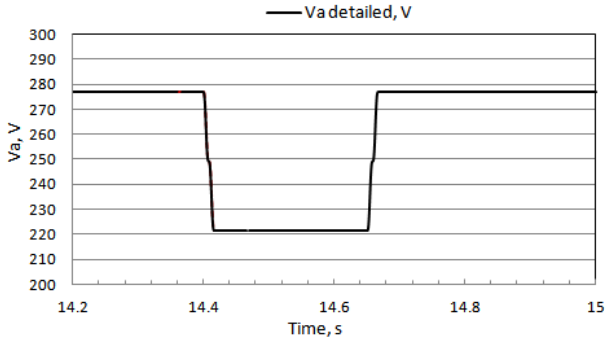

(a) Voltage Sag

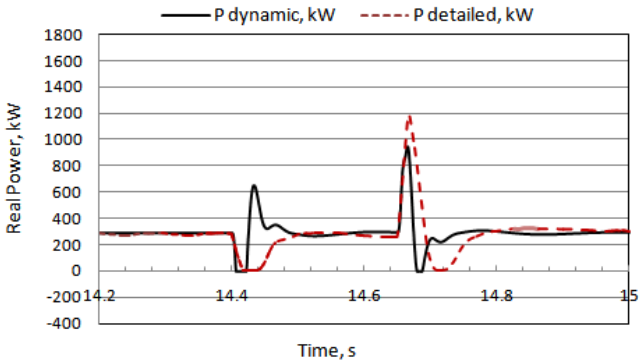

(b) Real Power P

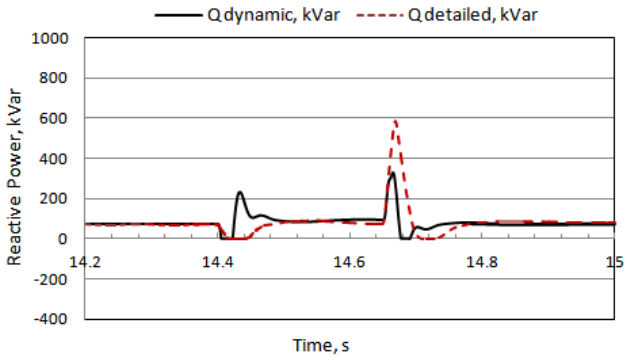

(c) Reactive Power Q

Figure 4.32 Dynamic responses of the dynamic and detailed switching models for the cascaded inverter motor drive system, 80% voltage sag

4.5.1.2 Frequence Dependence

The detailed switching model for the frequency dependence verification is shown in Figure 4.33. The frequency variation from 60 Hz step changed to 55 Hz is applied at the power source in the detailed switching model at 14.4 s and cleared at 14.65 s. The total simulation time is 15 seconds. The frequency variation and corresponding small voltage variation caused by the frequency variation are applied to the dynamic model. The dynamic responses of the dynamic model and the detailed switching model in this case are shown in Figure 4.34.

The comparison between the dynamic model and the detailed switching model for the sample system shows good agreements and similar tendency, which verify the adequacy of the dynamic model.

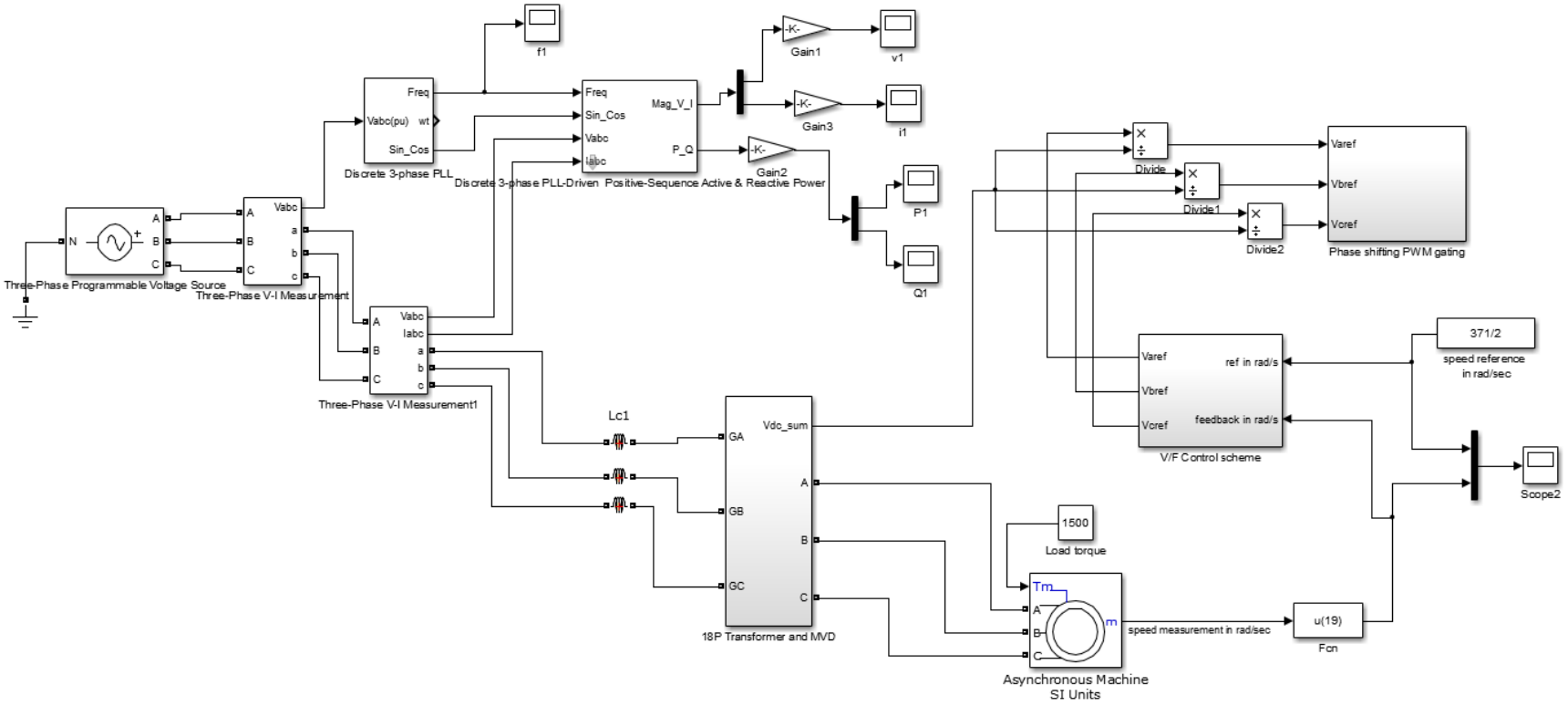

Figure 4.33 The detailed switching model for the 18-pulse cascaded inverter motor drive system (frequency dependence)

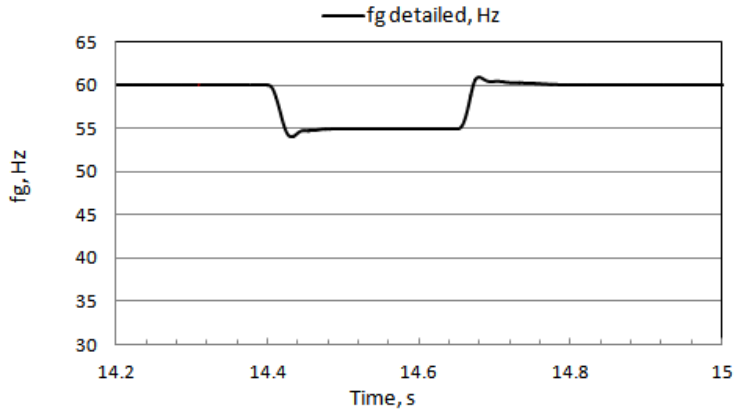

(a) Frequency variation

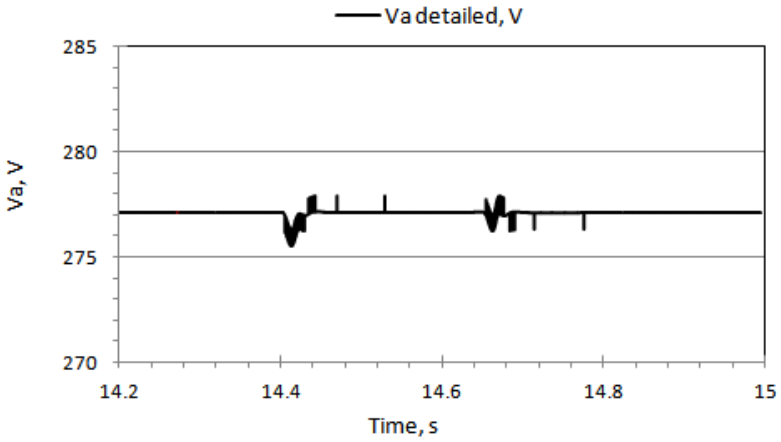

(b) Voltage variation

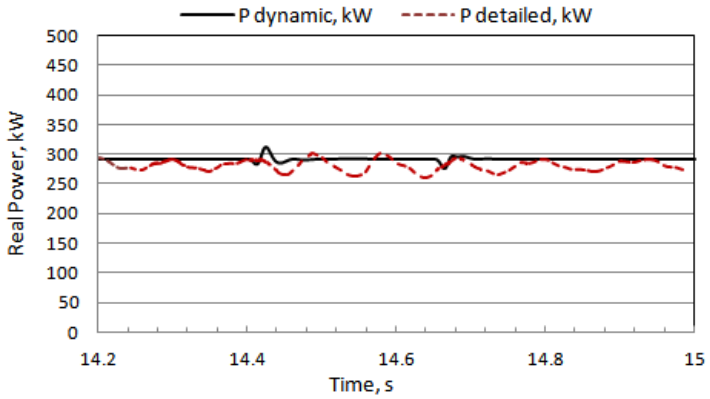

(c) Real Power P

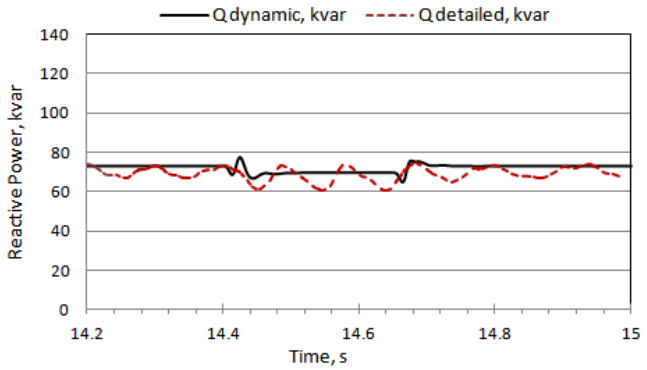

(d) Reactive Power Q

Figure 4.34 Dynamic responses of the dynamic and detailed switching models for the cascaded inverter motor drive system, frequency variation

4.5.2 Sensitivity Study

A sensitivity study is conducted for the equivalent dynamic model of the cascaded inverter motor drive system by evaluating the impact of the following three parameters on dynamic responses: 1) the speed controller parameters K_p and K_i, 2) the DC link capacitance C_{dc}, and 3) Load torque T_L of the induction motor.

Figure 4.35 shows the dynamic responses of the developed dynamic model for 90% voltage sag with the speed controller parameters K_p and K_i vary. The following three cases are considered: 1) K_p = 1.25, and K_i = 1.6; 2) K_p = 9, and K_i = 10; 3) K_p = 0.1, and K_i = 0.01. Other parameters are the same as that listed in Table 4.6. The control parameters with K_p = 9 and K_i = 10 in Case 2 show the best performance, the system is able to recover quickly after disturbances and reaches the previous steady-state values, which coincides with the detailed switching model response as shown in Figure 4.31. However, the control parameters in Cases 1 and 3 do not have good performance during disturbances. Therefore, it is very important that a proper control parameters for the speed controller are used in the dynamic model (such as K_p = 9 and K_i = 10), otherwise, the system will not be able to reach steady-state after disturbances.

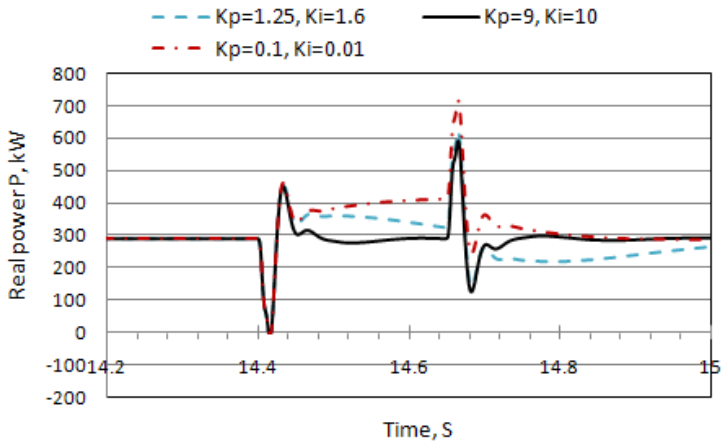

(a) Real power P

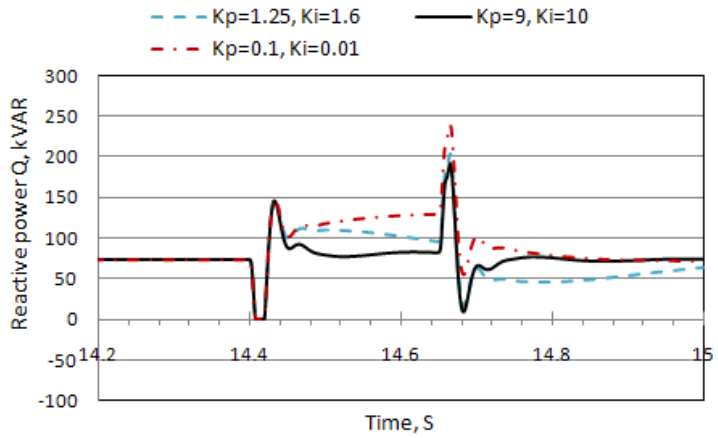

(b) Reactive power Q

Figure 4.35 The speed controller parameters K_p and K_i

The dynamic responses of the developed dynamic model for 90% voltage sag with the DC link capacitance C_{dc} varying are shown in Figure 4.36. The C_{dc} values considered in the simulation are 9200 µF, 10000 µF and 18000 µF. Other parameters are the same as that listed in Table 4.6. It is found that increasing the DC link capacitance tends to increase the magnitude of the dynamic transient for both real and reactive power. The DC link capacitance has no effect on the steady-state values for the real and reactive power.

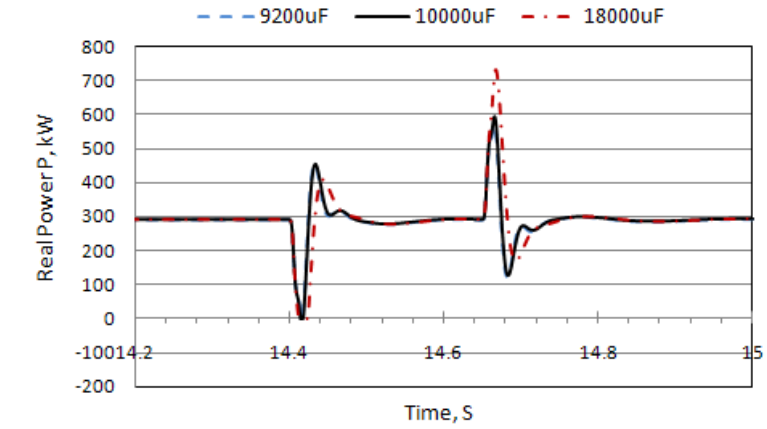

(a) Real power P

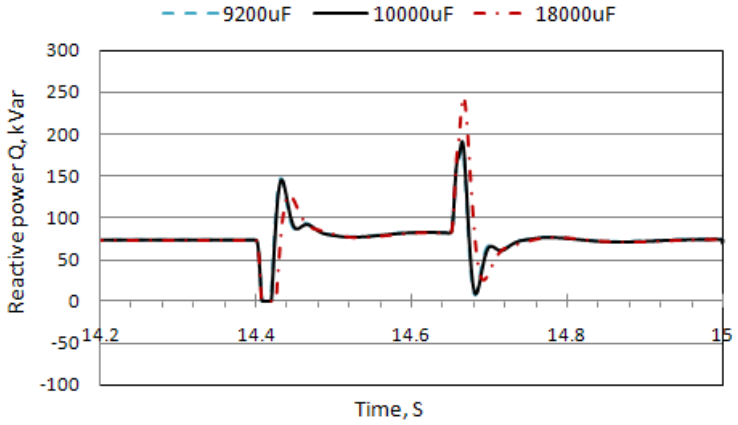

(b) Reactive power Q

Figure 4.36 DC link capacitance C_{dc}

The following three different load torques T_L are applied to the induction motor for 90% voltage sag for the derived dynamic model: 1000 NM, 1500 NM and 2000 NM, which correspond to 17.3%, 25.9% and 34.5% loading of the motor, respectively. Other parameters are the same as that listed in Table 4.6. The simulated dynamic responses of the developed dynamic model in this case are shown in Figure 4.37. It is found that the loading factor of the motor has significant effect on both steady-state and dynamic transient responses for the real and reactive power.

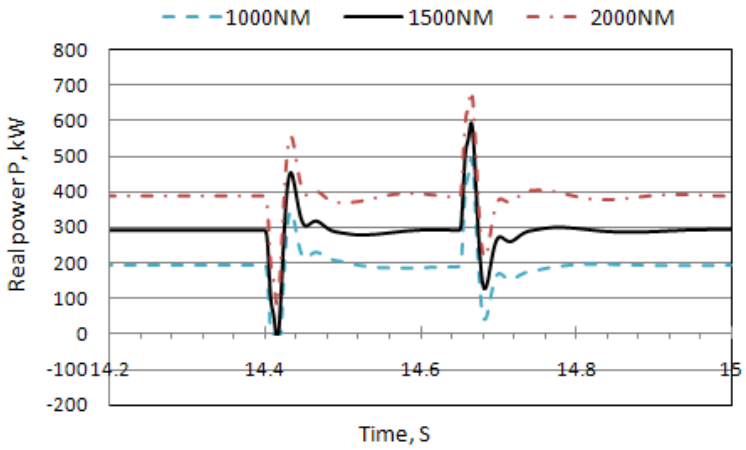

(a) Real power P

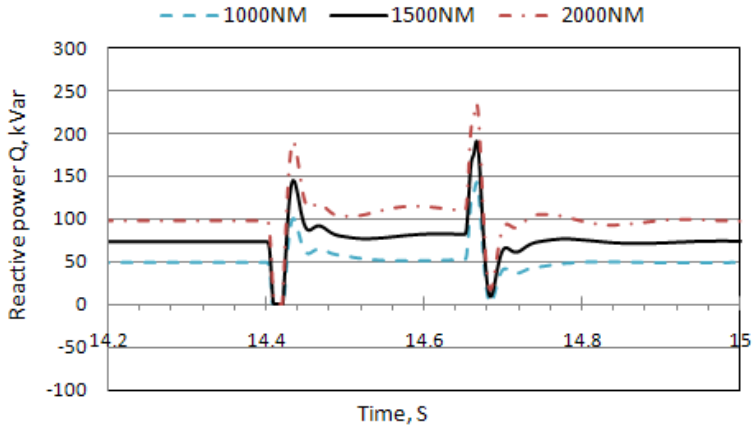

(b) Reactive power Q

Figure 4.37 The load torque of the motor T_L

4.6 Trip-Off Criteria of Variable Frequency Drives

The equivalent dynamic model for motor drive systems is proposed for the case that a drive is able to ride through during disturbances, which is extensively discussed in previous sections. However, when voltage sags are large and exceed the thresholds of the drive protection, the drive will trip out of lines, in this case, the motor drive system should be excluded from power systems dynamic studies.

To provide a generic motor drive system modeling technique, a VFD trip characteristic curve and a simple screening procedure are proposed in this thesis serving as criteria whether drives should be considered tripping or not. This VFD trip characteristic curve is developed based on the literature review for the drives protection and control, field survey regarding VFDs tripping status during disturbances, and also based on drive manufacturer specifications [31, 32, 33, 37, 123-128].

The under-voltage trip settings for the Siemens's Medium Voltage Drive, Robicon Perfect Harmony, which uses the cascaded H-bridge multi-level converter topology, will trip on voltage sags with duration of 100ms (6 cycles) or more and having a voltage drop of more than 30%, which is below 70% of rated voltage [123].

As the requirements to the equipment responding to voltage sags/dips, IEC 61000 (parts 6-1 and 6-2) specifies that all equipment must ride-through a voltage dip of a residual voltage of 70% for 10 ms, and must not be damaged for a voltage dip of a residual voltage of 40% for 100 ms [31]. CIGRE/CIRED/UIE Joint Working Group proposed immunity classes against voltage dips for balanced voltage dips (type III). The equipment will remain in service: 1) when the voltage dip is above 70% between 10 ms and 200 ms (1/2 cycle to 12 cycles), and 2) when the voltage dip is above 80% between 200 ms (12 cycles) to 3000 ms [124]. VFDs as electrical equipment should also follow such guidelines.

Voltage sag measurements in two industrial facilities for 17 months were conducted in [125], which provided solid proof about the levels of voltage sags causing tripping of VFDs. The two facilities for measurements were fed by 115 kV utility transmission lines. Even faults in 230 kV or 400 kV lines were felt by the utility entrance substation as voltage sags. The field records of voltage sags and subsequent VFD tripping status indicates that voltage sags with duration of 12 cycles or more and having a voltage drop of more than 20% will trip out a VFD [125].

Since most fault durations are between 10 ms and 3000 ms, a conservative VFD trip characteristic curve is proposed for this duration as shown in Figure 4.38. Based on this curve, voltage sags above 70% between 10 ms and 200 ms (12 cycles), and above 80% from 200 ms (12 cycles) to 3000 ms will not cause VFD tripping. A voltage sag marked as a "*" above the proposed curve will not cause the VFD tripping, while a voltage sag marked as a "#" below the proposed curve will cause the VFD tripping.

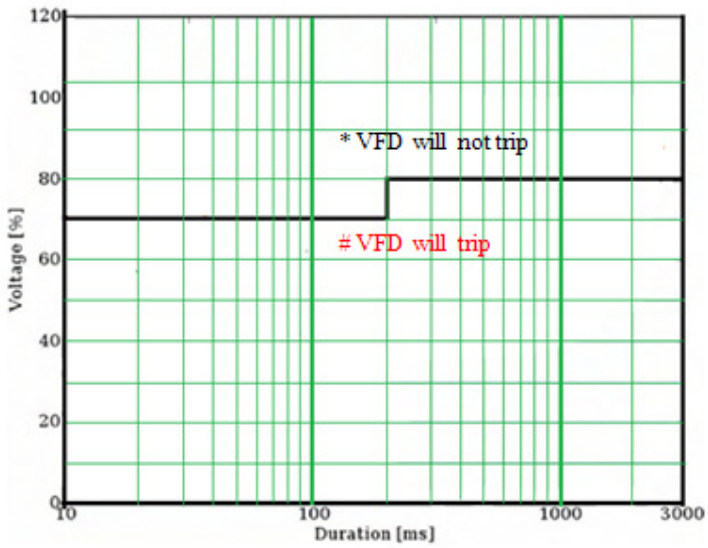

Figure 4.38 The VFD trip curve

A simple screening procedure is proposed to determine whether a VFD will trip subjected to a given disturbance as follows:

1) Conduct a three-phase short-circuit study on the system if the outage event of interest involves a short-circuit fault, which will yield a voltage sag magnitude at the VFD location. In the short circuit study, the VFDs can be omitted since they have little contributions to the fault current.

2) Check the relay setting involved in clearing the fault. This setting will provide the voltage sag duration value for the outage event.

3) The resulting magnitude and duration values for voltage sags are then compared with the VFD trip characteristic curve. If the point is below the curve, the VFD will trip and they shall not be modeled in power systems dynamic studies. If the point is above the trip curve, a motor drive system dynamic model proposed in Equations (4.2-42) and (4.2-43) are needed for dynamic simulation.

4.7 Summary and Conclusions

The equivalent dynamic model for motor drive systems is proposed for the case that a VFD is able to ride through voltage sags and remains in service. The linearization approach is used to create the model. To illustrate this approach, dynamic models are created for VSI and cascaded inverter drives and their induction motor loads. The developed dynamic models are expressed by 7^{th} order transfer functions and both voltage and frequency dependence are considered. These models can be inserted into commercially available computer simulation tools, suitable for three-phase balanced fault conditions when three phases of the rectifier remain in operation. The accuracy of the dynamic models is verified by comparing their simulation results with that of the detailed switching models.

For the case that a VFD will trip due to large voltage sags, the motor drive system should not be included in power systems dynamic studies. A VFD trip characteristic curve is proposed to evaluate whether the drive will trip or not based on the magnitude and duration of voltage sags. A simple screening

procedure is proposed for this purpose. This procedure provides instructions on how to use the VFD trip characteristic curve, and whether a dynamic model of motor drive system shall be developed and inserted into the simulation tool or simply take the VFD out of line due to tripping for the event.

The equivalent dynamic model for motor drive systems is based on linearization of differential equations, and it is suitable for small signal stability studies. On the other hand, VFDs will trip out of lines during large disturbances, the motor drive systems are only considered in dynamic modeling for small voltage sags, so the developed dynamic models will serve well for power systems dynamic studies.

CHAPTER 5 AGGREGATION OF MOTOR DRIVE SYSTEMS

5.1 Scenario 1: VFDs Connected to the Same Bus

As part of the load modeling study for industrial facilities, the aggregation method for VFDs connected to the same bus is investigated. The common configuration of a group of VFDs connected to a switchboard is shown in Figure 5.1.

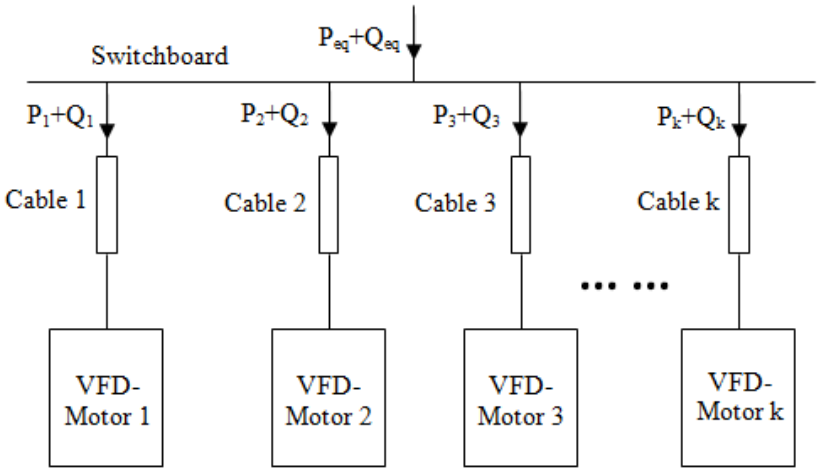

(a) A typical configuration connecting VFDs to a switchboard

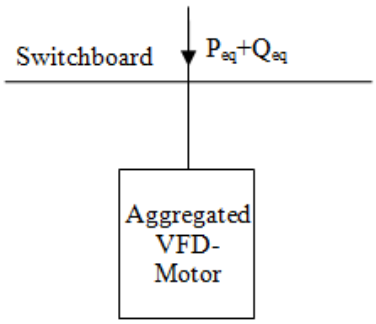

(b) The aggregated VFD-motor load

Figure 5.1 A group of VFDs connected to a common switchboard

Pade approximation method [129] is used to create the equivalent dynamic model aggregated from a group of motor drive systems. The goal of such

aggregation is to convert the system configuration from Figure 5.1 (a) to Figure 5.1 (b). The dynamic models for individual motor drive systems are listed as follows:

$$P_1 = P_{0\_1} + G_{P1\_1}\Delta E + G_{P2\_1}\Delta E^2 + \left(G_{P3\_1} + G_{P4\_1}\Delta E\right)\Delta f_g \tag{5.1-1}$$

$$Q_1 = Q_{0\_1} + G_{Q1\_1}\Delta E + G_{Q2\_1}\Delta E^2 + \left(G_{Q3\_1} + G_{Q4\_1}\Delta E\right)\Delta f_g \tag{5.1-2}$$

$$P_2 = P_{0\_2} + G_{P1\_2}\Delta E + G_{P2\_2}\Delta E^2 + \left(G_{P3\_2} + G_{P4\_2}\Delta E\right)\Delta f_g \tag{5.1-3}$$

$$Q_2 = Q_{0\_2} + G_{Q1\_2}\Delta E + G_{Q2\_2}\Delta E^2 + \left(G_{Q3\_2} + G_{Q4\_2}\Delta E\right)\Delta f_g \tag{5.1-4}$$

… … …

$$P_k = P_{0\_k} + G_{P1\_k}\Delta E + G_{P2\_k}\Delta E^2 + \left(G_{P3\_k} + G_{P4\_k}\Delta E\right)\Delta f_g \tag{5.1-5}$$

$$Q_k = Q_{0\_k} + G_{Q1\_k}\Delta E + G_{Q2\_k}\Delta E^2 + \left(G_{Q3\_k} + G_{Q4\_k}\Delta E\right)\Delta f_g \tag{5.1-6}$$

To make the two systems equivalent, the real and reactive power through the switchboard for the original and equivalent systems should remain the same. Adding real and reactive power for each individual VFDs connected to the switchboard, total real and reactive power through the switchboard can be determined as follows:

$$P_{eq} = P_1 + P_2 + \cdots + P_k = P_{0\_eq} + G_{P1\_eq}\Delta E + G_{P2\_eq}\Delta E^2 + \left(G_{P3\_eq} + G_{P4\_eq}\Delta E\right)\Delta f_g \tag{5.1-7}$$

$$P_{0\_eq} = \sum_{i=1}^{k} P_{0\_i} \tag{5.1-8}$$

$$G_{P1\_eq} = \sum_{i=1}^{k} G_{P1\_i} \tag{5.1-9}$$

$$G_{P2\_eq} = \sum_{i=1}^{k} G_{P2\_i} \tag{5.1-10}$$

$$G_{P3\_eq} = \sum_{i=1}^{k} G_{P3\_i} \tag{5.1-11}$$

$$G_{P4\_eq} = \sum_{i=1}^{k} G_{P4\_i} \tag{5.1-12}$$

$$Q_{eq} = Q_1 + Q_2 + \cdots + Q_k = Q_{0\_eq} + G_{Q1\_eq}\Delta E + G_{Q2\_eq}\Delta E^2 + \left(G_{Q3\_eq} + G_{Q4\_eq}\Delta E\right)\Delta f_g \tag{5.1-13}$$

$$Q_{0\_eq} = \sum_{i=1}^{k} Q_{0\_i} \tag{5.1-14}$$

$$G_{Q1\_eq} = \sum_{i=1}^{k} G_{Q1\_i} \tag{5.1-15}$$

$$G_{Q2\_eq} = \sum_{i=1}^{k} G_{Q2\_i} \tag{5.1-16}$$

$$G_{Q3\_eq} = \sum_{i=1}^{k} G_{Q3\_i} \tag{5.1-17}$$

$$G_{Q4\_eq} = \sum_{i=1}^{k} G_{Q4\_i} \tag{5.1-18}$$

Equations (5.1-7) and (5.1-13) represent the dynamic model for the aggregated equivalent motor drive system in Figure 5.1(b). The coefficients expressed by transfer functions in the dynamic model, G_{P1_eq}, G_{P2_eq}, G_{P3_eq}, G_{P4_eq}, G_{Q1_eq}, G_{Q2_eq}, G_{Q3_eq}, and G_{Q4_eq}, can be obtained based on Pade approximation from dynamic models of individual VFDs.

The application of Pade Approximation in this case is explained using a transfer function G(x) as follows:

$$G(x) = \frac{a_0 + a_1 x + a_2 x^2 + \cdots + a_m x^m}{b_0 + b_1 x + b_2 x^2 + \cdots + b_n x^n} \tag{5.1-19}$$

The transfer function G(x) can be expressed by a polynomial function f(x):

$$f(x) = c_0 + c_1 x + c_2 x^2 + \cdots + c_{m+n} x^{m+n} \tag{5.1-20}$$

$$a_0 = b_0 c_0 \tag{5.1-21}$$

$$a_1 = b_0 c_1 + b_1 c_0 \tag{5.1-22}$$

… …

$$a_m = b_0 c_m + b_1 c_{m-1} + \cdots + b_m c_0 \tag{5.1-23}$$

… …

$$0 = b_0 c_{m+n} + b_1 c_{m+n-1} + \cdots + b_n c_m \tag{5.1-24}$$

Based on Equations (5.1-21)-(5.1-24), the coefficients of the new function f(x) can be determined. The detailed derivation using Pade approximation in this case can be found in Appendix D.

To achieve the sum of transfer functions in Equation (5.1-9)-(5.1-12) and Equations (5.1-15)-(5.1-18), the three steps are required: 1) the transfer functions are converted to polynomials using Pade approximation; 2) the converted polynomials are added together to obtain an equivalent polynomial; 3) the equivalent polynomial are converted back to the equivalent transfer function using Pade approximation backwards.

$$\sum_{i=1}^{k} G_{P1\_i} = \sum_{i=1}^{k} f_{P1\_i} = G_{P1\_eq} \tag{5.1-25}$$

$$\sum_{i=1}^{k} G_{P2\_i} = \sum_{i=1}^{k} f_{P2\_i} = G_{P2\_eq} \tag{5.1-26}$$

$$\sum_{i=1}^{k} G_{P3\_i} = \sum_{i=1}^{k} f_{P3\_i} = G_{P3\_eq} \tag{5.1-27}$$

$$\sum_{i=1}^{k} G_{P4\_i} = \sum_{i=1}^{k} f_{P4\_i} = G_{P4\_eq} \tag{5.1-28}$$

$$\sum_{i=1}^{k} G_{Q1\_i} = \sum_{i=1}^{k} f_{Q1\_i} = G_{Q1\_eq} \tag{5.1-29}$$

$$\sum_{i=1}^{k} G_{Q2\_i} = \sum_{i=1}^{k} f_{Q2\_i} = G_{Q2\_eq} \tag{5.1-30}$$

$$\sum_{i=1}^{k} G_{Q3\_i} = \sum_{i=1}^{k} f_{Q3\_i} = G_{Q3\_eq} \tag{5.1-31}$$

$$\sum_{i=1}^{k} G_{Q4\_i} = \sum_{i=1}^{k} f_{Q4\_i} = G_{Q4\_eq} \tag{5.1-32}$$

The direct- and quadrature-axis components of AC current at the drive input can be aggregated and converted using Pade approximation in similar way. The AC current for individual drives are listed as follows:

$$i_{qg\_1} = i_{qg0\_1} + G_{Iqg1\_1}\Delta E + G_{Iqg2\_1}\Delta f_g \tag{5.1-33}$$

$$i_{dg\_1} = i_{dg0\_1} + G_{Idg1\_1}\Delta E + G_{Idg2\_1}\Delta f_g \tag{5.1-34}$$

$$i_{qg\_2} = i_{qg0\_2} + G_{Iqg1\_2}\Delta E + G_{Iqg2\_2}\Delta f_g \tag{5.1-35}$$

$$i_{dg\_2} = i_{dg0\_2} + G_{Idg1\_2}\Delta E + G_{Idg2\_2}\Delta f_g \tag{5.1-36}$$

… … …

$$i_{qg\_k} = i_{qg0\_k} + G_{Iqg1\_k}\Delta E + G_{Iqg2\_k}\Delta f_g \tag{5.1-37}$$

$$i_{dg\_k} = i_{dg0\_k} + G_{Idg1\_k}\Delta E + G_{Idg2\_k}\Delta f_g \tag{5.1-38}$$

To make the two systems, Figures 5.1 (a) and 5.1 (b), equivalent, the direct- and quadrature-axis components of AC current through the switchboard for both systems should remain the same. Adding up direct-axis components and quadrature-axis components of AC current for each individual VFDs, respectively, the direct- and quadrature-axis components of total equivalent AC current at the switchboard can be determined as follows:

$$i_{qg\_eq} = i_{qg\_1} + i_{qg\_2} + \cdots i_{qg\_k} = i_{qg0\_eq} + G_{Iqg1\_eq}\Delta E + G_{Iqg2\_eq}\Delta f_g \tag{5.1-39}$$

$$i_{qg0\_eq} = \sum_{i=1}^{k} i_{qg0\_i} \tag{5.1-40}$$

$$G_{Iqg1\_eq} = \sum_{i=1}^{k} G_{Iqg1\_i} \tag{5.1-41}$$

$$G_{Iqg2\_eq} = \sum_{i=1}^{k} G_{Iqg2\_i} \tag{5.1-42}$$

$$i_{dg\_eq} = i_{dg\_1} + i_{dg\_2} + \cdots i_{dg\_k} = i_{dg0\_eq} + G_{Idg1\_eq}\Delta E + G_{Idg2\_eq}\Delta f_g \tag{5.1-43}$$

$$i_{dg0\_eq} = \sum_{i=1}^{k} i_{dg0\_i} \tag{5.1-44}$$

$$G_{Idg1\_eq} = \sum_{i=1}^{k} G_{Idg1\_i} \tag{5.1-45}$$

$$G_{Idg2\_eq} = \sum_{i=1}^{k} G_{Idg2\_i} \tag{5.1-46}$$

Similarly, to achieve the sum of transfer functions in Equations (5.1-41), (5.1-42), (5.1-45) and (5.1-46), Pade approximation is used as follows:

$$\sum_{i=1}^{k} G_{Iqg1\_i} = \sum_{i=1}^{k} f_{Iqg1\_i} = G_{Iqg1\_eq} \tag{5.1-47}$$

$$\sum_{i=1}^{k} G_{Iqg2\_i} = \sum_{i=1}^{k} f_{Iqg2\_i} = G_{Iqg2\_eq} \tag{5.1-48}$$

$$\sum_{i=1}^{k} G_{Idg1\_i} = \sum_{i=1}^{k} f_{Idg1\_i} = G_{Idg1\_eq} \tag{5.1-49}$$

$$\sum_{i=1}^{k} G_{Idg2\_i} = \sum_{i=1}^{k} f_{Idg2\_i} = G_{Idg2\_eq} \tag{5.1-50}$$

5.2 Verification of Scenario 1

5.2.1 Voltage Dependence

The proposed aggregation method for a group of motor drive loads connected to the same bus is verified by a sample system consisting of low voltage 6-pulse VSI drives and their induction motor loads. In the case study, there are four VFD-induction motor loads connected to a switchboard, and each VFD- motor load has the same parameters and loading condition as that given in Table 4.1. The detailed switching model of the case study is shown in Figure 5.2. The dynamic model for the aggregated VFD-induction motor model can be found in Table 5.1.

A three phase fault is applied at the upstream of the switchboard in the detailed switching model in Figure 5.2, which results in 90% and 80% voltage

sags. The fault is applied at 1.4 s and cleared at 1.65 s. The total simulation time is 2 seconds.

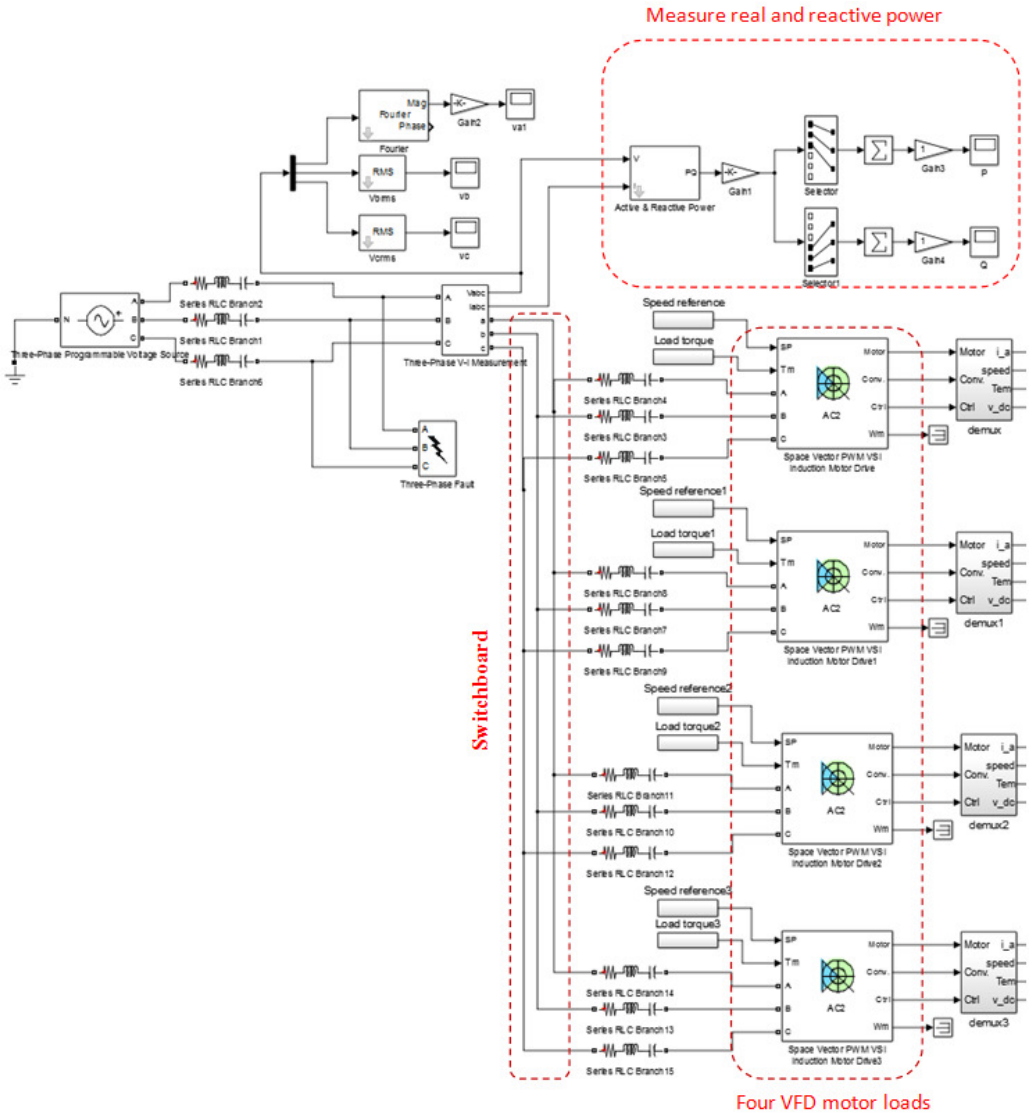

Figure 5.2 The detailed switching model for Scenario 1

Dynamic responses of the aggregated dynamic model and the detailed switching model are compared in Figures 5.3 and 5.4 for 90% and 80% voltage sags, respectively. It is found that there are good agreements between the two models. Therefore, it is verified that the proposed aggregation method considering voltage dependence for motor drive systems connected to the same bus is accurate.

Table 5.1 The aggregated dynamic model for Scenario 1 (Loading 1)

	Calculated transfer functions for the dynamic model
Derived Dynamic Model	$P = P_0 + G_{P1}\Delta E + G_{P2}\Delta E^2 + (G_{P3} + G_{P4}\Delta E)\Delta f_g$ $Q = Q_0 + G_{Q1}\Delta E + G_{Q2}\Delta E^2 + (G_{Q3} + G_{Q4}\Delta E)\Delta f_g$
P_0, Q_0	8.6537kW, 3.6659kVAR
G_{P1}	$G_{P1} = \frac{(-71.0971S^7 - 1.496\times10^5 S^6 - 3.4427\times10^7 S^5 - 1.731\times10^9 S^4 + 3.8654\times10^8 S^3 + 2.8504\times10^8 S^2 - 3.1806\times10^9 S - 2.5275\times10^8)}{(S^7 + 424.0744S^6 + 7.036\times10^4 S^5 + 5.626\times10^6 S^4 + 1.8181\times10^8 S^3 - 6.2966\times10^7 S^2 - 1.0949\times10^7 S + 3.2601\times10^8)}$
G_{P2}	$G_{P2} = \frac{(-0.0775S^7 - 926.095S^6 - 2.4489\times10^5 S^5 - 1.1997\times10^7 S^4 + 7.3805\times10^7 S^3 + 1.7552\times10^8 S^2 - 1.2681\times10^8 S - 2.4385\times10^8)}{(S^7 + 443.143S^6 + 7.5686\times10^4 S^5 + 6.2396\times10^6 S^4 + 2.1236\times10^8 S^3 + 3.2666\times10^8 S^2 - 3.5953\times10^8 S - 5.2886\times10^8)}$
G_{P3}	$G_{P3} = \frac{(9.6782S^7 + 2.6608\times10^4 S^6 - 2.5107\times10^6 S^5 - 3.6515\times10^8 S^4 - 3.7327\times10^9 S^3 - 1.0305\times10^9 S^2 + 3.6221\times10^9 S + 2.9071\times10^8)}{(S^7 + 100.S^6 - 1.5856\times10^4 S^5 - 3.6663\times10^6 S^4 - 2.1846\times10^8 S^3 - 1.992\times10^9 S^2 - 3.0207\times10^8 S + 1.9128\times10^9)}$
G_{P4}	$G_{P4} = \frac{(0.0869S^7 + 210.5258S^6 + 1.3999\times10^4 S^5 + 2.5258\times10^5 S^4 + 2.142\times10^7 S^3 + 1.7538\times10^7 S^2 - 9.4003\times10^6 S - 8.4141\times10^5)}{(S^7 + 252.3638S^6 + 2.7039\times10^4 S^5 + 1.3205\times10^6 S^4 + 3.4787\times10^7 S^3 + 1.543\times10^9 S^2 + 1.0624\times10^9 S - 7.3517\times10^8)}$
G_{Q1}	$G_{Q1} = \frac{(-16.9046S^7 - 8.8257\times10^4 S^6 - 2.6466\times10^7 S^5 - 1.3721\times10^9 S^4 + 6.9137\times10^9 S^3 + 8.4424\times10^9 S^2 - 1.6358\times10^8 S + 1.398\times10^9)}{(S^7 + 480.3395S^6 + 8.5297\times10^4 S^5 + 7.2325\times10^6 S^4 + 2.5064\times10^8 S^3 + 2.4674\times10^8 S^2 + 3.2715\times10^6 S + 4.0806\times10^7)}$
G_{Q2}	$G_{Q2} = \frac{(0.1436S^7 - 552.925S^6 - 1.536\times10^5 S^5 - 7.2452\times10^6 S^4 + 7.7943\times10^7 S^3 + 3.6849\times10^8 S^2 + 5.9677\times10^7 S - 2.8335\times10^8)}{(S^7 + 442.3046S^6 + 7.5818\times10^4 S^5 + 6.309\times10^6 S^4 + 2.212\times10^8 S^3 + 7.239\times10^8 S^2 + 6.153\times10^7 S - 5.5027\times10^8)}$
G_{Q3}	$G_{Q3} = \frac{(-28.9268S^7 + 4.0674\times10^3 S^6 + 1.9036\times10^6 S^5 + 1.7981\times10^7 S^4 - 6.8068\times10^9 S^3 - 5.2405\times10^9 S^2 - 7.4623\times10^9 S - 1.1749\times10^{10})}{(S^7 + 419.7837S^6 + 6.9422\times10^4 S^5 + 5.5567\times10^6 S^4 + 1.8219\times10^8 S^3 + 1.4312\times10^8 S^2 + 2.0489\times10^8 S + 3.0596\times10^8)}$
G_{Q4}	$G_{Q4} = \frac{(-0.3635S^7 + 534.5779S^6 - 1.3668\times10^5 S^5 - 4.2447\times10^6 S^4 + 6.1931\times10^8 S^3 - 3.9425\times10^9 S^2 - 5.7594\times10^8 S + 5.3625\times10^9)}{(S^7 - 1.6117\times10^3 S^6 - 4.4768\times10^5 S^5 - 4.6603\times10^7 S^4 - 1.6878\times10^9 S^3 + 1.3706\times10^{10} S^2 + 1.3522\times10^9 S - 1.8545\times10^{10})}$

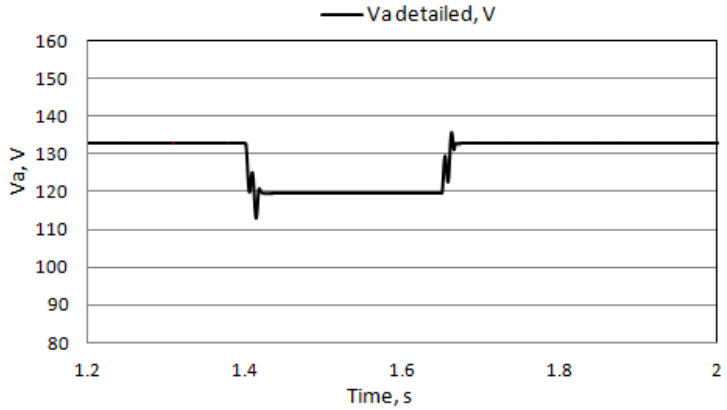

(a) Voltage sag

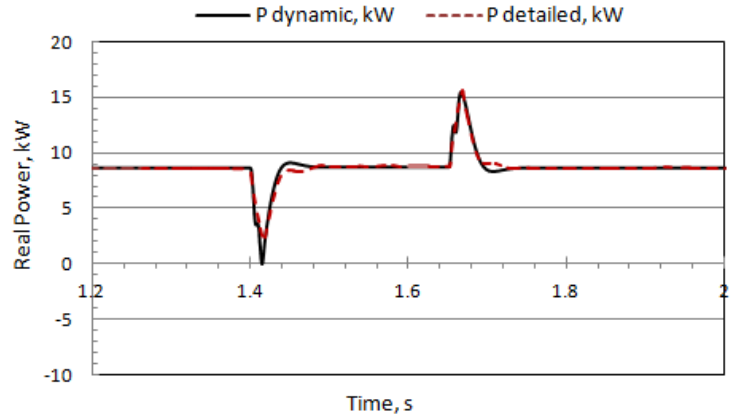

(b) Real Power P

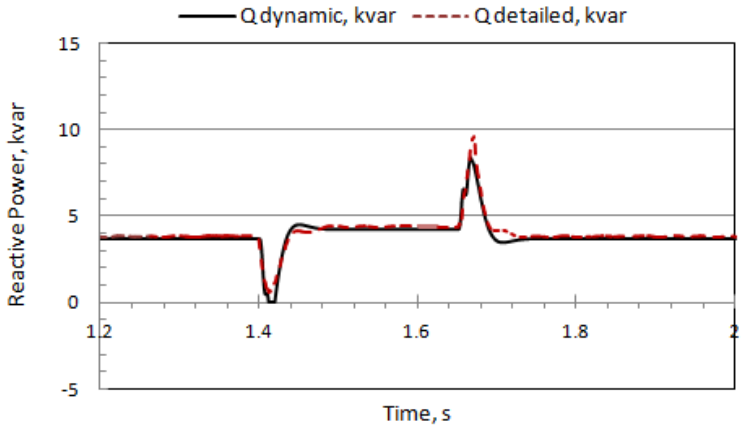

(c) Reactive Power Q

Figure 5.3 Dynamic responses of the aggregated dynamic and detailed switching models for Scenario 1, 90% voltage sag

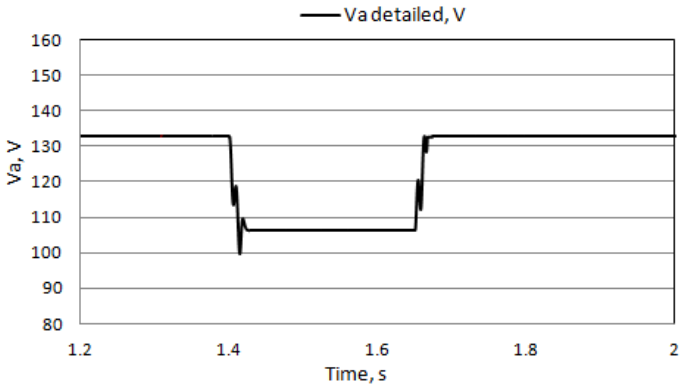

(a) Voltage sag

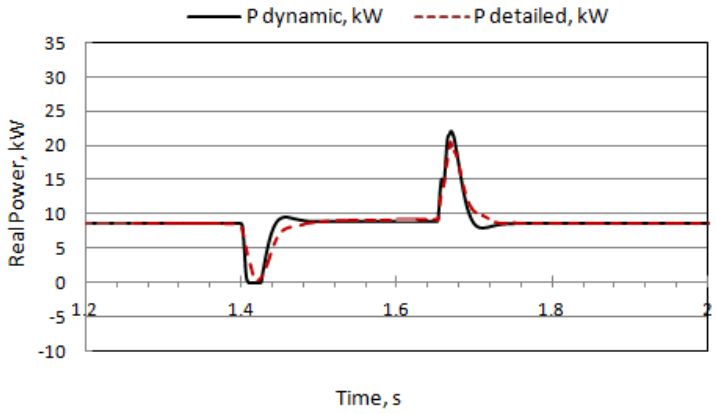

(b) Real Power P

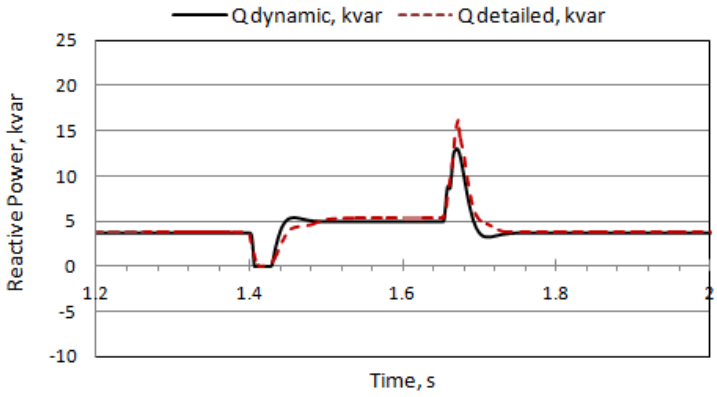

(c) Reactive Power Q

Figure 5.4 Dynamic responses of the aggregated dynamic and detailed switching models for Scenario 1, 80% voltage sag

5.2.2 Frequency Dependence

The frequency dependence of the aggregated dynamic model for motor drive systems is further verified using the same case study with four VFD-induction motor loads as Section 5.2.1. The parameters for individual VFD-induction motor load are the same as Table 4.1 except the following slight loading change for the induction motor: Load torque T_L= 12 NM, Target speed n_r = 1705 rpm. The derived dynamic model is provided in Table 5.2.

A step variation of the frequency from 60 Hz to 52 Hz is applied at the power source in the detailed switching model, the variation starts at 1.4 s and ends at 1.65 s. The total simulation time is 2 s. When the power source frequency is changed, the voltage will slightly vary accordingly. Both the frequency sag and the resultant small voltage variation were entered into the aggregated dynamic model as disturbances to represent real system conditions.

Dynamic responses of the aggregated dynamic model and the detailed switching model are compared in Figure 5.5 in this case. The simulated small voltage variation caused by the frequency variation from the detailed switching model is also shown in this figure.

It is found that there are good agreements between the two models. Therefore, the proposed aggregation method for motor drive loads connected to the same bus considering the frequency dependence is verified to be accurate.

Table 5.2 The aggregated dynamic model for Scenario 1 (Loading 2)

	Calculated transfer functions for the dynamic model
Derived Dynamic Model	$P = P_0 + G_{P1}\Delta E + G_{P2}\Delta E^2 + (G_{P3} + G_{P4}\Delta E)\Delta f_g$ $Q = Q_0 + G_{Q1}\Delta E + G_{Q2}\Delta E^2 + (G_{Q3} + G_{Q4}\Delta E)\Delta f_g$
P_0, Q_0	9.5582kW, 4.3148kVAR
G_{P1}	$G_{P1} = \frac{(-86.1499S^7 - 1.5612\times10^5 S^6 - 5.0423\times10^7 S^5 - 2.8409\times10^9 S^4 - 1.5057\times10^{10} S^3 - 2.6116\times10^7 S^2 + 1.9278\times10^{10} S + 2.876\times10^9)}{(S^7 + 536.2825S^6 + 9.9097\times10^4 S^5 + 8.6952\times10^6 S^4 + 3.2074\times10^6 S^3 + 1.5528\times10^9 S^2 - 3.3394\times10^8 S - 1.9318\times10^9)}$
G_{P2}	$G_{P2} = \frac{(-0.1559S^7 - 895.0652S^6 - 3.5911\times10^5 S^5 - 1.7112\times10^7 S^4 + 1.551\times10^8 S^3 - 3.5173\times10^6 S^2 - 4.6678\times10^7 S + 2.1296\times10^8)}{(S^7 + 567.4459S^6 + 1.0534\times10^5 S^5 + 9.085\times10^6 S^4 + 3.0987\times10^8 S^3 - 1.4735\times10^7 S^2 - 3.106\times10^7 S + 4.2499\times10^8)}$
G_{P3}	$G_{P3} = \frac{(18.7834S^7 + 3.4026\times10^4 S^6 + 1.0672\times10^7 S^5 + 5.5947\times10^8 S^4 + 7.5043\times10^8 S^3 - 6.8923\times10^8 S^2 - 1.0852\times10^9 S - 1.4652\times10^8)}{(S^7 + 524.8737S^6 + 9.4966\times10^4 S^5 + 8.0852\times10^6 S^4 + 2.7714\times10^8 S^3 + 3.0622\times10^8 S^2 - 3.9359\times10^8 S - 4.4939\times10^8)}$
G_{P4}	$G_{P4} = \frac{(0.1201S^7 + 239.987S^6 + 3.419\times10^4 S^5 + 1.1574\times10^6 S^4 - 5.2197\times10^6 S^3 + 3.097\times10^6 S^2 + 1.5017\times10^7 S + 2.1895\times10^6)}{(S^7 + 330.7902S^6 + 4.545\times10^4 S^5 + 2.968\times10^6 S^4 + 7.1459\times10^7 S^3 - 3.5392\times10^8 S^2 + 2.9297\times10^8 S + 8.9172\times10^8)}$
G_{Q1}	$G_{Q1} = \frac{(-23.5122S^7 - 9.335\times10^4 S^6 - 3.5817\times10^7 S^5 - 1.768\times10^9 S^4 + 1.064\times10^{10} S^3 + 1.9107\times10^{10} S^2 - 3.4675\times10^{10} S - 4.5858\times10^{10})}{(S^7 + 561.4916S^6 + 1.0418\times10^5 S^5 + 9.0179\times10^6 S^4 + 3.1254\times10^8 S^3 + 2.9176\times10^8 S^2 - 1.0404\times10^9 S - 1.116\times10^9)}$
G_{Q2}	$G_{Q2} = \frac{(-3.9336S^7 + 3.11\times10^3 S^6 - 7.3175\times10^6 S^5 - 4.1676\times10^8 S^4 + 5.1532\times10^9 S^3 + 2.5804\times10^{10} S^2 - 1.3337\times10^{10} S - 4.0546\times10^{10})}{(S^7 + 1.1441\times10^4 S^6 + 2.8823\times10^6 S^5 + 2.9649\times10^8 S^4 + 1.1908\times10^{10} S^3 + 4.0033\times10^{10} S^2 - 2.7725\times10^{10} S - 6.6313\times10^{10})}$
G_{Q3}	$G_{Q3} = \frac{(-33.079S^7 + 2.128\times10^3 S^6 + 3.1196\times10^6 S^5 + 2.7025\times10^7 S^4 - 1.0905\times10^{10} S^3 - 5.7312\times10^9 S^2 - 8.8401\times10^9 S - 1.8813\times10^{10})}{(S^7 + 490.8634S^6 + 8.6216\times10^4 S^5 + 7.1702\times10^6 S^4 + 2.3931\times10^8 S^3 + 1.2963\times10^8 S^2 + 2.0411\times10^8 S + 4.0497\times10^8)}$
G_{Q4}	$G_{Q4} = \frac{(-0.2668S^7 + 77.2327S^6 + 4.6731\times10^3 S^5 - 1.9824\times10^5 S^4 - 9.5746\times10^6 S^3 - 2.2762\times10^8 S^2 - 7.592\times10^7 S + 1.9529\times10^8)}{(S^7 + 280.0812S^6 + 3.372\times10^4 S^5 + 1.9368\times10^6 S^4 + 4.8796\times10^7 S^3 + 6.5835\times10^8 S^2 + 1.9796\times10^8 S - 5.5822\times10^8)}$

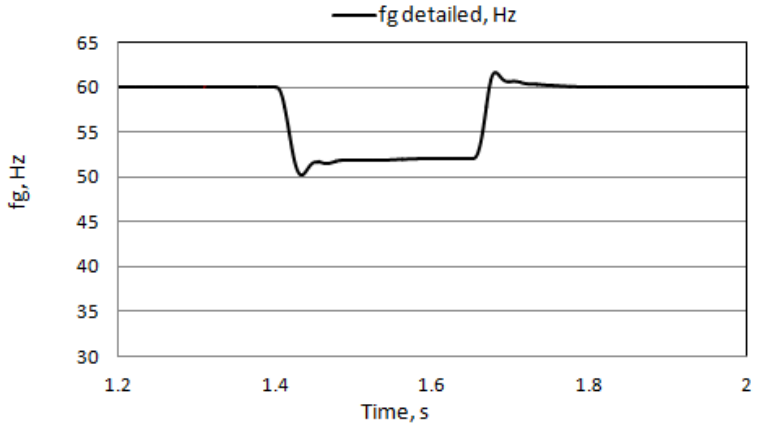

(c) Frequency variation

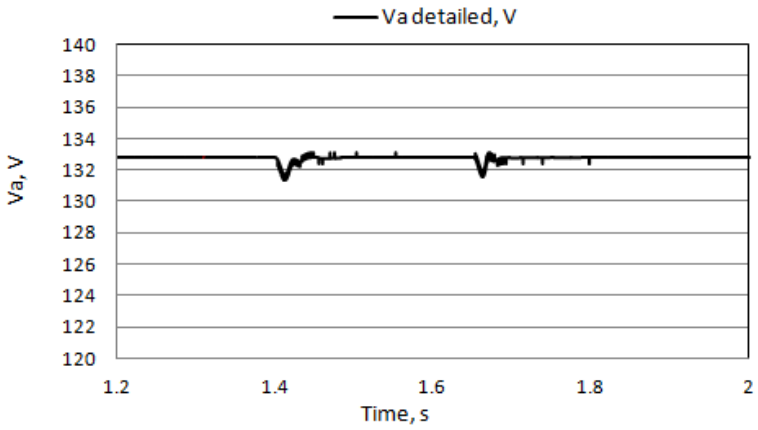

(d) Voltage variation

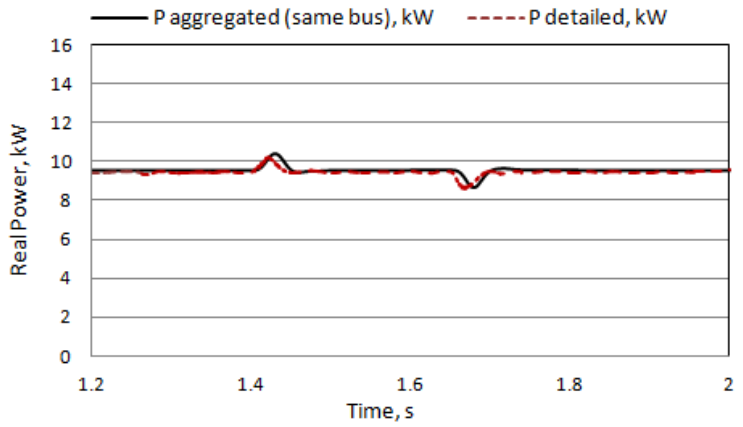

(c) Real Power P

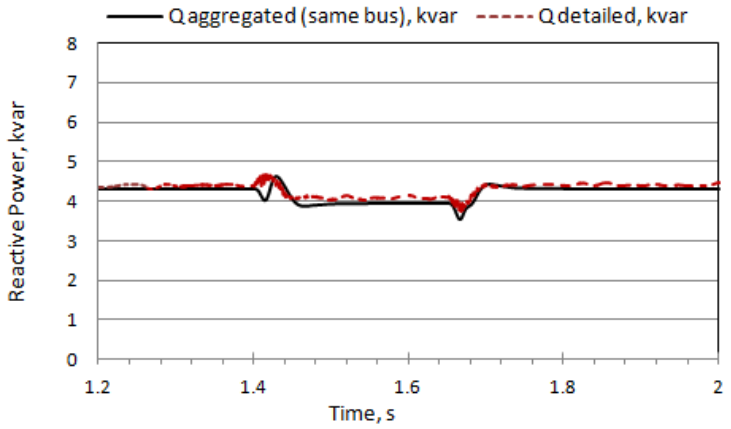

(d) Reactive Power Q

Figure 5.5 Dynamic responses of the aggregated dynamic and detailed switching models for Scenario 1, frequency variation

5.3 Scenario 2: VFDs with Upstream Series Impedance and Transformers

5.3.1 Upstream Series Impedance

The aggregated dynamic model of VFDs connected to the same bus might need to be aggregated further with upstream series impedance from cables, reactors, and transmission lines etc. To achieve such a system aggregation, the upstream series impedance in the form of R_L +jX_L is considered as shown in Figure 5.6.

The real and reactive power at Bus B, P_B and Q_B, in Figure 5.6 can be expressed based on Equations (5.1-7) and (5.1-13) as follows:

$$P_B = P_{0\_B} + G_{P1\_B}\Delta V_B + G_{P2\_B}\Delta V_B^2 + \left(G_{P3\_B} + G_{P4\_B}\Delta V_B\right)\Delta f_g \quad (5.3\text{-}1)$$

$$Q_B = Q_{0\_B} + G_{Q1\_B}\Delta V_B + G_{Q2\_B}\Delta V_B^2 + \left(G_{Q3\_B} + G_{Q4\_B}\Delta V_B\right)\Delta f_g \quad (5.3\text{-}2)$$

According to power invariant property, the active and reactive power at Bus A, P_A and Q_A, can be expressed using the branch current I and the impedance as follows [11]:

$$P_A = P_B + 3I^2 R_L \quad (5.3\text{-}3)$$

$$Q_A = Q_B + 3I^2(2\pi f_g L) \tag{5.3-4}$$

$$I^2 = i_{dg}^2 + i_{qg}^2 \tag{5.3-5}$$

The branch current, I, is determined by the downstream induction motors load demand, the branch current for the same load is considered to be the same through the whole branch without a transformer; with a transformer the current can be converted using the turn ratio of transformers accordingly. Equation (5.3-5) can be linearized as follows:

$$\Delta(I^2) = \Delta(i_{dg}^2 + i_{qg}^2) = 2I_0\Delta I = 2i_{dg0}\Delta i_{dg} + 2i_{qg0}\Delta i_{qg} \tag{5.3-6}$$

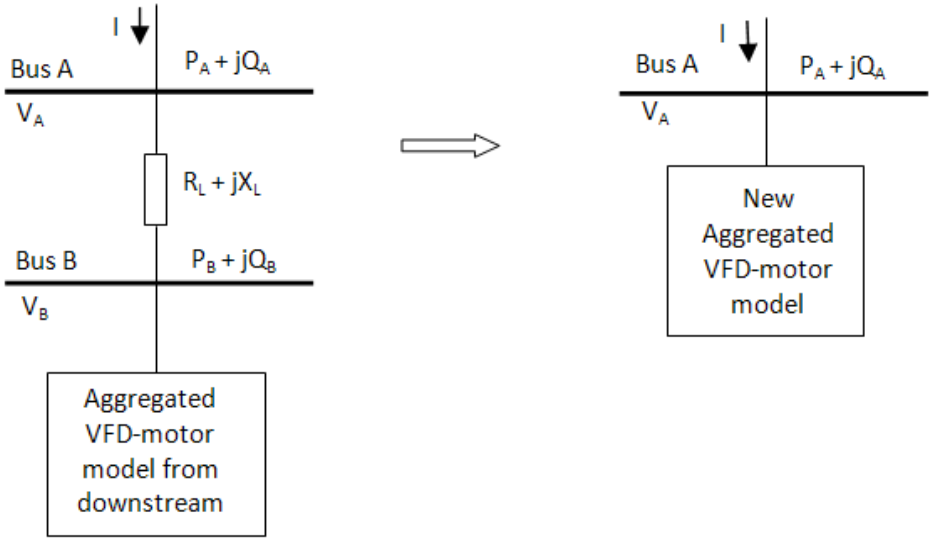

Figure 5.6 The motor drive model further aggregated with upstream series impedance

For the real power, substitute Equation (5.3-6) in the linearized Equation (5.3-3), we have

$$\Delta P_A = \Delta P_B + 3R_L\Delta(I^2) = \Delta P_B + (6R_L i_{dg0})\Delta i_{dg} + (6R_L i_{qg0})\Delta i_{qg} \tag{5.3-7}$$

$$\Delta P_A = P_A - P_{0\_A} \tag{5.3-8}$$

$$\Delta P_B = P_B - P_{0\_B} \tag{5.3-9}$$

$$\Delta i_{dg} = i_{dg} - i_{dg0} \tag{5.3-10}$$

$$\Delta i_{qg} = i_{qg} - i_{qg0} \tag{5.3-11}$$

$$P_{A0} = P_{B0} + 3I_0^2 R_L \tag{5.3-12}$$

$$I_0 = \sqrt{i_{dg0}^2 + i_{qg0}^2} \tag{5.3-13}$$

Similarly, substitute Equation (5.3-6) in the linearized Equation (5.3-4) for the reactive power, the following can be obtained:

$$\Delta Q_A = \Delta Q_B + (6\pi L)\Delta(I^2 f_g) = \Delta Q_B + (12\pi L f_{g0} i_{dg0})\Delta i_{dg} + (12\pi L f_{g0} i_{qg0})\Delta i_{qg} + (6\pi L I_0^2)\Delta f_g \tag{5.3-14}$$

$$\Delta Q_A = Q_A - Q_{0\_A} \tag{5.3-15}$$

$$\Delta Q_B = Q_B - Q_{0\_B} \tag{5.3-16}$$

$$\Delta f_g = f_g - f_{g0} \tag{5.3-17}$$

$$Q_{A0} = Q_{B0} + 3I_0^2(2\pi f_{g0} L) \tag{5.3-18}$$

Substitute Equations (4.2-44), (4.2-45), (5.3-1) and (5.3-2) in Equations (5.3-7) and (5.3-14), we have

$$P_A = P_{0\_A} + G_{PA11}\Delta V_B + G_{PA12}\Delta V_B^2 + (G_{PA13} + G_{PA14}\Delta V_B)\Delta f_g \tag{5.3-19}$$

$$G_{PA11} = G_{P1\_B} + (6R_L i_{dg0})G_{Idg1} + (6R_L i_{qg0})G_{Iqg1} \tag{5.3-20}$$

$$G_{PA12} = G_{P2\_B} \tag{5.3-21}$$

$$G_{PA13} = G_{P3\_B} + (6R_L i_{dg0})G_{Idg2} + (6R_L i_{qg0})G_{Iqg2} \tag{5.3-22}$$

$$G_{PA14} = G_{P4\_B} \tag{5.3-23}$$

$$Q_A = Q_{0\_A} + G_{QA11}\Delta V_B + G_{QA12}\Delta V_B^2 + (G_{QA13} + G_{QA14}\Delta V_B)\Delta f_g \tag{5.3-24}$$

$$G_{QA11} = G_{Q1\_B} + (12\pi L f_{g0} i_{dg0})G_{Idg1} + (12\pi L f_{g0} i_{qg0})G_{Iqg1} \tag{5.3-25}$$

$$G_{QA12} = G_{Q2\_B} \tag{5.3-26}$$

$$G_{QA13} = G_{Q3\_B} + (12\pi L f_{g0} i_{dg0})G_{Idg2} + (12\pi L f_{g0} i_{qg0})G_{Iqg2} + (6\pi L I_0^2) \tag{5.3-27}$$

$$G_{QA14} = G_{Q4\_B} \tag{5.3-28}$$

According to Reference [130], the voltage at Bus B and the voltage at Bus A have the following relationship:

$$V_A \approx V_B + \frac{P_B R_L + Q_B X_L}{3V_B} = V_B + \left(\frac{R_L}{3}\right)\left(P_B \frac{1}{V_B}\right) + \left(\frac{2\pi L}{3}\right)\left(f_g Q_B \frac{1}{V_B}\right) \tag{5.3-29}$$

$$V_{A0} = V_{B0} + \frac{P_{0\_B} R_L + Q_{0\_B} X_L}{3V_{B0}} \tag{5.3-30}$$

Linearize Equation (5.3-29), we have

$$\Delta V_A = \left(\frac{3V_{B0}^2 - R_L P_{0\_B} - 2\pi f_{g0} L Q_{0\_B}}{3V_{B0}^2}\right)\Delta V_B + \left(\frac{2\pi L Q_{0\_B}}{3V_{B0}}\right)\Delta f_g + \left(\frac{R_L}{3V_{B0}}\right)\Delta P_B + \left(\frac{2\pi L f_{g0}}{3V_{B0}}\right)\Delta Q_B \tag{5.3-31}$$

To simplify the problem, dynamic terms of ΔP and ΔQ are ignored from Equation (5.3-31), the voltage variation of Bus B can be expressed by the voltage variation of Bus A as follows:

$$\Delta V_B = V_{B11}\Delta V_A + V_{B12}\Delta f_g \tag{5.3-32}$$

$$V_{B11} = \frac{3V_{B0}^2}{3V_{B0}^2 - R_L P_{0\_B} - 2\pi f_{g0} L Q_{0\_B}} \tag{5.3-33}$$

$$V_{B12} = -\frac{2\pi L Q_{0\_B} V_{B0}}{3V_{B0}^2 - R_L P_{0\_B} - 2\pi f_{g0} L Q_{0\_B}} \tag{5.3-34}$$

Substitute Equation (5.3-32) in Equations (5.3-19) and (5.3-24), and ignoring the 2nd order f_g term, the real power can be obtained as follows:

$$P_A = P_{0\_A} + G_{P1\_A}\Delta V_A + G_{P2\_A}\Delta V_A^2 + \left(G_{P3\_A} + G_{P4\_A}\Delta V_A\right)\Delta f_g \tag{5.3-35}$$

Where,

$$G_{P1\_A} = V_{B11} G_{PA11} \tag{5.3-36}$$

$$G_{P2\_A} = V_{B11}^2 G_{PA12} \tag{5.3-37}$$

$$G_{P3\_A} = V_{B12} G_{PA11} + G_{PA13} \tag{5.3-38}$$

$$G_{P4\_A} = (2V_{B11}V_{B12})G_{PA12} + V_{B11}G_{PA14} \tag{5.3-39}$$

Substitute Equations (5.3-20) to (5.3-23) in Equations (5.3-36) to (5.3-39), the following equations are obtained:

$$G_{P1\_A} = V_{B11}G_{P1\_B} + (6R_L i_{dg0}V_{B11})G_{Idg1} + (6R_L i_{qg0}V_{B11})G_{Iqg1} \tag{5.3-40}$$

$$G_{P2\_A} = V_{B11}^2 G_{P2\_B} \tag{5.3-41}$$

$$\begin{aligned} G_{P3\_A} = {} & V_{B12}G_{P1\_B} + (6R_L i_{dg0}V_{B12})G_{Idg1} + (6R_L i_{qg0}V_{B12})G_{Iqg1} \\ & + G_{P3\_B} + (6R_L i_{dg0})G_{Idg2} + (6R_L i_{qg0})G_{Iqg2} \end{aligned} \tag{5.3-42}$$

$$G_{P4\_A} = (2V_{B11}V_{B12})G_{P2\_B} + V_{B11}G_{P4\_B} \tag{5.3-43}$$

Similarly, the reactive power can be determined as follows:

$$Q_A = Q_{0\_A} + G_{Q1\_A}\Delta V_A + G_{Q2\_A}\Delta V_A^2 + (G_{Q3\_A} + G_{Q4\_A}\Delta V_A)\Delta f_g \tag{5.3-44}$$

Where,

$$G_{Q1\_A} = V_{B11}G_{QA11} \tag{5.3-45}$$

$$G_{Q2\_A} = V_{B11}^2 G_{QA12} \tag{5.3-46}$$

$$G_{Q3\_A} = V_{B12}G_{QA11} + G_{QA13} \tag{5.3-47}$$

$$G_{Q4\_A} = (2V_{B11}V_{B12})G_{QA12} + V_{B11}G_{QA14} \tag{5.3-48}$$

Substitute Equations (5.3-25) to (5.3-28) in Equations (5.3-45) to (5.3-48), the following equations are obtained:

$$G_{Q1\_A} = V_{B11}G_{Q1\_B} + (12\pi L f_{g0} i_{dg0}V_{B11})G_{Idg1} + (12\pi L f_{g0} i_{qg0}V_{B11})G_{Iqg1} \tag{5.3-49}$$

$$G_{Q2\_A} = V_{B11}^2 G_{Q2\_B} \tag{5.3-50}$$

$$\begin{aligned} G_{Q3\_A} = {} & V_{B12}G_{Q1\_B} + (12\pi L f_{g0} i_{dg0}V_{B12})G_{Idg1} + (12\pi L f_{g0} i_{qg0}V_{B12})G_{Iqg1} \\ & + G_{Q3\_B} + (12\pi L f_{g0} i_{dg0})G_{Idg2} + (12\pi L f_{g0} i_{qg0})G_{Iqg2} + 6\pi L I_0^2 \end{aligned} \tag{5.3-51}$$

$$G_{Q4\_A} = (2V_{B11}V_{B12})G_{Q2\_B} + V_{B11}G_{Q4\_B} \tag{5.3-52}$$

The coefficients, G_{P1_A}, G_{P2_A}, G_{P3_A}, G_{P4_A}, G_{Q1_A}, G_{Q2_A}, G_{Q3_A}, and G_{Q4_A}, are calculated by adding several transfer functions, whose denominators

might not be the same. Therefore, the Pade approximation method is used in this case: 1) convert every transfer function for these coefficients into its polynomial format; 2) add the converted polynomials to obtain the resultant final polynomial; 3) convert the resultant final polynomial to a transfer function using Pade approximation.

To illustrate the above mentioned steps, the coefficient G_{P1_A} in Equation (5.3-40) is used as an example. G_{P1_A} is determined by three transfer functions, G_{P1_B}, G_{Idg1}, and G_{Iqg1}. The three transfer functions are converted to corresponding polynomials using Pade approximation in Equations (5.3-53) – (5.3-55), and the resultant final polynomial for the coefficient G_{P1_A} is determined by Equation (5.3-56).

$$G_{P1\_B}(S) = c_{0\_GP1B} + c_{1\_GP1B}S + \cdots c_{14\_GP1B}S^{14} \tag{5.3-53}$$

$$G_{Idg1}(S) = c_{0\_GIdg1} + c_{1\_GIdg1}S + \cdots c_{14\_GIdg1}S^{14} \tag{5.3-54}$$

$$G_{Iqg1}(S) = c_{0\_GIqg1} + c_{1\_GIqg1}S + \cdots c_{14\_GIqg1}S^{14} \tag{5.3-55}$$

$$G_{P1\_A}(S) = c_{0eq\_GP1A} + c_{1eq\_GP1A}S + \cdots c_{14eq\_GP1A}S^{14} \tag{5.3-56}$$

$$c_{0eq\_GP1A} = V_{B11}c_{0\_GP1B} + \left(6R_L i_{dg0}V_{B11}\right)c_{0\_GIdg1} + \left(6R_L i_{qg0}V_{B11}\right)c_{0\_GIqg1} \tag{5.3-57}$$

$$c_{1eq\_GP1A} = V_{B11}c_{1\_GP1B} + \left(6R_L i_{dg0}V_{B11}\right)c_{1\_GIdg1} + \left(6R_L i_{qg0}V_{B11}\right)c_{1\_GIqg1} \tag{5.3-58}$$

… … …

$$c_{14eq\_GP1A} = V_{B11}c_{14\_GP1B} + \left(6R_L i_{dg0}V_{B11}\right)c_{14\_GIdg1} + \left(6R_L i_{qg0}V_{B11}\right)c_{14\_GIqg1} \tag{5.3-59}$$

After obtaining the final polynomial for G_{P1_A} in Equation (5.3-56), the Pade approximation can be applied to convert it to the final 7th order transfer function for G_{P1_A} as follows:

$$G_{P1\_A} = \frac{\left(\begin{array}{l} a_{7eq\_GP1A}S^7 + a_{6eq\_GP1A}S^6 + a_{5eq\_GP1A}S^5 + a_{4eq\_GP1A}S^4 + \\ a_{3eq\_GP1A}S^3 + a_{2eq\_GP1A}S^2 + a_{1eq\_GP1A}S + a_{0eq\_GP1A} \end{array}\right)}{\left(\begin{array}{l} b_{7eq\_GP1A}S^7 + b_{6eq\_GP1A}S^6 + b_{5eq\_GP1A}S^5 + b_{4eq\_GP1A}S^4 + \\ b_{3eq\_GP1A}S^3 + b_{2eq\_GP1A}S^2 + b_{1eq\_GP1A}S + b_{0eq\_GP1A} \end{array}\right)} \tag{5.3-60}$$

All coefficients can be calculated in similar way and their 7th order transfer functions for VSI drive-induction motor loads are listed as follows:

$$G_{P2\_A}=\frac{\left(\begin{array}{l}a_{7eq\_GP2A}S^7+a_{6eq\_GP2A}S^6+a_{5eq\_GP2A}S^5+a_{4eq\_GP2A}S^4+\\a_{3eq\_GP2A}S^3+a_{2eq\_GP2A}S^2+a_{1eq\_GP2A}S+a_{0eq\_GP2A}\end{array}\right)}{\left(\begin{array}{l}b_{7eq\_GP2A}S^7+b_{6eq\_GP2A}S^6+b_{5eq\_GP2A}S^5+b_{4eq\_GP2A}S^4+\\b_{3eq\_GP2A}S^3+b_{2eq\_GP2A}S^2+b_{1eq\_GP2A}S+b_{0eq\_GP2A}\end{array}\right)} \tag{5.3-61}$$

$$G_{P3\_A}=\frac{\left(\begin{array}{l}a_{7eq\_GP3A}S^7+a_{6eq\_GP3A}S^6+a_{5eq\_GP3A}S^5+a_{4eq\_GP3A}S^4+\\a_{3eq\_GP3A}S^3+a_{2eq\_GP3A}S^2+a_{1eq\_GP3A}S+a_{0eq\_GP3A}\end{array}\right)}{\left(\begin{array}{l}b_{7eq\_GP3A}S^7+b_{6eq\_GP3A}S^6+b_{5eq\_GP3A}S^5+b_{4eq\_GP3A}S^4+\\b_{3eq\_GP3A}S^3+b_{2eq\_GP3A}S^2+b_{1eq\_GP3A}S+b_{0eq\_GP3A}\end{array}\right)} \tag{5.3-62}$$

$$G_{P4\_A}=\frac{\left(\begin{array}{l}a_{7eq\_GP4A}S^7+a_{6eq\_GP4A}S^6+a_{5eq\_GP4A}S^5+a_{4eq\_GP4A}S^4+\\a_{3eq\_GP4A}S^3+a_{2eq\_GP4A}S^2+a_{1eq\_GP4A}S+a_{0eq\_GP4A}\end{array}\right)}{\left(\begin{array}{l}b_{7eq\_GP4A}S^7+b_{6eq\_GP4A}S^6+b_{5eq\_GP4A}S^5+b_{4eq\_GP4A}S^4+\\b_{3eq\_GP4A}S^3+b_{2eq\_GP4A}S^2+b_{1eq\_GP4A}S+b_{0eq\_GP4A}\end{array}\right)} \tag{5.3-63}$$

$$G_{Q1\_A}=\frac{\left(\begin{array}{l}a_{7eq\_GQ1A}S^7+a_{6eq\_GQ1A}S^6+a_{5eq\_GQ1A}S^5+a_{4eq\_GQ1A}S^4+\\a_{3eq\_GQ1A}S^3+a_{2eq\_GQ1A}S^2+a_{1eq\_GQ1A}S+a_{0eq\_GQ1A}\end{array}\right)}{\left(\begin{array}{l}b_{7eq\_GQ1A}S^7+b_{6eq\_GQ1A}S^6+b_{5eq\_GQ1A}S^5+b_{4eq\_GQ1A}S^4+\\b_{3eq\_GQ1A}S^3+b_{2eq\_GQ1A}S^2+b_{1eq\_GQ1A}S+b_{0eq\_GQ1A}\end{array}\right)} \tag{5.3-64}$$

$$G_{Q2\_A}=\frac{\left(\begin{array}{l}a_{7eq\_GQ2A}S^7+a_{6eq\_GQ2A}S^6+a_{5eq\_GQ2A}S^5+a_{4eq\_GQ2A}S^4+\\a_{3eq\_GQ2A}S^3+a_{2eq\_GQ2A}S^2+a_{1eq\_GQ2A}S+a_{0eq\_GQ2A}\end{array}\right)}{\left(\begin{array}{l}b_{7eq\_GQ2A}S^7+b_{6eq\_GQ2A}S^6+b_{5eq\_GQ2A}S^5+b_{4eq\_GQ2A}S^4+\\b_{3eq\_GQ2A}S^3+b_{2eq\_GQ2A}S^2+b_{1eq\_GQ2A}S+b_{0eq\_GQ2A}\end{array}\right)} \tag{5.3-65}$$

$$G_{Q3\_A}=\frac{\left(\begin{array}{l}a_{7eq\_GQ3A}S^7+a_{6eq\_GQ3A}S^6+a_{5eq\_GQ3A}S^5+a_{4eq\_GQ3A}S^4+\\a_{3eq\_GQ3A}S^3+a_{2eq\_GQ3A}S^2+a_{1eq\_GQ3A}S+a_{0eq\_GQ3A}\end{array}\right)}{\left(\begin{array}{l}b_{7eq\_GQ3A}S^7+b_{6eq\_GQ3A}S^6+b_{5eq\_GQ3A}S^5+b_{4eq\_GQ3A}S^4+\\b_{3eq\_GQ3A}S^3+b_{2eq\_GQ3A}S^2+b_{1eq\_GQ3A}S+b_{0eq\_GQ3A}\end{array}\right)} \tag{5.3-66}$$

$$G_{Q4\_A} = \frac{\begin{pmatrix} a_{7eq\_GQ4A}S^7 + a_{6eq\_GQ4A}S^6 + a_{5eq\_GQ4A}S^5 + a_{4eq\_GQ4A}S^4 + \\ a_{3eq\_GQ4A}S^3 + a_{2eq\_GQ4A}S^2 + a_{1eq\_GQ4A}S + a_{0eq\_GQ4A} \end{pmatrix}}{\begin{pmatrix} b_{7eq\_GQ4A}S^7 + b_{6eq\_GQ4A}S^6 + b_{5eq\_GQ4A}S^5 + b_{4eq\_GQ4A}S^4 + \\ b_{3eq\_GQ4A}S^3 + b_{2eq\_GQ4A}S^2 + b_{1eq\_GQ4A}S + b_{0eq\_GQ4A} \end{pmatrix}} \quad (5.3\text{-}67)$$

5.3.2 Transformers

For the case that the upstream component of the aggregated dynamic model of the motor drive systems is a transformer, the transformer can be expressed by a series impedance (R_T + jX_T) and an ideal transformer with the ratio n:1 (Figure 5.7). In this case, the dynamic model of the system at the upstream Bus A can be obtained by further aggregation of the transformer with the dynamic model of the system at the downstream Bus B by the following two steps:

- Step 1: Convert the model to Bus B' by considering ideal transformer only
- Step 2: Aggregate the model from Bus B' to Bus A through the series impedance R_T + jX_T using the method proposed in Section 5.3.1.

For the ideal transformer, the power loss is zero and the voltage relationship is linear. The real power, reactive power and the voltage at the primary of the ideal transformer (Bus B') can be determined as follows:

$$V_B' = nV_B \quad (5.3\text{-}68)$$

$$P_B' = P_B \quad (5.3\text{-}69)$$

$$Q_B' = Q_B \quad (5.3\text{-}70)$$

$$I_B' = \frac{1}{n} I_B \quad (5.3\text{-}71)$$

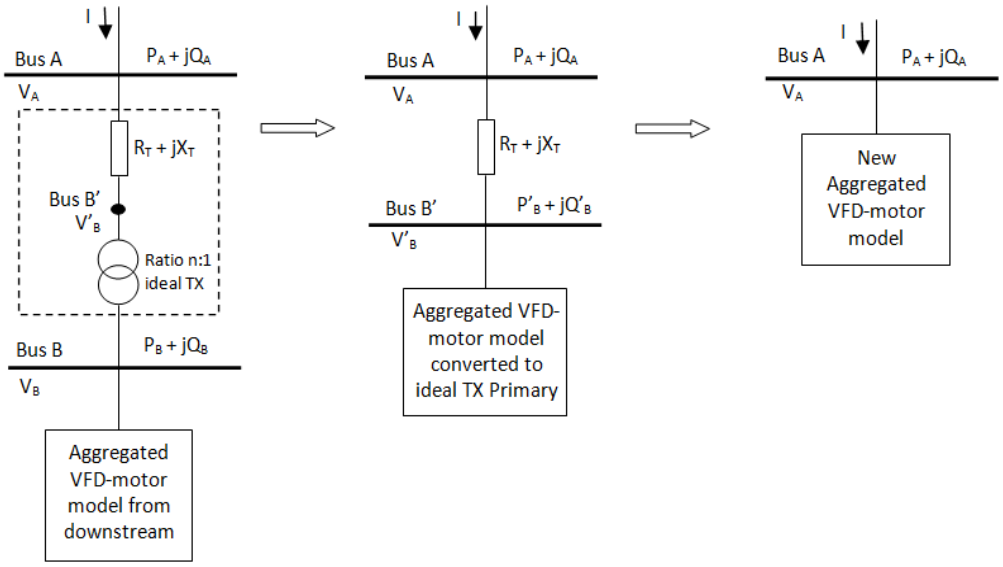

Figure 5.7 The motor drive model further aggregated with the upstream transformer

Linearize Equations (5.3-68) – (5.3-71), and submit Equations (5.3-1) and (5.3-2) in the linearized equations, the real power at Bus B' using the generic model format can be expressed as follows:

$$P'_B = P'_{0\_B} + G'_{P1\_B}\Delta V'_B + G'_{P2\_B}\Delta V'^2_B + \left(G'_{P3\_B} + G'_{P4\_B}\Delta V'_B\right)\Delta f_g \tag{5.3-72}$$

where,

$$G'_{P1\_B} = \left(\frac{1}{n}\right)G_{P1\_B} \tag{5.3-73}$$

$$G'_{P2\_B} = \left(\frac{1}{n^2}\right)G_{P2\_B} \tag{5.3-74}$$

$$G'_{P3\_B} = G_{P3\_B} \tag{5.3-75}$$

$$G'_{P4\_B} = \left(\frac{1}{n}\right)G_{P4\_B} \tag{5.3-76}$$

The reactive power can be obtained in similar way:

$$Q'_B = Q'_{0\_B} + G'_{Q1\_B}\Delta V'_B + G'_{Q2\_B}\Delta V'^2_B + \left(G'_{Q3\_B} + G'_{Q4\_B}\Delta V'_B\right)\Delta f_g \tag{5.3-77}$$

where,

$$G'_{Q1\_B} = \left(\frac{1}{n}\right) G_{Q1\_B} \tag{5.3-78}$$

$$G'_{Q2\_B} = \left(\frac{1}{n^2}\right) G_{Q2\_B} \tag{5.3-79}$$

$$G'_{Q3\_B} = G_{Q3\_B} \tag{5.3-80}$$

$$G'_{Q4\_B} = \left(\frac{1}{n}\right) G_{Q4\_B} \tag{5.3-81}$$

Once the dynamic model at Bus B' is determined by Equations (5.3-72) and (5.3-77), the dynamic model at Bus A can be calculated by the method proposed in Section 5.3.1 by aggregating the dynamic model of the system at Bus B' with the transformer impedance $R_T + jX_T$.

5.4 Verification of Scenario 2

5.4.1 Voltage Dependence

The verification is conducted for the aggregated dynamic model derived from four motor drive loads connected to the same bus, further aggregated with an upstream impedance $R_L + jX_L$ (R_L = 0.1 ohms, L = 0.18mH), and a step-down transformer rated at 1 MVA, 4160 V/230 V, wye-wye winding connection, the impedance Z of the transformer is 5.75% with X/R ratio = 5.79. The detailed switching model for the whole system set-up is shown in Figure 5.8. Individual motor drive loads are the same as that in Table 4.1. The aggregated dynamic model at Bus A can be found in Table 5.3.

A three-phase fault is applied to the detailed switching model, which results in 90% and 80% voltage sags. The fault is applied at 1.4 s and cleared at 1.65 s with the total simulation time equal to 2 s. The frequency of the power source remains constant. The dynamic responses of the aggregated dynamic model and the detailed switching model at Bus A are shown in Figures 5.9 and

5.10 for 90% and 80% voltage sags, respectively. It is found that dynamic responses of the aggregated dynamic model at Bus A using the proposed aggregation algorithms has good agreements with that of the detailed switching model. Therefore, it is verified that the proposed aggregation algorithms considering voltage dependence are accurate.

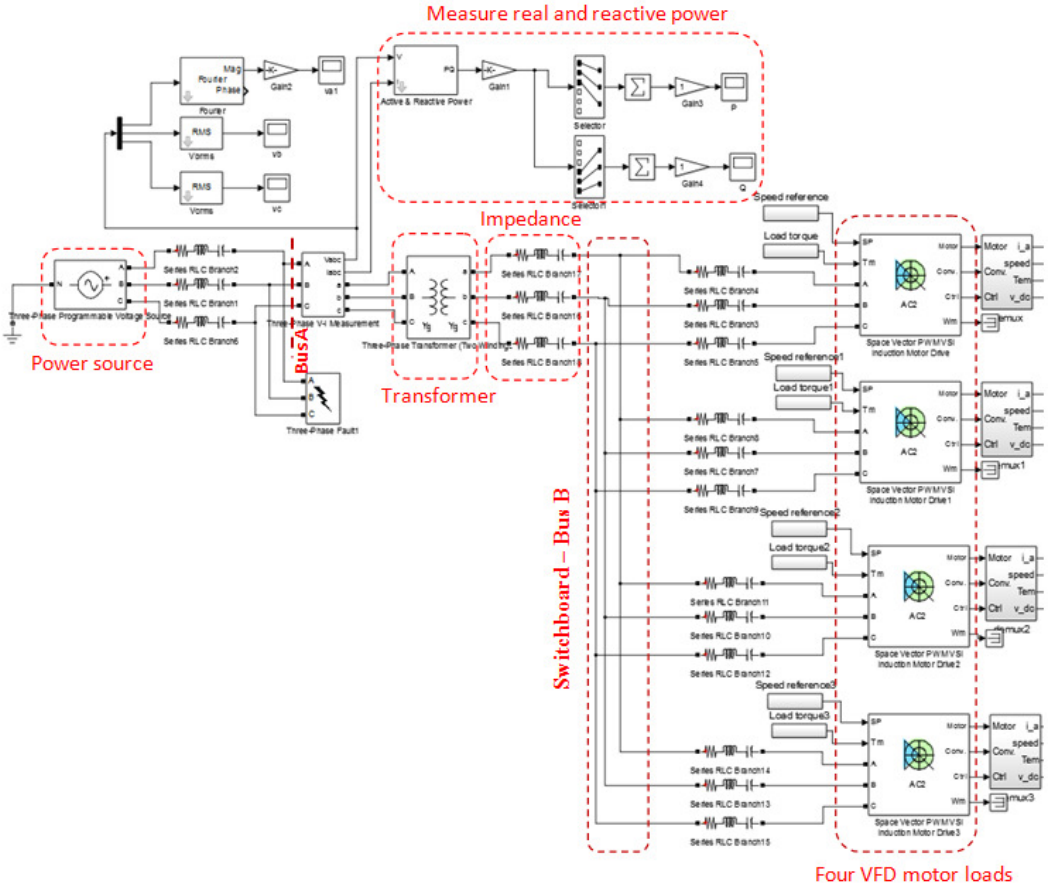

Figure 5.8 The detailed switching model for Scenario 2

Table 5.3 The aggregated dynamic model for Scenario 2 (Loading 1)

	Calculated transfer functions for the dynamic model
Derived Dynamic Model	$P = P_0 + G_{P1}\Delta E + G_{P2}\Delta E^2 + (G_{P3} + G_{P4}\Delta E)\Delta f_g$ $Q = Q_0 + G_{Q1}\Delta E + G_{Q2}\Delta E^2 + (G_{Q3} + G_{Q4}\Delta E)\Delta f_g$
P_0, Q_0	8.821kW, 3.7808kVAR
G_{P1}	$G_{P1} = \frac{(-4.1311S^7 - 7.91\times10^3 S^6 - 2.0383\times10^6 S^5 - 1.0794\times10^8 S^4 - 2.5373\times10^7 S^3 + 1.9429\times10^8 S^2 + 1.5014\times10^7 S - 7.6224\times10^7)}{(S^7 + 456.7627S^6 + 7.8812\times10^4 S^5 + 6.4996\times10^6 S^4 + 2.1548\times10^8 S^3 - 1.4092\times10^8 S^2 - 2.6477\times10^8 S + 1.8618\times10^8)}$
G_{P2}	$G_{P2} = \frac{(-0.0023S^7 - 2.3494S^6 - 4.5671\times10^3 S^5 - 2.7175\times10^5 S^4 + 3.4012\times10^6 S^3 - 8.567\times10^6 S^2 - 4.426\times10^6 S + 1.1633\times10^7)}{(S^7 + 1.6593\times10^3 S^6 + 3.8676\times10^5 S^5 + 3.7859\times10^7 S^4 + 1.373\times10^9 S^3 - 6.1516\times10^9 S^2 - 1.7447\times10^9 S + 7.905\times10^9)}$
G_{P3}	$G_{P3} = \frac{(15.7601S^7 + 2.9661\times10^4 S^6 + 9.1068\times10^6 S^5 + 5.22\times10^8 S^4 + 9.6808\times10^8 S^3 + 6.1235\times10^8 S^2 + 3.6317\times10^8 S + 1.5302\times10^8)}{(S^7 + 513.7506.S^6 + 9.4069\times10^4 S^5 + 8.1607\times10^6 S^4 + 2.8881\times10^8 S^3 + 3.231\times10^8 S^2 + 1.1089\times10^8 S + 1.1894\times10^8)}$
G_{P4}	$G_{P4} = \frac{(0.0065S^7 + 13.9108S^6 + 4.2307\times10^3 S^5 + 2.3499\times10^5 S^4 - 4.2698\times10^4 S^3 + 3.9138\times10^5 S^2 + 4.9924\times10^5 S - 4.3527\times10^5)}{(S^7 + 504.5856S^6 + 9.1473\times10^4 S^5 + 7.8571\times10^6 S^4 + 2.7327\times10^8 S^3 + 1.0654\times10^8 S^2 + 5.255\times10^8 S + 8.4701\times10^8)}$
G_{Q1}	$G_{Q1} = \frac{(-16.9046S^7 - 8.8257\times10^4 S^6 - 2.6466\times10^7 S^5 - 1.3721\times10^9 S^4 + 6.9137\times10^9 S^3 + 8.4424\times10^9 S^2 - 1.6358\times10^8 S + 1.398\times10^9)}{(S^7 + 472.3802S^6 + 8.3139\times10^4 S^5 + 6.9929\times10^6 S^4 + 2.3953\times10^8 S^3 + 1.3968\times10^8 S^2 - 5.2794\times10^8 S - 4.4034\times10^8)}$
G_{Q2}	$G_{Q2} = \frac{(4.7084\times10^{-4} S^7 - 1.7746S^6 - 470.7178S^5 - 2.2352\times10^4 S^4 + 1.999\times10^5 S^3 + 1.427\times10^6 S^2 + 2.2765\times10^6 S + 1.0737\times10^6)}{(S^7 + 432.5951S^6 + 7.3513\times10^4 S^5 + 6.1048\times10^6 S^4 + 2.1721\times10^8 S^3 + 1.0089\times10^9 S^2 + 1.4497\times10^9 S + 6.5331\times10^8)}$
G_{Q3}	$G_{Q3} = \frac{(-26.6347S^7 + 3.5595\times10^3 S^6 + 2.1637\times10^6 S^5 + 3.1486\times10^7 S^4 - 7.4436\times10^9 S^3 - 4.6123\times10^8 S^2 - 1.6572\times10^9 S - 1.2289\times10^{10})}{(S^7 + 445.9095S^6 + 7.6117\times10^4 S^5 + 6.239\times10^6 S^4 + 2.0743\times10^8 S^3 + 1.4379\times10^7 S^2 + 5.8121\times10^7 S + 3.4122\times10^8)}$
G_{Q4}	$G_{Q4} = \frac{(-0.0127S^7 + 3.1436S^6 + 741.0534S^5 + 6.1252\times10^3 S^4 - 2.0776\times10^6 S^3 - 5.0229\times10^6 S^2 + 3.6183\times10^7 S + 4.4588\times10^7)}{(S^7 + 370.2202S^6 + 5.6633\times10^4 S^5 + 4.2361\times10^6 S^4 + 1.3114\times10^8 S^3 + 2.1742\times10^8 S^2 - 2.2276\times10^9 S - 2.6255\times10^9)}$

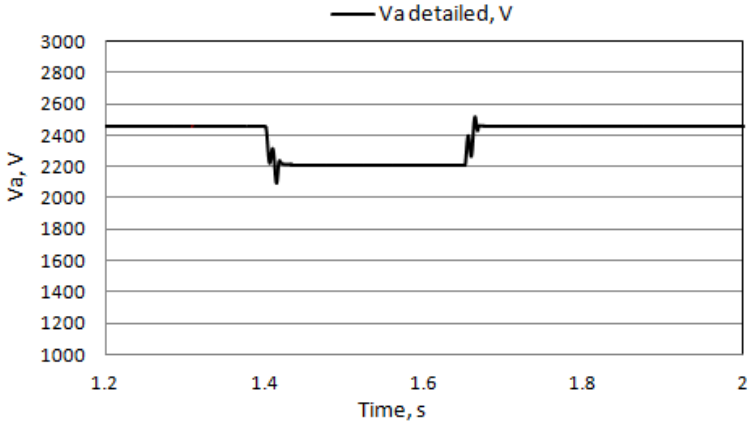

(a) Voltage sag at Phase a

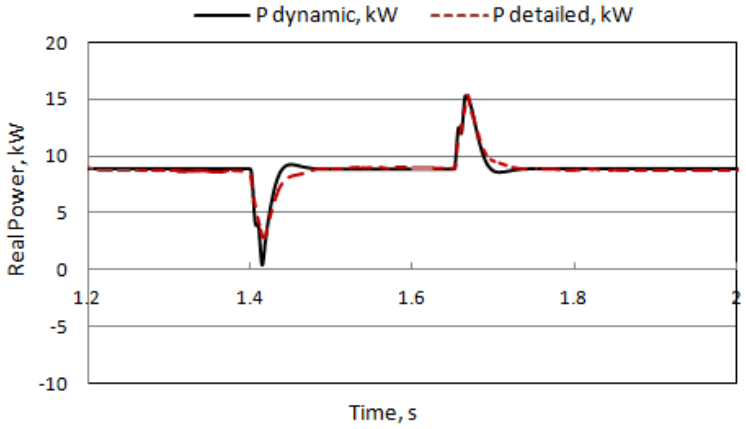

(b) Real Power P

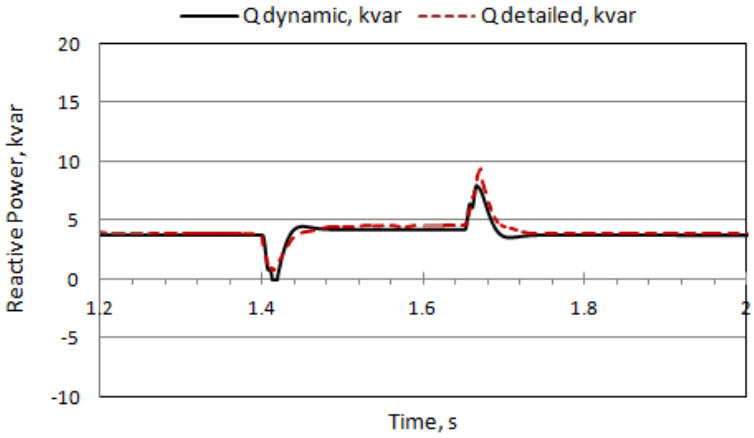

(c) Reactive Power Q

Figure 5.9 Dynamic responses of the aggregated dynamic and detailed switching models for Scenario 2, 90% voltage sag

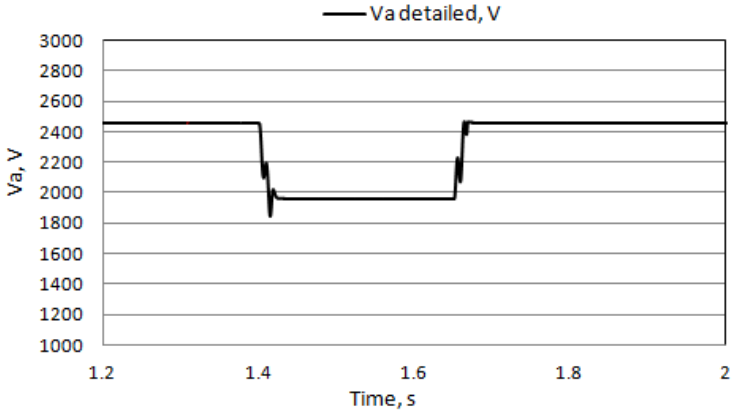

(a) Voltage sag at Phase a

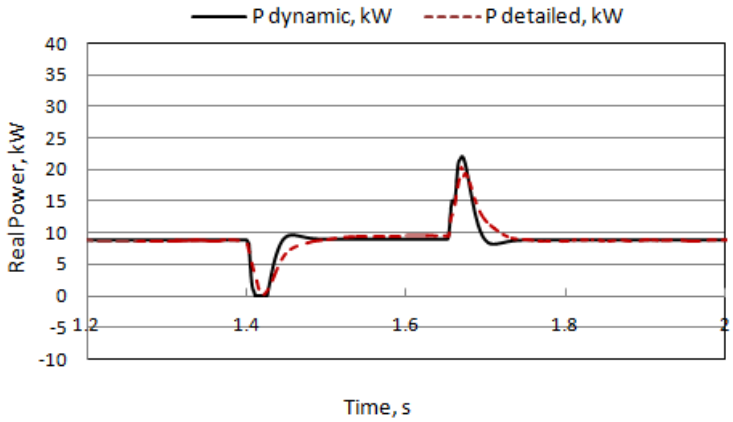

(b) Real Power P

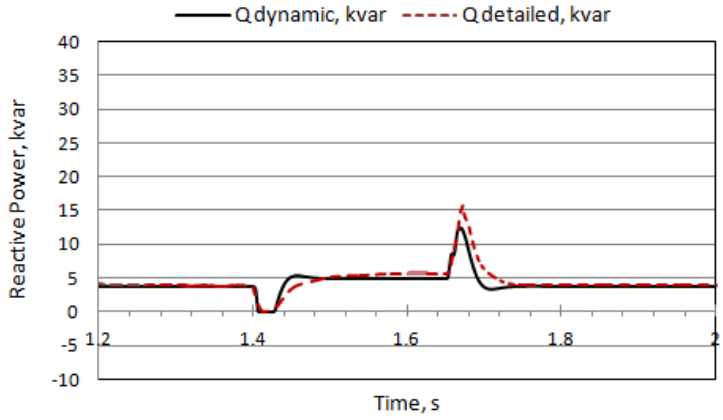

(c) Reactive Power Q

Figure 5.10 Dynamic responses of the aggregated dynamic and detailed switching models for Scenario 2, 80% voltage sag

5.4.2 Frequency Dependence

The frequency dependence is verified by applying frequency variation from 60 Hz to 52 Hz, which is applied at the power source at 1.4 s and cleared at 1.65 s with the total simulation time equal to 2 s. Individual VFDs and their motor loads are the same as Table 4.1 except the following slight loading changes for the induction motor: Load torque T_L = 12 NM, and target speed n_r = 1705 rpm. The derived aggregated dynamic model at Bus A can be found in Table 5.4.

Dynamic responses of the aggregated dynamic model and the detailed switching model at Bus A are shown in Figure 5.11. It is found that there are good agreements between the two models at Bus A, which verifies the accuracy of the proposed aggregation algorithms considering the frequency dependence.

Table 5.4 The aggregated dynamic model for Scenario 2 (Loading 2)

	Calculated transfer functions for the dynamic model
Derived Dynamic Model	$P = P_0 + G_{P1}\Delta E + G_{P2}\Delta E^2 + (G_{P3} + G_{P4}\Delta E)\Delta f_g$ $Q = Q_0 + G_{Q1}\Delta E + G_{Q2}\Delta E^2 + (G_{Q3} + G_{Q4}\Delta E)\Delta f_g$
P_0, Q_0	9.7665kW, 4.458kVAR
G_{P1}	$G_{P1} = \frac{(-6.0303S^7 - 9.1917\times10^3 S^6 - 5.1433\times10^6 S^5 - 3.0278\times10^8 S^4 - 6.9813\times10^8 S^3 + 2.4955\times10^8 S^2 + 1.5193\times10^9 S + 8.5649\times10^8)}{(S^7 + 878.9134S^6 + 1.8447\times10^5 S^5 + 1.7211\times10^7 S^4 + 6.3115\times10^8 S^3 + 7.0232\times10^8 S^2 - 1.3674\times10^9 S - 1.5638\times10^9)}$
G_{P2}	$G_{P2} = \frac{(-8.9328\times10^{-4} S^7 - 2.7685S^6 - 1.8889\times10^3 S^5 - 9.6825\times10^4 S^4 + 8.9015\times10^5 S^3 - 3.4848\times10^5 S^2 + 7.4294\times10^5 S + 2.8086\times10^6)}{(S^7 + 807.4461S^6 + 1.6559\times10^5 S^5 + 1.5166\times10^7 S^4 + 5.3933\times10^8 S^3 - 1.25\times10^8 S^2 + 7.1736\times10^8 S + 1.747\times10^9)}$
G_{P3}	$G_{P3} = \frac{(18.166S^7 + 3.215\times10^4 S^6 + 7.2032\times10^6 S^5 + 3.3248\times10^8 S^4 - 9.2248\times10^7 S^3 - 1.797\times10^9 S^2 - 1.8203\times10^9 S - 4.7886\times10^8)}{(S^7 + 421.6913.S^6 + 6.8471\times10^4 S^5 + 5.3212\times10^6 S^4 + 1.6329\times10^8 S^3 - 2.268\times10^8 S^2 - 6.7816\times10^8 S - 2.4632\times10^8)}$
G_{P4}	$G_{P4} = \frac{(0.0076S^7 + 15.4329S^6 + 3.6607\times10^3 S^5 + 1.6858\times10^5 S^4 - 2.7898\times10^5 S^3 + 4.9997\times10^5 S^2 + 7.3339\times10^5 S - 5.918\times10^5)}{(S^7 + 433.3348S^6 + 7.1418\times10^4 S^5 + 5.623\times10^6 S^4 + 1.7526\times10^8 S^3 - 1.8355\times10^8 S^2 + 4.3254\times10^8 S + 9.7843\times10^8)}$
G_{Q1}	$G_{Q1} = \frac{(-1.2296S^7 - 4.5418\times10^3 S^6 - 1.6379\times10^6 S^5 - 7.8104\times10^7 S^4 + 5.7329\times10^8 S^3 - 1.9125\times10^8 S^2 - 1.0543\times10^9 S + 4.0039\times10^7)}{(S^7 + 542.4446S^6 + 9.8862\times10^4 S^5 + 8.3996\times10^6 S^4 + 2.8061\times10^8 S^3 - 2.155\times10^8 S^2 - 5.7676\times10^8 S + 2.2063\times10^7)}$
G_{Q2}	$G_{Q2} = \frac{(5.2091\times10^{-4} S^7 - 1.8184S^6 - 558.139S^5 - 2.2839\times10^4 S^4 + 3.7631\times10^5 S^3 + 4.8925\times10^5 S^2 + 5.4646\times10^5 S + 5.8488\times10^5)}{(S^7 + 462.8682S^6 + 7.9317\times10^4 S^5 + 6.4938\times10^6 S^4 + 2.1593\times10^8 S^3 + 2.7523\times10^8 S^2 + 3.0513\times10^8 S + 2.9813\times10^8)}$
G_{Q3}	$G_{Q3} = \frac{(-30.7208S^7 + 3.2923\times10^3 S^6 + 2.9145\times10^6 S^5 + 3.1355\times10^7 S^4 - 9.4472\times10^9 S^3 - 9.6781\times10^9 S^2 + 1.5623\times10^9 S + 3.1849\times10^8)}{(S^7 + 473.9824S^6 + 8.2068\times10^4 S^5 + 6.7652\times10^6 S^4 + 2.2546\times10^8 S^3 + 2.2167\times10^8 S^2 - 3.6245\times10^7 S - 7.3361\times10^6)}$
G_{Q4}	$G_{Q4} = \frac{(-0.0149S^7 + 3.579S^6 + 954.3145S^5 + 8.5653\times10^3 S^4 - 2.5788\times10^6 S^3 - 1.6031\times10^7 S^2 + 4.3709\times10^7 S + 6.6815\times10^7)}{(S^7 + 382.0529S^6 + 5.9494\times10^4 S^5 + 4.5603\times10^6 S^4 + 1.4982\times10^8 S^3 + 6.9819\times10^8 S^2 - 2.2268\times10^9 S - 3.224\times10^9)}$

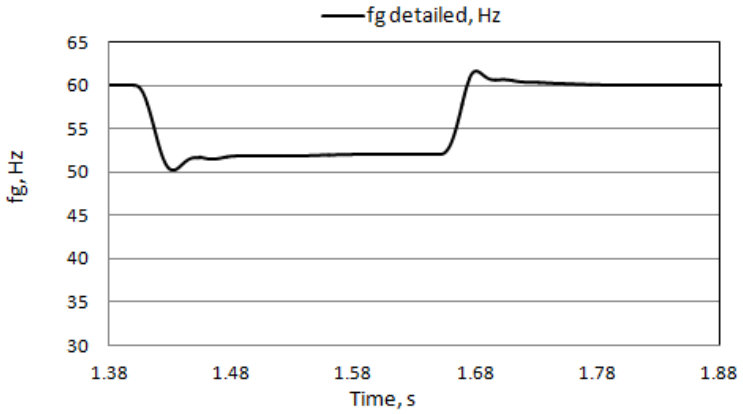

(a) Frequency sag

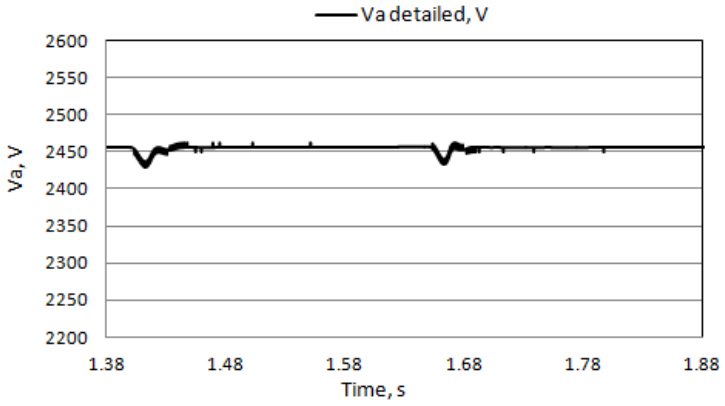

(b) Voltage variation with frequency sag

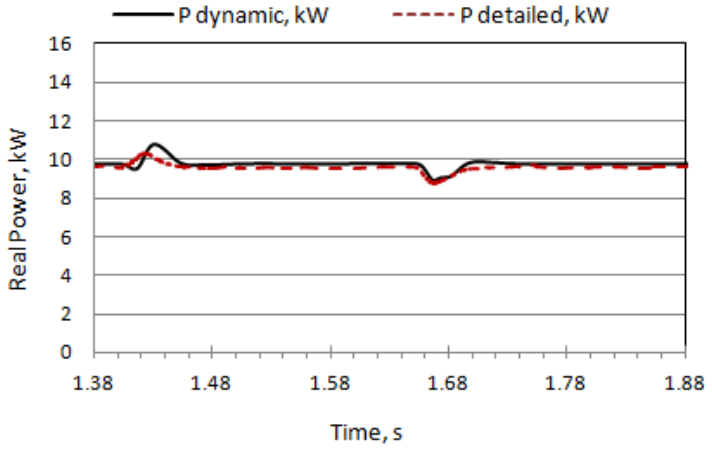

(c) Real Power P

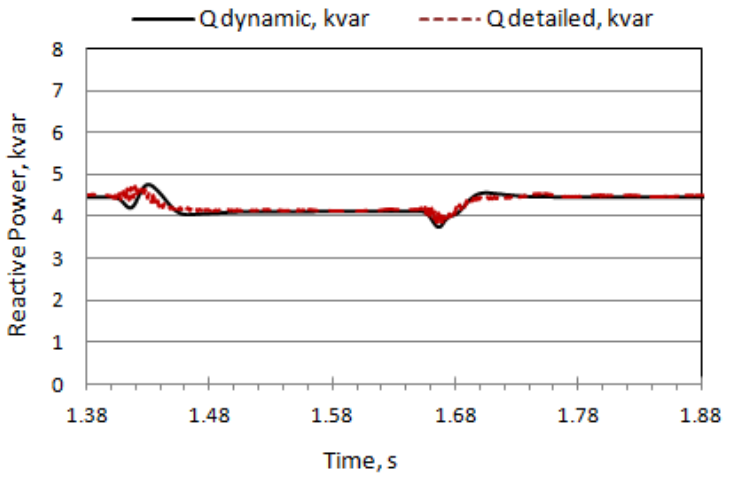

(d) Reactive power Q

Figure 5.11 Dynamic responses of the aggregated dynamic and detailed switching models for Scenario 2, frequency variation

5.5 Summary and Conclusions

Aggregation algorithms of motor drive loads are proposed in this chapter for two cases: 1) VFDs connected to the same bus, 2) VFDs further aggregated with upstream series impedance and transformers. Both voltage and frequency dependence are considered in the proposed aggregation algorithms.

The accuracy of the proposed aggregation algorithms for motor drive systems is verified by comparing dynamic responses of the aggregated dynamic models with that of the detailed switching models for both cases.

CHAPTER 6 CONCLUSIONS AND FUTURE WORK

6.1 A Generic Dynamic Load Model Structure for Industrial Facilities

The ultimate goal of the research work is to create adequate dynamic load models for industrial facilities. In Chapter 2, the template-based load modeling technique for industrial facilities is proposed. In Chapters 4 and 5, the equivalent dynamic model and aggregation algorithms for motor drive systems are proposed.

Commonly used loads could vary from one type of industrial facilities to another. For example, there are three common types of loads involved in oil refinery facilities: induction motors, synchronous motors and static loads, the number of VFDs are in very small amount in oil refinery facilities and thus VFDs can be ignored from load modeling. In newer Kraft paper mill facilities, three common types of loads could be present: induction motors, VFDs, and static loads [131], synchronous motors are not used in this type of facilities.

A generic dynamic load model structure for industrial facilities is proposed in this thesis, which consists of an induction motor, a synchronous motor, a static load, and a motor drive system as shown in Figure 6.1. This generic load model structure shall cover all commonly used loads and can be used to establish dynamic load models for any types of industrial facilities.

The final load model for an industrial facility of interest can be adjusted by removing certain load types that do not exist in the facility from the generic structure. For example, as discussed in Chapter 3, the “motor drive system” branch can be removed, and the “induction motor”, “synchronous motor” and “static load” are left in the final load model for oil refinery facilities. For newer Kraft paper mill facilities, the “synchronous motor” branch needs to be removed,

and the “induction motor”, “motor drive system” and “static load” are left in the final load model.

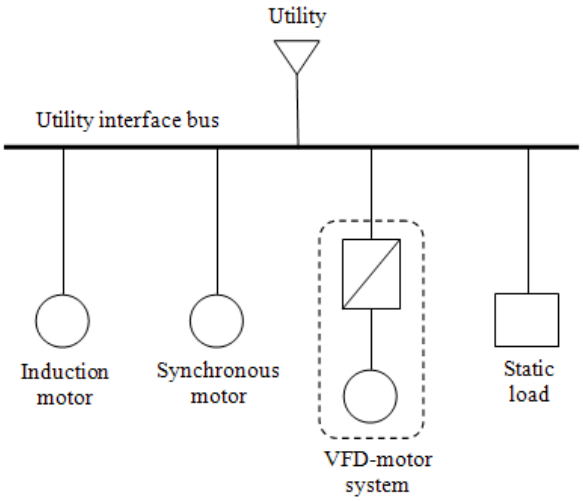

Figure 6.1 The generic dynamic load model structure for industrial facilities

More “motor drive system” branches might be added to the load model if the drives and/or motors are different types, which result in different order transfer functions for the dynamic model, and thus, need to be expressed by separate branches.

The procedure to create the final dynamic load model for an industrial facility of interest can be explained as follows:

1) Conduct survey for the industrial facility of interest, and determine major load types that will be included in the dynamic load modeling.
2) Tailor the generic dynamic load model structure based on major load types into the final load model structure.
3) Create the templates and template scaling rules, and establish the template-based full model of the facility based on the template-based load modeling technique.
4) If VFDs are one of major load types in the facility, they shall be included in the established template-based full model.

5) Apply the model equivalence algorithms for induction motors, synchronous motors, motor drive systems, and static loads (if present) in the template-based full model to achieve load aggregation of whole facility.

6.2 Conclusions

Two major contributions for dynamic load modeling of industrial facilities are presented in this thesis:

1) Template-based load modeling technique
2) Equivalent dynamic models and aggregation algorithms for motor drive systems

The combination of the above two contributions will lead to adequate dynamic load models for industrial facilities.

Large industrial facilities connected to power transmission systems typically draw large amounts of power and have complex dynamic responses to systems disturbances. Traditional load modeling approaches such as those based on load composition or site measurements are not adequate to produce dynamic models for such facilities.

A template-based load modeling technique is proposed to provide adequate dynamic load modeling for large industrial facilities. This technique consists of three main building blocks, electrical templates, template scaling rules and the model aggregation method. Oil refinery facilities are used as example to demonstrate the proposed technique. Various case studies conducted have shown that the template-based full model and equivalent models are able to capture major dynamic characteristics of actual oil refinery facilities and can be used to represent such facilities when detailed facility information is not available.

Due to increasing usage of VFDs in some types of industrial facilities, the influence of VFDs and their loads on overall system dynamics for such facilities

become essential. However, dynamic models for motor drive systems suitable for power systems dynamic studies are not available. To address this issue, the equivalent dynamic model for motor drive systems is proposed in this thesis for the case that VFDs can ride through voltage sags. This model is created by linearization of differential equations of the drive, the motor, and their control system. The voltage dependence and frequency dependence are considered. Dynamic models for VSI and cascaded inverter motor drive systems are created. As part of the load aggregation requirements for the whole facility, aggregation algorithms for motor drive systems are also proposed. The accuracy of the proposed aggregation algorithms for motor drive systems is verified using case studies.

The ultimate goal of the research work is to create adequate dynamic load models for industrial facilities. Therefore, a generic dynamic model structure for industrial facilities is proposed in this thesis, which consists of an induction motor, a synchronous motor, a static load, and a motor drive system. This generic structure shall cover all commonly used loads and can be used to establish dynamic load models for any types of industrial facilities. The final load model for an industrial facility of interest can be tailored from the generic structure based on load types practically involved in the facility. Procedure on how to use the proposed generic dynamic load model, template-based load modeling technique, and dynamic modeling and aggregation approaches for motor drive systems to establish the final dynamic load model for an industrial facility is recommended in the thesis.

6.3 Future Work

Based on current research results, the future work can be extended in the following directions:

1) If VFDs are connected to a same bus/switchboard with many induction motors, which is similar to the case induction motors and synchronous motors are connected to the same bus, how to split VFDs and induction motors for load aggregation purpose might need further investigations.
2) Develop equivalent dynamic models for CSI and NPC inverter motor drive systems for motor systems.
3) Dynamic load models for motor drive system under unbalanced fault conditions.

BIBLIOGRAPHY

[1] IEEE Task Force on Load Representation for Dynamic Performance, "Load Representation for Dynamic Performance Analysis", IEEE Transactions on Power Systems, Vol. 8, No.2, May 1993, Page(s): 472 – 482.

[2] IEEE Task Force on Load Representation for Dynamic Performance, System Dynamic Performance Subcommittee, Power System Engineering Committee, "Standard Load Models for Power Flow and Dynamic Performance Simulation", IEEE Transactions on Power Systems, Vol.10, No. 3, August 1995, Page(s): 1302 – 1313.

[3] Ellis, D. Kosterev, and Anatoliy Meklin, "Dynamic Load Models: Where Are We?", 2005/2006 IEEE PES Transmission and Distribution Conference and Exhibition, Page(s) 1320-1324.

[4] Graham J. Rogers, John Di Manno, Robert T.H. Alden, "An Aggregate Induction Motor Model for Industrial Plant", IEEE Transactions on Power Apparatus and Systems, Vol. PAS-103, No. 4, April 1984, Page(s): 683-690.

[5] Kip Morison, Hamid Hamadani, Lei Wang, "Practical Issues in Load Modeling for Voltage Stability Study", IEEE Power Engineering Society General Meeting, Vol. 3, 13-17 July 2003, Page(s): 1392-1397.

[6] Dmitry Kosterev and Anatoliy Meklin, "Load Modeling in WECC", 2006 IEEE PES Power Systems Conference and Exposition (PSCE '06), Oct. 29 -Nov. 1 2006, Page(s):576 – 581.

[7] S.A.Y. Sabir, and D.C. Lee, "Dynamic Load Models Derived from Data Acquired During System Transients", IEEE Transactions on Power

Apparatus and Systems, Vol. PAS-101, No. 9, September 1982, Page(s): 3365-3372.

[8] Sina Chiniforoosh, Ph.D. thesis, "Generalized Dynamic Average Modeling of Line-commutated Converter Systems in Transient Simulation Programs", University of British Columbia, 2012.

[9] Takao Omata, and Katsuhiko Uemura, "Effects of Series Impedance on Power System Load Dynamics", IEEE Transactions on Power Systems, Vol. 14, No. 3, August 1999, Page(s): 1070-1077.

[10] F.T. Dai, J.V. Milanovic, N. Jenkins, and V. Roberts, "Development of a Dynamic Power System Load Model", IEE Seventh International Conference on AC-DC Power Transmission, 28-30 November 2001, Page(s): 344-349.

[11] E. Welfonder, H. Weber, and B. Hall, "Investigations of the Frequency and Voltage Dependence of Load Part Systems Using a Digital Self-Acting Measuring and Identification System", IEEE Transactions on Power Systems, Vol. 4, No. 1, February 1989, Page(s): 19-25.

[12] Krishnaswamy Srinivasan, and Claude Lafond, "Statistical Analysis of Load Behavior Parameters at Four Major Loads", IEEE Transactions on Power Systems, Vol. 10, No. 1, February 1995, Page(s): 387-392.

[13] He Renmu, Ma Jin, David J. Hill, "Composite Load Modeling Via Measurement Approach", IEEE Transactions on Power Systems, Vol. 21, No.2, May 2006, Page(s): 663 – 672.

[14] Ma Jin, He Renmu, David J. Hill, "Load Modeling by Finding Support Vectors of Load Data from Field Measurements", IEEE Transactions on Power Systems, Vol. 21, No. 2, May 2006, Page(s):726 – 735.

[15] Aleksandar M. Stankovic and Andrija T. Saric, "Transient Power System Analysis with Measurement-Based Gray Box and Hybrid Dynamic

Equivalents", IEEE Transactions on Power Systems, Vol. 19, No. 1, February 2004, Page(s): 455 – 462.

[16] Qian Ai, Danzhen Gu, Chen Chen, "New Load Modeling Approaches Based on Field Tests for Fast Transient Stability Calculations", IEEE Transactions on Power Systems, Vol. 21, No. 4, November 2006, Page(s): 1864 – 1873.

[17] Jin-Cheng Wang, Hsiao-Dong Chiang, Chung-Liang Chang, Ah-Hsing Liu, Chang-Horng Huang, Chiung-Yi Huang, "Development of a Frequency-Dependent Composite Load Model Using the Measurement Approach", IEEE Transactions on Power Systems, Vol. 9, No. 3, August 1994, Page(s):1546 – 1556.

[18] Byoung-Kon Choi, Hsiao-Dong Chiang, Yinhong Li, Yung-Tien Chen, Der-Hua Huang, and Mark G. Lauby, "Development of Composite Load Models of Power Systems using On-line Measurement Data", 2006 IEEE Power Engineering Society General Meeting, Page(s): 1-8.

[19] Danlel Karlsson, and David J. Hill, "Modeling and Identification of Nonlinear Dynamic Loads in Power Systems", IEEE Transactions on Power System, Vol. 9, No. 1, February 1994, Page(s): 157-166.

[20] William U. Price, Kim A. Uirgau, Alexander Uurdoch, James V. Uitsche, Ebrahim Vaahedi, and Uoe A. El-Kady, "Load Modeling for Power Flow and Transient Stability Computer Studies", IEEE Transactions on Power Systems, Vol. 3, No. 1, February 1988, Page(s): 180-187.

[21] J.R. Ribeiro, and F.J. Lange, "A New Aggregation Method for Determination Composite Load Characteristics", IEEE Transactions on Power Apparatus and Systems, Vol. PAS-101, No. 8 August 1982, Page(s): 2869-2875.

[22] Jae-Yoon Lim, Jeung-Hoon Kim, Jin-O Kim, Chanan Singh, "Application of Expert System to Load Composition Rate Estimation Algorithm", IEEE Transactions on Power Systems, Vol. 14, No. 3, August 1999, Page(s): 1137-1143.

[23] Jin-Yi Kim, Dong-Jun Won, and Seung-11 Moon, "Development of the Dynamic Equivalent Model for Large Power System", 2001 IEEE Power Engineering Society Summer Meeting, Vol. 2, Page(s): 973 – 977.

[24] Ma Da-Qing, and Ju Ping, "A Novel Approach to Dynamic Load Modeling", IEEE Transactions on Power Systems, Vol. 4, No. 2, May 1989, Page(s): 396-402.

[25] Roderick J. Frowd, Robin Podmore, and Mark Waldron, "Synthesis of Dynamic Load Models for Stability Studies", IEEE Transactions on Power Apparatus and Systems, Vol. PAS-101, No. 1 January 1982, Page(s): 127-135.

[26] Lim, J.Y., Ji, P.S., Ozdemir, A, Singh, C, "Component-Based Load Modeling including Capacitor Banks", IEEE Power Engineering Society Summer Meeting, Vol. 2, 15-19 July 2001, Page(s): 1199-1204.

[27] Toshio Shimada, Shigem Agematsu, Toshiya Shoji, Toshihisa Funabshi, Hitomi Otoguro, and Akihiro Ametani , "Combining Power System Load Models at a Busbar", 2000 IEEE Power Engineering Society Summer Meeting, Vol. 1, Page(s): 383 – 388.

[28] P. Ju, and X.Y. Zhou, "Dynamic Equivalents of Distribution Systems for Voltage Stability Studies", IEE Proc.-Gener. Transm. Distrib., Vol. 148, No. 1, January 2001, Page(s): 49-53.

[29] Les Pereira, Dmitry Kosterev, Peter Mackin,, Donald Davies, John Undrill, and Wenchun Zhu, "An Interim Dynamic Induction Motor

Model for Stability Studies in the WSCC", IEEE Transactions on Power Systems, Vol. 17, No. 4, November 2002, Page(s): 1108-1115.

[30] IEEE Recommended Practice for Monitoring Electric Power Quality, 1995, IEEE Standard 1159, New York.

[31] Antoni Sudria, Miquel Teixido, Samuel Galceran, Oriol Gomis, Daniel Montesinos, Frede Blaabjerg, "Grid Voltage Sags Effects on Frequency Converter Drives and Controlled Rectifier Drives", IEEE Compatibility in Power Electronics, 2005, Page(s): 1-7.

[32] S. Z. Djokic, K. Stockman, J. V. Milanovic, J. J. M. Desmet, and R. Belmans, "Sensitivity of AC Adjustable Speed Drives to Voltage Sags and Short Interruptions", IEEE Transactions on Power Delivery, Vol. 20, No. 1, January 2005, pp. 494-505.

[33] S. Z. Djokic, S. M. Munshi, and C. E. Cresswell, "The Influence of Overcurrent and Undervoltage Protection Settings on ASD Sensitivity to Voltage Sags and Short Interruptions", 4th IET conference on Power Electronics, Machines and Drives, 2008 (PEMD 2008), pp. 130-134.

[34] Ran Cao, and E.R. Collins, Jr., "The Effects of Load Types on the Behaviors of AC Motor Drives During Voltage Sags", 10th International Conference on Harmonics and Quality of Power, Vol. 1, 2002, Page(s): 353-358.

[35] Debaprasad Kastha, and Bimal K. Bose, "Investigation of Fault Modes of Voltage-Fed Inverter System for Induction Motor Drive", IEEE Transactions on Industry Applications, Vol. 30, No. 4, July/August 1994, Page(s): 1028-1037.

[36] Jose Luis Duran-Gomez, Prasad N. Enjeti, and Byeong Ok Woo, "Effect of Voltage Sags on Adjustable-Speed Drives: A Critical Evaluation and an Approach to Improve Performance", IEEE Transactions on Industry

Applications, Vol. 35, No. 6, November/December 1999, Page(s): 1440-1449.

[37] C.P. Gupta, and Jovica V. Milanovic, "Probabilistic Assessment of Equipment Trips due to Voltage Sags", IEEE Transactions on Power Delivery, Vol. 21, No. 2, April 2006, Page(s): 711-718.

[38] Asma Merdassi, Laurent Gerbaud, and Seddik Bacha, "A New Automatic Average modelling Tool for Power Electronics Systems", 2008 IEEE Power Electronics Specialists Conference (PESC), Page(s): 3425-3431.

[39] Jian Sun, and Horst Grotstollen, "Averaged Modeling of Switching Power Converters: Reformulation and Theoretical Basis", 1992 IEEE 23rd Annual Power Electronics Specialists Conference (PESC'92), Vol. 2, Page(s): 1165 – 1172.

[40] S. Cuk, and R. D. Middlebrook, "A General Unified Approach to Modelling Switching-Power-Stages", IEEE PESC'76 Record, 1976, Page(s): 18-31.

[41] Antonio Griffo, Jiabin Wang, and David Howe, "State-Space Average Modeling of 18-Pulse Diode Rectifier", 3rd International Conference From Scientific Computing to Computational Engineering (IC-SCCE), Athens, 9-12 July, 2008.

[42] T.A. Meynard, M. Fadel, and N. Aouda, "Modeling of Multilevel Converters", IEEE Transactions on Industrial Electronics, Vol. 44, No. 3, June 1997, Page(s): 356-364.

[43] Alexander Uan-Zo-li, Rolando P. Burgos, Frederic Lacaux, Fred Wang and Dushan Boroyevich, "Assessment of Multi-Pulse Converter Average Models for Stability Studies Using a Quasi-Stationary Small-Signal

Technique", the 4th International Power Electronics and Motor Control Conferences, 2004, Vol. 3, Page(s): 1654-1658.

[44] Huiyu Zhu, Rolando P. Burgos, Frederic Lacaux, Alexander Uan-Zo-li, Douglas K. Lindner, Fred Wang, and Dushan Boroyevich, "Average Modeling of Three-phase and Nine-phase Diode Rectifiers with Improved AC Current and DC Voltage Dynamics", 2005 31st Annual Conference of IEEE Industrial Electronics Society, Page(s): 1024-1029.

[45] Sebastian Rosado, Rolando Burgos, Fred Wang, and Dushan Boroyevich, "Large- and Small-Signal Evaluation of Average Models for Multi-Pulse Diode Rectifiers", 2006 IEEE COMPEL Workshop, Rensselaer Polytechnic Institute, Troy, NY, USA, July 16-19, 2006, Page(s): 89-94.

[46] Sebastian Rosado, Rolando Burgos, Fred Wang, and Dushan Boroyevich, "Large-Signal Stability Assessment of AC/DC Systems with Multi-Pulse Rectification and DC-Fed PWM Motor Drives", 2007 IEEE Power Electronics Specialist Conference (PESC), Page(s): 2168-2173.

[47] J. Arrillaga, H.J. Al-Khashali, and J.G. Campos-Barros, **"**General formulation for dynamic studies in power systems including static convertors**",** Proc. IEE, Vol. 124, No. 11, November 1977, Page(s): 1047-1052.

[48] Alfred Baghramian, "Average, Dynamic Model of Multi-Pulse Rectifiers", 2010 18th IEEE Iranian Conference on Electrical Engineering (ICEE), Page(s): 716 – 721.

[49] Liqiu Han, Jiabin Wang and David Howe, "State-space average modeling of 6- and 12-pulse diode rectifiers", 2007 European Conference on Power Electronics and Applications, Page(s): 1 – 10.

[50] D. N. Kosterev, "Modeling Synchronous Voltage Source Converters in Transmission System Planning Studies", IEEE Transactions on Power Delivery, Vol. 12, No. **2,** April 1997, Page(s): 947-952.

[51] Giuseppe Saccomando, and Jan Svensson, "Transient Operation of Grid-connected Voltage Source Converter Under Unbalanced Voltage Conditions", 2001 IEEE 36th Industry Application Society (IAS) Annual Meeting, Vol. 4, Page(s): 2419-2424.

[52] Brad Lehman, and Richard M. Bass, "Switching Frequency Dependent Averaged Models for PWM DC-DC Converters", IEEE Transactions on Power Electronics, Vol. 11, No. 1, January 1996, Page(s): 89-98.

[53] S.D. Sudhoff, K.A. Corzine**,** H.J. Hegner, and D.E. Delisle, "Transient and Dynamic Average-value Modeling of Synchronous Machine Fed Load-Commutated Converters", IEEE Transactions on Energy Conversion, Vol. 11, No. 3, September 1996, Page(s): 508-514.

[54] Jian Sun, Daniel M. Mitchell*,* Matthew F. Greuel, Philip T. Krein, and Richard M. Bass, "Averaged Modeling of PWM Converters Operating in Discontinuous Conduction Mode", IEEE Transactions on Power Electronics, Vol. 16, No. 4, July 2001, Page(s): 482-492.

[55] Keith Corzine, Xiaomin Kou, and James R. Baker, "Dynamic Average-Value Modeling of a Four-Level Drive System", IEEE Transactions on Power Electronics, Vol. 18, No. 2, March 2003, Page(s): 619-627.

[56] Juri Jatskevich, and Tarek Aboul-Seoud, "Impedance Characterization of a Six-Phase Synchronous Generator-Rectifier System Using Average-Value Model", 2004 Canadian Conference on Electrical and Computer Engineering, Vol. 4, Page(s): 2231 – 2234.

[57] Juri Jatskevich*,* Steven D. Pekarek, and Ali Davoudi, "Parametric Average-Value Model of Synchronous Machine-Rectifier Systems",

IEEE TRANSACTIONS ON ENERGY CONVERSION, VOL. 21, NO. 1, MARCH 2006, Page(s): 9-18.

[58] Baghramian, and A.J. Forsyth, "Averaged-Value Models of Twelve-Pulse Rectifiers for Aerospace Applications", 2004 2nd international Conference on Power Electronics, Machines, and Drives, Vol. 1, Page(s): 220 – 225.

[59] Cross, A. Baghramian, and A. Forsyth, "Approximate, average, dynamic models of uncontrolled rectifiers for aircraft applications", IET Power Electron., 2009, Vol. 2, Issue. 4, Page(s): 398–409.

[60] Paul C. Krause, Oleg Wasynczuk, Scott D. Sudhoff, "Analysis of Electric Machinery and Drive Systems", 2nd Edition, IEEE Press Power Engineering Series.

[61] Ali Emadi, Alireza Khaligh, Claudio H. Rivetta, and Geoffrey A. Williamson, "Constant Power Loads and Negative Impedance Instability in Automotive Systems: Definition, Modeling, Stability, and Control of Power Electronic Converters and Motor Drives", IEEE Transaction on Vehicular Technology, Vol. 55, No. 4, July 2006, Page(s): 1112-1125.

[62] Ali Emadi, "Modeling of Power Electronic Loads in AC Distribution Systems Using the Generalized State-Space Averaging Method", IEEE Transactions on Industrial Electronics, Vol. 51, No. 5, OCTOBER 2004, Page(s): 992-1000.

[63] Planning and Design of Airports, 4th Edition, Robert Horonjeff, Francis X. McKelvey (Contributor), Richard D. Horonjeff, McGraw-Hill Professional, December 1, 1993.

[64] Airport Systems Planning, Design, and Management, Richard L. de Neufville, Amedeo R. Odoni, McGraw-Hill Professional, October 8, 2002.

[65] Jia Hou, Zhao Xu, and Zhao Yang Dong, "Load Modeling Practice in a Smart Grid Environment", the 4th International Conference on Electric Utility Deregulation and Restructuring and Power Technology (DRPT), 2011, Page(s): 7-13.

[66] D.C. Franklin and A. Morelato, "Improving Dynamic Aggregation of Induction Motor Models", IEEE Transactions on Power Systems, Vol. 9, No. 4, November 1994, Page(s): 1934 – 1941.

[67] M.M. Abdel Hakim and G.J. Berg, "Dynamic Single-Unit Representation of Induction Motor Groups", IEEE Transactions on Power Apparatus and Systems, Vol. PAS-95, no.1, January/February, 1976, Page(s):155 – 165.

[68] T. Kataoka, H. Uchida, S. Nishikata, T. Kai and T. Funabashi, "A Method for Aggregation of a Group of Induction Motor Loads", Proceedings of International Conference on Power System Technology, POWERCON 2000, Perth, Australia, Page(s): 1683-1688.

[69] M. Akbaba, and S.Q. Fakhro, "New model for single-unit representation of induction motor loads, including skin effect, for power system transient stability studies", IEE Proceedings-B, Vol. 139, NO. 6, November 1992, Page(s): 521-533.

[70] M. Taleb, M. Akbaba, and E. A. Abdullah, "Aggregation of Induction Machines for Power System Dynamic Studies", IEEE Transactions on Power Systems, Vol. *9,* No. 4, November 1994, Page(s): 2042-2048.

[71] Aleksandar M. Stanković, and Bernard C. Lesieutre, "A Probabilistic Approach to Aggregate Induction Machine Modeling", IEEE Transactions on Power Systems, Vol. 1 1, No. 4, November 1996, Page(s): 1983-1989.

[72] Aleksandar M. Stanković, and Bernard C. Lesieutre, "Parametric Variations in Dynamic Models of Induction Machine Clusters", IEEE

Transactions on Power Systems, Vol. 12, No. 4, November 1997, Page(s): 1549-1554.

[73] P. Piromthum, and A. Kunakom, "A Study of Starting Current due to a Group of Induction Motors Using an Aggregation Model", the Fifth International Conference on Power Electronics and Drive Systems (PEDS), 2003, Vol. 2, Page(s): 1054-1057.

[74] Joaquín Pedra, Luis Sainz, and Felipe Córcoles, "Study of Aggregate Models for Squirrel-Cage Induction Motors", IEEE Transactions on Power Systems, Vol. 20, No. 3, August 2005, Page(s): 1519-1527.

[75] K. W. Louie, "Aggregation of Induction Motors Based on Their Equivalent Circuits under Some Special Operating Conditions", Canadian Conference on Electrical and Computer Engineering, 2005, Page(s): 1966 – 1969.

[76] K. W. Louie, and P. Wilson, "Aggregation of Induction Motors Based on Their Specifications", Canadian Conference on Electrical and Computer Engineering, 2006, Page(s): 803-806.

[77] P. C. Krause, F. Nozari, T. L. Skvarenina, and D. W. Olive, "The Theory of Neglecting Stator Transients", IEEE Transactions on Power Apparatus and Systems, Vol.PAS-98, No.1 Jan/Feb 1979, Page(s): 141-148.

[78] N. Gunaratnam, and D. W. Novotny, "The Effects of Neglecting Stator Transients in Induction Machine Modeling", IEEE Transactions on Power Apparatus and Systems, Vol. PAS-99, No. 6 Nov/Dec 1980, Page(s): 2050-2059.

[79] R. Nath, and S.S. Lamba, "Development of Coherency-based Time-domain Equivalent Model Using Structure Constraints", IEE Proceedings on Generation, Transmission and Distribution, Vol. 133, Pl. C, No. 4, May 1986, Page(s): 165-175.

[80] M. Larbi Ourari, Louis-A. Dessaint, and Van-Que Do, "Dynamic Equivalent Modeling of Large Power Systems Using Structure Preservation Technique", IEEE Transactions on Power Systems, Vol. 21, No. 3, August 2006, Page(s): 1284-1295.

[81] X. Lei, D. Povh, and O. Ruhle, "Industrial Approaches for Dynamic Equivalents of Large Power Systems", IEEE Power Engineering Society Winter Meeting, Vol. 2, 2002, Page(s): 1036-1042.

[82] Federico Milano, and Kailash Srivastava, "Dynamic REI Equivalents for Short Circuit and Transient Stability Analyses", Electric Power Systems Research 79(2009), Page(s): 878-887, available online 3 January 2009.

[83] Prabha S. Kundur, "Power System Stability and Control", ISBN 0-07-035958-X, 1994, McGraw-Hill Inc.

[84] J. Germond, and R. Podmore, "Dynamic Aggregation of Generating Unit Models", IEEE Transactions on Power Apparatus and Systems, Vol. PAS-97, no. 4 July/Aug 1978, Page(s): 1060-1069.

[85] Federico Milano, and Kailash Srivastava, "Dynamic REI equivalents for short circuit and transient stability analyses", Electric Power Systems Research 79 (2009) 878–887, Elsevier.

[86] M. L. Ourari, L. A. Dessaint, V.Q. Do, "Coherency Approach for Dynamic Equivalents of Large Power Systems", International Conference on Power Systems Transients – IPST 2003 in New Orleans, USA, Page(s): 1-6.

[87] Mansoor, S. A. Mansoor, and S. A. K. Masud, "Aggregation and Dispatching of Captive Generator Sets for System Load Reduction and Capacity Relief", Second International Conference on Electrical and Computer Engineering, ICECE 2002, 26-28 December 2002, Dhaka, Bangladesh, Page(s): 220-224.

[88] R. Podmore, "A Comprehensive Program for Computing Coherency-Based Dynamic Equivalents", IEEE Conference Proceedings, 1979 Power Industry Computer Applications Conference, Page(s): 298 – 306.

[89] E.J.S. Pires de Souza, and A.M. Leite da Silva, "An Efficient Methodology for Coherency-Based Dynamic Equivalents", IEE Proceedings-C. Vol. 139, No 5, September 1992, Page(s): 371-382.

[90] Robin Podmore, "Identification of Coherent Generator for Dynamic Equivalents", IEEE Transactions on Power Apparatus and Systems, Vol. PAS-97, no. 4 July/Aug 1978, Page(s): 1344-1354.

[91] Lei Wang, Meir Klein, Solomon Yirga, and Prabha Kundur, "Dynamic Reduction of Large Power Systems for Stability Studies", IEEE Transactions on Power Systems, Vol. 12, No. 2, May 1997, Page(s): 889-895.

[92] M. L. Ourari, L. A. Dessaint, and V. Q. Do, "Generating Units Aggregation for Dynamic Equivalent of Large Power Systems", IEEE Power Engineering Society General Meeting, 2004, Vol. 2, Page(s): 1535-1541.

[93] R.J. Newell, M.D. Risan, L. Allen, IC.S. Rao, and D.L. Stuehm, "Utility Experience with Coherency-Based Dynamic Equivalents of Very Large Systems", IEEE Transactions on Power Apparatus and Systems, Vol. PAS-104, No. 11, November 1985, Page(s): 3056-3063.

[94] T.Y .J. Lem, and R.T.H. Alden, "Comparison of Experimental and Aggregate Induction Motor Responses", IEEE Transactions on Power Systems, Vol. 9, No. 4**,** November 1994, Page(s): 1895-1900.

[95] Luis Fernandez Fernandez, "Renovation for more Reliability", IEEE Industry Applications Magazine, Jan/Feb 2003, Page(s): 42-51.

[96] Cali, S. Conti, F. Santonoceto, G. Tina, "Benefits Assessment of Fault Current Limiters in a Refinery Power Plant: a Case Study", International Conference on Power System Technology (PowerCon), 2000, Vol. 3, Page(s): 1505-1510.

[97] Barry M. Wood, Cheri L. Oslen, Gregory D. Hartzo, John C. Rama, and Fred R. Szenasi, "Development of an 11000-r/min 3500-hp Induction Motor and Adjustable-Speed Drive for Refinery Service", IEEE Transactions on Industry Applications, Vol. 33, No. 3, May/June 1997, Page(s): 815-825.

[98] P. Pillay and S. M. A. Sabur, "Use of Reduced Order Models to Calculate Reclosing Transients in a Refinery", IEEE 30th IAS Annual Meeting, 1995, Vol. 3, Page(s): 2180-2188.

[99] Ronald M. Jackson, and Moon H. Yuen, "Integrating of Utility Distribution System into a Refinery Plant Generation/Distribution Network at Unocal Los Angeles Refinery", IEEE Transactions on Industry Applications, Vol. 25, No. 5, September/October 1989, Page(s): 918-927.

[100] Robert A. Hanna, Peter Bulmer, and Rasul Kohisani, "Minimizing Refinery Upset During Power Interruptions Using PLC Control", 39th Annual Petroleum and Chemical Industry Conference (PCIC), 1992, Page(s): 185-195.

[101] A.C. (Tony) Demassi and R.W. (Ron) Jurchuk, "Major Petroleum Refinery and Electric Utility Collaborate to Increase Value to Each Organization", 41st Annual Petroleum and Chemical Industry Conference (PCIC), 1994, Page(s): 251-259.

[102] Robert E. Young, "Petroleum Refining Process Control and Real-Time Optimization", IEEE Control Systems Magazine, December 2006, Page(s): 73-83.

[103] Overview of the Canadian Downstream Petroleum Industry, Natural Resources Canada, Oil Division, July 2005, http://fuelfocus.nrcan.gc.ca/reports/2005-07/overview/overview_july2005_e.pdf , visited on August 20, 2008 at 1:38p.m.

[104] Oil Refinery, http://en.wikipedia.org/wiki/Oil_refinery, visited on March 5, 2013.

[105] Ernst Worrell and Christina Galitsky, "Profile of the Petroleum Refining Industry in California, California Industries of the Future Program", March 2004, http://ies.lbl.gov/iespubs/55450.pdf, visited on August 19, 2008 at 3:07 p.m.

[106] Electricity Shortage in California: Issues for Petroleum and Natural Gas Supply, Energy Information Administration, http://www.eia.doe.gov/emeu/steo/pub/special/california/june01article/carefinery.html, visited on July 20, 2008 at 10:28 a.m.

[107] United States Patent, US 7,608,938 B2, Philip Lynn Andrew, Timothy Andrew Melsert, and John Edward Ford, "Methods and Apparatus for Electric Power Grid Frequency Stabilization", General Electric Company, October 27, 2009.

[108] Eduardo P. Wiechmann, Pablo Aqueveque, Rolando Burgos, and José Rodríguez, "On the Efficiency of Voltage Source and Current Source Inverters for High-Power Drives", IEEE Transactions on Industrial Electronics, Vol. 55, No. 4, April 2008, Page(s): 1771-1782.

[109] José R. Espinoza, and Géza Joós, "A Current-Source Inverter-Fed Induction Motor Drive System with Reduced Losses", IEEE Transactions on Industry Applications, Vol. 34, No. 4, July/August 1998, Page(s): 796-805.

[110] Ahmet M. Hava, "Carrier Based PWM-VSI Drives in the Over-modulation Region", University of Wisconsin - Madison, Ph.D. Thesis, 1995.

[111] Zhenyu Yu and David Figoli, "AC Induction Motor Control Using Constant V/Hz Principle and Space Vector PWM Technique with TMS320C240", Application Report: SPRA284A, Digital Signal Processing Solutions, April 1998, Texas Instruments, http://www.ti.com/lit/an/spra284a/spra284a.pdf, visited on Oct. 2, 2012 at 10:00 a.m.

[112] M.V. Palandurkar, J.P. Modak, and S.G. Tarnekar, "Torque Computation of Induction Motor with VVVF Drive Subjected to Severe Torque Fluctuation", Proceedings of the Third International Conference on Trends in Information, Telecommunication, and Computing, Ninu V. Das, Springer New York Heidelberg Dordrecht London, 2013.

[113] C.U. Ogbuka, and M.U. Agu, "Effects of Load and Speed Variations in a Modified Closed Loop V/F Induction Motor Drive", Nigerian Journal of Technology (NIJOTECH), Vol. 31, No. 3, November, 2012, Page(s): 365-369.

[114] C.U. Ogbuka, and M.U. Agu, "A Modified Closed Loop V/F Controlled Induction Motor Drive", The Pacific Journal of Science and Technology, Volume 10. Number 1. May 2009, Page(s): 52-58.

[115] M. S. Aspalli, Sunil Kalshetti, and P. V. Hunagund, "Speed Control of Induction Motor Using Volts Hertz Control Method**",** International Journal of Electronics Engineering, 3 (2), 2011, Page(s): 231– 236.

[116] Shalini.N. MaliPatil, M. S. Aspalli, and P.V.Hungund , "Speed Control of Three Phase Induction Motor Using VLSI", International Journal of Advanced Information Science and Technology (IJAIST) , Vol.8, No.8, December 2012 , Page(s): 20-26.

[117] Matlab/Simulink On-line manual.

[118] Peter W. Hammond, "A New Approach to Enhance Power Quality for Medium Voltage AC Drives", IEEE Transactions on Industry Applications, Vol. 33, No. 1, January/February, 1997, Page(s): 202-208.

[119] Walter A. Hill, and Cyrus D. Harbourt, "Performance of Medium Voltage Multi-Level Inverters", Proceedings of the 34th IEEE Industry Applications Society (IAS) Annual Meeting, 1999, Vol. 2, Page(s): 1186-1192.

[120] Peter W. Hammond, "Enhancing the Reliability of Modular Medium-Voltage Drives", IEEE Transactions on Industrial Electronics, Vol. 49, No. 5, October 2002, Page(s): 948-954.

[121] Yusuke Fukuta, and Giri Venkataramanan, "DC Bus Ripple Minimization in Cascaded H-Bridge Multilevel Converters under Staircase Modulation", Proceedings of the 37th IEEE Industry Applications Society (IAS) Annual Meeting, 2002, Vol. 3, Page(s): 1988-1993.

[122] Mukul Rastogi, and Peter W. Hammond, "Dual-Frequency Braking in AC Drives", IEEE Transactions on Power Electronics, Vol. 17, No. 6, November 2002, Page(s): 1032-1040.

[123] "Which medium-voltage drive fulfills highest demands to availability and versatility", https://www.automation.siemens.com/mcms/ infocenter/content/en/Pages/orderform.aspx?nodeKey=key_516862&InfoType=brochures, Siemens, visited at 4: 12 pm, June 30, 2011.

[124] Math H.J. Bollen, Mark Stephens, Sasa Z. Djokic, Robert Neumann, Alex McEachern, Jovica V. Milanovic, Jose Romero Gordon, Bill Brumsickle, Gaetan Ethier, Francise Zavoda, Kurt Stockman, "CIGRE/CIRED/UIE Joint Working Group C4.110, Voltage Dip

Immunity of Equipment in Installations – Main Contributions and Conclusions", 20th International Conference on Electricity Distribution, Prague, 8-11 June 2009.

[125] Hector G. Sarmiento, and Eduardo Estrada, "A Voltage Sag Study in an Industry with Adjustable Speed Drives", IEEE Industry Applications Magazine, January/February 1996, Page(s): 16-19.

[126] Van E Wagner, Allen A. Andreshak, and Joseph P. Staniak, "Power Quality and Factory Automation", IEEE Transactions on Industry Applications, Vol. 26, No. 4, July/August 1990, Page(s): 620-626.

[127] AK Keus, JM van Coller, RG Koch, "A Test Facility for Determining the Response of Industrial Equipment to Voltage Dips (SAGS)", International Conference Electric Machines and Drives, 1999 (IEMD'99), pp. 210-212.

[128] Math H. J. Bollen, "Comparing Voltage Dip Survey Results", IEEE Power Engineering Society Winter Meeting, 2002, Vol. 2, Page(s): 1130-1134.

[129] Y. Shamash, "Linear-System Reduction Using Pade Approximation to Allow Retention of Dominant Modes," *International Journal of Control,* vol. 21, pp. 257-272, 1975.

[130] Z. Han, Power System Analysis (Third Edition). Hangzhou: Zhejiang University Press, 2005.

[131] Shengqiang Li, "Load Modeling Techniques for Power System Dynamic Studies", Master of Science thesis, Spring 2013.

[132] Murray L. Macdonald, and Paresh S. Sen, "Control Loop Study of Induction Motor Drives Using DQ Model", IEEE Transactions on Industrial Electronics and Control Instrumentation, Vol. IECI-26, No. 4, Nov 1979, Page(s): 237-243.

[133] Debmalya Banerjee, and V. T. Ranganathan, "Load commutaed SCR current-Source-Inverter-Fed Induction Motor Drive with Sinusodial Motor Voltage and Current", IEEE Transactions on Power Electronics, Vol. 24, No. 4, April 2009, Page(s): 1048-1062.

[134] Duo Deng, and Thomas A. Lipo, "A Modified Control Method for Fast-Response Current Source Inverter Drives", IEEE Transactions on Industry Applications, Vol. 1A-22, No. 4, July/August 1986, Page(s): 653-665.

[135] S. H. Shahalami, and Abbas Mohammadi damirof, "Implementation of Variable-Speed Asynchronous Drive Fed by Current Source Inverter", 2012 3rd Power Electronics and Drive System Technology (PEDSTC), Page(s): 206 – 211.

[136] Mitsuyuki Hombu, Shigeta Ueda, and Akjteru Ueda," A New Current Source GTO Inverter with Sinusoidal Output Voltage and Current", IEEE Transactions on Industry Applications, Vol. IA-21, No. 5, September/October 1985, Page(s): 1192-1198.

[137] Mika Salo, and Heikki Tuusa, "A Vector-Controlled PWM Current-Source-Inverter-Fed Induction Motor Drive with a New Stator Current Control Method", IEEE Transactions on Industry Electronics, Vol. 52, No. 2, April 2005, Page(s): 523-531.

[138] José Espinoza, Géza Joós, and Phoivos Ziogas, "An Integrated Three Phase Voltage Regulated Current Source Inverter Topology", 1993 IEEE International Symposium on Industrial Electronics (ISIE'93), Page(s): 663 – 668.

[139] Daming Ma, Bin Wu, and Steve Rizzo, "A CSI-Based Medium Voltage Multi-Motor Drive", The 3rd International Power Electronics and Motion Control Conference (IPEMC 2000), 2000, Vol. 2, Page(s): 780 – 785.

[140] Bin Wu, Shashi B. Dewan, and Gordon R. Slemon, "PWM - CSI Inverter for Induction Motor Drives", IEEE Transactions on Industry Applications, Vol. 28, No. 1, January/February 1992, Page(s): 64-71.

[141] Bin Wu, Gordon R. Slemon, and Shashi B. Dewan, "PWM-CSI Induction Motor Drive with Phase Angle Control", 1989 IEEE Industry Application Society Annual Meeting, 1989, Vol. 1, Page(s): 674 - 679.

[142] A. Dakir, R. Barlik, M. Nowak, P. Grochal, "Computer Simulations for two Angular-Speed-Control Systems of a Current Source Inverter feeding an Induction Machine", IEEE International Symposium on Industrial Electronics (ISIE'96), 1996, Vol. 2, Page(s): 940 – 945.

[143] Ehsan Al-nabi, Bin Wu, Vijay Sood, and Jingya Dai, "High Power CSI-Fed IPM drive System Control with Minimum DC-Link Current", 36th Annual Conference on IEEE Industrial Electronics Society (IECON 2010), 2010, Page(s): 857 – 863.

[144] Yun Wei Li, "Control and Resonance Damping of Voltage-Source and Current-Source Converters With *LC* Filters", IEEE Transactions on Industrial Electronics, Vol. 56, No. 5, May 2009, Page(s): 1511 – 1521.

[145] Abdul Rahiman Beig, and V. T. Ranganathan, "A Novel CSI-Fed Induction Motor Drive", IEEE Transactions on Power Electronics, Vol. 21, No. 4, July 2006, Page(s): 1073-1082.

[146] Sakutaro Nonaka, and Yasuhiko Neba, "Current Regulated PWM-CSI Induction Motor Drive System without a Speed Sensor", 1992 IEEE Industry Application Society Annual Meeting, 1992, Vol. 1, Page(s): 347 – 354.

[147] A. Mohammadzadeh, P. Farmanzadeh , and M. Azizian, "An Improved Vector Controlled CSI – Fed Induction Motor Drive Using an Active

Filter", 2010 1st Power Electronic & Drive Systems & Technologies Conference (PEDSTC), 2010, Page(s): 201 – 207.

[148] Navid R. Zargari, Yuan Xiao, and Bin Wu, "Near Unity Displacement Factor for Current Source PWM Drives", IEEE Industry Application Magazine, Vol. 5, No. 4, 1999, Page(s): 19 – 25.

[149] J.-H. Song, T.-W. Yoon, K.-H. Kim, K.-B. Kim, and M.-J. Youn, "Control Loop Study of a Load Commutated CSI-Fed Induction Motor", IEE Proceedings-B, Vol. 139, No. 3, May 1992, Page(s): 183-190.

[150] W G Dunford, and E Mufford, "An Integrated Controller for Current Source Inverter Drives", 1993 IEEE International Symposium on Industrial Electronics (ISIE'93), 1993, Page(s): 67 – 72.

[151] Ahmed K. Abdelsalam, Mahmoud I. Masoud, Mostafa S. Hamad, and Barry W. Williams, "Modified Indirect Vector Control Technique for Current-Source Induction Motor Drive", IEEE Transactions on Industry Applications, Vol. 48, No. 6, November/December 2012, Page(s): 2433 - 2442.

[152] ETAP online manual and database

[153] "When to Use a Line or Load Reactor Protecting the Drive or the Motor", http://www.rae.ca/Support/Line%20Reactor%20White%20Paper%20AN0032.pdf, visited at 1:45pm March 19, 2013, Application Note, Lenze AC Tech.

[154] "Space Vector PWM VSI Induction Motor Drive", Matlab/Simulink library data and Matlab/Simulink on-line manual.

[155] "INT-A-PAK Power Module Thyristor/Diode, 300 A", http://www.vishay.com/docs/94557/vskl3008.pdf, visited at 2:40pm March 19, 2013, Vishay High Power Products, VSKL300-08PbF, Vishay.

[156] Jimmie J. Cathey, Ralph K. Cavin, III, and A.K. Ayoub, "Transient Load Model of an Induction Motor", IEEE Transactions on Power Apparatus and Systems, Vol. PAS-92 , No. 4, 1973, Page(s): 1399-1406.

[157] Xiaodong Liang, and Obinna Ilochonwu, "Induction Motor Starting in Practical Industrial Applications", IEEE Transactions on Industry Applications, Vol. 47, No. 1, January/February 2011, Page(s): 271-280.

[158] H. du Toit Mouton, "Natural Balancing of Three-Level Neutral-Point-Clamped PWM Inverters", IEEE Transactions on Industrial Electronics, Vol. 49, No. 5, October 2002, Page(s): 1017-1025.

[159] Akira Nabae, Isao Takahashi, and Hirofumi Akagi", A New Neutral-Point-Clamped PWM Inverter", IEEE Transactions on Industry Applications, Vol. 1A-17, No. 5, September/October, 1981, Page(s): 518-523.

[160] James Patrick Lyons et al, US patent, US 5,910,892, "High Power Motor Drive Converter System and Modulation Control", June 8, 1999.

[161] B. P. McGrath, and D.G. Holmes, "A Comparison of Multicarrier PWM Strategies for Cascaded and Neutral Point Clamped Multilevel Inverters", IEEE 31st Annual Power Electronics Specialist Conference (PESC00), 2000, Vol. 2, Page(s): 674-679.

APPENDIX A TYPICAL DATA FOR TEMPLATE-BASED FULL MODEL

1) Induction Motors Parameters Used in the Template

Table A.1 Equivalent circuit parameters of induction motors (60Hz) [152]

Motor HP	Voltage V	R_s Ω	X_s Ω	X_m Ω	R_r, Ω	X_r, Ω
200	460	0.02122	0.14032	5.79240	0.012055	0.17070
350	460	0.01212	0.08018	3.31000	0.006889	0.09754
800	460	0.00530	0.03508	1.44810	0.003014	0.04268
1000	460	0.00424	0.02806	1.15850	0.002411	0.03414
1200	460	0.00354	0.02339	0.96540	0.002009	0.02845
1500	460	0.00283	0.01871	0.77232	0.001607	0.02276
350	2300	0.39014	1.95401	53.9122	0.687706	2.00361
800	2300	0.15622	0.78205	21.5639	0.275060	0.80122
350	4000	1.18000	5.91000	163.060	2.080000	6.06000
800	4000	0.47250	2.36539	65.2221	0.831940	2.42336
1000	4000	0.29204	2.60472	79.1281	0.272311	2.34819
1500	4000	0.24520	2.23460	68.1497	0.246200	2.04430
2000	4000	0.19840	1.86450	57.1712	0.220000	1.74040
3000	4000	0.10480	1.12430	35.2143	0.167700	1.13260
4000	4000	0.01113	0.38406	13.2575	0.115370	0.52473
5500	4000	0.03260	0.32128	8.00000	0.065280	0.32128

The inertia J of the induction motors vs. HP ratings are shown in Figure A.1.

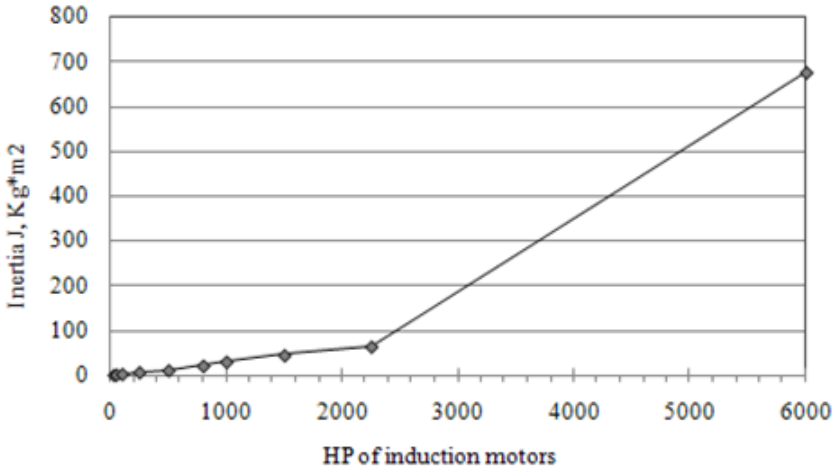

Figure A.1 Inertia vs. HP ratings of induction motors [156]

2) Transformer Parameters Used in the Template

The transformer data are based on information from ETAP online manual and database [152]. Transformer impedance and X/R ratios based on its KVA sizing are listed in Tables A.2, A.3 and A.4. The Industrial Power System Handbook by Beeman (page 96) specifies typical data for transformers that has rating not larger than 500 kVA and primary voltage not higher than 12.47 kV.

Table A.2 Typical impedances for transformers less than or equal to 500 kVA [152]

Rating	Group 1 *		Group2+	
	Percent Z	X/R	Percent Z	X/R
kVA ≤ 5	2.3	0.88	2.8	0.77
5< kVA ≤ 25	2.3	1.13	2.3	1.00
25< kVA ≤ 50	2.6	1.69	2.4	1.54
50< kVA ≤ 100	2.6	1.92	3.7	2.92
100< kVA ≤ 167	4.0	3.45	3.7	3.60
167< kVA ≤ 500	4.8	4.70	5.2	5.10
* Group 1: Transformers with high voltage windings of less than or equal to 8.32 kV + Group 2: Transformers that have high voltages of greater than 8.32 kV and less than or equal to 12.47 kV				

The American National Standard C57.12.10 specifies impedance values for transformers larger than 500 kVA.

Table A.3 Typical impedances for transformers more than 500 kVA [152]

High Voltage Side	Low Voltage Side < 2.4 kV	Low Voltage Side ≥ 2.4 kV	
		Without LTC	With LTC
kV ≤ 13.8	5.75 **	5.5**	
13.8 < kV ≤ 23	6.75	6.5	7.0
23 < kV ≤ 34.5	7.25	7.0	7.5
34.5 < kV ≤ 46	7.75	7.5	8.0
46 < kV ≤ 69		8.0	8.5
69 < kV ≤ 115		8.5	9.0
115 < kV ≤ 138		9.0	9.5
138 < kV ≤ 161		9.5	10.0
161 < kV ≤ (230)		10.0	10.5
** Self-cooled transformers with greater than 5000 kVA values shall be the same as those for 23 kV high voltage			

Table A.4 Typical X/R ratios for transformers more than 500 kVA [152]

Rating	X/R	Rating	X/R
MVA ≤ 1	5.790	8 < MVA ≤ 10	15.50
1 < MVA ≤ 2	7.098	10 < MVA ≤ 20	18.60
2 < MVA ≤ 3	10.67	20 < MVA ≤ 30	23.70
3 < MVA ≤ 4	11.41	30 < MVA ≤ 40	27.30
4 < MVA ≤ 5	12.14	40 < MVA ≤ 50	29.50
5 < MVA ≤ 6	12.85	50 < MVA ≤ 100	34.10
6 < MVA ≤ 7	13.55	100 < MVA ≤ 200	42.00
7 < MVA ≤ 8	14.23	200 < MVA ≤ 1000	50.00

3) Cable Parameters Used in the Template

Table A.5 Cable ratings and impedance for the TF model [152]

Parameters	Cables used in the template full model
Voltage level, kV	15
Size	500 AWG
Resistance, ohms	0.0284 ohms per 1000 ft
Reactance at 60Hz, ohms	0.0351 ohms per 1000 ft

4) Synchronous Machine Parameters Used in the Template

Table A.6 Parameters in per unit on individual synchronous motor MVA base

X_d'', p.u.	0.15385
X_d', p.u.	0.23
X_d, p.u.	1.10
X_{du}, p.u.	1.17
X_L, p.u.	0.11
X_2, p.u.	0.15385
X_0, p.u.	0.15385
X_q'', p.u.	0.12
X_q', p.u.	0.23
X_q, p.u.	1.08
X_{qu}, p.u.	1.15
T_{do}'', sec	0.002
T_{do}', sec	5.6
T_{qo}'', sec	0.002
T_{qo}', sec	3.7

APPENDIX B LOAD ASSIGNMENTS FOR THE TEMPLATE-BASED FULL MODEL

The load assignments in each process when creating the template-based full model for the 108MW coking refinery facility are illustrated in detail.

1) Process 1 – CDU

Table B.1 Load distribution for CDU

Load distribution inside the CDU	Loads in MW	Explanations
Rated total loads of the process, MW	2.89	2.68% of 108 MW
Rated static loads of the process, MW	1.33	1.23% of 108 MW
Rated synchronous motor loads of the process, MW	0	0% of 108 MW
Rated induction motor loads of the process, MW	1.566	1.45% of 108 MW
0.46 KV induction motors of the process, MW	0.149	0.138% of 108 MW
2.3 KV induction motors of the process, MW	1.417	1.312% of 108 MW
4 KV induction motors of the process, MW	0	0% of 108 MW

Table B.2 Voltage levels and sizes of loads for CDU

Voltage level, KV	Induction motor load		Synchronous motor load		Static load in MW
	#	Unit size, HP	#	Unit size, HP	
13.8	--	--	--	--	1.33
0.46	1	200	--	--	--
2.3	3	350, 800	--	--	--
4	--	--	--	--	--

Table B.3 Cables and transformers data for CDU

Cables	Transformers
Cable1 (to CDU-T1), 100 ft Cable3 (to CDU-T2), 100 ft Cable 34 (main feeder), 2000 ft	CDU-T1, 500KVA @ 13.8KV/0.48KV CDU-T2, 2.5MVA @ 13.8KV/2.4KV

The electrical single-line diagram of the process CDU is shown in Figure B.1. The electrical single-line diagrams for other processes will be created in similar way as CDU, so they will not be provided in this thesis due to page limits.

2) Process 2 – VDU

Table B.4 Load distribution for VDU

Load distribution inside VDU	Loads in MW	Explanations
Rated total loads of the process, MW	10.65	9.86% of 108 MW
Rated static loads of the process, MW	5.054	4.68% of 108 MW
Rated synchronous motor loads of the process, MW	0	0% of 108 MW
Rated induction motor loads of the process, MW	5.594	5.18% of 108 MW
0.46 KV induction motors of the process, MW	2.276	2.107% of 108 MW
2.3 KV induction motors of the process, MW	0.261	0.242% of 108 MW
4 KV induction motors of the process, MW	3.060	2.832% of 108 MW

Table B.5 Voltage levels and sizes of loads for VDU

Voltage level, KV	Induction motor load		Synchronous motor load		Static load in MW
	#	Unit size, HP	#	Unit size, HP	
13.8	--	--	--	--	5.054
0.46	4	200, 1200, 1500	--	--	--
2.3	1	350	--	--	--
4	8	350, 1000	--	--	--

Table B.6 Cables and transformers data for VDU

Cables	Transformers
Cable5 (to VDU-T1), 100 ft Cable6 (to VDU-T2), 100 ft Cable7 (to VDU-T3), 100 ft Cable 36 (main feeder), 2000 ft	VDU-T1, 3.5 MVA @ 13.8KV/0.48KV VDU-T2, 0.5 MVA @ 13.8KV/2.4KV VDU-T3, 7.5 MVA @ 13.8KV/4.16KV

The electrical single-line diagram of the process VDU is shown in Figure B.2. The electrical single-line diagrams for other processes will be created in similar way as CDU and VDU, so they will not be provided in this thesis due to page limits.

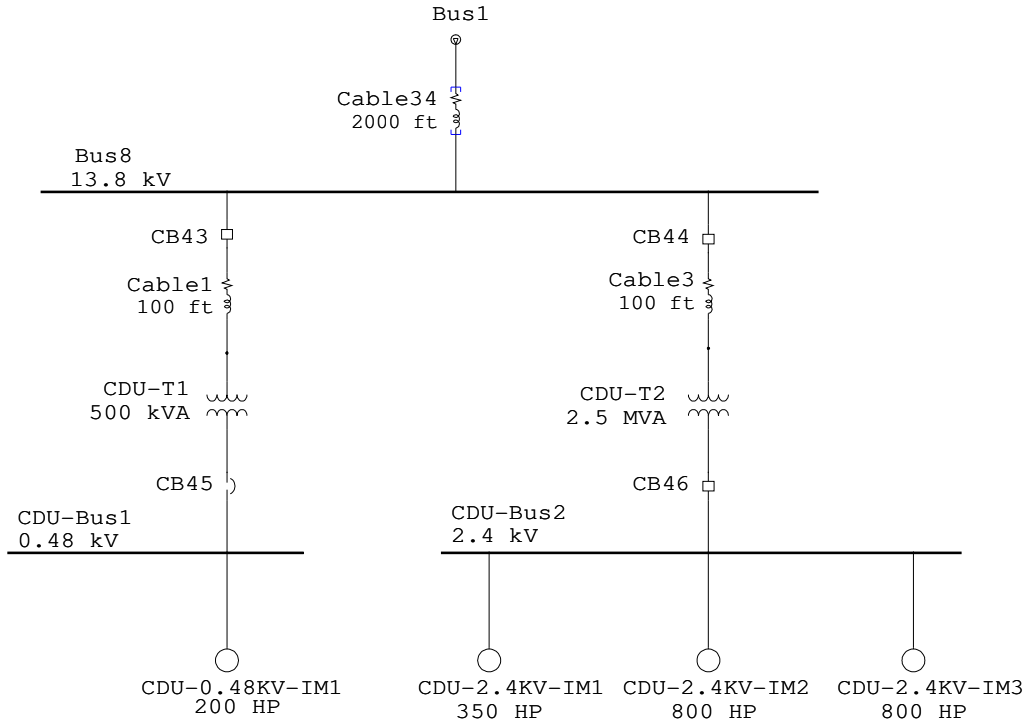

Figure B.1 Single-line diagram of the process CDU

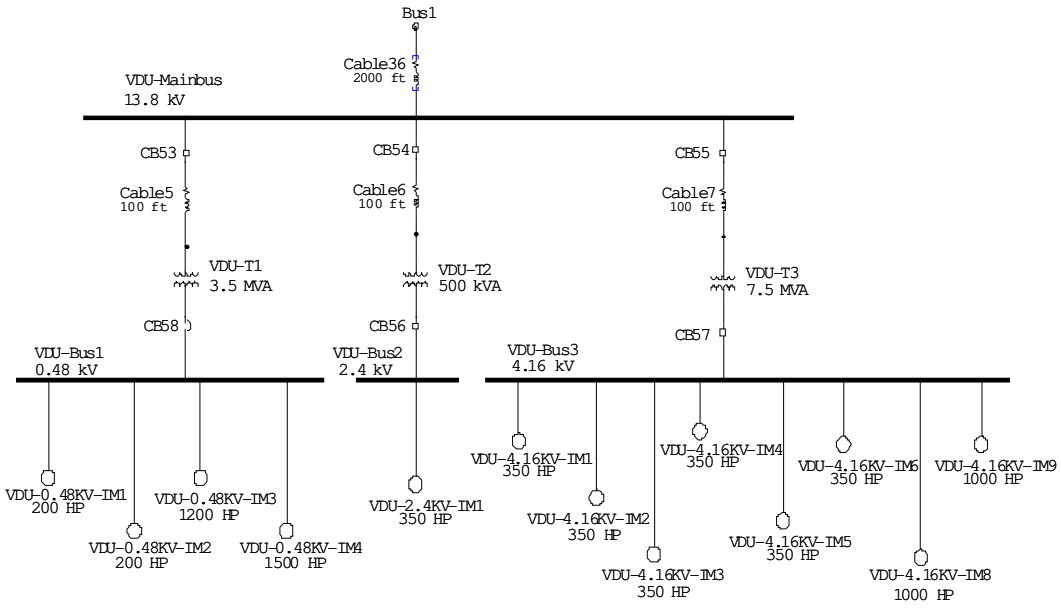

Figure B.2 Single-line diagram of the process VDU

3) Process 3 – Hydrotreater

Table B.7 Load distribution for Hydrotreater

Load distribution inside the Hydrotreater	Loads in MW	Explanations
Rated total loads of the process, MW	2.311	2.14% of 108 MW
Rated static loads of the process, MW	0	0% of 108 MW
Rated synchronous motor loads of the process, MW	1.307	1.21% of 108 MW
Rated induction motor loads of the process, MW	1.004	0.93% of 108 MW
0.46 KV induction motors of the process, MW	0.046	0.043% of 108 MW
2.3 KV induction motors of the process, MW	0.958	0.887% of 108 MW
4 KV induction motors of the process, MW	0	0% of 108 MW

Table B.8 Voltage levels and sizes of loads for Hydrotreater

Voltage level, KV	Induction motor load		Synchronous motor load		Static load in MW
	#	Unit size, HP	#	Unit size, HP	
13.8	--	--	--	--	0
0.46	1	200	--	--	--
2.3	2	350, 800	--	--	--
4	--	--	1	1750	--

Table B.9 Cables and transformers data for Hydrotreater

Cables	Transformers
Cable8 (to Hydrotreater-T1), 100 ft Cable9 (to Hydrotreater-T2), 100 ft Cable 37 (main feeder), 2000 ft	Hydrotreater-T1, 0.5 MVA @ 13.8KV/0.48KV Hydrotreater-T2, 2.0MVA @ 13.8KV/2.4KV

4) Process 4 – Coking

Table B.10 Load distribution for Coking

Load distribution inside Coking/Thermal cracking	Loads in MW	Explanations
Rated total loads of the process, MW	9.256	8.57% of 108 MW
Rated static loads of the process, MW	2.96	2.74% of 108 MW
Rated synchronous motor loads of the process, MW	0	0% of 108 MW
Rated induction motor loads of the process, MW	6.296	5.83% of 108 MW
0.46 KV induction motors of the process, MW	1.851	1.714% of 108 MW
2.3 KV induction motors of the process, MW	0.187	0.173% of 108 MW
4 KV induction motors of the process, MW	4.258	3.943% of 108 MW

Table B.11 Voltage levels and sizes of loads for Coking

Voltage level, KV	Induction motor load		Synchronous motor load		Static load in MW
	#	Unit size, HP	#	Unit size, HP	
13.8	--	--	--	--	2.96
0.46	7	200, 800	--	--	--
2.3	1	350	--	--	--
4	5	350, 1500, 3000	--	--	--

Table B.12 Cables and transformers data for Coking

Cables	Transformers
Cable10 (to Coking-T1), 100 ft Cable11 (to Coking-T2), 100 ft Cable12 (to Coking-T3), 100 ft Cable 38 (main feeder), 2000 ft	Coking-T1, 3.0 MVA @ 13.8KV/0.48KV Coking-T2, 0.5 MVA @ 13.8KV/2.4KV Coking-T3, 7.5 MVA @ 13.8KV/4.16KV

5) Process 5 – FCC

Table B.13 Load distribution for FCC

Load distribution inside FCC	Loads in MW	Explanations
Rated total loads of the process, MW	3.208	2.97% of 108 MW
Rated static loads of the process, MW	1.458	1.35% of 108 MW
Rated synchronous motor loads of the process, MW	0	0% of 108 MW
Rated induction motor loads of the process, MW	1.75	1.62% of 108 MW
0.46 KV induction motors of the process, MW	0.734	0.68% of 108 MW
2.3 KV induction motors of the process, MW	0.448	0.415% of 108 MW
4 KV induction motors of the process, MW	0.559	0.518% of 108 MW

Table B.14 Voltage levels and sizes of loads for FCC

Voltage level, KV	Induction motor load		Synchronous motor load		Static load in MW
	#	Unit size, HP	#	Unit size, HP	
13.8	--	--	--	--	1.49
0.46	4	200	--	--	--
2.3	2	350	--	--	--
4	2	350	--	--	--

Table B.15 Cables and transformers data for FCC

Cables	Transformers
Cable13 (to FCC-T1), 100 ft Cable14 (to FCC-T2), 100 ft Cable15 (to FCC-T3), 100 ft Cable 39 (main feeder), 2000 ft	FCC-T1, 3 MVA @ 13.8KV/0.48KV FCC-T2, 5 MVA @ 13.8KV/2.4KV FCC-T3, 5 MVA @ 13.8KV/4.16KV

6) Process 6 – Hydrocracker

Table B.16 Load distribution for Hydrocracker

Load distribution inside Hydrocracker	Loads in MW	Explanations
Rated total loads of the process, MW	32.422	30.02% of 108 MW
Rated static loads of the process, MW	5.314	4.92% of 108 MW
Rated synchronous motor loads of the process, MW	12.68	11.74% of 108 MW
Rated induction motor loads of the process, MW	14.43	13.36% of 108 MW
0.46 KV induction motors of the process, MW	1.585	1.468% of 108 MW
2.3 KV induction motors of the process, MW	0	0% of 108 MW
4 KV induction motors of the process, MW	12.843	11.892% of 108 MW

Table B.17 Voltage levels and sizes of loads for Hydrocracker

Voltage level, KV	Induction motor load		Synchronous motor load		Static load in MW
	#	Unit size, HP	#	Unit size, HP	
13.8	--	--	--	--	5.314
0.46	13	200, 350, 800, 1000	--	--	--
2.3	--	--	--	--	--
4	8	350, 2000, 3000, 4000	4	2000, 3000, 2×6000	--

Table B.18 Cables and transformers data for Hydrocracker

Cables	Transformers
Cable16 (to Hydrocracker-T1), 100 ft Cable17 (to Hydrocracker-T2), 100 ft Cable 34 (main feeder), 2000 ft	Hydrocracker-T1, 5 MVA @ 13.8KV/0.48KV Hydrocracker-T2, 15 MVA @ 13.8KV/4.16KV

7) Process 7 – Reforming

Table B.19 Load distribution for Reforming

Load distribution inside Reforming	Loads in MW	Explanations
Rated total loads of the process, MW	0.724	0.67% of 108 MW
Rated static loads of the process, MW	0.530	0.49% of 108 MW
Rated synchronous motor loads of the process, MW	0	0% of 108 MW
Rated induction motor loads of the process, MW	0.194	0.18% of 108 MW
0.46 KV induction motors of the process, MW	0.194	0.18% of 108 MW
2.3 KV induction motors of the process, MW	0	0% of 108 MW
4 KV induction motors of the process, MW	0	0% of 108 MW

Table B.20 Voltage levels and sizes of loads for Reforming

Voltage level, KV	Induction motor load		Synchronous motor load		Static load in MW
	#	Unit size, HP	#	Unit size, HP	
13.8	--	--	--	--	0.53
0.46	1	200	--	--	--
2.3	--	--	--	--	--
4	--	--	--	--	--

Table B.21 Cables and transformers data for Reforming

Cables	Transformers
Cable18 (to Reforming-T1), 100 ft Cable 41 (main feeder), 2000 ft	Reforming-T1, 0.75 MVA @ 13.8KV/0.48KV

8) Process 8 – Alkylates

Table B.22 Load distribution for Alkylates

Load distribution inside Alkylates	Loads in MW	Explanations
Rated total loads of the process, MW	1.361	1.26% of 108 MW
Rated static loads of the process, MW	0.983	0.91% of 108 MW
Rated synchronous motor loads of the process, MW	0	0% of 108 MW
Rated induction motor loads of the process, MW	0.378	0.35% of 108 MW
0.46 KV induction motors of the process, MW	0.113	0.105% of 108 MW
2.3 KV induction motors of the process, MW	0.265	0.245% of 108 MW
4 KV induction motors of the process, MW	0	0% of 108 MW

Table B.23 Voltage levels and sizes of loads for Alkylates

Voltage level, KV	Induction motor load		Synchronous motor load		Static load in MW
	#	Unit size, HP	#	Unit size, HP	
13.8	--	--	--	--	0.983
0.46	1	200	--	--	--
2.3	1	350	--	--	--
4	--	--	--	--	--

Table B.24 Cables and transformers data for Alkylates

Cables	Transformers
Cable19 (to Alkylates-T1), 100 ft Cable20 (to Alkylates-T2), 100 ft Cable 42 (main feeder), 2000 ft	Alkylates-T1, 0.5 MVA @ 13.8KV/0.48KV Alkylates-T2, 0.5 MVA @ 13.8KV/2.4KV

9) Process 9 – Isomers

Table B.25 Load distribution for Isomers

Load distribution inside Isomers	Loads in MW	Explanations
Rated total loads of the process, MW	6.448	5.97% of 108 MW
Rated static loads of the process, MW	1.026	0.95% of 108 MW
Rated synchronous motor loads of the process, MW	0	0% of 108 MW
Rated induction motor loads of the process, MW	5.422	5.02% of 108 MW
0.46 KV induction motors of the process, MW	0.187	0.173% of 108 MW
2.3 KV induction motors of the process, MW	0	0% of 108 MW
4 KV induction motors of the process, MW	5.235	4.847% of 108 MW

Table B.26 Voltage levels and sizes of loads for Isomers

Voltage level, KV	Induction motor load		Synchronous motor load		Static load in MW
	#	Unit size, HP	#	Unit size, HP	
13.8	--	--	--	--	1.026
0.46	1	200	--	--	--
2.3	--	--	--	--	--
4	2	1500, 5500	--	--	--

Table B.27 Cables and transformers data for Isomers

Cables	Transformers
Cable21 (to Isomers-T1), 100 ft Cable22 (to Isomers-T2), 100 ft Cable 43 (main feeder), 2000 ft	Isomers-T1, 0.5 MVA @ 13.8KV/0.48KV Isomers-T2, 8.0MVA @ 13.8KV/4.16KV

10) Process 10 – Sulfur

Table B.28 Load distribution for Sulfur

Load distribution inside Sulfur	Loads in MW	Explanations
Rated total loads of the process, MW	6.448	2.3% of 108 MW
Rated static loads of the process, MW	1.026	1.27% of 108 MW
Rated synchronous motor loads of the process, MW	0	0% of 108 MW
Rated induction motor loads of the process, MW	5.422	1.03% of 108 MW
0.46 KV induction motors of the process, MW	0.187	0.953% of 108 MW
2.3 KV induction motors of the process, MW	0.083	0.077% of 108 MW
4 KV induction motors of the process, MW	0	0% of 108 MW

Table B.29 Voltage levels and sizes of loads for Sulfur

Voltage level, KV	Induction motor load		Synchronous motor load		Static load in MW
	#	Unit size, HP	#	Unit size, HP	
13.8	--	--	--	--	1.026
0.46	1	200	--	--	--
2.3	--	--	--	--	--
4	--	--	--	--	--

Table B.30 Cables and transformers data for Sulfur

Cables	Transformers
Cable23 (to Sulfur-T1), 100 ft Cable44 (main feeder), 2000 ft	Sulfur-T1, 3 MVA @ 13.8KV/0.48KV

11) Process 11 – Hydrogen

Table B.31 Load distribution for Hydrogen

Load distribution inside Hydrogen	Loads in MW	Explanations
Rated total loads of the process, MW	3.888	3.6% of 108 MW
Rated static loads of the process, MW	0	0% of 108 MW
Rated synchronous motor loads of the process, MW	2.981	2.76% of 108 MW
Rated induction motor loads of the process, MW	0.907	0.84% of 108 MW
0.46 KV induction motors of the process, MW	0.062	0.057% of 108 MW
2.3 KV induction motors of the process, MW	0	0% of 108 MW
4 KV induction motors of the process, MW	0.846	0.783% of 108 MW

Table B.32 Voltage levels and sizes of loads for Hydrogen

Voltage level, KV	Induction motor load		Synchronous motor load		Static load in MW
	#	Unit size, HP	#	Unit size, HP	
13.8	--	--	--	--	0
0.46	1	200	--	--	--
2.3	--	--	--	--	--
4	3	350	2	2000	--

Table B.33 Cables and transformers data for Hydrogen

Cables	Transformers
Cable25 (to Hydrogen-T1), 100 ft Cable26 (to Hydrogen-T2), 100 ft Cable 45 (main feeder), 2000 ft	Hydrogen-T1, 0.5 MVA @ 13.8KV/0.48KV Hydrogen-T2, 1.0 MVA @ 13.8KV/4.16KV

12) Process 12 – Gasplant

Table B.34 Load distribution for Gasplant

Load distribution inside Gasplant	Loads in MW	Explanations
Rated total loads of the process, MW	3.337	3.09% of 108 MW
Rated static loads of the process, MW	1.48	1.37% of 108 MW
Rated synchronous motor loads of the process, MW	0	0% of 108 MW
Rated induction motor loads of the process, MW	1.858	1.72% of 108 MW
0.46 KV induction motors of the process, MW	0.553	0.512% of 108 MW
2.3 KV induction motors of the process, MW	0.708	0.656% of 108 MW
4 KV induction motors of the process, MW	0.597	0.553% of 108 MW

Table B.35 Voltage levels and sizes of loads for Gasplant

Voltage level, KV	Induction motor load		Synchronous motor load		Static load in MW
	#	Unit size, HP	#	Unit size, HP	
13.8	--	--	--	--	1.49
0.46	3	200	--	--	--
2.3	3	350	--	--	--
4	1	800	--	--	--

Table B.36 Cables and transformers data for Gasplant

Cables	Transformers
Cable27 (to Gasplant-T1), 100 ft Cable28 (to Gasplant-T2), 100 ft Cable29 (to Gasplant-T3), 100 ft Cable46 (main feeder), 2000 ft	Gasplant-T1, 1.0 MVA @ 13.8KV/0.48KV Gasplant-T2, 1.5 MVA @ 13.8KV/2.4KV Gasplant-T3, 1.5 MVA @ 13.8KV/4.16KV

13) Process 13 – Others

Table B.37 Load distribution for Other

Load distribution inside Other	Loads in MW	Explanations
Rated total loads of the process, MW	29.02	26.87% of 108 MW
Rated static loads of the process, MW	9.817	9.09% of 108 MW
Rated synchronous motor loads of the process, MW	0	0% of 108 MW
Rated induction motor loads of the process, MW	19.202	17.78% of 108 MW
0.46 KV induction motors of the process, MW	1.461	1.353% of 108 MW
2.3 KV induction motors of the process, MW	3.879	3.592% of 108 MW
4 KV induction motors of the process, MW	13.862	12.835% of 108 MW

Table B.38 Voltage levels and sizes of loads for Other

Voltage level, KV	Induction motor load		Synchronous motor load		Static load in MW
	#	Unit size, HP	#	Unit size, HP	
13.8	--	--	--	--	9.817
0.46	23	200	--	--	--
2.3	8	350, 800	--	--	--
4	22	800	--	--	--

Table B.39 Cables and transformers data for Other

Cables	Transformers
Cable 30 (to Other-T1), 100 ft Cable 31 (to Other-T2), 100 ft Cable 32 (to Other-T3), 100 ft Cable 47 (main feeder), 2000 ft	Other-T1, 5 MVA @ 13.8KV/0.48KV Other-T2, 2.5MVA @ 13.8KV/2.4KV Other-T3, 2.5MVA @ 13.8KV/4.16KV

APPENDIX C DYNAMIC MODEL FOR VSI MOTOR DRIVE SYSTEMS

C.1 Diode Converter

The output voltage v_d from the diode converter can be expressed as follows:

$$v_d = \frac{3\sqrt{6}}{\pi} E - \frac{3}{\pi} l_c (2\pi f_g) i_d - 2l_c \frac{di_d}{dt} - 2V_{diode} \quad \text{(C.1-1)}$$

where v_d is output voltage from the diode converter, i_d is the dc link current from diode converter, E is rms source voltage per phase, l_c is the source commutation inductance in front of the VFD, f_g is the power grid frequency in Hz, V_{diode} is diode on-state voltage. The source resistance is ignored.

The DC link consists of a DC link resistor r_{dc}, DC link reactor L_{dc}, and DC link capacitor C_{dc}. The voltage and currents at DC link can be calculated as follows:

$$v_d = r_{dc} i_d + L_{dc} \frac{di_d}{dt} + e_d \quad \text{(C.1-2)}$$

$$i_d = i_c + i_I \quad \text{(C.1-3)}$$

$$i_c = C_{dc} \frac{de_d}{dt} \quad \text{(C.1-4)}$$

Where e_d is the dc link voltage supplying to inverter, i_c is the current flowing through the DC link capacitor, i_I is the current flowing into the inverter.

Combining Equations (C.1-1) and (C.1-2), the dc link current i_d can be expressed as follows:

$$\frac{di_d}{dt} = \left(\frac{1}{L_{dc} + 2l_c}\right)\left[\frac{3\sqrt{6}}{\pi}E - \left(r_{dc} + \frac{3}{\pi}l_c\left(2\pi f_g\right)\right)i_d - 2V_{diode} - e_d\right] \quad \text{(C.1-5)}$$

Substitute (C.1-5) in (C.1-2), the dc link voltage from output of the diode converter can be rewritten as follows:

$$v_d = \frac{\frac{3\sqrt{6}}{\pi}L_{dc}}{L_{dc} + 2l_c}E + \frac{l_c\left(2r_{dc} - \frac{3}{\pi}L_{dc}\left(2\pi f_g\right)\right)}{L_{dc} + 2l_c}i_d + \frac{2l_c}{L_{dc} + 2l_c}e_d - \frac{2L_{dc}}{L_{dc} + 2l_c}V_{diode} \quad \text{(C.1-6)}$$

Linearize Equation (C.1-5):

$$\Delta i_d = \frac{\left(\frac{3\sqrt{6}}{\pi}\right)\Delta E - \Delta e_d - \left(6l_c i_{d0}\right)\Delta f_g}{\left(L_{dc} + 2l_c\right)S + \left(r_{dc} + \frac{3}{\pi}l_c\left(2\pi f_{g0}\right)\right)} = \frac{L_{21}}{L_{11}S + L_{12}}\Delta E - \frac{1}{L_{11}S + L_{12}}\Delta e_d + \frac{L_{22}}{L_{11}S + L_{12}}\Delta f_g$$

(C.1-7)

$$L_{21} = \frac{3\sqrt{6}}{\pi} \quad \text{(C.1-8)}$$

$$L_{11} = L_{dc} + 2l_c \quad \text{(C.1-9)}$$

$$L_{12} = r_{dc} + \frac{3}{\pi}l_c\left(2\pi f_{g0}\right) \quad \text{(C.1-10)}$$

$$L_{22} = 6l_c i_{d0} \quad \text{(C.1-11)}$$

Linearize Equation (C.1-6):

$$v_d = v_{d0} + a_{E\_Vd}\Delta E + a_{id\_Vd}\Delta i_d + a_{fg\_Vd}\Delta f_g + a_{ed\_Vd}\Delta e_d \quad \text{(C.1-12)}$$

$$a_{E\_Vd} = \frac{\frac{3\sqrt{6}}{\pi}L_{dc}}{L_{dc} + 2l_c} \quad \text{(C.1-13)}$$

$$a_{id\_Vd} = \frac{2l_c\left(r_{dc} - 3L_{dc}f_{g0}\right)}{L_{dc} + 2l_c} \quad \text{(C.1-14)}$$

$$a_{fg\_Vd} = -\frac{6l_c L_{dc} i_{d0}}{L_{dc} + 2l_c} \tag{C.1-15}$$

$$a_{ed\_Vd} = \frac{2l_c}{L_{dc} + 2l_c} \tag{C.1-16}$$

Substitute Equation (C.1-7) in Equation (C.1-12), the dc link voltage can be derived as follows:

$$v_d = v_{d0} + M_{21}\Delta E + M_{22}\Delta e_d + M_{23}\Delta f_g \tag{C.1-17}$$

$$M_{21} = \frac{\left(a_{E\_Vd} L_{11}\right)S + \left(a_{E\_Vd} L_{12} + a_{id\_Vd} L_{21}\right)}{L_{11}S + L_{12}} = \frac{M_{31}S + M_{32}}{L_{11}S + L_{12}} \tag{C.1-18}$$

$$M_{22} = \frac{\left(a_{ed\_Vd} L_{11}\right)S + \left(a_{ed\_Vd} L_{12} - a_{id\_Vd}\right)}{L_{11}S + L_{12}} = \frac{M_{33}S + M_{34}}{L_{11}S + L_{12}} \tag{C.1-19}$$

$$M_{23} = \frac{\left(a_{fg\_Vd} L_{11}\right)S + \left(a_{fg\_Vd} L_{12} + a_{id\_Vd} L_{22}\right)}{L_{11}S + L_{12}} = \frac{M_{35}S + M_{36}}{L_{11}S + L_{12}} \tag{C.1-20}$$

$$M_{31} = a_{E\_Vd} L_{11} \tag{C.1-21}$$

$$M_{32} = a_{E\_Vd} L_{12} + a_{id\_Vd} L_{21} \tag{C.1-22}$$

$$M_{33} = a_{ed\_Vd} L_{11} \tag{C.1-23}$$

$$M_{34} = a_{ed\_Vd} L_{12} - a_{id\_Vd} \tag{C.1-24}$$

$$M_{35} = a_{fg\_Vd} L_{11} \tag{C.1-25}$$

$$M_{36} = a_{fg\_Vd} L_{12} + a_{id\_Vd} L_{22} \tag{C.1-26}$$

The power source voltage in dq reference frame can be expressed as follows:

$$v_{dg} = 0 \tag{C.1-27}$$

$$v_{qg} = \sqrt{2}E \tag{C.1-28}$$

The current at the input of the VFD in dq reference frame can be calculated as follows:

$$i_{qg} = i_{qgcom} + i_{qgcond} \tag{C.1-29}$$

$$i_{dg} = i_{dgcom} + i_{dgcond} \tag{C.1-30}$$

$$i_{qgcom} = \frac{2\sqrt{3}}{\pi} i_d \left[\sin\left(u - \frac{5\pi}{6} \right) - \sin\left(-\frac{5\pi}{6} \right) \right] + \frac{3\sqrt{2}}{\pi l_c (2\pi f_g)} E(\cos u - 1) + \frac{3\sqrt{2}}{4\pi l_c (2\pi f_g)} E(1 - \cos 2u) \tag{C.1-31}$$

$$i_{qgcond} = \frac{2\sqrt{3}}{\pi} i_d \left[\sin\left(\frac{7\pi}{6} \right) - \sin\left(u + \frac{5\pi}{6} \right) \right] \tag{C.1-32}$$

$$i_{dgcom} = \frac{2\sqrt{3}}{\pi} i_d \left[-\cos\left(u - \frac{5\pi}{6} \right) + \cos\left(-\frac{5\pi}{6} \right) \right] + \frac{3\sqrt{2}}{\pi l_c (2\pi f_g)} E \sin u - \frac{3\sqrt{2}}{4\pi l_c (2\pi f_g)} E \sin 2u - \frac{3\sqrt{2}}{2\pi l_c (2\pi f_g)} Eu \tag{C.1-33}$$

$$i_{dgcond} = \frac{2\sqrt{3}}{\pi} i_d \left[-\cos\left(\frac{7\pi}{6} \right) + \cos\left(u + \frac{5\pi}{6} \right) \right] \tag{C.1-34}$$

$$u = \arccos\left(1 - \frac{2 l_c (2\pi f_g) i_d}{\sqrt{6} E} \right) \tag{C.1-35}$$

where u is the commutation angle.

The real power P and reactive power at the power source in front of the commutation inductor l_c can be calculated as follows:

$$P = \frac{3}{2} \left(v_{dg} i_{dg} + v_{qg} i_{qg} \right) \tag{C.1-36}$$

$$Q = \frac{3}{2} \left(v_{qg} i_{dg} - v_{dg} i_{qg} \right) \tag{C.1-37}$$

Substitute equations (C.1-27) and (C.1-28) in Equations (C.1-36) and (C.1-37),

$$P = \frac{3}{2} \left(\sqrt{2} E i_{qg} \right) = \frac{3}{\sqrt{2}} E i_{qg} = \frac{3}{\sqrt{2}} E \left(i_{qgcom} + i_{qgcond} \right) \tag{C.1-38}$$

$$Q=\frac{3}{2}\left(\sqrt{2}Ei_{dg}\right)=\frac{3}{\sqrt{2}}Ei_{dg}=\frac{3}{\sqrt{2}}E\left(i_{dgcom}+i_{dgcond}\right) \tag{C.1-39}$$

Linearize Equations (C.1-31)-(C.1-35):

$$i_{qgcom}=i_{qgcom0}+a_{id\_qgcom}\Delta i_d+a_{E\_qgcom}\Delta E+a_{u\_qgcom}\Delta u+a_{fg\_qgcom}\Delta f_g \tag{C.1-40}$$

$$\begin{aligned} i_{qgcom0}=&\frac{2\sqrt{3}}{\pi}i_{d0}\left[\sin\left(u_0-\frac{5\pi}{6}\right)-\sin\left(-\frac{5\pi}{6}\right)\right]+\frac{3\sqrt{2}}{\pi l_c\left(2\pi f_{g0}\right)}E_0\left(\cos u_0-1\right)\\ &+\frac{3\sqrt{2}}{4\pi l_c\left(2\pi f_{g0}\right)}E_0\left(1-\cos\left(2u_0\right)\right)\end{aligned} \tag{C.1-41}$$

$$a_{id\_qgcom}=\frac{\sqrt{3}}{\pi}-\frac{3}{\pi}\sin\left(u_0\right)-\frac{\sqrt{3}}{\pi}\cos\left(u_0\right)=\frac{\sqrt{3}}{\pi}\left(1-\sqrt{3}\sin\left(u_0\right)-\cos\left(u_0\right)\right) \tag{C.1-42}$$

$$a_{E\_qgcom}=\frac{3\sqrt{2}}{2\pi^2 l_c f_{g0}}\left(\cos\left(u_0\right)-\frac{3}{4}-\frac{1}{4}\cos\left(2u_0\right)\right) \tag{C.1-43}$$

$$a_{u\_qgcom}=\frac{3\sqrt{2}E_0}{2\pi^2 l_c f_{g0}}\left(\frac{\sin\left(2u_0\right)}{2}-\sin\left(u_0\right)\right)+\frac{\sqrt{3}i_{d0}}{\pi}\left(\sin\left(u_0\right)-\sqrt{3}\cos\left(u_0\right)\right) \tag{C.1-44}$$

$$a_{fg\_qgcom}=\frac{3\sqrt{2}E_0}{2\pi^2 l_c f_{g0}^2}\left(-\cos\left(u_0\right)+\frac{3}{4}+\frac{1}{4}\cos\left(2u_0\right)\right) \tag{C.1-45}$$

$$i_{qgcond}=i_{qgcond0}+a_{id\_qgcond}\Delta i_d+a_{u\_qgcond}\Delta u \tag{C.1-46}$$

$$i_{qgcond0}=\frac{2\sqrt{3}}{\pi}i_{d0}\left[\sin\left(\frac{7\pi}{6}\right)-\sin\left(u_0+\frac{5\pi}{6}\right)\right] \tag{C.1-47}$$

$$a_{id\_qgcond}=-\frac{\sqrt{3}}{\pi}+\frac{3}{\pi}\sin\left(u_0\right)-\frac{\sqrt{3}}{\pi}\cos\left(u_0\right)=\frac{\sqrt{3}}{\pi}\left(\sqrt{3}\sin\left(u_0\right)-\cos\left(u_0\right)-1\right) \tag{C.1-48}$$

$$a_{u\_qgcond}=\frac{3i_{d0}}{\pi}\cos\left(u_0\right)+\frac{\sqrt{3}i_{d0}}{\pi}\sin\left(u_0\right)=\frac{\sqrt{3}}{\pi}i_{d0}\left(\sin\left(u_0\right)-\sqrt{3}\cos\left(u_0\right)\right) \tag{C.1-49}$$

$$i_{dgcom}=i_{dgcom0}+a_{id\_dgcom}\Delta i_d+a_{E\_dgcom}\Delta E+a_{u\_dgcom}\Delta u+a_{fg\_dgcom}\Delta f_g \tag{C.1-50}$$

$$i_{dgcom0} = \frac{2\sqrt{3}}{\pi} i_{d0}\left[-\cos\left(u_0 - \frac{5\pi}{6}\right) + \cos\left(-\frac{5\pi}{6}\right)\right] + \frac{3\sqrt{2}}{\pi l_c (2\pi f_{g0})} E_0 \sin(u_0) - \frac{3\sqrt{2}}{4\pi l_c (2\pi f_{g0})} E_0 \sin(2u_0) - \frac{3\sqrt{2}}{2\pi l_c (2\pi f_{g0})} E_0 u_0 \quad \text{(C.1-51)}$$

$$a_{id\_dgcom} = \frac{3}{\pi}\cos(u_0) - \frac{\sqrt{3}}{\pi}\sin(u_0) - \frac{3}{\pi} = \frac{\sqrt{3}}{\pi}\left(\sqrt{3}\cos(u_0) - \sin(u_0) - \sqrt{3}\right) \quad \text{(C.1-52)}$$

$$a_{E\_dgcom} = \frac{3\sqrt{2}}{2\pi^2 l_c f_{g0}}\left(\sin(u_0) - \frac{1}{4}\sin(2u_0) - \frac{u_0}{2}\right) \quad \text{(C.1-53)}$$

$$a_{u\_dgcom} = \frac{3\sqrt{2}E_0}{2\pi^2 l_c f_{g0}}\left(\cos(u_0) - \frac{\cos(2u_0)}{2} - \frac{1}{2}\right) - \frac{\sqrt{3}i_{d0}}{\pi}\left(\sqrt{3}\sin(u_0) + \cos(u_0)\right) \quad \text{(C.1-54)}$$

$$a_{fg\_dgcom} = \frac{3\sqrt{2}E_0}{2\pi^2 l_c f_{g0}^2}\left(-\sin(u_0) + \frac{u_0}{2} + \frac{1}{4}\sin(2u_0)\right) \quad \text{(C.1-55)}$$

$$i_{dgcond} = i_{dgcond0} + a_{id\_dgcond}\Delta i_d + a_{u\_dgcond}\Delta u \quad \text{(C.1-56)}$$

$$i_{dgcond0} = \frac{2\sqrt{3}}{\pi} i_{d0}\left[-\cos\left(\frac{7\pi}{6}\right) + \cos\left(u_0 + \frac{5\pi}{6}\right)\right] \quad \text{(C.1-57)}$$

$$a_{id\_dgcond} = \frac{3}{\pi} - \frac{3}{\pi}\cos(u_0) - \frac{\sqrt{3}}{\pi}\sin(u_0) = \frac{\sqrt{3}}{\pi}\left(\sqrt{3} - \sqrt{3}\cos(u_0) - \sin(u_0)\right) \quad \text{(C.1-58)}$$

$$a_{u\_dgcond} = \frac{3i_{d0}}{\pi}\sin(u_0) - \frac{\sqrt{3}i_{d0}}{\pi}\cos(u_0) = \frac{\sqrt{3}}{\pi} i_{d0}\left(\sqrt{3}\sin(u_0) - \cos(u_0)\right) \quad \text{(C.1-59)}$$

For the real power P, the Taylor expansion for Equation (C.1-38) can be written as follows:

$$\begin{aligned} P &= P_0 + a_{E\_P}(E - E_0) + a_{iqgcom}\left(i_{qgcom} - i_{qgcom0}\right) + a_{iqgcond}\left(i_{qgcond} - i_{qgcond0}\right) \\ &\quad + a_{Eiqgcom}(E - E_0)\left(i_{qgcom} - i_{qgcom0}\right) + a_{Eiqgcond}(E - E_0)\left(i_{qgcond} - i_{qgcond0}\right) \\ &\quad + a_{EE\_P}(E - E_0)^2 \\ &= P_0 + a_{E\_P}\Delta E + a_{iqgcom}\Delta i_{qgcom} + a_{iqgcond}\Delta i_{qgcond} + a_{Eiqgcom}\Delta E\Delta i_{qgcom} \\ &\quad + a_{Eiqgcond}\Delta E\Delta i_{qgcond} + a_{EE\_P}\Delta E^2 \end{aligned} \quad \text{(C.1-60)}$$

$$a_{E\_P} = \frac{3}{\sqrt{2}}\left(i_{qgcom0} + i_{qgcond0}\right) \tag{C.1-61}$$

$$a_{iqgcom\_P} = \frac{3}{\sqrt{2}} E_0 \tag{C.1-62}$$

$$a_{iqgcond\_P} = \frac{3}{\sqrt{2}} E_0 \tag{C.1-63}$$

$$a_{Eiqgcom\_P} = \frac{3}{\sqrt{2}} \tag{C.1-64}$$

$$a_{Eiqgcond\_P} = \frac{3}{\sqrt{2}} \tag{C.1-65}$$

$$a_{EE\_P} = \frac{3}{2\sqrt{2}} a_{Eiqgcom} \tag{C.1-66}$$

Substitute Equations (C.1-40) and (C.1-46) in Equation (C.1-60), the real power P can be expressed as follows:

$$\begin{aligned} P = {} & P_0 + GP_{11}\Delta E + GP_{12}\Delta i_d + GP_{13}\Delta u + GP_{14}\Delta f_g + GP_{15}\Delta E\Delta u \\ & + GP_{16}\Delta E\Delta i_d + GP_{17}\Delta E^2 + GP_{18}\Delta E\Delta f_g \end{aligned} \tag{C.1-67}$$

$$GP_{11} = a_{E\_P} + a_{iqgcom} a_{E\_qgcom} \tag{C.1-68}$$

$$GP_{12} = a_{iqgcom} a_{id\_qgcom} + a_{iqgcond} a_{id\_qgcond} \tag{C.1-69}$$

$$GP_{13} = a_{iqgcom} a_{u\_qgcom} + a_{iqgcond} a_{u\_qgcond} \tag{C.1-70}$$

$$GP_{14} = a_{iqgcom} a_{fg\_qgcom} \tag{C.1-71}$$

$$GP_{15} = a_{Eiqgcom} a_{u\_qgcom} + a_{Eiqgcond} a_{u\_qgcond} \tag{C.1-72}$$

$$GP_{16} = a_{Eiqgcom} a_{id\_qgcom} + a_{Eiqgcond} a_{id\_qgcond} \tag{C.1-73}$$

$$GP_{17} = a_{Eiqgcom} a_{E\_qgcom} + a_{EE\_P} \tag{C.1-74}$$

$$GP_{18} = a_{Eiqgcom} a_{fg\_qgcom} \tag{C.1-75}$$

Based on Equation (C.1-35), the commutation angle can be expressed as follows:

$$\cos(u) = 1 - \frac{2l_c(2\pi f_g)i_d}{\sqrt{6}E} = 1 - \frac{4\pi l_c}{\sqrt{6}} f_g i_d \left(\frac{1}{E}\right) \tag{C.1-76}$$

Linearize Equation (C.1-76), we have

$$\Delta u = u_{21}\Delta i_d + u_{22}\Delta E + u_{23}\Delta f_g \tag{C.1-77}$$

$$u_{21} = \frac{4\pi l_c f_{g0}}{\sqrt{6}E_0 \sin(u_0)} \tag{C.1-78}$$

$$u_{22} = -\frac{4\pi l_c f_{g0} i_{d0}}{\sqrt{6}E_0^2 \sin(u_0)} \tag{C.1-79}$$

$$u_{23} = \frac{4\pi l_c i_{d0}}{\sqrt{6}E_0 \sin(u_0)} \tag{C.1-80}$$

Substitute Equation (C.1-77) in Equation (C.1-67),

$$P = P_0 + GP_{21}\Delta E + GP_{22}\Delta i_d + GP_{23}\Delta f_g + GP_{24}\Delta i_d \Delta E + GP_{25}\Delta E^2 + GP_{26}\Delta E \Delta f_g \tag{C.1-81}$$

$$GP_{21} = GP_{11} + GP_{13}u_{22} \tag{C.1-82}$$

$$GP_{22} = GP_{12} + GP_{13}u_{21} \tag{C.1-83}$$

$$GP_{23} = GP_{14} + GP_{13}u_{23} \tag{C.1-84}$$

$$GP_{24} = GP_{16} + GP_{15}u_{21} \tag{C.1-85}$$

$$GP_{25} = GP_{17} + GP_{15}u_{22} \tag{C.1-86}$$

$$GP_{26} = GP_{18} + GP_{15}u_{23} \tag{C.1-87}$$

For the reactive power Q, the Taylor expansion for Equation (C.1-39) can be written as follows:

$$
\begin{aligned}
Q &= Q_0 + a_{E\_Q}(E - E_0) + a_{idgcom}\left(i_{dgcom} - i_{dgcom0}\right) + a_{idgcond}\left(i_{dgcond} - i_{dgcond0}\right) \\
&\quad + a_{Eidgcom}(E - E_0)\left(i_{dgcom} - i_{dgcom0}\right) + a_{Eidgcond}(E - E_0)\left(i_{dgcond} - i_{dgcond0}\right) \\
&\quad + a_{EE\_Q}(E - E_0)^2 \\
&= Q_0 + a_{E\_Q}\Delta E + a_{idgcom}\Delta i_{dgcom} + a_{idgcond}\Delta i_{dgcond} + a_{Eidgcom}\Delta E\Delta i_{dgcom} \\
&\quad + a_{Eidgcond}\Delta E\Delta i_{dgcond} + a_{EE\_Q}\Delta E^2
\end{aligned}
\tag{C.1-88}
$$

$$
a_{E\_Q} = \frac{3}{\sqrt{2}}\left(i_{dgcom0} + i_{dgcond0}\right) \tag{C.1-89}
$$

$$
a_{idgcom\_Q} = \frac{3}{\sqrt{2}}E_0 \tag{C.1-90}
$$

$$
a_{idgcond\_Q} = \frac{3}{\sqrt{2}}E_0 \tag{C.1-91}
$$

$$
a_{Eidgcom\_Q} = \frac{3}{\sqrt{2}} \tag{C.1-92}
$$

$$
a_{Eidgcond\_Q} = \frac{3}{\sqrt{2}} \tag{C.1-93}
$$

$$
a_{EE\_Q} = \frac{3}{2\sqrt{2}}a_{Eidgcom} \tag{C.1-94}
$$

Substitute Equations (C.1-50) and (C.1-56) in Equation (C.1-88), the reactive power Q can be expressed as follows:

$$
\begin{aligned}
Q &= Q_0 + GQ_{11}\Delta E + GQ_{12}\Delta i_d + GQ_{13}\Delta u + GQ_{14}\Delta f_g + GQ_{15}\Delta E\Delta u \\
&\quad + GQ_{16}\Delta E\Delta i_d + GQ_{17}\Delta E^2 + GQ_{18}\Delta E\Delta f_g
\end{aligned}
\tag{C.1-95}
$$

$$
GQ_{11} = a_{E\_Q} + a_{idgcom}a_{E\_dgcom} \tag{C.1-96}
$$

$$
GQ_{12} = a_{idgcom}a_{id\_dgcom} + a_{idgcond}a_{id\_dgcond} \tag{C.1-97}
$$

$$
GQ_{13} = a_{idgcom}a_{u\_dgcom} + a_{idgcond}a_{u\_dgcond} \tag{C.1-98}
$$

$$
GQ_{14} = a_{idgcom}a_{fg\_dgcom} \tag{C.1-99}
$$

$$
GQ_{15} = a_{Eidgcom}a_{u\_dgcom} + a_{Eidgcond}a_{u\_dgcond} \tag{C.1-100}
$$

$$GQ_{16} = a_{Eidgcom} a_{id\_dgcom} + a_{Eidgcond} a_{id\_dgcond} \quad \text{(C.1-101)}$$

$$GQ_{17} = a_{Eidgcom} a_{E\_dgcom} + a_{EE\_Q} \quad \text{(C.1-102)}$$

$$GQ_{18} = a_{Eidgcom} a_{fg\_dgcom} \quad \text{(C.1-103)}$$

Substitute Equation (C.1-77) in Equation (C.1-95),

$$Q = Q_0 + GQ_{21}\Delta E + GQ_{22}\Delta i_d + GQ_{23}\Delta f_g + GQ_{24}\Delta i_d \Delta E + GQ_{25}\Delta E^2 + GQ_{26}\Delta E \Delta f_g \quad \text{(C.1-104)}$$

$$GQ_{21} = GQ_{11} + GQ_{13}u_{22} \quad \text{(C.1-105)}$$

$$GQ_{22} = GQ_{12} + GQ_{13}u_{21} \quad \text{(C.1-106)}$$

$$GQ_{23} = GQ_{14} + GQ_{13}u_{23} \quad \text{(C.1-107)}$$

$$GQ_{24} = GQ_{16} + GQ_{15}u_{21} \quad \text{(C.1-108)}$$

$$GQ_{25} = GQ_{17} + GQ_{15}u_{22} \quad \text{(C.1-109)}$$

$$GQ_{26} = GQ_{18} + GQ_{15}u_{23} \quad \text{(C.1-110)}$$

C.2 Induction Motors

The induction motors can be represented by the following differential equations:

$$v_{ds} = R_s i_{ds} - \omega_s \Psi_{qs} + \frac{d\Psi_{ds}}{dt} \quad \text{(C.2-1)}$$

$$v_{qs} = R_s i_{qs} + \omega_s \Psi_{ds} + \frac{d\Psi_{qs}}{dt} \quad \text{(C.2-2)}$$

$$v_{dr} = R_r i_{dr} - (\omega_s - \omega_r)\Psi_{qr} + \frac{d\Psi_{dr}}{dt} \quad \text{(C.2-3)}$$

$$v_{qr} = R_r i_{qr} + (\omega_s - \omega_r)\Psi_{dr} + \frac{d\Psi_{qr}}{dt} \quad \text{(C.2-4)}$$

$$\Psi_{ds} = L_s i_{ds} + L_m i_{dr} \quad \text{(C.2-5)}$$

$$\Psi_{qs} = L_s i_{qs} + L_m i_{qr} \tag{C.2-6}$$

$$\Psi_{dr} = L_m i_{ds} + L_r i_{dr} \tag{C.2-7}$$

$$\Psi_{qr} = L_m i_{qs} + L_r i_{qr} \tag{C.2-8}$$

$$T_e = 1.5P\left(\Psi_{ds} i_{qs} - \Psi_{qs} i_{ds}\right) \tag{C.2-9}$$

$$\frac{d\omega_r}{dt} = \frac{P}{2H}\left(T_e - T_m\right) \tag{C.2-10}$$

$$L_s = l_s + L_m \tag{C.2-11}$$

$$L_r = l_r + L_m \tag{C.2-12}$$

$$J = \frac{2H}{p} \tag{C.2-13}$$

where p is pole pair, l_s and l_r is the leakage inductance of the stator and the rotor, J is inertia.

The stator transients are negligible,

$$\frac{d\Psi_{ds}}{dt} = 0, \qquad \frac{d\Psi_{qs}}{dt} = 0 \tag{C.2-14}$$

For induction motors, the rotor is shorted:

$$v_{dr} = 0, \qquad v_{qr} = 0 \tag{C.2-15}$$

Substitute Equations (C.2-5)-(C.2-8), (C.2-14) and (C.2-15) in Equations (C.2-1)-(C.2-4), and (C.2-9):

$$v_{ds} = R_s i_{ds} - \omega_s\left(L_s i_{qs} + L_m i_{qr}\right) \tag{C.2-16}$$

$$v_{qs} = R_s i_{qs} + \omega_s\left(L_s i_{ds} + L_m i_{dr}\right) \tag{C.2-17}$$

$$0 = R_r i_{dr} - \left(\omega_s - \omega_r\right)\left(L_m i_{qs} + L_r i_{qr}\right) + \left(L_m \frac{di_{ds}}{dt} + L_r \frac{di_{dr}}{dt}\right) \tag{C.2-18}$$

$$0 = R_r i_{qr} + (\omega_s - \omega_r)(L_m i_{ds} + L_r i_{dr}) + \left(L_m \frac{di_{qs}}{dt} + L_r \frac{di_{qr}}{dt} \right) \quad \text{(C.2-19)}$$

$$T_e = 1.5 p L_m (i_{dr} i_{qs} - i_{qr} i_{ds}) \quad \text{(C.2-20)}$$

Linearize Equations (C.2-10), (C.2-16)-(C.2-19):

$$\Delta v_{ds} = R_s \Delta i_{ds} - L_s \omega_{s0} \Delta i_{qs} - L_m \omega_{s0} \Delta i_{qr} - (L_s i_{qs0} + L_m i_{qr0}) \Delta \omega_s \quad \text{(C.2-21)}$$

$$\Delta v_{qs} = R_s \Delta i_{qs} + L_s \omega_{s0} \Delta i_{ds} + L_m \omega_{s0} \Delta i_{dr} + (L_s i_{ds0} + L_m i_{dr0}) \Delta \omega_s \quad \text{(C.2-22)}$$

$$\begin{aligned} 0 = {} & (R_r + L_r S) \Delta i_{dr} + L_m (\omega_{r0} - \omega_{s0}) \Delta i_{qs} + L_r (\omega_{r0} - \omega_{s0}) \Delta i_{qr} \\ & + (L_m S) \Delta i_{ds} + (L_m i_{qs0} + L_r i_{qr0}) \Delta \omega_r - (L_m i_{qs0} + L_r i_{qr0}) \Delta \omega_s \end{aligned} \quad \text{(C.2-23)}$$

$$\begin{aligned} 0 = {} & (R_r + L_r S) \Delta i_{qr} - L_m (\omega_{r0} - \omega_{s0}) \Delta i_{ds} - L_r (\omega_{r0} - \omega_{s0}) \Delta i_{dr} \\ & + (L_m S) \Delta i_{qs} - (L_m i_{ds0} + L_r i_{dr0}) \Delta \omega_r + (L_m i_{ds0} + L_r i_{dr0}) \Delta \omega_s \end{aligned} \quad \text{(C.2-24)}$$

$$S \Delta \omega_r = \frac{1.5 P^2 L_m}{2H} (i_{dr0} \Delta i_{qs} + i_{qs0} \Delta i_{dr} - i_{qr0} \Delta i_{ds} - i_{ds0} \Delta i_{qr}) \quad \text{(C.2-25)}$$

From Equation (C.2-21), i_{qr} can be determined as follows:

$$\Delta i_{qr} = \left(\frac{1}{L_m \omega_{s0}} \right) [R_s \Delta i_{ds} - L_s \omega_{s0} \Delta i_{qs} - (L_s i_{qs0} + L_m i_{qr0}) \Delta \omega_s - \Delta v_{ds}] \quad \text{(C.2-26)}$$

From Equation (C.2-22), i_{dr} can be determined as follows:

$$\Delta i_{dr} = \left(\frac{1}{L_m \omega_{s0}} \right) [\Delta v_{qs} - R_s \Delta i_{qs} - L_s \omega_{s0} \Delta i_{ds} - (L_s i_{ds0} + L_m i_{dr0}) \Delta \omega_s] \quad \text{(C.2-27)}$$

Substitute Equations (C.2-26) and (C.2-27) in Equations (C.2-23)-(C.2-25):

$$\begin{aligned} 0 = {} & (R_r + L_r S) \Delta v_{qs} - L_r (\omega_{r0} - \omega_{s0}) \Delta v_{ds} + [\omega_{s0} (\omega_{r0} - \omega_{s0}) (L_m^2 - L_r L_s) - R_s (R_r + L_r S)] \Delta i_{qs} \\ & + [\omega_{s0} (L_m^2 - L_r L_s) S + R_s L_r (\omega_{r0} - \omega_{s0}) - R_r L_s \omega_{s0}] \Delta i_{ds} + [L_m \omega_{s0} (L_m i_{qs0} + L_r i_{qr0})] \Delta \omega_r \\ & - [(R_r + L_r S)(L_s i_{ds0} + L_m i_{dr0}) + L_r (\omega_{r0} - \omega_{s0})(L_s i_{qs0} + L_m i_{qr0}) + L_m \omega_{s0} (L_m i_{qs0} + L_r i_{qr0})] \Delta \omega_s \end{aligned} \quad \text{(C.2-28)}$$

$$0 = -L_r(\omega_{r0} - \omega_{s0})\Delta v_{qs} - (R_r + L_r S)\Delta v_{ds} + \left[\omega_{s0}\left(L_m^2 - L_r L_s\right)S + R_s L_r(\omega_{r0} - \omega_{s0}) - R_r L_s \omega_{s0}\right]\Delta i_{qs}$$
$$+ \left[R_s(R_r + L_r S) - \omega_{s0}(\omega_{r0} - \omega_{s0})\left(L_m^2 - L_r L_s\right)\right]\Delta i_{ds} - \left[L_m \omega_{s0}(L_m i_{ds0} + L_r i_{dr0})\right]\Delta\omega_r$$
$$+ \left[L_r(\omega_{r0} - \omega_{s0})(L_s i_{ds0} + L_m i_{dr0}) + L_m \omega_{s0}(L_m i_{ds0} + L_r i_{dr0}) - (R_r + L_r S)\left(L_s i_{qs0} + L_m i_{qr0}\right)\right]\Delta\omega_s \quad \text{(C.2-29)}$$

$$\left(\frac{4H\omega_{s0}S}{3P^2}\right)\Delta\omega_r = i_{qs0}\Delta v_{qs} + i_{ds0}\Delta v_{ds} + \left[i_{dr0}L_m\omega_{s0} - i_{qs0}R_s + i_{ds0}L_s\omega_{s0}\omega_{s0}\right]\Delta i_{qs}$$
$$- \left[i_{qs0}L_s\omega_{s0} + i_{qr0}L_m\omega_{s0} + i_{ds0}R_s\right]\Delta i_{ds} + \left[i_{ds0}\left(L_s i_{qs0} + L_m i_{qr0}\right) - i_{qs0}\left(L_s i_{ds0} + L_m i_{dr0}\right)\right]\Delta\omega_s \quad \text{(C.2-30)}$$

C.3 PWM-Controlled VSI and the Voltage per Hz Control

The output voltage from the PWM controlled voltage source inverter:

$$v_{ds} = 0 \quad \text{(C.3-1)}$$

$$v_{qs} = \frac{1}{2}de_d \quad \text{(C.3-2)}$$

Where d is duty cycle.

The real power from the inverter supplying to the motor load is

$$P_{inv\_out} = \frac{3}{2}\left(v_{ds}i_{ds} + v_{qs}i_{qs}\right) \quad \text{(C.3-3)}$$

The dc link power to the inverter can be expressed as

$$P_{inv\_in} = e_d i_I \quad \text{(C.3-4)}$$

When the losses of the inverter are ignored, the power at the input of the inverter, P_{inv_in}, and at the output of the inverter, P_{inv_out}, is considered to be the same:

$$\frac{3}{2}\left(v_{ds}i_{ds} + v_{qs}i_{qs}\right) = e_d i_I \quad \text{(C.3-5)}$$

From Equations (C.1-3) and (C.1-4), the current entering inverter at the DC link can be determined as follows:

$$i_I = i_d - C_{dc}\frac{de_d}{dt} \tag{C.3-6}$$

Substitute Equations (C.3-1), (C.3-2), and (C.3-6) in Equation (C.3-5), the following equation can be obtained:

$$i_{qs} = \frac{4}{3}\frac{\left(i_d - C_{dc}\frac{de_d}{dt}\right)}{d} \tag{C.3-7}$$

At the time t=0, Equation (C.3-7) can be expressed using the initial values:

$$i_{qs0} = \frac{4}{3}\frac{\left(i_{d0} - C_{dc}\frac{de_d}{dt}\Big|_{t=0}\right)}{d_0} \tag{C.3-8}$$

Rearrange Equation (C.3-8),

$$\frac{de_d}{dt}\Big|_{t=0} = \frac{\left(i_{d0} - \frac{3}{4}i_{qs0}d_0\right)}{C_{dc}} \tag{C.3-9}$$

Linearize Equation (C.3-7) and combining with Equation (C.3-9),

$$\Delta i_{qs} = \frac{4}{3d_0}\Delta i_d - \frac{4C_{dc}S}{3d_0}\Delta e_d - \frac{i_{qs0}}{d_0}\Delta d \tag{C.3-10}$$

For the speed controller, the following relationship exists:

$$\begin{bmatrix} v_{qs}^e \\ v_{ds}^e \end{bmatrix} = \begin{bmatrix} \cos\theta_{ce} & \sin\theta_{ce} \\ -\sin\theta_{ce} & \cos\theta_{ce} \end{bmatrix} \begin{bmatrix} v_{qs}^c \\ v_{ds}^c \end{bmatrix} \tag{C.3-11}$$

Replace v_{qs}^{e} by the command value v_{qs}^{e*}, v_{ds}^{e} by the command value v_{ds}^{e*}, v_{qs}^{c} and v_{ds}^{c} by Equations (C.3-1) and (C.3-2),

$$\begin{bmatrix} v_{qs}^{e*} \\ v_{ds}^{e*} \end{bmatrix} = \begin{bmatrix} \cos\theta_{ce} & \sin\theta_{ce} \\ -\sin\theta_{ce} & \cos\theta_{ce} \end{bmatrix} \begin{bmatrix} \frac{1}{2} de_d \\ 0 \end{bmatrix} \tag{C.3-12}$$

The duty cycle d can be calculated as follows:

$$d = \frac{\sqrt{\left(v_{qs}^{e*}\right)^2 + \left(v_{ds}^{e*}\right)^2}}{\frac{1}{2} e_d} \tag{C.3-13}$$

The voltage per Hz control scheme for the low voltage 6-pulse VSI based drive is shown in Figure C.1.

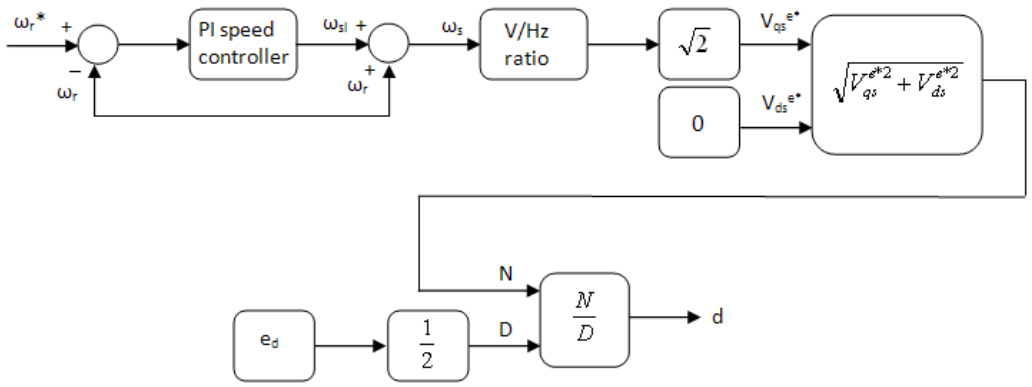

Figure C.1 Voltage per Hz control scheme for VSI motor drive systems

Based on Figure C.1, equations for the control system can be written as follows:

$$\omega_{SL} = K_{pm}\left(\omega_r^* - \omega_r\right) + \int_0^t K_{im}\left(\omega_r^* - \omega_r\right)dt + \left(\omega_{s0} - \omega_{r0}\right) \tag{C.3-14}$$

$$\omega_{SL} + \omega_r = \omega_s \tag{C.3-15}$$

$$\frac{\omega_s\left(\frac{V_b}{\omega_b}\right)\sqrt{2}}{\frac{1}{2}e_d} = d \tag{C.3-16}$$

Linearize Equation (C.3-14),

$$\Delta\omega_{SL} = -\left(\frac{K_{pm}S + K_{im}}{S}\right)\Delta\omega_r \tag{C.3-17}$$

Linearize Equation (C.3-15),

$$\Delta\omega_{SL} + \Delta\omega_r = \Delta\omega_s \tag{C.3-18}$$

Combining Equations (C.3-17) and (C.3-18),

$$\Delta\omega_s = \frac{A_{11}S + A_{12}}{S}\Delta\omega_r \tag{C.3-19}$$

$$A_{11} = 1 - K_{pm} \tag{C.3-20}$$

$$A_{12} = -K_{im} \tag{C.3-21}$$

Linearize Equation (C.3-16):

$$\Delta d = \left(-\frac{2\sqrt{2}V_b\omega_{s0}}{\omega_b e_{d0}^2}\right)\Delta e_d + \left(\frac{2\sqrt{2}V_b}{\omega_b e_{d0}}\right)\Delta\omega_s \tag{C.3-22}$$

Substitute Equation (C.3-22) in Equation (C.3-10):

$$\Delta i_{qs} = A_{21}\Delta i_d + A_{22}\Delta\omega_s + \left(A_{231}S + A_{232}\right)\Delta e_d \tag{C.3-23}$$

$$A_{21} = \frac{4}{3d_0} \tag{C.3-24}$$

$$A_{22} = -\frac{2\sqrt{2}V_b i_{qs0}}{\omega_b e_{d0} d_0} \tag{C.3-25}$$

$$A_{231} = -\frac{4C_{dc}}{3d_0} \tag{C.3-26}$$

$$A_{232} = \frac{2\sqrt{2}V_b \omega_{s0} i_{qs0}}{\omega_b e_{d0}^2 d_0} \tag{C.3-27}$$

Linearize Equations (C.3-1) and (C.3-2):

$$\Delta v_{ds} = 0 \tag{C.3-28}$$

$$\Delta v_{qs} = A_{31}\Delta\omega_s + A_{32}\Delta e_d \tag{C.3-29}$$

$$A_{31} = \frac{\sqrt{2}V_b}{\omega_b} \tag{C.3-30}$$

$$A_{32} = \frac{d_0}{2} - \frac{\sqrt{2}V_b \omega_{s0}}{\omega_b e_{d0}} \tag{C.3-31}$$

Substitute Equation (C.3-19) in Equations (C.3-23) and (C.3-29):

$$\Delta i_{qs} = A_{21}\Delta i_d + \left(\frac{A_{22}A_{11}S + A_{22}A_{12}}{S}\right)\Delta\omega_r + \left(A_{231}S + A_{232}\right)\Delta e_d \tag{C.3-32}$$

$$\Delta v_{qs} = \frac{A_{31}A_{11}S + A_{31}A_{12}}{S}\Delta\omega_r + A_{32}\Delta e_d \tag{C.3-33}$$

Substitute Equations (C.3-28), (C.3-32) and (C.3-33) in Equations (C.2-28), (C.2-29) and (C.2-30):

$$0 = A_{41}\Delta V_{qs} + A_{42}\Delta V_{ds} + A_{43}\Delta i_{qs} + A_{44}\Delta\omega_s + A_{45}\Delta i_{ds} + A_{46}\Delta\omega_r \tag{C.3-34}$$

$$0 = A_{51}\Delta V_{qs} + A_{52}\Delta V_{ds} + A_{53}\Delta i_{qs} + A_{54}\Delta\omega_s + A_{55}\Delta i_{ds} + A_{56}\Delta\omega_r \tag{C.3-35}$$

$$0 = A_{61}\Delta V_{qs} + A_{62}\Delta V_{ds} + A_{63}\Delta i_{qs} + A_{64}\Delta\omega_s + A_{65}\Delta i_{ds} + A_{66}\Delta\omega_r \tag{C.3-36}$$

$$A_{41} = A_{411}S + A_{412} \tag{C.3-37}$$

$$A_{411} = L_r \tag{C.3-38}$$

$$A_{412} = R_r \tag{C.3-39}$$

$$A_{42} = -L_r\left(\omega_{r0} - \omega_{s0}\right) \tag{C.3-40}$$

$$A_{43} = A_{431}S + A_{432} \tag{C.3-41}$$

$$A_{431} = -R_s L_r \tag{C.3-42}$$

$$A_{432} = \omega_{s0}\left(\omega_{r0} - \omega_{s0}\right)\left(L_m^2 - L_r L_s\right) - R_s R_r \tag{C.3-43}$$

$$A_{44} = A_{441} S + A_{442} \tag{C.3-44}$$

$$A_{441} = -L_r\left(L_s i_{ds0} + L_m i_{dr0}\right) \tag{C.3-45}$$

$$A_{442} = -L_m \omega_{s0}\left(L_m i_{qs0} + L_r i_{qr0}\right) - R_r\left(L_s i_{ds0} + L_m i_{dr0}\right) - L_r\left(\omega_{r0} - \omega_{s0}\right)\left(L_s i_{qs0} + L_m i_{qr0}\right) \tag{C.3-46}$$

$$A_{45} = A_{451} S + A_{452} \tag{C.3-47}$$

$$A_{451} = \omega_{s0}\left(L_m^2 - L_r L_s\right) \tag{C.3-48}$$

$$A_{452} = L_r R_s\left(\omega_{r0} - \omega_{s0}\right) - R_r L_s \omega_{s0} \tag{C.3-49}$$

$$A_{46} = L_m \omega_{s0}\left(L_m i_{qs0} + L_r i_{qr0}\right) \tag{C.3-50}$$

$$A_{51} = -L_r\left(\omega_{r0} - \omega_{s0}\right) \tag{C.3-51}$$

$$A_{52} = A_{521} S + A_{522} \tag{C.3-52}$$

$$A_{521} = -L_r \tag{C.3-53}$$

$$A_{522} = -R_r \tag{C.3-54}$$

$$A_{53} = A_{531} S + A_{532} \tag{C.3-55}$$

$$A_{531} = \omega_{s0}\left(L_m^2 - L_r L_s\right) = A_{451} \tag{C.3-56}$$

$$A_{532} = L_r R_s\left(\omega_{r0} - \omega_{s0}\right) - R_r L_s \omega_{s0} = A_{452} \tag{C.3-57}$$

$$A_{54} = A_{541} S + A_{542} \tag{C.3-58}$$

$$A_{541} = -L_r\left(L_s i_{qs0} + L_m i_{qr0}\right) \tag{C.3-59}$$

$$A_{542} = -L_m \omega_{s0}\left(L_m i_{ds0} + L_r i_{dr0}\right) - R_r\left(L_s i_{qs0} + L_m i_{qr0}\right) + L_r\left(\omega_{r0} - \omega_{s0}\right)\left(L_s i_{ds0} + L_m i_{dr0}\right) \tag{C.3-60}$$

$$A_{55} = A_{551} S + A_{552} \tag{C.3-61}$$

$$A_{551} = R_s L_r \tag{C.3-62}$$

$$A_{552} = R_s R_r - \omega_{s0}\left(\omega_{r0} - \omega_{s0}\right)\left(L_m^2 - L_r L_s\right) \tag{C.3-63}$$

$$A_{56} = -L_m \omega_{s0}\left(L_m i_{ds0} + L_r i_{dr0}\right) \tag{C.3-64}$$

$$A_{61} = i_{qs0} \tag{C.3-65}$$

$$A_{62} = i_{ds0} \tag{C.3-66}$$

$$A_{63} = L_m \omega_{s0} i_{dr0} - R_s i_{qs0} + L_s \omega_{s0} i_{ds0} \tag{C.3-67}$$

$$A_{64} = i_{ds0}\left(L_s i_{qs0} + L_m i_{qr0}\right) - i_{qs0}\left(L_s i_{ds0} + L_m i_{dr0}\right) \tag{C.3-68}$$

$$A_{65} = -\left(i_{qs0} L_s \omega_{s0} + i_{ds0} R_s + i_{qr0} L_m \omega_{s0}\right) \tag{C.3-69}$$

$$A_{66} = A_{661} S \tag{C.3-70}$$

$$A_{661} = -\frac{4H\omega_{s0}}{3p^2} \tag{C.3-71}$$

Substitute Equation (C.3-28) in Equation (C.3-36), and rearrange Equation (C.3-36) as follows:

$$\Delta i_{ds} = \left(-\frac{1}{A_{65}}\right)\left(A_{61}\Delta V_{qs} + A_{63}\Delta i_{qs} + A_{64}\Delta\omega_s + A_{66}\Delta\omega_r\right) \tag{C.3-72}$$

Substitute Equations (C.3-28) and (C.3-72) in Equations (C.3-34) and (C.3-35):

$$0 = \left(B_{11}S + B_{12}\right)\Delta V_{qs} + \left(B_{21}S + B_{22}\right)\Delta i_{qs} + \left(B_{31}S + B_{32}\right)\Delta\omega_s + \left(B_{41}S^2 + B_{42}S + B_{43}\right)\Delta\omega_r \tag{C.3-73}$$

$$0 = \left(B_{51}S + B_{52}\right)\Delta V_{qs} + \left(B_{61}S + B_{62}\right)\Delta i_{qs} + \left(B_{71}S + B_{72}\right)\Delta\omega_s + \left(B_{81}S^2 + B_{82}S + B_{83}\right)\Delta\omega_r \tag{C.3-74}$$

$$B_{11} = A_{411}A_{65} - A_{451}A_{61} \tag{C.3-75}$$

$$B_{12} = A_{412}A_{65} - A_{452}A_{61} \tag{C.3-76}$$

$$B_{21} = A_{431}A_{65} - A_{451}A_{63} \tag{C.3-77}$$

$$B_{22} = A_{432}A_{65} - A_{452}A_{63} \tag{C.3-78}$$

$$B_{31} = A_{441}A_{65} - A_{451}A_{64} \quad \text{(C.3-79)}$$

$$B_{32} = A_{442}A_{65} - A_{452}A_{64} \quad \text{(C.3-80)}$$

$$B_{41} = -A_{451}A_{661} \quad \text{(C.3-81)}$$

$$B_{42} = -A_{452}A_{661} \quad \text{(C.3-82)}$$

$$B_{43} = A_{46}A_{65} \quad \text{(C.3-83)}$$

$$B_{51} = -A_{551}A_{61} \quad \text{(C.3-84)}$$

$$B_{52} = A_{51}A_{65} - A_{552}A_{61} \quad \text{(C.3-85)}$$

$$B_{61} = A_{531}A_{65} - A_{551}A_{63} \quad \text{(C.3-86)}$$

$$B_{62} = A_{532}A_{65} - A_{552}A_{63} \quad \text{(C.3-87)}$$

$$B_{71} = A_{541}A_{65} - A_{551}A_{64} \quad \text{(C.3-88)}$$

$$B_{72} = A_{542}A_{65} - A_{552}A_{64} \quad \text{(C.3-89)}$$

$$B_{81} = -A_{551}A_{661} \quad \text{(C.3-90)}$$

$$B_{82} = -A_{552}A_{661} \quad \text{(C.3-91)}$$

$$B_{83} = A_{56}A_{65} \quad \text{(C.3-92)}$$

Substitute Equations (C.3-29) and (C.3-32) in Equations (C.3-73) and (C.3-74):

$$0 = D_{11}\Delta i_d + D_{12}\Delta e_d + D_{13}\Delta\omega_r \quad \text{(C.3-93)}$$

$$0 = D_{21}\Delta i_d + D_{22}\Delta e_d + D_{23}\Delta\omega_r \quad \text{(C.3-94)}$$

$$D_{11} = D_{111}S^2 + D_{112}S \quad \text{(C.3-95)}$$

$$D_{111} = A_{21}B_{21} \quad \text{(C.3-96)}$$

$$D_{112} = A_{21}B_{22} \quad \text{(C.3-97)}$$

$$D_{12} = D_{121}S^3 + D_{122}S^2 + D_{123}S \quad \text{(C.3-98)}$$

$$D_{121} = B_{21}A_{231} \quad \text{(C.3-99)}$$

$$D_{122} = B_{21}A_{232} + B_{22}A_{231} + A_{32}B_{11} \quad \text{(C.3-100)}$$

$$D_{123} = A_{32}B_{12} + B_{22}A_{232} \tag{C.3-101}$$

$$D_{13} = D_{131}S^3 + D_{132}S^2 + D_{133}S + D_{134} \tag{C.3-102}$$

$$D_{131} = B_{41} \tag{C.3-103}$$

$$D_{132} = A_{11}\left(A_{31}B_{11} + B_{31}\right) + B_{21}A_{22}A_{11} + B_{42} \tag{C.3-104}$$

$$D_{133} = A_{11}\left(A_{31}B_{12} + B_{32}\right) + A_{12}\left(A_{31}B_{11} + B_{31}\right) + B_{21}A_{22}A_{12} + B_{22}A_{22}A_{11} + B_{43} \tag{C.3-105}$$

$$D_{134} = A_{12}\left(A_{31}B_{12} + B_{32}\right) + B_{22}A_{22}A_{12} \tag{C.3-106}$$

$$D_{21} = D_{211}S^2 + D_{212}S \tag{C.3-107}$$

$$D_{211} = A_{21}B_{61} \tag{C.3-108}$$

$$D_{212} = A_{21}B_{62} \tag{C.3-109}$$

$$D_{22} = D_{221}S^3 + D_{222}S^2 + D_{223}S \tag{C.3-110}$$

$$D_{221} = B_{61}A_{231} \tag{C.3-111}$$

$$D_{222} = B_{62}A_{231} + B_{61}A_{232} + A_{32}B_{51} \tag{C.3-112}$$

$$D_{223} = A_{32}B_{52} + B_{62}A_{232} \tag{C.3-113}$$

$$D_{23} = D_{231}S^3 + D_{232}S^2 + D_{233}S + D_{234} \tag{C.3-114}$$

$$D_{231} = B_{81} \tag{C.3-115}$$

$$D_{232} = A_{11}\left(A_{31}B_{51} + B_{71}\right) + B_{61}A_{22}A_{11} + B_{82} \tag{C.3-116}$$

$$D_{233} = A_{11}\left(A_{31}B_{52} + B_{72}\right) + A_{12}\left(A_{31}B_{51} + B_{71}\right) + B_{62}A_{22}A_{11} + B_{61}A_{22}A_{12} + B_{83} \tag{C.3-117}$$

$$D_{234} = A_{12}\left(A_{31}B_{52} + B_{72}\right) + B_{62}A_{22}A_{12} \tag{C.3-118}$$

Based on Equations (C.3-93) and (C.3-94),

$$\Delta\omega_r = \left(-\frac{1}{D_{13} - D_{23}}\right)\left[\left(D_{11} - D_{21}\right)\Delta i_d + \left(D_{12} - D_{22}\right)\Delta e_d\right] \tag{C.3-119}$$

Substitute Equation (C.3-119) in Equation (C.3-93), the relationship between i_d and e_d can then be determined as follows:

$$\Delta i_d = \left[\frac{D_{13}(D_{12} - D_{22}) - D_{12}(D_{13} - D_{23})}{D_{11}(D_{13} - D_{23}) - D_{13}(D_{11} - D_{21})} \right] \Delta e_d \tag{C.3-120}$$

Equation (C.3-120) can be further derived to be:

$$\Delta i_d = G_{13} \Delta e_d \tag{C.3-121}$$

$$G_{13} = \frac{F_{11}S^5 + F_{12}S^4 + F_{13}S^3 + F_{14}S^2 + F_{15}S + F_{16}}{F_{21}S^4 + F_{22}S^3 + F_{23}S^2 + F_{24}S + F_{25}} \tag{C.3-122}$$

$$F_{11} = E_{11} - E_{21} \tag{C.3-123}$$

$$F_{12} = E_{12} - E_{22} \tag{C.3-124}$$

$$F_{13} = E_{13} - E_{23} \tag{C.3-125}$$

$$F_{14} = E_{14} - E_{24} \tag{C.3-126}$$

$$F_{15} = E_{15} - E_{25} \tag{C.3-127}$$

$$F_{16} = E_{16} - E_{26} \tag{C.3-128}$$

$$F_{21} = E_{31} - E_{41} \tag{C.3-129}$$

$$F_{22} = E_{32} - E_{42} \tag{C.3-130}$$

$$F_{23} = E_{33} - E_{43} \tag{C.3-131}$$

$$F_{24} = E_{34} - E_{44} \tag{C.3-132}$$

$$F_{25} = E_{35} - E_{45} \tag{C.3-133}$$

$$E_{11} = D_{131}(D_{121} - D_{221}) \tag{C.3-134}$$

$$E_{12} = D_{132}(D_{121} - D_{221}) + D_{131}(D_{122} - D_{222}) \tag{C.3-135}$$

$$E_{13} = D_{133}(D_{121} - D_{221}) + D_{132}(D_{122} - D_{222}) + D_{131}(D_{123} - D_{223}) \tag{C.3-136}$$

$$E_{14} = D_{134}(D_{121} - D_{221}) + D_{133}(D_{122} - D_{222}) + D_{132}(D_{123} - D_{223}) \tag{C.3-137}$$

$$E_{15} = D_{134}(D_{122} - D_{222}) + D_{133}(D_{123} - D_{223}) \tag{C.3-138}$$

$$E_{16} = D_{134}(D_{123} - D_{223}) \tag{C.3-139}$$

$$E_{21} = D_{121}(D_{131} - D_{231}) \tag{C.3-140}$$

$$E_{22} = D_{122}(D_{131} - D_{231}) + D_{121}(D_{132} - D_{232}) \quad \text{(C.3-141)}$$

$$E_{23} = D_{123}(D_{131} - D_{231}) + D_{122}(D_{132} - D_{232}) + D_{121}(D_{133} - D_{233}) \quad \text{(C.3-142)}$$

$$E_{24} = D_{123}(D_{132} - D_{232}) + D_{122}(D_{133} - D_{233}) + D_{121}(D_{134} - D_{234}) \quad \text{(C.3-143)}$$

$$E_{25} = D_{123}(D_{133} - D_{233}) + D_{122}(D_{134} - D_{234}) \quad \text{(C.3-144)}$$

$$E_{26} = D_{123}(D_{134} - D_{234}) \quad \text{(C.3-145)}$$

$$E_{31} = D_{111}(D_{131} - D_{231}) \quad \text{(C.3-146)}$$

$$E_{32} = D_{111}(D_{132} - D_{232}) + D_{112}(D_{131} - D_{231}) \quad \text{(C.3-147)}$$

$$E_{33} = D_{111}(D_{133} - D_{233}) + D_{112}(D_{132} - D_{232}) \quad \text{(C.3-148)}$$

$$E_{34} = D_{111}(D_{134} - D_{234}) + D_{112}(D_{133} - D_{233}) \quad \text{(C.3-149)}$$

$$E_{35} = D_{112}(D_{134} - D_{234}) \quad \text{(C.3-150)}$$

$$E_{41} = D_{131}(D_{111} - D_{211}) \quad \text{(C.3-151)}$$

$$E_{42} = D_{132}(D_{111} - D_{211}) + D_{131}(D_{112} - D_{212}) \quad \text{(C.3-152)}$$

$$E_{43} = D_{133}(D_{111} - D_{211}) + D_{132}(D_{112} - D_{212}) \quad \text{(C.3-153)}$$

$$E_{44} = D_{134}(D_{111} - D_{211}) + D_{133}(D_{112} - D_{212}) \quad \text{(C.3-154)}$$

$$E_{45} = D_{134}(D_{112} - D_{212}) \quad \text{(C.3-155)}$$

Combined Equations (C.1-7) and (C.3-121), the relationship between E and e_d is obtained:

$$\Delta e_d = G_{11}\Delta E + G_{12}\Delta f_g \quad \text{(C.3-156)}$$

$$G_{11} = \frac{F_{41}S^4 + F_{42}S^3 + F_{43}S^2 + F_{44}S + F_{45}}{F_{31}S^6 + F_{32}S^5 + F_{33}S^4 + F_{34}S^3 + F_{35}S^2 + F_{36}S + F_{37}} \quad \text{(C.3-157)}$$

$$G_{12} = \left(\frac{L_{22}}{L_{21}}\right) G_{11} \quad \text{(C.3-158)}$$

$$F_{31} = L_{11}F_{11} \quad \text{(C.3-159)}$$

$$F_{32} = L_{11}F_{12} + L_{12}F_{11} \quad \text{(C.3-160)}$$

$$F_{33} = L_{11}F_{13} + L_{12}F_{12} + F_{21} \quad \text{(C.3-161)}$$

$$F_{34} = L_{11}F_{14} + L_{12}F_{13} + F_{22} \quad \text{(C.3-162)}$$

$$F_{35} = L_{11}F_{15} + L_{12}F_{14} + F_{23} \quad \text{(C.3-163)}$$

$$F_{36} = L_{11}F_{16} + L_{12}F_{15} + F_{24} \quad \text{(C.3-164)}$$

$$F_{37} = L_{12}F_{16} + F_{25} \quad \text{(C.3-165)}$$

$$F_{41} = L_{21}F_{21} \quad \text{(C.3-166)}$$

$$F_{42} = L_{21}F_{22} \quad \text{(C.3-167)}$$

$$F_{43} = L_{21}F_{23} \quad \text{(C.3-168)}$$

$$F_{44} = L_{21}F_{24} \quad \text{(C.3-169)}$$

$$F_{45} = L_{21}F_{25} \quad \text{(C.3-170)}$$

C.4 Overall System Combination

Rewrite Equation (C.1-7) as follows:

$$\Delta i_d = N_{11}\Delta E + N_{12}\Delta e_d + N_{13}\Delta f_g \quad \text{(C.4-1)}$$

$$N_{11} = \frac{L_{21}}{L_{11}S + L_{12}} \quad \text{(C.4-2)}$$

$$N_{12} = -\frac{1}{L_{11}S + L_{12}} \quad \text{(C.4-3)}$$

$$N_{13} = \frac{L_{22}}{L_{11}S + L_{12}} \quad \text{(C.4-4)}$$

Rewrite Equation (C.3-156) as follows:

$$\Delta e_d = G_{11}\Delta E + \left(\frac{L_{22}}{L_{21}}\right)G_{11}\Delta f_g \quad \text{(C.4-5)}$$

Submit Equations (C.4-1) and (C.4-5) in Equations (C.1-81) and (C.1-104), the dynamic model of VFDs using the real power and reactive power at the input of the VFD can be determined as follows:

$$P = P_0 + G_{P1}\Delta E + G_{P2}\Delta E^2 + \left(G_{P3} + G_{P4}\Delta E\right)\Delta f \tag{C.4-6}$$

$$G_{P1} = GP_{21} + GP_{22}N_{11} + GP_{22}N_{12}G_{11} \tag{C.4-7}$$

$$G_{P2} = GP_{25} + GP_{24}N_{11} + GP_{24}N_{12}G_{11} \tag{C.4-8}$$

$$G_{P3} = GP_{23} + GP_{22}N_{13} + \frac{L_{22}GP_{22}}{L_{21}}N_{12}G_{11} \tag{C.4-9}$$

$$G_{P4} = GP_{26} + GP_{24}N_{13} + \frac{L_{22}GP_{24}}{L_{21}}N_{12}G_{11} \tag{C.4-10}$$

$$Q = Q_0 + G_{Q1}\Delta E + G_{Q2}\Delta E^2 + \left(G_{Q3} + G_{Q4}\Delta E\right)\Delta f \tag{C.4-11}$$

$$G_{Q1} = GQ_{21} + GQ_{22}N_{11} + GQ_{22}N_{12}G_{11} \tag{C.4-12}$$

$$G_{Q2} = GQ_{25} + GQ_{24}N_{11} + GQ_{24}N_{12}G_{11} \tag{C.4-13}$$

$$G_{Q3} = GQ_{23} + GQ_{22}N_{13} + \frac{L_{22}GQ_{22}}{L_{21}}N_{12}G_{11} \tag{C.4-14}$$

$$G_{Q4} = GQ_{26} + GQ_{24}N_{13} + \frac{L_{22}GQ_{24}}{L_{21}}N_{12}G_{11} \tag{C.4-15}$$

The coefficient of the real power and reactive power are transfer functions, they can be derived as follows:

$$G_{P1} = \frac{GP_{51}S^7 + GP_{52}S^6 + GP_{53}S^5 + GP_{54}S^4 + GP_{55}S^3 + GP_{56}S^2 + GP_{57}S + GP_{58}}{P_{b1}S^7 + P_{b2}S^6 + P_{b3}S^5 + P_{b4}S^4 + P_{b5}S^3 + P_{b6}S^2 + P_{b7}S + P_{b8}} \tag{C.4-16}$$

$$G_{P2} = \frac{GP_{71}S^7 + GP_{72}S^6 + GP_{73}S^5 + GP_{74}S^4 + GP_{75}S^3 + GP_{76}S^2 + GP_{77}S + GP_{78}}{P_{b1}S^7 + P_{b2}S^6 + P_{b3}S^5 + P_{b4}S^4 + P_{b5}S^3 + P_{b6}S^2 + P_{b7}S + P_{b8}} \tag{C.4-17}$$

$$G_{P3} = \frac{GP_{91}S^7 + GP_{92}S^6 + GP_{93}S^5 + GP_{94}S^4 + GP_{95}S^3 + GP_{96}S^2 + GP_{97}S + GP_{98}}{P_{b1}S^7 + P_{b2}S^6 + P_{b3}S^5 + P_{b4}S^4 + P_{b5}S^3 + P_{b6}S^2 + P_{b7}S + P_{b8}}$$

(C.4-18)

$$G_{P4} = \frac{HP_{21}S^7 + HP_{22}S^6 + HP_{23}S^5 + HP_{24}S^4 + HP_{25}S^3 + HP_{26}S^2 + HP_{27}S + HP_{28}}{P_{b1}S^7 + P_{b2}S^6 + P_{b3}S^5 + P_{b4}S^4 + P_{b5}S^3 + P_{b6}S^2 + P_{b7}S + P_{b8}}$$

(C.4-19)

$$G_{Q1} = \frac{GQ_{51}S^7 + GQ_{52}S^6 + GQ_{53}S^5 + GQ_{54}S^4 + GQ_{55}S^3 + GQ_{56}S^2 + GQ_{57}S + GQ_{58}}{P_{b1}S^7 + P_{b2}S^6 + P_{b3}S^5 + P_{b4}S^4 + P_{b5}S^3 + P_{b6}S^2 + P_{b7}S + P_{b8}}$$

(C.4-20)

$$G_{Q2} = \frac{GQ_{71}S^7 + GQ_{72}S^6 + GQ_{73}S^5 + GQ_{74}S^4 + GQ_{75}S^3 + GQ_{76}S^2 + GQ_{77}S + GQ_{78}}{P_{b1}S^7 + P_{b2}S^6 + P_{b3}S^5 + P_{b4}S^4 + P_{b5}S^3 + P_{b6}S^2 + P_{b7}S + P_{b8}}$$

(C.4-21)

$$G_{Q3} = \frac{GQ_{91}S^7 + GQ_{92}S^6 + GQ_{93}S^5 + GQ_{94}S^4 + GQ_{95}S^3 + GQ_{96}S^2 + GQ_{97}S + GQ_{98}}{P_{b1}S^7 + P_{b2}S^6 + P_{b3}S^5 + P_{b4}S^4 + P_{b5}S^3 + P_{b6}S^2 + P_{b7}S + P_{b8}}$$

(C.4-22)

$$G_{Q4} = \frac{HQ_{21}S^7 + HQ_{22}S^6 + HQ_{23}S^5 + HQ_{24}S^4 + HQ_{25}S^3 + HQ_{26}S^2 + HQ_{27}S + HQ_{28}}{P_{b1}S^7 + P_{b2}S^6 + P_{b3}S^5 + P_{b4}S^4 + P_{b5}S^3 + P_{b6}S^2 + P_{b7}S + P_{b8}}$$

(C.4-23)

$$\Delta E = E - E_0 \quad \text{(C.4-24)}$$

$$\Delta f = f_g - f_{g0} \quad \text{(C.4-25)}$$

Where P_0, Q_0, E_0, f_{g0} are steady-state values for real power, reactive power, voltage per phase, power supply frequency, respectively.

$$P_{b1} = L_{11}F_{31} \quad \text{(C.4-26)}$$

$$P_{b2} = L_{11}F_{32} + L_{12}F_{31} \quad \text{(C.4-27)}$$

$$P_{b3} = L_{11}F_{33} + L_{12}F_{32} \quad \text{(C.4-28)}$$

$$P_{b4} = L_{11}F_{34} + L_{12}F_{33} \quad \text{(C.4-29)}$$

$$P_{b5} = L_{11}F_{35} + L_{12}F_{34} \quad \text{(C.4-30)}$$

$$P_{b6} = L_{11}F_{36} + L_{12}F_{35} \quad \text{(C.4-31)}$$

$$P_{b7} = L_{11}F_{37} + L_{12}F_{36} \quad \text{(C.4-32)}$$

$$P_{b8} = L_{12}F_{37} \quad \text{(C.4-33)}$$

$$GP_{41} = GP_{21}L_{11} \quad \text{(C.4-34)}$$

$$GP_{42} = GP_{21}L_{12} + GP_{22}L_{21} \quad \text{(C.4-35)}$$

$$GP_{51} = GP_{41}F_{31} \quad \text{(C.4-36)}$$

$$GP_{52} = GP_{41}F_{32} + GP_{42}F_{31} \quad \text{(C.4-37)}$$

$$GP_{53} = GP_{41}F_{33} + GP_{42}F_{32} \quad \text{(C.4-38)}$$

$$GP_{54} = GP_{41}F_{34} + GP_{42}F_{33} - GP_{22}F_{41} \quad \text{(C.4-39)}$$

$$GP_{55} = GP_{41}F_{35} + GP_{42}F_{34} - GP_{22}F_{42} \quad \text{(C.4-40)}$$

$$GP_{56} = GP_{41}F_{36} + GP_{42}F_{35} - GP_{22}F_{43} \quad \text{(C.4-41)}$$

$$GP_{57} = GP_{41}F_{37} + GP_{42}F_{36} - GP_{22}F_{44} \quad \text{(C.4-42)}$$

$$GP_{58} = GP_{42}F_{37} - GP_{22}F_{45} \quad \text{(C.4-43)}$$

$$GP_{61} = GP_{23}L_{11} \quad \text{(C.4-44)}$$

$$GP_{62} = GP_{23}L_{12} + GP_{22}L_{22} \quad \text{(C.4-45)}$$

$$GP_{63} = \frac{GP_{22}L_{22}}{L_{21}} \quad \text{(C.4-46)}$$

$$GP_{64} = GP_{25}L_{11} \quad \text{(C.4-47)}$$

$$GP_{65} = GP_{25}L_{12} + GP_{24}L_{21} \quad \text{(C.4-48)}$$

$$GP_{71} = GP_{64}F_{31} \quad \text{(C.4-49)}$$

$$GP_{72} = GP_{64}F_{32} + GP_{65}F_{31} \quad \text{(C.4-50)}$$

$$GP_{73} = GP_{64}F_{33} + GP_{65}F_{32} \quad \text{(C.4-51)}$$

$$GP_{74} = GP_{64}F_{34} + GP_{65}F_{33} - GP_{24}F_{41} \quad \text{(C.4-52)}$$

$$GP_{75} = GP_{64}F_{35} + GP_{65}F_{34} - GP_{24}F_{42} \quad \text{(C.4-53)}$$

$$GP_{76} = GP_{64}F_{36} + GP_{65}F_{35} - GP_{24}F_{43} \quad \text{(C.4-54)}$$

$$GP_{77} = GP_{64}F_{37} + GP_{65}F_{36} - GP_{24}F_{44} \quad \text{(C.4-55)}$$

$$GP_{78} = GP_{65}F_{37} - GP_{24}F_{45} \quad \text{(C.4-56)}$$

$$GP_{91} = GP_{61}F_{31} \quad \text{(C.4-57)}$$

$$GP_{92} = GP_{61}F_{32} + GP_{62}F_{31} \quad \text{(C.4-58)}$$

$$GP_{93} = GP_{61}F_{33} + GP_{62}F_{32} \quad \text{(C.4-59)}$$

$$GP_{94} = GP_{61}F_{34} + GP_{62}F_{33} - GP_{63}F_{41} \quad \text{(C.4-60)}$$

$$GP_{95} = GP_{61}F_{35} + GP_{62}F_{34} - GP_{63}F_{42} \quad \text{(C.4-61)}$$

$$GP_{96} = GP_{61}F_{36} + GP_{62}F_{35} - GP_{63}F_{43} \quad \text{(C.4-62)}$$

$$GP_{97} = GP_{61}F_{37} + GP_{62}F_{36} - GP_{63}F_{44} \quad \text{(C.4-63)}$$

$$GP_{98} = GP_{62}F_{37} - GP_{63}F_{45} \quad \text{(C.4-64)}$$

$$HP_{11} = GP_{26}L_{11} \quad \text{(C.4-65)}$$

$$HP_{12} = GP_{26}L_{12} + GP_{24}L_{22} \quad \text{(C.4-66)}$$

$$HP_{13} = \frac{GP_{24}L_{22}}{L_{21}} \quad \text{(C.4-67)}$$

$$HP_{21} = HP_{11}F_{31} \quad \text{(C.4-68)}$$

$$HP_{22} = HP_{11}F_{32} + HP_{12}F_{31} \quad \text{(C.4-69)}$$

$$HP_{23} = HP_{11}F_{33} + HP_{12}F_{32} \quad \text{(C.4-70)}$$

$$HP_{24} = HP_{11}F_{34} + HP_{12}F_{33} - HP_{13}F_{41} \quad \text{(C.4-71)}$$

$$HP_{25} = HP_{11}F_{35} + HP_{12}F_{34} - HP_{13}F_{42} \quad \text{(C.4-72)}$$

$$HP_{26} = HP_{11}F_{36} + HP_{12}F_{35} - HP_{13}F_{43} \quad \text{(C.4-73)}$$

$$HP_{27} = HP_{11}F_{37} + HP_{12}F_{36} - HP_{13}F_{44} \quad \text{(C.4-74)}$$

$$HP_{28} = HP_{12}F_{37} - HP_{13}F_{45} \quad \text{(C.4-75)}$$

$$GQ_{41} = GQ_{21}L_{11} \tag{C.4-76}$$

$$GQ_{42} = GQ_{21}L_{12} + GQ_{22}L_{21} \tag{C.4-77}$$

$$GQ_{51} = GQ_{41}F_{31} \tag{C.4-78}$$

$$GQ_{52} = GQ_{41}F_{32} + GQ_{42}F_{31} \tag{C.4-79}$$

$$GQ_{53} = GQ_{41}F_{33} + GQ_{42}F_{32} \tag{C.4-80}$$

$$GQ_{54} = GQ_{41}F_{34} + GQ_{42}F_{33} - GQ_{22}F_{41} \tag{C.4-81}$$

$$GQ_{55} = GQ_{41}F_{35} + GQ_{42}F_{34} - GQ_{22}F_{42} \tag{C.4-82}$$

$$GQ_{56} = GQ_{41}F_{36} + GQ_{42}F_{35} - GQ_{22}F_{43} \tag{C.4-83}$$

$$GQ_{57} = GQ_{41}F_{37} + GQ_{42}F_{36} - GQ_{22}F_{44} \tag{C.4-84}$$

$$GQ_{58} = GQ_{42}F_{37} - GQ_{22}F_{45} \tag{C.4-85}$$

$$GQ_{61} = GQ_{25}L_{11} \tag{C.4-86}$$

$$GQ_{62} = GQ_{25}L_{12} + GQ_{24}L_{22} \tag{C.4-87}$$

$$GQ_{81} = GQ_{23}L_{11} \tag{C.4-88}$$

$$GQ_{82} = GQ_{23}L_{12} + GQ_{22}L_{22} \tag{C.4-89}$$

$$GP_{83} = \frac{GQ_{22}L_{22}}{L_{21}} \tag{C.4-90}$$

$$GQ_{71} = GQ_{61}F_{31} \tag{C.4-91}$$

$$GQ_{72} = GQ_{61}F_{32} + GQ_{62}F_{31} \tag{C.4-92}$$

$$GQ_{73} = GQ_{61}F_{33} + GQ_{62}F_{32} \tag{C.4-93}$$

$$GQ_{74} = GQ_{61}F_{34} + GQ_{62}F_{33} - GQ_{24}F_{41} \tag{C.4-94}$$

$$GQ_{75} = GQ_{61}F_{35} + GQ_{62}F_{34} - GQ_{24}F_{42} \tag{C.4-95}$$

$$GQ_{76} = GQ_{61}F_{36} + GQ_{62}F_{35} - GQ_{24}F_{43} \tag{C.4-96}$$

$$GQ_{77} = GQ_{61}F_{37} + GQ_{62}F_{36} - GQ_{24}F_{44} \tag{C.4-97}$$

$$GQ_{78} = GQ_{62}F_{37} - GP_{24}F_{45} \tag{C.4-98}$$

$$GQ_{91} = GQ_{81}F_{31} \tag{C.4-99}$$

$$GQ_{92} = GQ_{81}F_{32} + GQ_{82}F_{31} \tag{C.4-100}$$

$$GQ_{93} = GQ_{81}F_{33} + GQ_{82}F_{32} \tag{C.4-101}$$

$$GQ_{94} = GQ_{81}F_{34} + GQ_{82}F_{33} - GQ_{83}F_{41} \tag{C.4-102}$$

$$GQ_{95} = GQ_{81}F_{35} + GQ_{82}F_{34} - GQ_{83}F_{42} \tag{C.4-103}$$

$$GQ_{96} = GQ_{81}F_{36} + GQ_{82}F_{35} - GQ_{83}F_{43} \tag{C.4-104}$$

$$GQ_{97} = GQ_{81}F_{37} + GQ_{82}F_{36} - GQ_{83}F_{44} \tag{C.4-105}$$

$$GQ_{98} = GQ_{82}F_{37} - GQ_{83}F_{45} \tag{C.4-106}$$

$$HQ_{11} = GQ_{26}L_{11} \tag{C.4-107}$$

$$HQ_{12} = GQ_{26}L_{12} + GQ_{24}L_{22} \tag{C.4-108}$$

$$HQ_{13} = \frac{GQ_{24}L_{22}}{L_{21}} \tag{C.4-109}$$

$$HQ_{21} = HQ_{11}F_{31} \tag{C.4-110}$$

$$HQ_{22} = HQ_{11}F_{32} + HQ_{12}F_{31} \tag{C.4-111}$$

$$HQ_{23} = HQ_{11}F_{33} + HQ_{12}F_{32} \tag{C.4-112}$$

$$HQ_{24} = HQ_{11}F_{34} + HQ_{12}F_{33} - HQ_{13}F_{41} \tag{C.4-113}$$

$$HQ_{25} = HQ_{11}F_{35} + HQ_{12}F_{34} - HQ_{13}F_{42} \tag{C.4-114}$$

$$HQ_{26} = HQ_{11}F_{36} + HQ_{12}F_{35} - HQ_{13}F_{43} \tag{C.4-115}$$

$$HQ_{27} = HQ_{11}F_{37} + HQ_{12}F_{36} - HQ_{13}F_{44} \tag{C.4-116}$$

$$HQ_{28} = HQ_{12}F_{37} - HQ_{13}F_{45} \tag{C.4-117}$$

Table C.1 Parameters used in real power and reactive power

$G_{P1\_1} = GP_{51}$	$G_{P2\_1} = GP_{71}$	$G_{P3\_1} = GP_{91}$	$G_{P4\_1} = HP_{21}$
$G_{P1\_2} = GP_{52}$	$G_{P2\_2} = GP_{72}$	$G_{P3\_2} = GP_{92}$	$G_{P4\_2} = HP_{22}$
$G_{P1\_3} = GP_{53}$	$G_{P2\_3} = GP_{73}$	$G_{P3\_3} = GP_{93}$	$G_{P4\_3} = HP_{23}$
$G_{P1\_4} = GP_{54}$	$G_{P2\_4} = GP_{74}$	$G_{P3\_4} = GP_{94}$	$G_{P4\_4} = HP_{24}$
$G_{P1\_5} = GP_{55}$	$G_{P2\_5} = GP_{75}$	$G_{P3\_5} = GP_{95}$	$G_{P4\_5} = HP_{25}$
$G_{P1\_6} = GP_{56}$	$G_{P2\_6} = GP_{76}$	$G_{P3\_6} = GP_{96}$	$G_{P4\_6} = HP_{26}$
$G_{P1\_7} = GP_{57}$	$G_{P2\_7} = GP_{77}$	$G_{P3\_7} = GP_{97}$	$G_{P4\_7} = HP_{27}$
$G_{P1\_8} = GP_{58}$	$G_{P2\_8} = GP_{78}$	$G_{P3\_8} = GP_{98}$	$G_{P4\_8} = HP_{28}$
$G_{Q1\_1} = GQ_{51}$	$G_{Q2\_1} = GQ_{71}$	$G_{Q3\_1} = GQ_{91}$	$G_{Q4\_1} = HQ_{21}$
$G_{Q1\_2} = GQ_{52}$	$G_{Q2\_2} = GQ_{72}$	$G_{Q3\_2} = GQ_{92}$	$G_{Q4\_2} = HQ_{22}$
$G_{Q1\_3} = GQ_{53}$	$G_{Q2\_3} = GQ_{73}$	$G_{Q3\_3} = GQ_{93}$	$G_{Q4\_3} = HQ_{23}$
$G_{Q1\_4} = GQ_{54}$	$G_{Q2\_4} = GQ_{74}$	$G_{Q3\_4} = GQ_{94}$	$G_{Q4\_4} = HQ_{24}$
$G_{Q1\_5} = GQ_{55}$	$G_{Q2\_5} = GQ_{75}$	$G_{Q3\_5} = GQ_{95}$	$G_{Q4\_5} = HQ_{25}$
$G_{Q1\_6} = GQ_{56}$	$G_{Q2\_6} = GQ_{76}$	$G_{Q3\_6} = GQ_{96}$	$G_{Q4\_6} = HQ_{26}$
$G_{Q1\_7} = GQ_{57}$	$G_{Q2\_7} = GQ_{77}$	$G_{Q3\_7} = GQ_{97}$	$G_{Q4\_7} = HQ_{27}$
$G_{Q1\_8} = GQ_{58}$	$G_{Q2\_8} = GQ_{78}$	$G_{Q3\_8} = GQ_{98}$	$G_{Q4\_8} = HQ_{28}$

The coefficient of the real power and reactive power as 7th transfer functions can be rewritten as follows:

$$G_{P1} = \frac{G_{P1\_1}S^7 + G_{P1\_2}S^6 + G_{P1\_3}S^5 + G_{P1\_4}S^4 + G_{P1\_5}S^3 + G_{P1\_6}S^2 + G_{P1\_7}S + G_{P1\_8}}{P_{b1}S^7 + P_{b2}S^6 + P_{b3}S^5 + P_{b4}S^4 + P_{b5}S^3 + P_{b6}S^2 + P_{b7}S + P_{b8}} \tag{C.4-118}$$

$$G_{P2} = \frac{G_{P2\_1}S^7 + G_{P2\_2}S^6 + G_{P2\_3}S^5 + G_{P2\_4}S^4 + G_{P2\_5}S^3 + G_{P2\_6}S^2 + G_{P2\_7}S + G_{P2\_8}}{P_{b1}S^7 + P_{b2}S^6 + P_{b3}S^5 + P_{b4}S^4 + P_{b5}S^3 + P_{b6}S^2 + P_{b7}S + P_{b8}} \tag{C.4-119}$$

$$G_{P3} = \frac{G_{P3\_1}S^7 + G_{P3\_2}S^6 + G_{P3\_3}S^5 + G_{P3\_4}S^4 + G_{P3\_5}S^3 + G_{P3\_6}S^2 + G_{P3\_7}S + G_{P3\_8}}{P_{b1}S^7 + P_{b2}S^6 + P_{b3}S^5 + P_{b4}S^4 + P_{b5}S^3 + P_{b6}S^2 + P_{b7}S + P_{b8}} \tag{C.4-120}$$

$$G_{P4} = \frac{G_{P4\_1}S^7 + G_{P4\_2}S^6 + G_{P4\_3}S^5 + G_{P4\_4}S^4 + G_{P4\_5}S^3 + G_{P4\_6}S^2 + G_{P4\_7}S + G_{P4\_8}}{P_{b1}S^7 + P_{b2}S^6 + P_{b3}S^5 + P_{b4}S^4 + P_{b5}S^3 + P_{b6}S^2 + P_{b7}S + P_{b8}}$$

(C.4-121)

$$G_{Q1} = \frac{G_{Q1\_1}S^7 + G_{Q1\_2}S^6 + G_{Q1\_3}S^5 + G_{Q1\_4}S^4 + G_{Q1\_5}S^3 + G_{Q1\_6}S^2 + G_{Q1\_7}S + G_{Q1\_8}}{P_{b1}S^7 + P_{b2}S^6 + P_{b3}S^5 + P_{b4}S^4 + P_{b5}S^3 + P_{b6}S^2 + P_{b7}S + P_{b8}}$$

(C.4-122)

$$G_{Q2} = \frac{G_{Q2\_1}S^7 + G_{Q2\_2}S^6 + G_{Q2\_3}S^5 + G_{Q2\_4}S^4 + G_{Q2\_5}S^3 + G_{Q2\_6}S^2 + G_{Q2\_7}S + G_{Q2\_8}}{P_{b1}S^7 + P_{b2}S^6 + P_{b3}S^5 + P_{b4}S^4 + P_{b5}S^3 + P_{b6}S^2 + P_{b7}S + P_{b8}}$$

(C.4-123)

$$G_{Q3} = \frac{G_{Q3\_1}S^7 + G_{Q3\_2}S^6 + G_{Q3\_3}S^5 + G_{Q3\_4}S^4 + G_{Q3\_5}S^3 + G_{Q3\_6}S^2 + G_{Q3\_7}S + G_{Q3\_8}}{P_{b1}S^7 + P_{b2}S^6 + P_{b3}S^5 + P_{b4}S^4 + P_{b5}S^3 + P_{b6}S^2 + P_{b7}S + P_{b8}}$$

(C.4-124)

$$G_{Q4} = \frac{G_{Q4\_1}S^7 + G_{Q4\_2}S^6 + G_{Q4\_3}S^5 + G_{Q4\_4}S^4 + G_{Q4\_5}S^3 + G_{Q4\_6}S^2 + G_{Q4\_7}S + G_{Q4\_8}}{P_{b1}S^7 + P_{b2}S^6 + P_{b3}S^5 + P_{b4}S^4 + P_{b5}S^3 + P_{b6}S^2 + P_{b7}S + P_{b8}}$$

(C.4-125)

To calculate the ac current at the drive input, substitute Equation (C.1-77) in Equations (C.1-40), (C.1-46), (C.1-50), and (C.1-56), the following can be obtained:

$$i_{qgcom} = i_{qgcom\,0} + G_{Iq1}\Delta i_d + G_{Iq2}\Delta E + G_{Iq3}\Delta f_g \quad \text{(C.4-126)}$$

$$G_{Iq1} = a_{id\_qgcom} + a_{u\_qgcom}u_{21} \quad \text{(C.4-127)}$$

$$G_{Iq2} = a_{E\_qgcom} + a_{u\_qgcom}u_{22} \quad \text{(C.4-128)}$$

$$G_{Iq3} = a_{fg\_qgcom} + a_{u\_qgcom}u_{23} \quad \text{(C.4-129)}$$

$$i_{qgcond} = i_{qgcond\,0} + G_{Iq4}\Delta i_d + G_{Iq5}\Delta E + G_{Iq6}\Delta f_g \quad \text{(C.4-130)}$$

$$G_{Iq4} = a_{id\_qgcond} + a_{u\_qgcond}u_{21} \quad \text{(C.4-131)}$$

$$G_{Iq5} = a_{u\_qgcond}u_{22} \quad \text{(C.4-132)}$$

$$G_{Iq6} = a_{u\_qgcond} u_{23} \tag{C.4-133}$$

$$i_{qg} = i_{qgcom} + i_{qgcond} = i_{qg0} + G_{Iq7}\Delta i_d + G_{Iq8}\Delta E + G_{Iq9}\Delta f_g \tag{C.4-134}$$

$$i_{qg0} = i_{qgcom0} + i_{qgcond0} \tag{C.4-135}$$

$$G_{Iq7} = G_{Iq1} + G_{Iq4} \tag{C.4-136}$$

$$G_{Iq8} = G_{Iq2} + G_{Iq5} \tag{C.4-137}$$

$$G_{Iq9} = G_{Iq3} + G_{Iq6} \tag{C.4-138}$$

$$i_{dgcom} = i_{dgcom0} + G_{Id1}\Delta i_d + G_{Id2}\Delta E + G_{Id3}\Delta f_g \tag{C.4-139}$$

$$G_{Id1} = a_{id\_dgcom} + a_{u\_dgcom} u_{21} \tag{C.4-140}$$

$$G_{Id2} = a_{E\_dgcom} + a_{u\_dgcom} u_{22} \tag{C.4-141}$$

$$G_{Id3} = a_{fg\_dgcom} + a_{u\_dgcom} u_{23} \tag{C.4-142}$$

$$i_{dgcond} = i_{dgcond0} + G_{Id4}\Delta i_d + G_{Id5}\Delta E + G_{Id6}\Delta f_g \tag{C.4-143}$$

$$G_{Id4} = a_{id\_dgcond} + a_{u\_dgcond} u_{21} \tag{C.4-144}$$

$$G_{Id5} = a_{u\_dgcond} u_{22} \tag{C.4-145}$$

$$G_{Id6} = a_{u\_dgcond} u_{23} \tag{C.4-146}$$

$$i_{dg} = i_{dgcom} + i_{dgcond} = i_{dg0} + G_{Id7}\Delta i_d + G_{Id8}\Delta E + G_{Id9}\Delta f_g \tag{C.4-147}$$

$$i_{dg0} = i_{dgcom0} + i_{dgcond0} \tag{C.4-148}$$

$$G_{Id7} = G_{Id1} + G_{Id4} \tag{C.4-149}$$

$$G_{Id8} = G_{Id2} + G_{Id5} \tag{C.4-150}$$

$$G_{Id9} = G_{Id3} + G_{Id6} \tag{C.4-151}$$

Substitute Equation (C.4-1) in Equations (C.4-134) and (C.4-147), we have

$$i_{qg} = i_{qg0} + G_{Iqg1}\Delta E + G_{Iqg2}\Delta f_g \tag{C.4-152}$$

$$i_{dg} = i_{dg0} + G_{Idg1}\Delta E + G_{Idg2}\Delta f_g \tag{C.4-153}$$

$$G_{Iqg1} = G_{Iq8} + G_{Iq7}N_{11} + G_{Iq7}N_{12}G_{11} \tag{C.4-154}$$

$$G_{Iqg2} = G_{Iq9} + G_{Iq7}N_{13} + \frac{G_{Iq7}L_{22}}{L_{21}}N_{12}G_{11} \tag{C.4-155}$$

$$G_{Idg1} = G_{Id8} + G_{Id7}N_{11} + G_{Id7}N_{12}G_{11} \tag{C.4-156}$$

$$G_{Idg2} = G_{Id9} + G_{Id7}N_{13} + \frac{G_{Id7}L_{22}}{L_{21}}N_{12}G_{11} \tag{C.4-157}$$

The four coefficients in Equations (C.4-152) and (C.4-153) are 7th order transfer functions as follows:

$$G_{Iqg1} = \frac{IQ_{q1}S^7 + IQ_{q2}S^6 + IQ_{q3}S^5 + IQ_{q4}S^4 + IQ_{q5}S^3 + IQ_{q6}S^2 + IQ_{q7}S + IQ_{q8}}{P_{b1}S^7 + P_{b2}S^6 + P_{b3}S^5 + P_{b4}S^4 + P_{b5}S^3 + P_{b6}S^2 + P_{b7}S + P_{b8}} \tag{C.4-158}$$

$$IQ_{q1} = G_{Iq8}L_{11}F_{31} \tag{C.4-159}$$

$$IQ_{q2} = G_{Iq8}L_{11}F_{32} + \left(G_{Iq8}L_{12} + G_{Iq7}L_{21}\right)F_{31} \tag{C.4-160}$$

$$IQ_{q3} = G_{Iq8}L_{11}F_{33} + \left(G_{Iq8}L_{12} + G_{Iq7}L_{21}\right)F_{32} \tag{C.4-161}$$

$$IQ_{q4} = G_{Iq8}L_{11}F_{34} + \left(G_{Iq8}L_{12} + G_{Iq7}L_{21}\right)F_{33} - G_{Iq7}F_{41} \tag{C.4-162}$$

$$IQ_{q5} = G_{Iq8}L_{11}F_{35} + \left(G_{Iq8}L_{12} + G_{Iq7}L_{21}\right)F_{34} - G_{Iq7}F_{42} \tag{C.4-163}$$

$$IQ_{q6} = G_{Iq8}L_{11}F_{36} + \left(G_{Iq8}L_{12} + G_{Iq7}L_{21}\right)F_{35} - G_{Iq7}F_{43} \tag{C.4-164}$$

$$IQ_{q7} = G_{Iq8}L_{11}F_{37} + \left(G_{Iq8}L_{12} + G_{Iq7}L_{21}\right)F_{36} - G_{Iq7}F_{44} \tag{C.4-165}$$

$$IQ_{q8} = \left(G_{Iq8}L_{12} + G_{Iq7}L_{21}\right)F_{37} - G_{Iq7}F_{45} \tag{C.4-166}$$

$$G_{Iqg2} = \frac{HQ_{q1}S^7 + HQ_{q2}S^6 + HQ_{q3}S^5 + HQ_{q4}S^4 + HQ_{q5}S^3 + HQ_{q6}S^2 + HQ_{q7}S + HQ_{q8}}{P_{b1}S^7 + P_{b2}S^6 + P_{b3}S^5 + P_{b4}S^4 + P_{b5}S^3 + P_{b6}S^2 + P_{b7}S + P_{b8}} \tag{C.4-167}$$

$$HQ_{q1} = G_{Iq9} L_{11} F_{31} \tag{C.4-168}$$

$$HQ_{q2} = G_{Iq9} L_{11} F_{32} + \left(G_{Iq9} L_{12} + G_{Iq7} L_{22}\right) F_{31} \tag{C.4-169}$$

$$HQ_{q3} = G_{Iq9} L_{11} F_{33} + \left(G_{Iq9} L_{12} + G_{Iq7} L_{22}\right) F_{32} \tag{C.4-170}$$

$$HQ_{q4} = G_{Iq9} L_{11} F_{34} + \left(G_{Iq9} L_{12} + G_{Iq7} L_{22}\right) F_{33} - \frac{G_{Iq7} L_{22}}{L_{21}} F_{41} \tag{C.4-171}$$

$$HQ_{q5} = G_{Iq9} L_{11} F_{35} + \left(G_{Iq9} L_{12} + G_{Iq7} L_{22}\right) F_{34} - \frac{G_{Iq7} L_{22}}{L_{21}} F_{42} \tag{C.4-172}$$

$$HQ_{q6} = G_{Iq9} L_{11} F_{36} + \left(G_{Iq9} L_{12} + G_{Iq7} L_{22}\right) F_{35} - \frac{G_{Iq7} L_{22}}{L_{21}} F_{43} \tag{C.4-173}$$

$$HQ_{q7} = G_{Iq9} L_{11} F_{37} + \left(G_{Iq9} L_{12} + G_{Iq7} L_{21}\right) F_{36} - \frac{G_{Iq7} L_{22}}{L_{21}} F_{44} \tag{C.4-174}$$

$$HQ_{q8} = \left(G_{Iq9} L_{12} + G_{Iq7} L_{22}\right) F_{37} - \frac{G_{Iq7} L_{22}}{L_{21}} F_{45} \tag{C.4-175}$$

$$G_{Idg1} = \frac{IQ_{d1} S^7 + IQ_{d2} S^6 + IQ_{d3} S^5 + IQ_{d4} S^4 + IQ_{d5} S^3 + IQ_{d6} S^2 + IQ_{d7} S + IQ_{d8}}{P_{b1} S^7 + P_{b2} S^6 + P_{b3} S^5 + P_{b4} S^4 + P_{b5} S^3 + P_{b6} S^2 + P_{b7} S + P_{b8}} \tag{C.4-176}$$

$$IQ_{d1} = G_{Id8} L_{11} F_{31} \tag{C.4-177}$$

$$IQ_{d2} = G_{Id8} L_{11} F_{32} + \left(G_{Id8} L_{12} + G_{Id7} L_{21}\right) F_{31} \tag{C.4-178}$$

$$IQ_{d3} = G_{Id8} L_{11} F_{33} + \left(G_{Id8} L_{12} + G_{Id7} L_{21}\right) F_{32} \tag{C.4-179}$$

$$IQ_{d4} = G_{Id8} L_{11} F_{34} + \left(G_{Id8} L_{12} + G_{Id7} L_{21}\right) F_{33} - G_{Id7} F_{41} \tag{C.4-180}$$

$$IQ_{d5} = G_{Id8} L_{11} F_{35} + \left(G_{Id8} L_{12} + G_{Id7} L_{21}\right) F_{34} - G_{Id7} F_{42} \tag{C.4-181}$$

$$IQ_{d6} = G_{Id8} L_{11} F_{36} + \left(G_{Id8} L_{12} + G_{Id7} L_{21}\right) F_{35} - G_{Id7} F_{43} \tag{C.4-182}$$

$$IQ_{d7} = G_{Id8} L_{11} F_{37} + \left(G_{Id8} L_{12} + G_{Id7} L_{21}\right) F_{36} - G_{Id7} F_{44} \tag{C.4-183}$$

$$IQ_{d8} = \left(G_{Id8} L_{12} + G_{Id7} L_{21}\right) F_{37} - G_{Id7} F_{45} \tag{C.4-184}$$

$$G_{Idg2} = \frac{HQ_{d1}S^7 + HQ_{d2}S^6 + HQ_{d3}S^5 + HQ_{d4}S^4 + HQ_{d5}S^3 + HQ_{d6}S^2 + HQ_{d7}S + HQ_{d8}}{P_{b1}S^7 + P_{b2}S^6 + P_{b3}S^5 + P_{b4}S^4 + P_{b5}S^3 + P_{b6}S^2 + P_{b7}S + P_{b8}}$$

(C.4-185)

$$HQ_{d1} = G_{Id9}L_{11}F_{31} \tag{C.4-186}$$

$$HQ_{d2} = G_{Id9}L_{11}F_{32} + (G_{Id9}L_{12} + G_{Id7}L_{22})F_{31} \tag{C.4-187}$$

$$HQ_{d3} = G_{Id9}L_{11}F_{33} + (G_{Id9}L_{12} + G_{Id7}L_{22})F_{32} \tag{C.4-188}$$

$$HQ_{d4} = G_{Id9}L_{11}F_{34} + (G_{Id9}L_{12} + G_{Id7}L_{22})F_{33} - \frac{G_{Id7}L_{22}}{L_{21}}F_{41} \tag{C.4-189}$$

$$HQ_{d5} = G_{Id9}L_{11}F_{35} + (G_{Id9}L_{12} + G_{Id7}L_{22})F_{34} - \frac{G_{Id7}L_{22}}{L_{21}}F_{42} \tag{C.4-190}$$

$$HQ_{d6} = G_{Id9}L_{11}F_{36} + (G_{Id9}L_{12} + G_{Id7}L_{22})F_{35} - \frac{G_{Id7}L_{22}}{L_{21}}F_{43} \tag{C.4-191}$$

$$HQ_{d7} = G_{Id9}L_{11}F_{37} + (G_{Id9}L_{12} + G_{Id7}L_{22})F_{36} - \frac{G_{Id7}L_{22}}{L_{21}}F_{44} \tag{C.4-192}$$

$$HQ_{d8} = (G_{Id9}L_{12} + G_{Id7}L_{22})F_{37} - \frac{G_{Id7}L_{22}}{L_{21}}F_{45} \tag{C.4-193}$$

Table C.2 Parameters used in ac currents in d- and q-axis

$G_{Iqg11} = IQ_{q1}$	$G_{Iqg21} = HQ_{q1}$	$G_{Idg11} = IQ_{d1}$	$G_{Idg21} = HQ_{d1}$
$G_{Iqg12} = IQ_{q2}$	$G_{Iqg22} = HQ_{q2}$	$G_{Idg12} = IQ_{d2}$	$G_{Idg22} = HQ_{d2}$
$G_{Iqg13} = IQ_{q3}$	$G_{Iqg23} = HQ_{q3}$	$G_{Idg13} = IQ_{d3}$	$G_{Idg23} = HQ_{d3}$
$G_{Iqg14} = IQ_{q4}$	$G_{Iqg24} = HQ_{q4}$	$G_{Idg14} = IQ_{d4}$	$G_{Idg24} = HQ_{d4}$
$G_{Iqg15} = IQ_{q5}$	$G_{Iqg25} = HQ_{q5}$	$G_{Idg15} = IQ_{d5}$	$G_{Idg25} = HQ_{d5}$
$G_{Iqg16} = IQ_{q6}$	$G_{Iqg26} = HQ_{q6}$	$G_{Idg16} = IQ_{d6}$	$G_{Idg26} = HQ_{d6}$
$G_{Iqg17} = IQ_{q7}$	$G_{Iqg27} = HQ_{q7}$	$G_{Idg17} = IQ_{d7}$	$G_{Idg27} = HQ_{d7}$
$G_{Iqg18} = IQ_{q8}$	$G_{Iqg28} = HQ_{q8}$	$G_{Idg18} = IQ_{d8}$	$G_{Idg28} = HQ_{d8}$

The four coefficients as 7th order transfer functions for the d- and q-axis ac currents are rewritten as follows:

$$G_{Iqg1} = \frac{G_{Iqg11}S^7 + G_{Iqg12}S^6 + G_{Iqg13}S^5 + G_{Iqg14}S^4 + G_{Iqg15}S^3 + G_{Iqg16}S^2 + G_{Iqg17}S + G_{Iqg18}}{P_{b1}S^7 + P_{b2}S^6 + P_{b3}S^5 + P_{b4}S^4 + P_{b5}S^3 + P_{b6}S^2 + P_{b7}S + P_{b8}}$$

(C.4-194)

$$G_{Iqg2} = \frac{G_{Iqg21}S^7 + G_{Iqg22}S^6 + G_{Iqg23}S^5 + G_{Iqg24}S^4 + G_{Iqg25}S^3 + G_{Iqg26}S^2 + G_{Iqg27}S + G_{Iqg28}}{P_{b1}S^7 + P_{b2}S^6 + P_{b3}S^5 + P_{b4}S^4 + P_{b5}S^3 + P_{b6}S^2 + P_{b7}S + P_{b8}}$$

(C.4-195)

$$G_{Idg1} = \frac{G_{Idg11}S^7 + G_{Idg12}S^6 + G_{Idg13}S^5 + G_{Idg14}S^4 + G_{Idg15}S^3 + G_{Idg16}S^2 + G_{Idg17}S + G_{Idg18}}{P_{b1}S^7 + P_{b2}S^6 + P_{b3}S^5 + P_{b4}S^4 + P_{b5}S^3 + P_{b6}S^2 + P_{b7}S + P_{b8}}$$

(C.4-196)

$$G_{Idg2} = \frac{G_{Idg21}S^7 + G_{Idg22}S^6 + G_{Idg23}S^5 + G_{Idg24}S^4 + G_{Idg25}S^3 + G_{Idg26}S^2 + G_{Idg27}S + G_{Idg28}}{P_{b1}S^7 + P_{b2}S^6 + P_{b3}S^5 + P_{b4}S^4 + P_{b5}S^3 + P_{b6}S^2 + P_{b7}S + P_{b8}}$$

(C.4-197)

Note: due to the characteristics of diode rectifier which does not allow the power flowing backward to the power grid, the dynamic response results calculated from the developed dynamic model need to manually assign all negative real power and reactive power values to be 0.

C.5 Initial Values

The initial values used in the formulas are determined in this section. Some parameters are given values, such as

L_{dc}: dc link inductance

r_{dc} : dc link resistance

C_{dc}: dc link capacitance

l_c: commutation inductance

R_s: stator resistance

l_s: stator leakage inductance

R_r: rotor resistance

l_r: rotor leakage inductance

L_m: exciting inductance

H: Motor inertia

p: pole pair

V_{diode}: diode on-state voltage

E_0: power source steady-state rms voltage per phase

ω_g: power source angular frequency

ω_{r0}: rotor steady-state electric angular frequency

ω_{s0}: stator steady-state electric angular frequency

K_{pm}: speed controller proportional gain

K_{im}: speed controller integral gain

V_b: nominal voltage of the motor per phase

ω_b: nominal frequency of the motor

T_{Load}: the load torque

PF: power factor in front of the commutation inductance

P_0: real power

Q_0: reactive power

S_0: apparent power

Some parameters or initial values need to be calculated. The DC link voltage from the diode front-end rectifier can be calculated as follows:

$$v_{d0} = \frac{3\sqrt{6}}{\pi} E_0 - \frac{3}{\pi} l_c \omega_{g0} i_{d0} - 2V_{diode} \tag{C.5-1}$$

$$v_{d0} = r_{dc} i_{d0} + e_{d0} \tag{C.5-2}$$

Based on Equations (C.5-1) and (C.5-2), the DC link voltage after the capacitor is calculated by

$$e_{d0} = \frac{3\sqrt{6}}{\pi} E_0 - \left(\frac{3}{\pi} l_c \omega_{g0} + r_{dc} \right) i_{d0} - 2V_{diode} \tag{C.5-3}$$

The initial value for the commutation angle, AC input current components of the drive at d- and q-axis, and real power and reactive power at the input circuit can be determined as follows:

$$u_0 = \arccos\left(1 - \frac{2l_c\omega_{g0}i_{d0}}{\sqrt{6}E_0}\right) \tag{C.5-4}$$

$$i_{qgcom0} = \frac{2\sqrt{3}}{\pi}i_{d0}\left[\sin\left(u_0 - \frac{5\pi}{6}\right) - \sin\left(-\frac{5\pi}{6}\right)\right] + \frac{3\sqrt{2}E_0}{\pi l_c\omega_{g0}}(\cos u_0 - 1) + \frac{3\sqrt{2}E_0}{4\pi l_c\omega_{g0}}(1 - \cos 2u_0)$$

(C.5-5)

$$i_{dgcom0} = \frac{2\sqrt{3}}{\pi}i_{d0}\left[-\cos\left(u_0 - \frac{5\pi}{6}\right) + \cos\left(-\frac{5\pi}{6}\right)\right] + \frac{3\sqrt{2}E_0}{\pi l_c\omega_{g0}}\sin u_0 - \frac{3\sqrt{2}E_0}{4\pi l_c\omega_{g0}}\sin 2u_0 - \frac{3\sqrt{2}E_0}{2\pi l_c\omega_{g0}}u_0$$

(C.5-6)

$$i_{qgcond0} = \frac{2\sqrt{3}}{\pi}i_{d0}\left[\sin\left(\frac{7\pi}{6}\right) - \sin\left(u_0 + \frac{5\pi}{6}\right)\right] \tag{C.5-7}$$

$$i_{dgcond0} = \frac{2\sqrt{3}}{\pi}i_{d0}\left[-\cos\left(\frac{7\pi}{6}\right) + \cos\left(u_0 + \frac{5\pi}{6}\right)\right] \tag{C.5-8}$$

$$i_{qg0} = i_{qgcom0} + i_{qgcond0} \tag{C.5-9}$$

$$i_{dg0} = i_{dgcom0} + i_{dgcond0} \tag{C.5-10}$$

$$P_0 = \frac{3}{\sqrt{2}}E_0 i_{qg0} \tag{C.5-11}$$

$$S_0 = \frac{P_0}{PF_0} \tag{C.5-12}$$

where PF_0 is assumed based on the commutation inductance values. If the commutation inductance is 0-1mH, PF_0 = 96% (a typical power factor at the ac input of a diode rectifier), if the commutation inductance is 10mH, PF_0 = 92%. Other values can be estimated based on them.

$$Q_0 = \sqrt{S_0^2 - P_0^2} \tag{C.5-13}$$

To determine the parameters in Equations (C.5-3) - (C.5-13), the dc link current i_{d0} must be determined first. Based on induction motors equations and inverter equations, we have:

$$v_{ds0} = R_s i_{ds0} - \omega_{s0}\left(L_s i_{qs0} + L_m i_{qr0}\right) \tag{C.5-14}$$

$$v_{qs0} = R_s i_{qs0} + \omega_{s0}\left(L_s i_{ds0} + L_m i_{dr0}\right) \tag{C.5-15}$$

$$0 = R_r i_{dr0} - \left(\omega_{s0} - \omega_{r0}\right)\left(L_r i_{qr0} + L_m i_{qs0}\right) \tag{C.5-16}$$

$$0 = R_r i_{qr0} + \left(\omega_{s0} - \omega_{r0}\right)\left(L_r i_{dr0} + L_m i_{ds0}\right) \tag{C.5-17}$$

$$v_{ds0} = 0 \tag{C.5-18}$$

$$v_{qs0} = \frac{1}{2} d_0 e_{d0} \tag{C.5-19}$$

From Equation (C.5-16),

$$i_{dr0} = \frac{\left(\omega_{s0} - \omega_{r0}\right)}{R_r}\left(L_r i_{qr0} + L_m i_{qs0}\right) \tag{C.5-20}$$

Substitute Equation (C.5-20) in Equation (C.5-17), after rearrangement, the following equation can be obtained:

$$\left[\frac{R_r^2 + \left(\omega_{s0} - \omega_{r0}\right)^2 L_r^2}{R_r}\right] i_{qr0} + \left[L_m\left(\omega_{s0} - \omega_{r0}\right)\right] i_{ds0} + \left[\frac{\left(\omega_{s0} - \omega_{r0}\right)^2 L_r L_m}{R_r}\right] i_{qs0} = 0 \tag{C.5-21}$$

From Equations (C.5-14) and (C.5-18),

$$i_{qr0} = \left(\frac{R_s}{\omega_{s0} L_m}\right) i_{ds0} - \left(\frac{L_s}{L_m}\right) i_{qs0} \tag{C.5-22}$$

Substitute Equation (C.5-22) in Equation (C.5-21), the following is determined:

$$i_{ds0} = S_{11} i_{qs0} \tag{C.5-23}$$

$$S_{11} = \frac{\left(R_r^2 + \left(\omega_{s0} - \omega_{r0}\right)^2 L_r^2\right) L_s \omega_{s0} - \left(\omega_{s0} - \omega_{r0}\right)^2 L_r L_m^2 \omega_{s0}}{\left(R_r^2 + \left(\omega_{s0} - \omega_{r0}\right)^2 L_r^2\right) R_s + \left(\omega_{s0} - \omega_{r0}\right)^2 R_r L_m^2 \omega_{s0}} \tag{C.5-24}$$

Substitute Equation (C.5-23) in Equation (C.5-22),

$$i_{qr0} = S_{12} i_{qs0} \tag{C.5-25}$$

$$S_{12} = \frac{R_s S_{11} - \omega_{s0} L_s}{\omega_{s0} L_m} \tag{C.5-26}$$

Substitute Equation (C.5-25) in Equation (C.5-20),

$$i_{dr0} = S_{13} i_{qs0} \tag{C.5-27}$$

$$S_{13} = \frac{(\omega_{s0} - \omega_{r0})(L_m + L_r S_{12})}{R_r} \tag{C.5-28}$$

Under the steady-state condition, the motor electromagnetic torque should be balanced with the load torque as follows:

$$T_{e0} = 1.5 p L_m \left(i_{dr0} i_{qs0} - i_{qr0} i_{ds0}\right) = T_{Load0} \tag{C.5-29}$$

Substitute Equations (C.5-23), (C.5-25) and (C.5-27) in Equation (C.5-29), i_{qs0} can be calculated as follows:

$$i_{qs0} = \sqrt{\frac{T_{Load0}}{1.5 P L_m (S_{13} - S_{12} S_{11})}} \tag{C.5-30}$$

Substitute Equation (C.5-30) in Equations (C.5-23), (C.5-25) and (C.5-27), i_{ds0}, i_{qr0}, and i_{dr0} can be calculated.

Substitute Equations (C.5-23) and (C.5-27) in Equation (C.5-15), and combining with Equation (C.5-19),

$$v_{qs0} = R_s i_{qs0} + \omega_{s0} \left(L_s S_{11} i_{qs0} + L_m S_{13} i_{qs0}\right) = \frac{1}{2} d_0 e_{d0} \tag{C.5-31}$$

Define a new parameter S_{14} as follows:

$$S_{14} = d_0 e_{d0} = 2 R_s i_{qs0} + 2 \omega_{s0} \left(L_s S_{11} i_{qs0} + L_m S_{13} i_{qs0}\right) \tag{C.5-32}$$

Based on Equation (C.3-5),

$$\frac{3}{2}\left(v_{ds0}i_{ds0}+v_{qs0}i_{qs0}\right)=e_{d0}i_{I0} \tag{C.5-33}$$

Under steady-state, $i_{I0}=i_{d0}$, combining this with Equations (C.5-18), (C.5-19) and (C.5-33),

$$\frac{3}{2}\left(\frac{1}{2}d_0e_{d0}\right)i_{qs0}=e_{d0}i_{d0} \tag{C.5-34}$$

The dc link steady-state current i_{d0} can be obtained from Equation (C.5-34) as follows:

$$i_{d0}=\frac{3}{4}d_0i_{qs0} \tag{C.5-35}$$

Multiplying both sides of Equation (C.5-3) by d_0 as follows:

$$S_{14}=e_{d0}d_0=\frac{3\sqrt{6}}{\pi}E_0d_0-\left(\frac{3}{\pi}l_c\omega_g+r_{dc}\right)i_{d0}d_0-2V_{diode}d_0 \tag{C.5-36}$$

Substitute Equation (C.5-35) in Equation (C.5-36), we obtain the function of the duty cycle d_0 as follows:

$$\left[\frac{3}{4}\left(\frac{3}{\pi}l_c\omega_g+r_{dc}\right)i_{qs0}\right]d_0^2-\left(\frac{3\sqrt{6}}{\pi}E_0-2V_{diode}\right)d_0+S_{14}=0 \tag{C.5-37}$$

Solving Equation (C.5-37), the duty cycle d_0 are determined. All required initial values can be determined accordingly.

APPENDIX D AGGREGATION USING PADE APPROXIMATION

The Pade Approximation can be expressed as follows [129]:

$$G(x)=\frac{a_0+a_1x+a_2x^2+\cdots+a_mx^m}{b_0+b_1x+b_2x^2+\cdots+b_nx^n} \tag{D-1}$$

The function G(x) can be expressed by the function f(x) as follows:

$$f(x)=c_0+c_1x+c_2x^2+\cdots+c_{m+n}x^{m+n} \tag{D-2}$$

$$a_0=b_0c_0 \tag{D-3}$$

$$a_1=b_0c_1+b_1c_0 \tag{D-4}$$

… …

$$a_m=b_0c_m+b_1c_{m-1}+\cdots+b_mc_0 \tag{D-5}$$

… …

$$0=b_0c_{m+n}+b_1c_{m+n-1}+\cdots+b_nc_m \tag{D-6}$$

Based on Equations (D-3)-(D-6), the coefficient c of the new function f(x) can be determined. As an example, one of the transfer functions for the real power G_{p1} is converted to a polynomial f_{P1} using Pade Approximation.

$$G_{P1}=\frac{GP_{51}S^7+GP_{52}S^6+GP_{53}S^5+GP_{54}S^4+GP_{55}S^3+GP_{56}S^2+GP_{57}S+GP_{58}}{P_{b1}S^7+P_{b2}S^6+P_{b3}S^5+P_{b4}S^4+P_{b5}S^3+P_{b6}S^2+P_{b7}S+P_{b8}} \tag{D-7}$$

In Equation (D-7), m = 7 and n = 7, a new polynomial function $f_{P1}(S)$ equivalent to $G_{P1}(S)$ can be determined as follows:

$$f_{P1}(S)=c_0+c_1S+c_2S^2+\cdots+c_{14}S^{14} \tag{D-8}$$

Assign the following parameters as shown in Table D-1:

Table D. 1 Parameters used in G_{p1} for Pade Approximation

$a_0 = GP_{58}$	$b_0 = P_{b8}$
$a_1 = GP_{57}$	$b_1 = P_{b7}$
$a_2 = GP_{56}$	$b_2 = P_{b6}$
$a_3 = GP_{55}$	$b_3 = P_{b5}$
$a_4 = GP_{54}$	$b_4 = P_{b4}$
$a_5 = GP_{53}$	$b_5 = P_{b3}$
$a_6 = GP_{52}$	$b_6 = P_{b2}$
$a_7 = GP_{51}$	$b_7 = P_{b1}$

Equation (D-7) can be rewritten as follows:

$$G_{P1}(S) = \frac{a_7 S^7 + a_6 S^6 + a_5 S^5 + a_4 S^4 + a_3 S^3 + a_2 S^2 + a_1 S + a_0}{b_7 S^7 + b_6 S^6 + b_5 S^5 + b_4 S^4 + b_3 S^3 + b_2 S^2 + b_1 S + b_0} \tag{D-9}$$

Based on Equations (D-2) – (D-6), Equation (D-9) in the transfer function format can be converted to a polynomial format as follows:

$$f_{P1}(S) = c_0 + c_1 S + c_2 S^2 + \cdots + c_{14} S^{14} \tag{D-10}$$

$$c_0 = \frac{a_0}{b_0} \tag{D-11}$$

$$c_1 = \frac{1}{b_0}(a_1 - b_1 c_0) \tag{D-12}$$

$$c_2 = \frac{1}{b_0}(a_2 - b_1 c_1 - b_2 c_0) \tag{D-13}$$

$$c_3 = \frac{1}{b_0}(a_3 - b_1 c_2 - b_2 c_1 - b_3 c_0) \tag{D-14}$$

$$c_4 = \frac{1}{b_0}(a_4 - b_1 c_3 - b_2 c_2 - b_3 c_1 - b_4 c_0) \tag{D-15}$$

$$c_5 = \frac{1}{b_0}(a_5 - b_1 c_4 - b_2 c_3 - b_3 c_2 - b_4 c_1 - b_5 c_0) \tag{D-16}$$

$$c_6 = \frac{1}{b_0}(a_6 - b_1 c_5 - b_2 c_4 - b_3 c_3 - b_4 c_2 - b_5 c_1 - b_6 c_0) \tag{D-17}$$

$$c_7 = \frac{1}{b_0}\left(a_7 - b_1c_6 - b_2c_5 - b_3c_4 - b_4c_3 - b_5c_2 - b_6c_1 - b_7c_0\right) \quad \text{(D-18)}$$

$$c_8 = \frac{1}{b_0}\left(- b_1c_7 - b_2c_6 - b_3c_5 - b_4c_4 - b_5c_3 - b_6c_2 - b_7c_1\right) \quad \text{(D-19)}$$

$$c_9 = \frac{1}{b_0}\left(- b_1c_8 - b_2c_7 - b_3c_6 - b_4c_5 - b_5c_4 - b_6c_3 - b_7c_2\right) \quad \text{(D-20)}$$

$$c_{10} = \frac{1}{b_0}\left(- b_1c_9 - b_2c_8 - b_3c_7 - b_4c_6 - b_5c_5 - b_6c_4 - b_7c_3\right) \quad \text{(D-21)}$$

$$c_{11} = \frac{1}{b_0}\left(- b_1c_{10} - b_2c_9 - b_3c_8 - b_4c_7 - b_5c_6 - b_6c_5 - b_7c_4\right) \quad \text{(D-22)}$$

$$c_{12} = \frac{1}{b_0}\left(- b_1c_{11} - b_2c_{10} - b_3c_9 - b_4c_8 - b_5c_7 - b_6c_6 - b_7c_5\right) \quad \text{(D-23)}$$

$$c_{13} = \frac{1}{b_0}\left(- b_1c_{12} - b_2c_{11} - b_3c_{10} - b_4c_9 - b_5c_8 - b_6c_7 - b_7c_6\right) \quad \text{(D-24)}$$

$$c_{14} = \frac{1}{b_0}\left(- b_1c_{13} - b_2c_{12} - b_3c_{11} - b_4c_{10} - b_5c_9 - b_6c_8 - b_7c_7\right) \quad \text{(D-25)}$$

For n VFDs connected to the same bus, $f_1(S)$, $f_2(S)$, …, and $f_n(S)$ are obtained. The equivalent aggregated VFD should have the following function:

$$f_{P1\_eq}(S) = f_{P1\_1}(S) + f_{P1\_2}(S) + \cdots + f_{P1\_n}(S) = c_{0eq} + c_{1eq}S + c_{2eq}S^2 + \cdots + c_{14eq}S^{14} \quad \text{(D-26)}$$

$$c_{0eq} = c_{01} + c_{02} + \cdots c_{0n} \quad \text{(D-27)}$$

$$c_{1eq} = c_{11} + c_{12} + \cdots c_{1n} \quad \text{(D-28)}$$

$$c_{2eq} = c_{21} + c_{22} + \cdots c_{2n} \quad \text{(D-29)}$$

… …

$$c_{14eq} = c_{141} + c_{142} + \cdots c_{14n} \quad \text{(D-30)}$$

Now the task is to convert Equation (D-26) back to the transfer function format as follows:

$$G_{P1eq}(S)=\frac{a_7'S^7+a_6'S^6+a_5'S^5+a_4'S^4+a_3'S^3+a_2'S^2+a_1'S+a_0'}{b_7'S^7+b_6'S^6+b_5'S^5+b_4'S^4+b_3'S^3+b_2'S^2+b_1'S+b_0'} \quad \text{(D-31)}$$

Assign $b_7'=1$. Please note, when using Pade approximation method for VFDs, $b_0'=1$ cannot be assigned. The reason is that it could cause ill-conditioned matrix operation, and result in incorrect calculation result using Matlab. Based on Equations (D-3) – (D-6):

$$a_0'=b_0'c_0' \quad \text{(D-32)}$$

$$a_1'=b_0'c_1'+b_1'c_0' \quad \text{(D-33)}$$

$$a_2'=b_0'c_2'+b_1'c_1'+b_2'c_0' \quad \text{(D-34)}$$

$$a_3'=b_0'c_3'+b_1'c_2'+b_2'c_1'+b_3'c_0' \quad \text{(D-35)}$$

$$a_4'=b_0'c_4'+b_1'c_3'+b_2'c_2'+b_3'c_1'+b_4'c_0' \quad \text{(D-36)}$$

$$a_5'=b_0'c_5'+b_1'c_4'+b_2'c_3'+b_3'c_2'+b_4'c_1'+b_5'c_0' \quad \text{(D-37)}$$

$$a_6'=b_0'c_6'+b_1'c_5'+b_2'c_4'+b_3'c_3'+b_4'c_2'+b_5'c_1'+b_6'c_0' \quad \text{(D-38)}$$

$$a_7'=b_0'c_7'+b_1'c_6'+b_2'c_5'+b_3'c_4'+b_4'c_3'+b_5'c_2'+b_6'c_1'+b_7'c_0' \quad \text{(D-39)}$$

$$0=b_0'c_8'+b_1'c_7'+b_2'c_6'+b_3'c_5'+b_4'c_4'+b_5'c_3'+b_6'c_2'+b_7'c_1' \quad \text{(D-40)}$$

$$0=b_0'c_9'+b_1'c_8'+b_2'c_7'+b_3'c_6'+b_4'c_5'+b_5'c_4'+b_6'c_3'+b_7'c_2' \quad \text{(D-41)}$$

$$0=b_0'c_{10}'+b_1'c_9'+b_2'c_8'+b_3'c_7'+b_4'c_6'+b_5'c_5'+b_6'c_4'+b_7'c_3' \quad \text{(D-42)}$$

$$0=b_0'c_{11}'+b_1'c_{10}'+b_2'c_9'+b_3'c_8'+b_4'c_7'+b_5'c_6'+b_6'c_5'+b_7'c_4' \quad \text{(D-43)}$$

$$0=b_0'c_{12}'+b_1'c_{11}'+b_2'c_{10}'+b_3'c_9'+b_4'c_8'+b_5'c_7'+b_6'c_6'+b_7'c_5' \quad \text{(D-44)}$$

$$0=b_0'c_{13}'+b_1'c_{12}'+b_2'c_{11}'+b_3'c_{10}'+b_4'c_9'+b_5'c_8'+b_6'c_7'+b_7'c_6' \quad \text{(D-45)}$$

$$0=b_0'c_{14}'+b_1'c_{13}'+b_2'c_{12}'+b_3'c_{11}'+b_4'c_{10}'+b_5'c_9'+b_6'c_8'+b_7'c_7' \quad \text{(D-46)}$$

Solving Equations (D-40) - (D-46), b_0' to b_6' can be obtained. Further solving Equations (D-32) – (D-39) using the calculated b_0' to b_6' values, a_0' and a_7' can be obtained. Now the equivalent transfer function for the real power in Equation (D-31) is determined. The equivalent transfer function for the reactive power can be calculated using the similar method.

APPENDIX E TYPICAL PARAMETERS FOR DYNAMIC MODELS OF MOTOR DRIVE SYSTEMS

The input data and their typical/sample values used to derive the dynamic models for VSI based drive-induction motor systems are listed in Table E.1. Once the input data in this table are input into the Matlab program, all initial values will be calculated, and all transfer functions as the coefficients of the dynamic model are determined using the Matlab program.

Table E.1 Typical parameters for equivalent dynamic models

Symbols	Parameters Descriptions	Typical values
	For power source	
E_0	Rms value of the power source phase-to-ground voltage supplied to the drive (in front of the commutation inductance)	User defined or based on load flow study results at the bus the VFDs are connected to (V)
f_{g0}	Power supply frequency at the drive input	User defined, 50Hz or 60Hz (Hz)
l_c	Commutation inductance in front of the drive (include ac line reactor and the power system impedance at the input of the drive)	User defined or inductance of the 3% or 5% ac line reactor plus the power source inductance, either based on short circuit study results or assumptions (H) [153]
	For VFDs	
V_{diode}	Diode on-state voltage	1.2 or 1.3 (V) [154, 155]
r_{dc}	Resistance of DC link	0 (Ω) [154]
L_{dc}	Inductance of DC link reactor	0 (Ω) [154]
C_{dc}	Capacitance of DC link capacitor	User defined or 10%–20% of the base impedance (F) [36]
K_{pm}	Speed PI controller proportional gain for the closed-loop voltage per Hz control	9 [154]
K_{im}	Speed PI controller integral gain for the closed-loop voltage per Hz control	10 [154]
f_{out}	Output frequency of the drive	User defined, or estimated from (motor expected operating speed in rpm)*(motor nominal frequency) /(motor nominal speed in rpm) (Hz) [154]
npulse	Pulse number of the cascaded H-bridge inverter drives	User defined, 18, 24 etc
	For induction motors	
V_b	Rated voltage of the motor	User defined or from Tables E.2 or A.1 (V) [156]
R_s	Stator resistance	User defined or from Tables E.2 or A.1 (Ω) [156]
l_s	Stator leakage inductance	User defined or from Tables E.2 or A.1 (H) [156]
L_m	Magnetizing inductance	User defined or from Tables E.2 or A.1 (H) [156]
R_r	Rotor resistance	User defined or from Tables E.2 or A.1 (Ω) [156]

l_r	Rotor leakage inductance	User defined or from Tables E.2 or A.1 (H) [156]
P	Number of pole pairs	User defined or 2 (assumed to be 4 poles)
f_{rated}	Nominal frequency of the motor	User defined or 60 (Hz)
J	Inertia of the induction motor	User defined, or from Tables E.2 or A.1, or estimate from Figure A.1 (kg* m^2) [156]
n_{rated}	Nominal speed of the motor	User defined, or estimated from Table E.2 (rpm) [156]
T_L	Load torque (Motor operating data 1)	User defined or assumed to be equal to 25% - 80% of the rated electromagnetic torque calculated from Equation (E-1) (NM) [157]
n_r	Operating target speed of the motor (Motor operating data 2)	User defined, or assumed to be equal to nominal speed of the motor (rpm)
	For Transformers (aggregation VFDs)	
Stx	Transformer rated capacity, VA	User defined
Vptx	Transformer primary rated voltage, V	User defined
Vstx	Transformer secondary rated voltage, V	User defined
Ztx	Transformer impedance in %	User defined, or from Tables A.2 and A.3 [152]
X/R	Transformer X/R ratio	User defined, or from Tables A.2 and A.4 [152]
	For upstream series impedance (aggregation VFDs)	
Rimp	Resistance of series impedance, ohms	User defined
Limp	Inductance of series impedance, H	User defined

Table E.2 Equivalent circuit parameters of induction motors
(4 poles, 60Hz, 3-phase) [156]

Motor HP	Voltage, V	Rated speed rpm	R_s, Ω	$L_s = L'_r$, H	L_m, H	R'_r, Ω	J, Kg* m^2	D, N*m*s
3	220	1710	0.435	0.0713	0.0693	0.816	0.089	0.008
25	460	1695	0.249	0.0602	0.0587	0.536	0.554	0.040
50	460	1705	0.087	0.0355	0.0347	0.228	1.662	0.073
100	460	1700	0.031	0.0193	0.0189	0.134	4.449	0.121
250	2300	1769	0.681	0.2342	0.2277	0.401	6.918	0.124
500	2300	1773	0.262	0.1465	0.1433	0.187	11.062	0.402
800	2300	1778	0.131	0.0976	0.0957	0.094	21.262	0.283
1000	2300	1778	0.112	0.1452	0.1436	0.074	29.871	0.786
1500	2300	1783	0.056	0.0537	0.0527	0.037	44.548	0.500
2250	2300	1786	0.029	0.0352	0.0346	0.022	63.869	1.607
6000	4160	1787	0.022	0.0597	0.0589	0.022	674.971	2.444

Note 1: The inertia J include the inertia of load, which is assumed to be equal to inertia of motor

Note 2: These parameters were determined from manufacturer's published data for all motors except the 3HP machine, its parameters were determined from laboratory test data. All resistances are given for a temperature of 75ºC.

$L_s = l_s + L_m$

$L'_r = l'_r + L_m$

The rated electromagnetic torque calculation [157]:

$$T_{em} = \frac{3PR_r}{2\pi f_{rated} S_1} \left| \frac{jX_m}{\left(\frac{R_s R_r}{S_1} - X_s X_r - X_m (X_s + X_r) \right) + j\left(R_s X_r + \frac{R_r X_s}{S_1} + X_m \left(R_s + \frac{R_r}{S_1} \right) \right)} \right|^2 \times \left(\frac{V_b}{\sqrt{3}} \right)^2 \quad \text{(E-1)}$$

where

$$X_s = 2\pi f_{rated} l_s$$

$$X_m = 2\pi f_{rated} L_m$$

$$X_r = 2\pi f_{rated} l_r$$

APPENDIX F DYNAMIC MODEL FOR CASCADED INVERTER MOTOR DRIVE SYSTEMS

F.1 Each Power Module

The generic calculation method introduced in this Appendix is suitable to VFDs with either 18-pulse or 24-pulse. The 18-pulse medium voltage cascaded H-bridge inverter based drive consists of three power modules per phase. The derivation of the dynamic model for this type of MVD started from each low voltage power module.

The DC link voltage v_d from each power module can be expressed as follows:

$$v_d = \frac{3\sqrt{6}}{\pi} E - \frac{3}{\pi} l_c (2\pi f_g) i_d - 2l_c \frac{di_d}{dt} - 2V_{diode} \tag{F.1-1}$$

where v_d is output voltage from the diode converter at each power module, i_d is the dc link current from diode converter at each power module, E is rms source voltage per phase at each power module, l_c is the source commutation inductance in front of the MVD, f_g is the power grid frequency in Hz, V_{diode} is diode on-state voltage. The power source resistance is ignored.

It is verified that the DC link voltage in Equation (F.1-1) is not affected by the phase-shifting angle from the transformer, and each module has exactly the same voltage at DC links.

In each power module, the DC link consists of a DC link resistor r_{dc}, DC link reactor L_{dc}, and DC link capacitor C_{dc}. The voltage and currents at DC link can be calculated as follows:

$$v_d = r_{dc} i_d + L_{dc} \frac{di_d}{dt} + e_d \tag{F.1-2}$$

$$i_d = i_c + i_I \tag{F.1-3}$$

$$i_c = C_{dc}\frac{de_d}{dt} \tag{F.1-4}$$

Where e_d is the dc link voltage supplying to inverter, i_c is the current flowing through the DC link capacitor, i_I is the current flowing into the inverter.

Combining Equations (F.1-1) and (F.1-2), the dc link current i_d can be expressed as follows:

$$\frac{di_d}{dt} = \left(\frac{1}{L_{dc}+2l_c}\right)\left[\frac{3\sqrt{6}}{\pi}E - \left(r_{dc} + \frac{3}{\pi}l_c\left(2\pi f_g\right)\right)i_d - 2V_{diode} - e_d\right] \tag{F.1-5}$$

Substitute (F.1-5) in (F.1-2), the dc link voltage from output of the diode converter can be rewritten as follows:

$$v_d = \frac{\frac{3\sqrt{6}}{\pi}L_{dc}}{L_{dc}+2l_c}E + \frac{l_c\left(2r_{dc} - \frac{3}{\pi}L_{dc}\left(2\pi f_g\right)\right)}{L_{dc}+2l_c}i_d + \frac{2l_c}{L_{dc}+2l_c}e_d - \frac{2L_{dc}}{L_{dc}+2l_c}V_{diode} \tag{F.1-6}$$

Linearize Equation (F.1-5):

$$\Delta i_d = \frac{\left(\frac{3\sqrt{6}}{\pi}\right)\Delta E - \Delta e_d - \left(6l_c i_{d0}\right)\Delta f_g}{\left(L_{dc}+2l_c\right)S + \left(r_{dc} + \frac{3}{\pi}l_c\left(2\pi f_{g0}\right)\right)} = \frac{L_{21}}{L_{11}S+L_{12}}\Delta E - \frac{1}{L_{11}S+L_{12}}\Delta e_d + \frac{L_{22}}{L_{11}S+L_{12}}\Delta f_g$$

(F.1-7)

$$L_{21} = \frac{3\sqrt{6}}{\pi} \tag{F.1-8}$$

$$L_{11} = L_{dc} + 2l_c \tag{F.1-9}$$

$$L_{12} = r_{dc} + \frac{3}{\pi}l_c\left(2\pi f_{g0}\right) \tag{F.1-10}$$

$$L_{22} = 6l_c i_{d0} \tag{F.1-11}$$

Linearize Equation (F.1-6):

$$v_d = v_{d0} + a_{E\_Vd}\Delta E + a_{id\_Vd}\Delta i_d + a_{fg\_Vd}\Delta f_g + a_{ed\_Vd}\Delta e_d \tag{F.1-12}$$

$$a_{E\_Vd} = \frac{\frac{3\sqrt{6}}{\pi}L_{dc}}{L_{dc} + 2l_c} \tag{F.1-13}$$

$$a_{id\_Vd} = \frac{2l_c\left(r_{dc} - 3L_{dc}f_{g0}\right)}{L_{dc} + 2l_c} \tag{F.1-14}$$

$$a_{fg\_Vd} = -\frac{6l_c L_{dc} i_{d0}}{L_{dc} + 2l_c} \tag{F.1-15}$$

$$a_{ed\_Vd} = \frac{2l_c}{L_{dc} + 2l_c} \tag{F.1-16}$$

Substitute Equation (F.1-7) in Equation (F.1-12), the dc link voltage can be derived as follows:

$$v_d = v_{d0} + M_{21}\Delta E + M_{22}\Delta e_d + M_{23}\Delta f_g \tag{F.1-17}$$

$$M_{21} = \frac{\left(a_{E\_Vd}L_{11}\right)S + \left(a_{E\_Vd}L_{12} + a_{id\_Vd}L_{21}\right)}{L_{11}S + L_{12}} = \frac{M_{31}S + M_{32}}{L_{11}S + L_{12}} \tag{F.1-18}$$

$$M_{22} = \frac{\left(a_{ed\_Vd}L_{11}\right)S + \left(a_{ed\_Vd}L_{12} - a_{id\_Vd}\right)}{L_{11}S + L_{12}} = \frac{M_{33}S + M_{34}}{L_{11}S + L_{12}} \tag{F.1-19}$$

$$M_{23} = \frac{\left(a_{fg\_Vd}L_{11}\right)S + \left(a_{fg\_Vd}L_{12} + a_{id\_Vd}L_{22}\right)}{L_{11}S + L_{12}} = \frac{M_{35}S + M_{36}}{L_{11}S + L_{12}} \tag{F.1-20}$$

$$M_{31} = a_{E\_Vd}L_{11} \tag{F.1-21}$$

$$M_{32} = a_{E\_Vd}L_{12} + a_{id\_Vd}L_{21} \tag{F.1-22}$$

$$M_{33} = a_{ed\_Vd}L_{11} \tag{F.1-23}$$

$$M_{34} = a_{ed\_Vd}L_{12} - a_{id\_Vd} \tag{F.1-24}$$

$$M_{35} = a_{fg\_Vd}L_{11} \tag{F.1-25}$$

$$M_{36} = a_{fg\_Vd}L_{12} + a_{id\_Vd}L_{22} \tag{F.1-26}$$

The power source voltage in dq reference frame at the input of each power module can be expressed as follows:

$$v_{dg} = 0 \tag{F.1-27}$$

$$v_{qg} = \sqrt{2}E \tag{F.1-28}$$

The current at the input of the power module (without phase shifting) in dq reference frame can be calculated as follows:

$$i_{qg} = i_{qgcom} + i_{qgcond} \tag{F.1-29}$$

$$i_{dg} = i_{dgcom} + i_{dgcond} \tag{F.1-30}$$

$$i_{qgcom} = \frac{2\sqrt{3}}{\pi} i_d \left[\sin\left(u - \frac{5\pi}{6} \right) - \sin\left(-\frac{5\pi}{6} \right) \right] + \frac{3\sqrt{2}}{\pi l_c (2\pi f_g)} E(\cos u - 1) + \frac{3\sqrt{2}}{4\pi l_c (2\pi f_g)} E(1 - \cos 2u) \tag{F.1-31}$$

$$i_{qgcond} = \frac{2\sqrt{3}}{\pi} i_d \left[\sin\left(\frac{7\pi}{6} \right) - \sin\left(u + \frac{5\pi}{6} \right) \right] \tag{F.1-32}$$

$$i_{dgcom} = \frac{2\sqrt{3}}{\pi} i_d \left[-\cos\left(u - \frac{5\pi}{6} \right) + \cos\left(-\frac{5\pi}{6} \right) \right] + \frac{3\sqrt{2}}{\pi l_c (2\pi f_g)} E \sin u - \frac{3\sqrt{2}}{4\pi l_c (2\pi f_g)} E \sin 2u - \frac{3\sqrt{2}}{2\pi l_c (2\pi f_g)} Eu \tag{F.1-33}$$

$$i_{dgcond} = \frac{2\sqrt{3}}{\pi} i_d \left[-\cos\left(\frac{7\pi}{6} \right) + \cos\left(u + \frac{5\pi}{6} \right) \right] \tag{F.1-34}$$

$$u = \arccos\left(1 - \frac{2 l_c (2\pi f_g) i_d}{\sqrt{6}E} \right) \tag{F.1-35}$$

where u is the commutation angle.

The real and reactive power at the input of each power module can be calculated as follows:

$$P_{ac\_per\,module} = \frac{3}{2} \left(v_{dg} i_{dg} + v_{qg} i_{qg} \right) \tag{F.1-36}$$

$$Q_{ac\_per\,module} = \frac{3}{2}\left(v_{qg} i_{dg} - v_{dg} i_{qg}\right) \tag{F.1-37}$$

The total real and reactive power at the input of the 18-pulse MVD can be calculated by substituting equations (F.1-27) and (F.1-28) as follows:

$$n_{pulse} = 18$$

$$\begin{aligned} P_{ac} &= \left(\frac{n_{pulse}}{2}\right) P_{ac\_per\,module} = \frac{n_{pulse}}{2} \times \frac{3}{2}\left(\sqrt{2} E i_{qg}\right) \\ &= \frac{3 n_{pulse}}{2\sqrt{2}} E\left(i_{qgcom} + i_{qgcond}\right) \end{aligned} \tag{F.1-38}$$

$$\begin{aligned} Q_{ac} &= \left(\frac{n_{pulse}}{2}\right) Q_{ac\_per\,module} = \frac{n_{pulse}}{2} \times \frac{3}{2}\left(\sqrt{2} E i_{dg}\right) \\ &= \frac{3 n_{pulse}}{2\sqrt{2}} E\left(i_{dgcom} + i_{dgcond}\right) \end{aligned} \tag{F.1-39}$$

where n_{pulse} is the pulse number of the MVD, P_{ac} and Q_{ac} are the total real and reactive power at the MVD input, $P_{ac\_permodule}$ and $Q_{ac\_permodule}$ is the real and reactive power at each power module.

Linearize Equations (F.1-31)-(F.1-34) for each power module:

$$i_{qgcom} = i_{qgcom\ 0} + a_{id\_qgcom} \Delta i_d + a_{E\_qgcom} \Delta E + a_{u\_qgcom} \Delta u + a_{fg\_qgcom} \Delta f_g \tag{F.1-40}$$

$$\begin{aligned} i_{qgcom0} &= \frac{2\sqrt{3}}{\pi} i_{d0}\left[\sin\left(u_0 - \frac{5\pi}{6}\right) - \sin\left(-\frac{5\pi}{6}\right)\right] + \frac{3\sqrt{2}}{\pi l_c (2\pi f_{g0})} E_0 (\cos u_0 - 1) \\ &\quad + \frac{3\sqrt{2}}{4\pi l_c (2\pi f_{g0})} E_0 (1 - \cos(2u_0)) \end{aligned} \tag{F.1-41}$$

$$a_{id\_qgcom} = \frac{\sqrt{3}}{\pi} - \frac{3}{\pi}\sin(u_0) - \frac{\sqrt{3}}{\pi}\cos(u_0) = \frac{\sqrt{3}}{\pi}\left(1 - \sqrt{3}\sin(u_0) - \cos(u_0)\right) \tag{F.1-42}$$

$$a_{E\_qgcom} = \frac{3\sqrt{2}}{2\pi^2 l_c f_{g0}}\left(\cos(u_0) - \frac{3}{4} - \frac{1}{4}\cos(2u_0)\right) \tag{F.1-43}$$

$$a_{u\_qgcom} = \frac{3\sqrt{2}E_0}{2\pi^2 l_c f_{g0}}\left(\frac{\sin(2u_0)}{2} - \sin(u_0)\right) + \frac{\sqrt{3}i_{d0}}{\pi}\left(\sin(u_0) - \sqrt{3}\cos(u_0)\right) \tag{F.1-44}$$

$$a_{fg\_qgcom} = \frac{3\sqrt{2}E_0}{2\pi^2 l_c f_{g0}^2}\left(-\cos(u_0) + \frac{3}{4} + \frac{1}{4}\cos(2u_0)\right) \tag{F.1-45}$$

$$i_{qgcond} = i_{qgcond\ 0} + a_{id\_qgcond}\Delta i_d + a_{u\_qgcond}\Delta u \tag{F.1-46}$$

$$i_{qgcond0} = \frac{2\sqrt{3}}{\pi} i_{d0}\left[\sin\left(\frac{7\pi}{6}\right) - \sin\left(u_0 + \frac{5\pi}{6}\right)\right] \tag{F.1-47}$$

$$a_{id\_qgcond} = -\frac{\sqrt{3}}{\pi} + \frac{3}{\pi}\sin(u_0) - \frac{\sqrt{3}}{\pi}\cos(u_0) = \frac{\sqrt{3}}{\pi}\left(\sqrt{3}\sin(u_0) - \cos(u_0) - 1\right) \tag{F.1-48}$$

$$a_{u\_qgcond} = \frac{3i_{d0}}{\pi}\cos(u_0) + \frac{\sqrt{3}i_{d0}}{\pi}\sin(u_0) = \frac{\sqrt{3}}{\pi} i_{d0}\left(\sin(u_0) - \sqrt{3}\cos(u_0)\right) \tag{F.1-49}$$

$$i_{dgcom} = i_{dgcom\ 0} + a_{id\_dgcom}\Delta i_d + a_{E\_dgcom}\Delta E + a_{u\_dgcom}\Delta u + a_{fg\_dgcom}\Delta f_g \tag{F.1-50}$$

$$\begin{aligned} i_{dgcom0} = {} & \frac{2\sqrt{3}}{\pi} i_{d0}\left[-\cos\left(u_0 - \frac{5\pi}{6}\right) + \cos\left(-\frac{5\pi}{6}\right)\right] + \frac{3\sqrt{2}}{\pi l_c(2\pi f_{g0})} E_0 \sin(u_0) - \\ & \frac{3\sqrt{2}}{4\pi l_c(2\pi f_{g0})} E_0 \sin(2u_0) - \frac{3\sqrt{2}}{2\pi l_c(2\pi f_{g0})} E_0 u_0 \end{aligned} \tag{F.1-51}$$

$$a_{id\_dgcom} = \frac{3}{\pi}\cos(u_0) - \frac{\sqrt{3}}{\pi}\sin(u_0) - \frac{3}{\pi} = \frac{\sqrt{3}}{\pi}\left(\sqrt{3}\cos(u_0) - \sin(u_0) - \sqrt{3}\right) \tag{F.1-52}$$

$$a_{E\_dgcom} = \frac{3\sqrt{2}}{2\pi^2 l_c f_{g0}}\left(\sin(u_0) - \frac{1}{4}\sin(2u_0) - \frac{u_0}{2}\right) \tag{F.1-53}$$

$$a_{u\_dgcom} = \frac{3\sqrt{2}E_0}{2\pi^2 l_c f_{g0}}\left(\cos(u_0) - \frac{\cos(2u_0)}{2} - \frac{1}{2}\right) - \frac{\sqrt{3}i_{d0}}{\pi}\left(\sqrt{3}\sin(u_0) + \cos(u_0)\right) \tag{F.1-54}$$

$$a_{fg\_dgcom} = \frac{3\sqrt{2}E_0}{2\pi^2 l_c f_{g0}^2}\left(-\sin(u_0) + \frac{u_0}{2} + \frac{1}{4}\sin(2u_0)\right) \tag{F.1-55}$$

$$i_{dgcond} = i_{dgcond\ 0} + a_{id\_dgcond}\Delta i_d + a_{u\_dgcond}\Delta u \tag{F.1-56}$$

$$i_{dgcond0} = \frac{2\sqrt{3}}{\pi} i_{d0}\left[-\cos\left(\frac{7\pi}{6}\right) + \cos\left(u_0 + \frac{5\pi}{6}\right)\right] \tag{F.1-57}$$

$$a_{id\_dgcond} = \frac{3}{\pi} - \frac{3}{\pi}\cos(u_0) - \frac{\sqrt{3}}{\pi}\sin(u_0) = \frac{\sqrt{3}}{\pi}\left(\sqrt{3} - \sqrt{3}\cos(u_0) - \sin(u_0)\right) \quad \text{(F.1-58)}$$

$$a_{u\_dgcond} = \frac{3i_{d0}}{\pi}\sin(u_0) - \frac{\sqrt{3}i_{d0}}{\pi}\cos(u_0) = \frac{\sqrt{3}}{\pi}i_{d0}\left(\sqrt{3}\sin(u_0) - \cos(u_0)\right) \quad \text{(F.1-59)}$$

For the total real power, the Taylor expansion for Equation (F.1-38) can be written as follows:

$$\begin{aligned} P_{ac} &= P_0 + a_{E\_P}(E - E_0) + a_{iqgcom}\left(i_{qgcom} - i_{qgcom0}\right) + a_{iqgcond}\left(i_{qgcond} - i_{qgcond0}\right) \\ &\quad + a_{Eiqgcom}(E - E_0)\left(i_{qgcom} - i_{qgcom0}\right) + a_{Eiqgcond}(E - E_0)\left(i_{qgcond} - i_{qgcond0}\right) \\ &\quad + a_{EE\_P}(E - E_0)^2 \\ &= P_0 + a_{E\_P}\Delta E + a_{iqgcom}\Delta i_{qgcom} + a_{iqgcond}\Delta i_{qgcond} + a_{Eiqgcom}\Delta E\Delta i_{qgcom} \\ &\quad + a_{Eiqgcond}\Delta E\Delta i_{qgcond} + a_{EE\_P}\Delta E^2 \end{aligned} \quad \text{(F.1-60)}$$

$$a_{E\_P} = \frac{3n_{pulse}}{2\sqrt{2}}\left(i_{qgcom0} + i_{qgcond0}\right) \quad \text{(F.1-61)}$$

$$a_{iqgcom\_P} = \frac{3n_{pulse}}{2\sqrt{2}}E_0 \quad \text{(F.1-62)}$$

$$a_{iqgcond\_P} = \frac{3n_{pulse}}{2\sqrt{2}}E_0 \quad \text{(F.1-63)}$$

$$a_{Eiqgcom\_P} = \frac{3n_{pulse}}{2\sqrt{2}} \quad \text{(F.1-64)}$$

$$a_{Eiqgcond\_P} = \frac{3n_{pulse}}{2\sqrt{2}} \quad \text{(F.1-65)}$$

$$a_{EE\_P} = \frac{3n_{pulse}}{4\sqrt{2}}a_{Eiqgcom} \quad \text{(F.1-66)}$$

Substitute Equations (F.1-40) and (F.1-46) in Equation (F.1-60), the real power P can be expressed as follows:

$$P_{ac} = P_0 + GP_{11}\Delta E + GP_{12}\Delta i_d + GP_{13}\Delta u + GP_{14}\Delta f_g + GP_{15}\Delta E\Delta u + GP_{16}\Delta E\Delta i_d + GP_{17}\Delta E^2 + GP_{18}\Delta E\Delta f_g \quad \text{(F.1-67)}$$

$$GP_{11} = a_{E\_P} + a_{iqgcom}a_{E\_qgcom} \quad \text{(F.1-68)}$$

$$GP_{12} = a_{iqgcom}a_{id\_qgcom} + a_{iqgcond}a_{id\_qgcond} \quad \text{(F.1-69)}$$

$$GP_{13} = a_{iqgcom}a_{u\_qgcom} + a_{iqgcond}a_{u\_qgcond} \quad \text{(F.1-70)}$$

$$GP_{14} = a_{iqgcom}a_{fg\_qgcom} \quad \text{(F.1-71)}$$

$$GP_{15} = a_{Eiqgcom}a_{u\_qgcom} + a_{Eiqgcond}a_{u\_qgcond} \quad \text{(F.1-72)}$$

$$GP_{16} = a_{Eiqgcom}a_{id\_qgcom} + a_{Eiqgcond}a_{id\_qgcond} \quad \text{(F.1-73)}$$

$$GP_{17} = a_{Eiqgcom}a_{E\_qgcom} + a_{EE\_P} \quad \text{(F.1-74)}$$

$$GP_{18} = a_{Eiqgcom}a_{fg\_qgcom} \quad \text{(F.1-75)}$$

Based on Equation (F.1-35), the commutation angle can be expressed as follows:

$$\cos(u) = 1 - \frac{2l_c(2\pi f_g)i_d}{\sqrt{6}E} = 1 - \frac{4\pi l_c}{\sqrt{6}} f_g i_d \left(\frac{1}{E}\right) \quad \text{(F.1-76)}$$

Linearize Equation (F.1-76), we have

$$\Delta u = u_{21}\Delta i_d + u_{22}\Delta E + u_{23}\Delta f_g \quad \text{(F.1-77)}$$

$$u_{21} = \frac{4\pi l_c f_{g0}}{\sqrt{6}E_0 \sin(u_0)} \quad \text{(F.1-78)}$$

$$u_{22} = -\frac{4\pi l_c f_{g0} i_{d0}}{\sqrt{6}E_0^2 \sin(u_0)} \quad \text{(F.1-79)}$$

$$u_{23} = \frac{4\pi l_c i_{d0}}{\sqrt{6}E_0 \sin(u_0)} \quad \text{(F.1-80)}$$

Substitute Equation (F.1-77) in Equation (F.1-67),

$$P_{ac} = P_0 + GP_{21}\Delta E + GP_{22}\Delta i_d + GP_{23}\Delta f_g + GP_{24}\Delta i_d\Delta E + GP_{25}\Delta E^2 + GP_{26}\Delta E\Delta f_g$$

(F.1-81)

$$GP_{21} = GP_{11} + GP_{13}u_{22} \tag{F.1-82}$$

$$GP_{22} = GP_{12} + GP_{13}u_{21} \tag{F.1-83}$$

$$GP_{23} = GP_{14} + GP_{13}u_{23} \tag{F.1-84}$$

$$GP_{24} = GP_{16} + GP_{15}u_{21} \tag{F.1-85}$$

$$GP_{25} = GP_{17} + GP_{15}u_{22} \tag{F.1-86}$$

$$GP_{26} = GP_{18} + GP_{15}u_{23} \tag{F.1-87}$$

For the total reactive power, the Taylor expansion for Equation (F.1-39) can be written as follows:

$$\begin{aligned} Q_{ac} &= Q_0 + a_{E\_Q}(E - E_0) + a_{idgcom}\left(i_{dgcom} - i_{dgcom0}\right) + a_{idgcond}\left(i_{dgcond} - i_{dgcond0}\right) \\ &\quad + a_{Eidgcom}(E - E_0)\left(i_{dgcom} - i_{dgcom0}\right) + a_{Eidgcond}(E - E_0)\left(i_{dgcond} - i_{dgcond0}\right) \\ &\quad + a_{EE\_Q}(E - E_0)^2 \\ &= Q_0 + a_{E\_Q}\Delta E + a_{idgcom}\Delta i_{dgcom} + a_{idgcond}\Delta i_{dgcond} + a_{Eidgcom}\Delta E\Delta i_{dgcom} \\ &\quad + a_{Eidgcond}\Delta E\Delta i_{dgcond} + a_{EE\_Q}\Delta E^2 \end{aligned} \tag{F.1-88}$$

$$a_{E\_Q} = \frac{3n_{pulse}}{2\sqrt{2}}\left(i_{dgcom0} + i_{dgcond0}\right) \tag{F.1-89}$$

$$a_{idgcom\_Q} = \frac{3n_{pulse}}{2\sqrt{2}}E_0 \tag{F.1-90}$$

$$a_{idgcond\_Q} = \frac{3n_{pulse}}{2\sqrt{2}}E_0 \tag{F.1-91}$$

$$a_{Eidgcom\_Q} = \frac{3n_{pulse}}{2\sqrt{2}} \tag{F.1-92}$$

$$a_{Eidgcond\_Q} = \frac{3n_{pulse}}{2\sqrt{2}} \tag{F.1-93}$$

$$a_{EE\_Q} = \frac{3n_{pulse}}{4\sqrt{2}}a_{Eidgcom} \tag{F.1-94}$$

Substitute Equations (F.1-50) and (F.1-56) in Equation (F.1-88), the total reactive power can be expressed as follows:

$$Q_{ac} = Q_0 + GQ_{11}\Delta E + GQ_{12}\Delta i_d + GQ_{13}\Delta u + GQ_{14}\Delta f_g + GQ_{15}\Delta E\Delta u + GQ_{16}\Delta E\Delta i_d + GQ_{17}\Delta E^2 + GQ_{18}\Delta E\Delta f_g \quad \text{(F.1-95)}$$

$$GQ_{11} = a_{E\_Q} + a_{idgcom}a_{E\_dgcom} \quad \text{(F.1-96)}$$

$$GQ_{12} = a_{idgcom}a_{id\_dgcom} + a_{idgcond}a_{id\_dgcond} \quad \text{(F.1-97)}$$

$$GQ_{13} = a_{idgcom}a_{u\_dgcom} + a_{idgcond}a_{u\_dgcond} \quad \text{(F.1-98)}$$

$$GQ_{14} = a_{idgcom}a_{fg\_dgcom} \quad \text{(F.1-99)}$$

$$GQ_{15} = a_{Eidgcom}a_{u\_dgcom} + a_{Eidgcond}a_{u\_dgcond} \quad \text{(F.1-100)}$$

$$GQ_{16} = a_{Eidgcom}a_{id\_dgcom} + a_{Eidgcond}a_{id\_dgcond} \quad \text{(F.1-101)}$$

$$GQ_{17} = a_{Eidgcom}a_{E\_dgcom} + a_{EE\_Q} \quad \text{(F.1-102)}$$

$$GQ_{18} = a_{Eidgcom}a_{fg\_dgcom} \quad \text{(F.1-103)}$$

Substitute Equation (F.1-77) in Equation (F.1-95),

$$Q_{ac} = Q_0 + GQ_{21}\Delta E + GQ_{22}\Delta i_d + GQ_{23}\Delta f_g + GQ_{24}\Delta i_d\Delta E + GQ_{25}\Delta E^2 + GQ_{26}\Delta E\Delta f_g \quad \text{(F.1-104)}$$

$$GQ_{21} = GQ_{11} + GQ_{13}u_{22} \quad \text{(F.1-105)}$$

$$GQ_{22} = GQ_{12} + GQ_{13}u_{21} \quad \text{(F.1-106)}$$

$$GQ_{23} = GQ_{14} + GQ_{13}u_{23} \quad \text{(F.1-107)}$$

$$GQ_{24} = GQ_{16} + GQ_{15}u_{21} \quad \text{(F.1-108)}$$

$$GQ_{25} = GQ_{17} + GQ_{15}u_{22} \quad \text{(F.1-109)}$$

$$GQ_{26} = GQ_{18} + GQ_{15}u_{23} \quad \text{(F.1-110)}$$

F.2 Induction Motors

The induction motors are exactly the same as Section C.2, and the three main equations are copied here for convenience:

$$0=(R_r+L_rS)\Delta v_{qs}-L_r(\omega_{r0}-\omega_{s0})\Delta v_{ds}+\left[\omega_{s0}(\omega_{r0}-\omega_{s0})(L_m^2-L_rL_s)-R_s(R_r+L_rS)\right]\Delta i_{qs}$$
$$+\left[\omega_{s0}(L_m^2-L_rL_s)S+R_sL_r(\omega_{r0}-\omega_{s0})-R_rL_s\omega_{s0}\right]\Delta i_{ds}+\left[L_m\omega_{s0}(L_mi_{qs0}+L_ri_{qr0})\right]\Delta\omega_r$$
$$-\left[(R_r+L_rS)(L_si_{ds0}+L_mi_{dr0})+L_r(\omega_{r0}-\omega_{s0})(L_si_{qs0}+L_mi_{qr0})+L_m\omega_{s0}(L_mi_{qs0}+L_ri_{qr0})\right]\Delta\omega_s \quad \text{(F.2-1)}$$

$$0=-L_r(\omega_{r0}-\omega_{s0})\Delta v_{qs}-(R_r+L_rS)\Delta v_{ds}+\left[\omega_{s0}(L_m^2-L_rL_s)S+R_sL_r(\omega_{r0}-\omega_{s0})-R_rL_s\omega_{s0}\right]\Delta i_{qs}$$
$$+\left[R_s(R_r+L_rS)-\omega_{s0}(\omega_{r0}-\omega_{s0})(L_m^2-L_rL_s)\right]\Delta i_{ds}-\left[L_m\omega_{s0}(L_mi_{ds0}+L_ri_{dr0})\right]\Delta\omega_r$$
$$+\left[L_r(\omega_{r0}-\omega_{s0})(L_si_{ds0}+L_mi_{dr0})+L_m\omega_{s0}(L_mi_{ds0}+L_ri_{dr0})-(R_r+L_rS)(L_si_{qs0}+L_mi_{qr0})\right]\Delta\omega_s \quad \text{(F.2-2)}$$

$$\left(\frac{4H\omega_{s0}S}{3P^2}\right)\Delta\omega_r=i_{qs0}\Delta v_{qs}+i_{ds0}\Delta v_{ds}+\left[i_{dr0}L_m\omega_{s0}-i_{qs0}R_s+i_{ds0}L_s\omega_{s0}\omega_{s0}\right]\Delta i_{qs}$$
$$-\left[i_{qs0}L_s\omega_{s0}+i_{qr0}L_m\omega_{s0}+i_{ds0}R_s\right]\Delta i_{ds}+\left[i_{ds0}(L_si_{qs0}+L_mi_{qr0})-i_{qs0}(L_si_{ds0}+L_mi_{dr0})\right]\Delta\omega_s \quad \text{(F.2-3)}$$

F.3 Voltage per Hz Control

The output voltage from the single phase full bridge inverter for each power module can be determined as follows:

$$V_0=de_d \quad \text{(F.3-1)}$$

where V_0 is the output voltage from each power module, d is duty cycle.

For an 18-pulse system with three power modules each phase connected to the induction motors, the phase a voltage of the induction motor can be determined as follows:

$$V_{an}=\left(\frac{n_{pulse}}{6}\right)de_d\cos\theta \quad \text{(F.3-2)}$$

where V_{an} is the voltage at phase a of the induction motor.

The voltages at phases b and c can be determined similarly as follows:

$$V_{bn} = \left(\frac{n_{pulse}}{6}\right) de_d \cos\left(\theta - \frac{2\pi}{3}\right)$$

$$V_{cn} = \left(\frac{n_{pulse}}{6}\right) de_d \cos\left(\theta + \frac{2\pi}{3}\right)$$

The three phases voltages of the induction motor in *abc* frame are converted to the *dq0* frame as follows:

$$V_{qs} = \left(\frac{n_{pulse}}{6}\right) de_d \qquad \text{(F.3-3)}$$

$$V_{ds} = 0 \qquad \text{(F.3-4)}$$

where,

v_{qs} – q-axis voltage at the terminal of induction motor

v_{ds} – d-axis voltage at the terminal of induction motor

The real power supplying to the induction motor for an 18-pulse MVD P_{ac_IM} is:

$$P_{ac\_IM} = \frac{3}{2}\left(V_{ds} i_{qs} + V_{qs} i_{qs}\right) = \frac{3}{2} V_{qs} i_{qs} = \frac{3}{2} \times \left(\frac{n_{pulse}}{6} de_d\right) i_{qs} = \left(\frac{n_{pulse}}{4}\right) de_d i_{qs} \qquad \text{(F.3-5)}$$

The total DC power at DC links for all power modules corresponding to real power supplying to the induction motor for an 18-pulse MVD is:

$$P_{dc} = \left(\frac{n_{pulse}}{2}\right) P_{dc\_per\,module} = \left(\frac{n_{pulse}}{2}\right) e_d i_I \qquad \text{(F.3-6)}$$

Ignoring the losses at the inverters at the power modules, the following equation is satisfied:

$$P_{ac\_IM} = P_{dc} \qquad \text{(F.3-7)}$$

Substitute Equations (F.3-5) and (F.3-6) in Equation (F.3-7):

$$\left(\frac{n_{pulse}}{4}\right) de_d i_{qs} = \left(\frac{n_{pulse}}{2}\right) e_d i_I \tag{F.3-8}$$

Substitute Equations (F.1-3) and (F.1-4) in Equation (F.3-8), we have

$$\frac{1}{2} de_d i_{qs} = e_d \left(i_d - C_{dc} \frac{de_d}{dt} \right) \tag{F.3-9}$$

The q-axis component of the motor stator current can be determined from Equation (F.3-9) as follows:

$$i_{qs} = \frac{2i_d}{d} - 2C_{dc} \left(\frac{de_d}{dt} \frac{1}{d} \right) \tag{F.3-10}$$

At the time t=0, Equation (F.3-10) can be expressed using the initial values:

$$i_{qs0} = \frac{2i_{d0}}{d_0} - 2C_{dc} \left(\left. \frac{de_d}{dt} \right|_{t=0} \frac{1}{d_0} \right) \tag{F.3-11}$$

Rearrange Equation (F.3-11),

$$\left. \frac{de_d}{dt} \right|_{t=0} = \frac{\left(2i_{d0} - i_{qs0} d_0\right)}{2C_{dc}} \tag{F.3-12}$$

Linearize Equation (F.3-10):

$$\Delta i_{qs} = \frac{2}{d_0} \Delta i_d - \frac{i_{qs0}}{d_0} \Delta d - \frac{2C_{dc}}{d_0} S \Delta e_d \tag{F.3-13}$$

Replace V_{qs}^{e*} in Equation (4.2-34) by v_{qs} in Equation (4.6-17) yield:

$$\begin{bmatrix} v_{qs}^{e*} \\ v_{ds}^{e*} \end{bmatrix} = \begin{bmatrix} \cos\theta_{ce} & \sin\theta_{ce} \\ -\sin\theta_{ce} & \cos\theta_{ce} \end{bmatrix} \begin{bmatrix} v_{qs} \\ v_{ds} \end{bmatrix} = \begin{bmatrix} \cos\theta_{ce} & \sin\theta_{ce} \\ -\sin\theta_{ce} & \cos\theta_{ce} \end{bmatrix} \begin{bmatrix} \frac{n_{pulse}}{6} de_d \\ 0 \end{bmatrix} \tag{F.3-14}$$

From Equation (F.3-14), the following relationships are obtained:

$$d = \frac{\sqrt{\left(v_{qs}^{e*}\right)^2 + \left(v_{ds}^{e*}\right)^2}}{\left(\frac{n_{pulse}}{6}\right)e_d} \tag{F.3-15}$$

The developed simplified block diagram for the closed-loop voltage per Hz control scheme used for the formula derivation is shown in Figure 4.27. The equations for the closed-loop voltage per Hz control are given as follows:

$$\omega_{SL} = K_{pm}\left(\omega_r^* - \omega_r\right) + \int_0^t K_{im}\left(\omega_r^* - \omega_r\right)dt + \left(\omega_{s0} - \omega_{r0}\right) \tag{F.3-16}$$

$$\omega_{SL} + \omega_r = \omega_s \tag{F.3-17}$$

$$d = \frac{\omega_s\left(\frac{V_b}{\omega_b}\right)\sqrt{2}}{\left(\frac{n_{pulse}}{6}\right)e_d} \tag{F.3-18}$$

$$V_{qs}^{e*} = \omega_s\left(\frac{V_b}{\omega_b}\right)\sqrt{2} \tag{F.3-19}$$

$$V_{ds}^{e*} = 0 \tag{F.3-20}$$

where K_{pm} is speed PI controller proportional gain, and K_{im} is speed PI controller integral gain.

Linearize Equations (F.3-16) and (F.3-17), the relationship between ω_s and ω_r can be determined as follows:

$$\Delta\omega_s = \frac{A_{11}S + A_{12}}{S}\Delta\omega_r \tag{F.3-21}$$

$$A_{11} = 1 - K_{pm}$$

$$A_{12} = -K_{im}$$

Linearize Equation (F.3-18):

$$\Delta d = \left(-\frac{\sqrt{2}V_b\omega_{s0}}{\frac{n_{pulse}}{6}\omega_b e_{d0}^2} \right)\Delta e_d + \left(\frac{\sqrt{2}V_b}{\frac{n_{pulse}}{6}\omega_b e_{d0}} \right)\Delta\omega_s \qquad (F.3\text{-}22)$$

Substitute Equation (F.3-22) in Equation (F.3-13):

$$\Delta i_{qs} = A_{21}\Delta i_d + A_{22}\Delta\omega_s + (A_{231}S + A_{232})\Delta e_d \qquad (F.3\text{-}23)$$

$$A_{21} = \frac{2}{d_0} \qquad (F.3\text{-}24)$$

$$A_{22} = -\frac{\sqrt{2}i_{qs0}V_b}{\frac{n_{pulse}}{6}d_0\omega_b e_{d0}} \qquad (F.3\text{-}25)$$

$$A_{231} = -\frac{2C_{dc}}{d_0} \qquad (F.3\text{-}26)$$

$$A_{232} = \frac{\sqrt{2}i_{qs0}V_b\omega_{s0}}{\frac{n_{pulse}}{6}d_0\omega_b e_{d0}^2} \qquad (F.3\text{-}27)$$

Linearize Equation (F.3-3):

$$\Delta V_{qs} = \left(\frac{n_{pulse}}{6} \right) d_0\Delta e_d + \left(\frac{n_{pulse}}{6} \right) e_{d0}\Delta d \qquad (F.3\text{-}28)$$

Substitute Equation (F.3-22) in Equation (F.3-28), we have

$$\begin{aligned}\Delta V_{qs} &= \left(\frac{n_{pulse}}{6} \right) d_0\Delta e_d + \left(\frac{n_{pulse}}{6} e_{d0} \right)\left(-\frac{\sqrt{2}V_b\omega_{s0}}{\frac{n_{pulse}}{6}\omega_b e_{d0}^2}\Delta e_d + \frac{\sqrt{2}V_b}{\frac{n_{pulse}}{6}\omega_b e_{d0}}\Delta\omega_s \right) \qquad (F.3\text{-}29)\\ &= A_{31}\Delta\omega_s + A_{32}\Delta e_d\end{aligned}$$

$$A_{31} = \frac{\sqrt{2}V_b}{\omega_b} \tag{F.3-30}$$

$$A_{32} = \frac{n_{pulse}}{6} d_0 - \frac{\sqrt{2}V_b \omega_{s0}}{\omega_b e_{d0}} \tag{F.3-31}$$

Linearize Equation (F.3-4):

$$\Delta v_{ds} = 0 \tag{F.3-32}$$

Substitute Equation (F.3-21) in Equations (F.3-23) and (F.3-28):

$$\Delta i_{qs} = A_{21}\Delta i_d + \left(\frac{A_{22}A_{11}S + A_{22}A_{12}}{S} \right) \Delta\omega_r + \left(A_{231}S + A_{232} \right) \Delta e_d \tag{F.3-33}$$

$$\Delta v_{qs} = \frac{A_{31}A_{11}S + A_{31}A_{12}}{S} \Delta\omega_r + A_{32}\Delta e_d \tag{F.3-34}$$

Equations (F.2-1), (F.2-2) and (F.2-3) are rewritten as follows:

$$0 = A_{41}\Delta V_{qs} + A_{42}\Delta V_{ds} + A_{43}\Delta i_{qs} + A_{44}\Delta\omega_s + A_{45}\Delta i_{ds} + A_{46}\Delta\omega_r \tag{F.3-35}$$

$$0 = A_{51}\Delta V_{qs} + A_{52}\Delta V_{ds} + A_{53}\Delta i_{qs} + A_{54}\Delta\omega_s + A_{55}\Delta i_{ds} + A_{56}\Delta\omega_r \tag{F.3-36}$$

$$0 = A_{61}\Delta V_{qs} + A_{62}\Delta V_{ds} + A_{63}\Delta i_{qs} + A_{64}\Delta\omega_s + A_{65}\Delta i_{ds} + A_{66}\Delta\omega_r \tag{F.3-37}$$

$$A_{41} = A_{411}S + A_{412} \tag{F.3-38}$$

$$A_{411} = L_r \tag{F.3-39}$$

$$A_{412} = R_r \tag{F.3-40}$$

$$A_{42} = -L_r \left(\omega_{r0} - \omega_{s0} \right) \tag{F.3-41}$$

$$A_{43} = A_{431}S + A_{432} \tag{F.3-42}$$

$$A_{431} = -R_s L_r \tag{F.3-43}$$

$$A_{432} = \omega_{s0} \left(\omega_{r0} - \omega_{s0} \right) \left(L_m^2 - L_r L_s \right) - R_s R_r \tag{F.3-44}$$

$$A_{44} = A_{441}S + A_{442} \tag{F.3-45}$$

$$A_{441} = -L_r\left(L_s i_{ds0} + L_m i_{dr0}\right) \tag{F.3-46}$$

$$A_{442} = -L_m\omega_{s0}\left(L_m i_{qs0} + L_r i_{qr0}\right) - R_r\left(L_s i_{ds0} + L_m i_{dr0}\right) - L_r\left(\omega_{r0} - \omega_{s0}\right)\left(L_s i_{qs0} + L_m i_{qr0}\right) \tag{F.3-47}$$

$$A_{45} = A_{451}S + A_{452} \tag{F.3-48}$$

$$A_{451} = \omega_{s0}\left(L_m^2 - L_r L_s\right) \tag{F.3-49}$$

$$A_{452} = L_r R_s\left(\omega_{r0} - \omega_{s0}\right) - R_r L_s \omega_{s0} \tag{F.3-50}$$

$$A_{46} = L_m\omega_{s0}\left(L_m i_{qs0} + L_r i_{qr0}\right) \tag{F.3-51}$$

$$A_{51} = -L_r\left(\omega_{r0} - \omega_{s0}\right) \tag{F.3-52}$$

$$A_{52} = A_{521}S + A_{522} \tag{F.3-53}$$

$$A_{521} = -L_r \tag{F.3-54}$$

$$A_{522} = -R_r \tag{F.3-55}$$

$$A_{53} = A_{531}S + A_{532} \tag{F.3-56}$$

$$A_{531} = \omega_{s0}\left(L_m^2 - L_r L_s\right) = A_{451} \tag{F.3-57}$$

$$A_{532} = L_r R_s\left(\omega_{r0} - \omega_{s0}\right) - R_r L_s \omega_{s0} = A_{452} \tag{F.3-58}$$

$$A_{54} = A_{541}S + A_{542} \tag{F.3-59}$$

$$A_{541} = -L_r\left(L_s i_{qs0} + L_m i_{qr0}\right) \tag{F.3-60}$$

$$A_{542} = -L_m\omega_{s0}\left(L_m i_{ds0} + L_r i_{dr0}\right) - R_r\left(L_s i_{qs0} + L_m i_{qr0}\right) + L_r\left(\omega_{r0} - \omega_{s0}\right)\left(L_s i_{ds0} + L_m i_{dr0}\right) \tag{F.3-61}$$

$$A_{55} = A_{551}S + A_{552} \tag{F.3-62}$$

$$A_{551} = R_s L_r \tag{F.3-63}$$

$$A_{552} = R_s R_r - \omega_{s0}\left(\omega_{r0} - \omega_{s0}\right)\left(L_m^2 - L_r L_s\right) \tag{F.3-64}$$

$$A_{56} = -L_m\omega_{s0}\left(L_m i_{ds0} + L_r i_{dr0}\right) \tag{F.3-65}$$

$$A_{61} = i_{qs0} \tag{F.3-66}$$

$$A_{62} = i_{ds0} \tag{F.3-67}$$

$$A_{63} = L_m \omega_{s0} i_{dr0} - R_s i_{qs0} + L_s \omega_{s0} i_{ds0} \tag{F.3-68}$$

$$A_{64} = i_{ds0}\left(L_s i_{qs0} + L_m i_{qr0}\right) - i_{qs0}\left(L_s i_{ds0} + L_m i_{dr0}\right) \tag{F.3-69}$$

$$A_{65} = -\left(i_{qs0} L_s \omega_{s0} + i_{ds0} R_s + i_{qr0} L_m \omega_{s0}\right) \tag{F.3-70}$$

$$A_{66} = A_{661} S \tag{F.3-71}$$

$$A_{661} = -\frac{4H\omega_{s0}}{3p^2} \tag{F.3-72}$$

Rearrange Equation (F.3-37), and substitute Equation (F.3-32) in Equation (F.3-37):

$$\Delta i_{ds} = \left(-\frac{1}{A_{65}}\right)\left(A_{61}\Delta V_{qs} + A_{63}\Delta i_{qs} + A_{64}\Delta\omega_s + A_{66}\Delta\omega_r\right) \tag{F.3-73}$$

Substitute Equations (F.3-32) and (F.3-73) in Equations (F.3-35) and (F.3-36):

$$0 = \left(B_{11}S + B_{12}\right)\Delta V_{qs} + \left(B_{21}S + B_{22}\right)\Delta i_{qs} + \left(B_{31}S + B_{32}\right)\Delta\omega_s + \left(B_{41}S^2 + B_{42}S + B_{43}\right)\Delta\omega_r \tag{F.3-74}$$

$$0 = \left(B_{51}S + B_{52}\right)\Delta V_{qs} + \left(B_{61}S + B_{62}\right)\Delta i_{qs} + \left(B_{71}S + B_{72}\right)\Delta\omega_s + \left(B_{81}S^2 + B_{82}S + B_{83}\right)\Delta\omega_r \tag{F.3-75}$$

$$B_{11} = A_{411}A_{65} - A_{451}A_{61} \tag{F.3-76}$$

$$B_{12} = A_{412}A_{65} - A_{452}A_{61} \tag{F.3-77}$$

$$B_{21} = A_{431}A_{65} - A_{451}A_{63} \tag{F.3-78}$$

$$B_{22} = A_{432}A_{65} - A_{452}A_{63} \tag{F.3-79}$$

$$B_{31} = A_{441}A_{65} - A_{451}A_{64} \tag{F.3-80}$$

$$B_{32} = A_{442}A_{65} - A_{452}A_{64} \tag{F.3-81}$$

$$B_{41} = -A_{451}A_{661} \tag{F.3-82}$$

$$B_{42} = -A_{452}A_{661} \tag{F.3-83}$$

$$B_{43} = A_{46}A_{65} \tag{F.3-84}$$

$$B_{51} = -A_{551}A_{61} \tag{F.3-85}$$

$$B_{52} = A_{51}A_{65} - A_{552}A_{61} \tag{F.3-86}$$

$$B_{61} = A_{531}A_{65} - A_{551}A_{63} \tag{F.3-87}$$

$$B_{62} = A_{532}A_{65} - A_{552}A_{63} \tag{F.3-88}$$

$$B_{71} = A_{541}A_{65} - A_{551}A_{64} \tag{F.3-89}$$

$$B_{72} = A_{542}A_{65} - A_{552}A_{64} \tag{F.3-90}$$

$$B_{81} = -A_{551}A_{661} \tag{F.3-91}$$

$$B_{82} = -A_{552}A_{661} \tag{F.3-92}$$

$$B_{83} = A_{56}A_{65} \tag{F.3-93}$$

Substitute Equations (F.3-21), (F.3-33) and (F.3-34) in Equations (F.3-74) and (F.3-75):

$$0 = D_{11}\Delta i_d + D_{12}\Delta e_d + D_{13}\Delta\omega_r \tag{F.3-94}$$

$$0 = D_{21}\Delta i_d + D_{22}\Delta e_d + D_{23}\Delta\omega_r \tag{F.3-95}$$

$$D_{11} = D_{111}S^2 + D_{112}S \tag{F.3-96}$$

$$D_{111} = A_{21}B_{21} \tag{F.3-97}$$

$$D_{112} = A_{21}B_{22} \tag{F.3-98}$$

$$D_{12} = D_{121}S^3 + D_{122}S^2 + D_{123}S \tag{F.3-99}$$

$$D_{121} = B_{21}A_{231} \tag{F.3-100}$$

$$D_{122} = B_{21}A_{232} + B_{22}A_{231} + A_{32}B_{11} \tag{F.3-101}$$

$$D_{123} = A_{32}B_{12} + B_{22}A_{232} \tag{F.3-102}$$

$$D_{13} = D_{131}S^3 + D_{132}S^2 + D_{133}S + D_{134} \tag{F.3-103}$$

$$D_{131} = B_{41} \tag{F.3-104}$$

$$D_{132} = A_{11}\left(A_{31}B_{11} + B_{31}\right) + B_{21}A_{22}A_{11} + B_{42} \tag{F.3-105}$$

$$D_{133} = A_{11}\left(A_{31}B_{12} + B_{32}\right) + A_{12}\left(A_{31}B_{11} + B_{31}\right) + B_{21}A_{22}A_{12} + B_{22}A_{22}A_{11} + B_{43} \tag{F.3-106}$$

$$D_{134} = A_{12}\left(A_{31}B_{12} + B_{32}\right) + B_{22}A_{22}A_{12} \tag{F.3-107}$$

$$D_{21} = D_{211}S^2 + D_{212}S \tag{F.3-108}$$

$$D_{211} = A_{21}B_{61} \tag{F.3-109}$$

$$D_{212} = A_{21}B_{62} \tag{F.3-110}$$

$$D_{22} = D_{221}S^3 + D_{222}S^2 + D_{223}S \tag{F.3-111}$$

$$D_{221} = B_{61}A_{231} \tag{F.3-112}$$

$$D_{222} = B_{62}A_{231} + B_{61}A_{232} + A_{32}B_{51} \tag{F.3-113}$$

$$D_{223} = A_{32}B_{52} + B_{62}A_{232} \tag{F.3-114}$$

$$D_{23} = D_{231}S^3 + D_{232}S^2 + D_{233}S + D_{234} \tag{F.3-115}$$

$$D_{231} = B_{81} \tag{F.3-116}$$

$$D_{232} = A_{11}\left(A_{31}B_{51} + B_{71}\right) + B_{61}A_{22}A_{11} + B_{82} \tag{F.3-117}$$

$$D_{233} = A_{11}\left(A_{31}B_{52} + B_{72}\right) + A_{12}\left(A_{31}B_{51} + B_{71}\right) + B_{62}A_{22}A_{11} + B_{61}A_{22}A_{12} + B_{83} \tag{F.3-118}$$

$$D_{234} = A_{12}\left(A_{31}B_{52} + B_{72}\right) + B_{62}A_{22}A_{12} \tag{F.3-119}$$

Based on Equations (F.3-94) and (F.3-95),

$$\Delta\omega_r = \left(-\frac{1}{D_{13} - D_{23}}\right)\left[\left(D_{11} - D_{21}\right)\Delta i_d + \left(D_{12} - D_{22}\right)\Delta e_d\right] \tag{F.3-120}$$

Substitute Equation (F.3-120) in Equation (F.3-94), the relationship between i_d and e_d can then be determined as follows:

$$\Delta i_d = \left[\frac{D_{13}\left(D_{12} - D_{22}\right) - D_{12}\left(D_{13} - D_{23}\right)}{D_{11}\left(D_{13} - D_{23}\right) - D_{13}\left(D_{11} - D_{21}\right)}\right]\Delta e_d \tag{F.3-121}$$

Equation (F.3-121) can be further derived to be:

$$\Delta i_d = G_{13}\Delta e_d \tag{F.3-122}$$

$$G_{13} = \frac{F_{11}S^5 + F_{12}S^4 + F_{13}S^3 + F_{14}S^2 + F_{15}S + F_{16}}{F_{21}S^4 + F_{22}S^3 + F_{23}S^2 + F_{24}S + F_{25}} \tag{F.3-123}$$

$$F_{11} = E_{11} - E_{21} \tag{F.3-124}$$

$$F_{12} = E_{12} - E_{22} \tag{F.3-125}$$

$$F_{13} = E_{13} - E_{23} \tag{F.3-126}$$

$$F_{14} = E_{14} - E_{24} \tag{F.3-127}$$

$$F_{15} = E_{15} - E_{25} \tag{F.3-128}$$

$$F_{16} = E_{16} - E_{26} \tag{F.3-129}$$

$$F_{21} = E_{31} - E_{41} \tag{F.3-130}$$

$$F_{22} = E_{32} - E_{42} \tag{F.3-131}$$

$$F_{23} = E_{33} - E_{43} \tag{F.3-132}$$

$$F_{24} = E_{34} - E_{44} \tag{F.3-133}$$

$$F_{25} = E_{35} - E_{45} \tag{F.3-134}$$

$$E_{11} = D_{131}(D_{121} - D_{221}) \tag{F.3-135}$$

$$E_{12} = D_{132}(D_{121} - D_{221}) + D_{131}(D_{122} - D_{222}) \tag{F.3-136}$$

$$E_{13} = D_{133}(D_{121} - D_{221}) + D_{132}(D_{122} - D_{222}) + D_{131}(D_{123} - D_{223}) \tag{F.3-137}$$

$$E_{14} = D_{134}(D_{121} - D_{221}) + D_{133}(D_{122} - D_{222}) + D_{132}(D_{123} - D_{223}) \tag{F.3-138}$$

$$E_{15} = D_{134}(D_{122} - D_{222}) + D_{133}(D_{123} - D_{223}) \tag{F.3-139}$$

$$E_{16} = D_{134}(D_{123} - D_{223}) \tag{F.3-140}$$

$$E_{21} = D_{121}(D_{131} - D_{231}) \tag{F.3-141}$$

$$E_{22} = D_{122}(D_{131} - D_{231}) + D_{121}(D_{132} - D_{232}) \tag{F.3-142}$$

$$E_{23} = D_{123}(D_{131} - D_{231}) + D_{122}(D_{132} - D_{232}) + D_{121}(D_{133} - D_{233}) \tag{F.3-143}$$

$$E_{24} = D_{123}(D_{132} - D_{232}) + D_{122}(D_{133} - D_{233}) + D_{121}(D_{134} - D_{234}) \quad \text{(F.3-144)}$$

$$E_{25} = D_{123}(D_{133} - D_{233}) + D_{122}(D_{134} - D_{234}) \quad \text{(F.3-145)}$$

$$E_{26} = D_{123}(D_{134} - D_{234}) \quad \text{(F.3-146)}$$

$$E_{31} = D_{111}(D_{131} - D_{231}) \quad \text{(F.3-147)}$$

$$E_{32} = D_{111}(D_{132} - D_{232}) + D_{112}(D_{131} - D_{231}) \quad \text{(F.3-148)}$$

$$E_{33} = D_{111}(D_{133} - D_{233}) + D_{112}(D_{132} - D_{232}) \quad \text{(F.3-149)}$$

$$E_{34} = D_{111}(D_{134} - D_{234}) + D_{112}(D_{133} - D_{233}) \quad \text{(F.3-150)}$$

$$E_{35} = D_{112}(D_{134} - D_{234}) \quad \text{(F.3-151)}$$

$$E_{41} = D_{131}(D_{111} - D_{211}) \quad \text{(F.3-152)}$$

$$E_{42} = D_{132}(D_{111} - D_{211}) + D_{131}(D_{112} - D_{212}) \quad \text{(F.3-153)}$$

$$E_{43} = D_{133}(D_{111} - D_{211}) + D_{132}(D_{112} - D_{212}) \quad \text{(F.3-154)}$$

$$E_{44} = D_{134}(D_{111} - D_{211}) + D_{133}(D_{112} - D_{212}) \quad \text{(F.3-155)}$$

$$E_{45} = D_{134}(D_{112} - D_{212}) \quad \text{(F.3-156)}$$

Combined Equations (F.1-7) and (F.3-122), the relationship between E and e_d is obtained:

$$\Delta e_d = G_{11}\Delta E + G_{12}\Delta f_g \quad \text{(F.3-157)}$$

$$G_{11} = \frac{F_{41}S^4 + F_{42}S^3 + F_{43}S^2 + F_{44}S + F_{45}}{F_{31}S^6 + F_{32}S^5 + F_{33}S^4 + F_{34}S^3 + F_{35}S^2 + F_{36}S + F_{37}} \quad \text{(F.3-158)}$$

$$G_{12} = \left(\frac{L_{22}}{L_{21}}\right) G_{11} \quad \text{(F.3-159)}$$

$$F_{31} = L_{11}F_{11} \quad \text{(F.3-160)}$$

$$F_{32} = L_{11}F_{12} + L_{12}F_{11} \quad \text{(F.3-161)}$$

$$F_{33} = L_{11}F_{13} + L_{12}F_{12} + F_{21} \quad \text{(F.3-162)}$$

$$F_{34} = L_{11}F_{14} + L_{12}F_{13} + F_{22} \quad \text{(F.3-163)}$$

$$F_{35} = L_{11}F_{15} + L_{12}F_{14} + F_{23} \tag{F.3-164}$$

$$F_{36} = L_{11}F_{16} + L_{12}F_{15} + F_{24} \tag{F.3-165}$$

$$F_{37} = L_{12}F_{16} + F_{25} \tag{F.3-166}$$

$$F_{41} = L_{21}F_{21} \tag{F.3-167}$$

$$F_{42} = L_{21}F_{22} \tag{F.3-168}$$

$$F_{43} = L_{21}F_{23} \tag{F.3-169}$$

$$F_{44} = L_{21}F_{24} \tag{F.3-170}$$

$$F_{45} = L_{21}F_{25} \tag{F.3-171}$$

F.4 Overall System Combination

Rewrite Equation (F.1-7) as follows:

$$\Delta i_d = N_{11}\Delta E + N_{12}\Delta e_d + N_{13}\Delta f_g \tag{F.4-1}$$

$$N_{11} = \frac{L_{21}}{L_{11}S + L_{12}} \tag{F.4-2}$$

$$N_{12} = -\frac{1}{L_{11}S + L_{12}} \tag{F.4-3}$$

$$N_{13} = \frac{L_{22}}{L_{11}S + L_{12}} \tag{F.4-4}$$

Rewrite Equation (F.3-157) as follows:

$$\Delta e_d = G_{11}\Delta E + \left(\frac{L_{22}}{L_{21}}\right)G_{11}\Delta f_g \tag{F.4-5}$$

Submit Equations (F.4-1) and (F.4-5) in Equations (F.1-81) and (F.1-104), the dynamic model represented by real and reactive power at the input of the MVD can be determined as follows:

$$P = P_0 + G_{P1}\Delta E + G_{P2}\Delta E^2 + \left(G_{P3} + G_{P4}\Delta E\right)\Delta f \tag{F.4-6}$$

$$G_{P1} = GP_{21} + GP_{22}N_{11} + GP_{22}N_{12}G_{11} \tag{F.4-7}$$

$$G_{P2} = GP_{25} + GP_{24}N_{11} + GP_{24}N_{12}G_{11} \tag{F.4-8}$$

$$G_{P3} = GP_{23} + GP_{22}N_{13} + \frac{L_{22}GP_{22}}{L_{21}}N_{12}G_{11} \tag{F.4-9}$$

$$G_{P4} = GP_{26} + GP_{24}N_{13} + \frac{L_{22}GP_{24}}{L_{21}}N_{12}G_{11} \tag{F.4-10}$$

$$Q = Q_0 + G_{Q1}\Delta E + G_{Q2}\Delta E^2 + \left(G_{Q3} + G_{Q4}\Delta E\right)\Delta f \tag{F.4-11}$$

$$G_{Q1} = GQ_{21} + GQ_{22}N_{11} + GQ_{22}N_{12}G_{11} \tag{F.4-12}$$

$$G_{Q2} = GQ_{25} + GQ_{24}N_{11} + GQ_{24}N_{12}G_{11} \tag{F.4-13}$$

$$G_{Q3} = GQ_{23} + GQ_{22}N_{13} + \frac{L_{22}GQ_{22}}{L_{21}}N_{12}G_{11} \tag{F.4-14}$$

$$G_{Q4} = GQ_{26} + GQ_{24}N_{13} + \frac{L_{22}GQ_{24}}{L_{21}}N_{12}G_{11} \tag{F.4-15}$$

The coefficient of the real power and reactive power are 7th order transfer functions, they can be derived as follows:

$$G_{P1} = \frac{GP_{51}S^7 + GP_{52}S^6 + GP_{53}S^5 + GP_{54}S^4 + GP_{55}S^3 + GP_{56}S^2 + GP_{57}S + GP_{58}}{P_{b1}S^7 + P_{b2}S^6 + P_{b3}S^5 + P_{b4}S^4 + P_{b5}S^3 + P_{b6}S^2 + P_{b7}S + P_{b8}} \tag{F.4-16}$$

$$G_{P2} = \frac{GP_{71}S^7 + GP_{72}S^6 + GP_{73}S^5 + GP_{74}S^4 + GP_{75}S^3 + GP_{76}S^2 + GP_{77}S + GP_{78}}{P_{b1}S^7 + P_{b2}S^6 + P_{b3}S^5 + P_{b4}S^4 + P_{b5}S^3 + P_{b6}S^2 + P_{b7}S + P_{b8}} \tag{F.4-17}$$

$$G_{P3} = \frac{GP_{91}S^7 + GP_{92}S^6 + GP_{93}S^5 + GP_{94}S^4 + GP_{95}S^3 + GP_{96}S^2 + GP_{97}S + GP_{98}}{P_{b1}S^7 + P_{b2}S^6 + P_{b3}S^5 + P_{b4}S^4 + P_{b5}S^3 + P_{b6}S^2 + P_{b7}S + P_{b8}} \tag{F.4-18}$$

$$G_{P4} = \frac{HP_{21}S^7 + HP_{22}S^6 + HP_{23}S^5 + HP_{24}S^4 + HP_{25}S^3 + HP_{26}S^2 + HP_{27}S + HP_{28}}{P_{b1}S^7 + P_{b2}S^6 + P_{b3}S^5 + P_{b4}S^4 + P_{b5}S^3 + P_{b6}S^2 + P_{b7}S + P_{b8}}$$

(F.4-19)

$$G_{Q1} = \frac{GQ_{51}S^7 + GQ_{52}S^6 + GQ_{53}S^5 + GQ_{54}S^4 + GQ_{55}S^3 + GQ_{56}S^2 + GQ_{57}S + GQ_{58}}{P_{b1}S^7 + P_{b2}S^6 + P_{b3}S^5 + P_{b4}S^4 + P_{b5}S^3 + P_{b6}S^2 + P_{b7}S + P_{b8}}$$

(F.4-20)

$$G_{Q2} = \frac{GQ_{71}S^7 + GQ_{72}S^6 + GQ_{73}S^5 + GQ_{74}S^4 + GQ_{75}S^3 + GQ_{76}S^2 + GQ_{77}S + GQ_{78}}{P_{b1}S^7 + P_{b2}S^6 + P_{b3}S^5 + P_{b4}S^4 + P_{b5}S^3 + P_{b6}S^2 + P_{b7}S + P_{b8}}$$

(F.4-21)

$$G_{Q3} = \frac{GQ_{91}S^7 + GQ_{92}S^6 + GQ_{93}S^5 + GQ_{94}S^4 + GQ_{95}S^3 + GQ_{96}S^2 + GQ_{97}S + GQ_{98}}{P_{b1}S^7 + P_{b2}S^6 + P_{b3}S^5 + P_{b4}S^4 + P_{b5}S^3 + P_{b6}S^2 + P_{b7}S + P_{b8}}$$

(F.4-22)

$$G_{Q4} = \frac{HQ_{21}S^7 + HQ_{22}S^6 + HQ_{23}S^5 + HQ_{24}S^4 + HQ_{25}S^3 + HQ_{26}S^2 + HQ_{27}S + HQ_{28}}{P_{b1}S^7 + P_{b2}S^6 + P_{b3}S^5 + P_{b4}S^4 + P_{b5}S^3 + P_{b6}S^2 + P_{b7}S + P_{b8}}$$

(F.4-23)

$$\Delta E = E - E_0 \quad \text{(F.4-24)}$$

$$\Delta f = f_g - f_{g0} \quad \text{(F.4-25)}$$

Where P_0, Q_0, E_0, f_{g0} are steady-state values for real power, reactive power, voltage per phase, power supply frequency, respectively.

$$P_{b1} = L_{11}F_{31} \quad \text{(F.4-26)}$$

$$P_{b2} = L_{11}F_{32} + L_{12}F_{31} \quad \text{(F.4-27)}$$

$$P_{b3} = L_{11}F_{33} + L_{12}F_{32} \quad \text{(F.4-28)}$$

$$P_{b4} = L_{11}F_{34} + L_{12}F_{33} \quad \text{(F.4-29)}$$

$$P_{b5} = L_{11}F_{35} + L_{12}F_{34} \quad \text{(F.4-30)}$$

$$P_{b6} = L_{11}F_{36} + L_{12}F_{35} \quad \text{(F.4-31)}$$

$$P_{b7} = L_{11}F_{37} + L_{12}F_{36} \tag{F.4-32}$$

$$P_{b8} = L_{12}F_{37} \tag{F.4-33}$$

$$GP_{41} = GP_{21}L_{11} \tag{F.4-34}$$

$$GP_{42} = GP_{21}L_{12} + GP_{22}L_{21} \tag{F.4-35}$$

$$GP_{51} = GP_{41}F_{31} \tag{F.4-36}$$

$$GP_{52} = GP_{41}F_{32} + GP_{42}F_{31} \tag{F.4-37}$$

$$GP_{53} = GP_{41}F_{33} + GP_{42}F_{32} \tag{F.4-38}$$

$$GP_{54} = GP_{41}F_{34} + GP_{42}F_{33} - GP_{22}F_{41} \tag{F.4-39}$$

$$GP_{55} = GP_{41}F_{35} + GP_{42}F_{34} - GP_{22}F_{42} \tag{F.4-40}$$

$$GP_{56} = GP_{41}F_{36} + GP_{42}F_{35} - GP_{22}F_{43} \tag{F.4-41}$$

$$GP_{57} = GP_{41}F_{37} + GP_{42}F_{36} - GP_{22}F_{44} \tag{F.4-42}$$

$$GP_{58} = GP_{42}F_{37} - GP_{22}F_{45} \tag{F.4-43}$$

$$GP_{61} = GP_{23}L_{11} \tag{F.4-44}$$

$$GP_{62} = GP_{23}L_{12} + GP_{22}L_{22} \tag{F.4-45}$$

$$GP_{63} = \frac{GP_{22}L_{22}}{L_{21}} \tag{F.4-46}$$

$$GP_{64} = GP_{25}L_{11} \tag{F.4-47}$$

$$GP_{65} = GP_{25}L_{12} + GP_{24}L_{21} \tag{F.4-48}$$

$$GP_{71} = GP_{64}F_{31} \tag{F.4-49}$$

$$GP_{72} = GP_{64}F_{32} + GP_{65}F_{31} \tag{F.4-50}$$

$$GP_{73} = GP_{64}F_{33} + GP_{65}F_{32} \tag{F.4-51}$$

$$GP_{74} = GP_{64}F_{34} + GP_{65}F_{33} - GP_{24}F_{41} \tag{F.4-52}$$

$$GP_{75} = GP_{64}F_{35} + GP_{65}F_{34} - GP_{24}F_{42} \tag{F.4-53}$$

$$GP_{76} = GP_{64}F_{36} + GP_{65}F_{35} - GP_{24}F_{43} \tag{F.4-54}$$

$$GP_{77} = GP_{64}F_{37} + GP_{65}F_{36} - GP_{24}F_{44} \quad \text{(F.4-55)}$$

$$GP_{78} = GP_{65}F_{37} - GP_{24}F_{45} \quad \text{(F.4-56)}$$

$$GP_{91} = GP_{61}F_{31} \quad \text{(F.4-57)}$$

$$GP_{92} = GP_{61}F_{32} + GP_{62}F_{31} \quad \text{(F.4-58)}$$

$$GP_{93} = GP_{61}F_{33} + GP_{62}F_{32} \quad \text{(F.4-59)}$$

$$GP_{94} = GP_{61}F_{34} + GP_{62}F_{33} - GP_{63}F_{41} \quad \text{(F.4-60)}$$

$$GP_{95} = GP_{61}F_{35} + GP_{62}F_{34} - GP_{63}F_{42} \quad \text{(F.4-61)}$$

$$GP_{96} = GP_{61}F_{36} + GP_{62}F_{35} - GP_{63}F_{43} \quad \text{(F.4-62)}$$

$$GP_{97} = GP_{61}F_{37} + GP_{62}F_{36} - GP_{63}F_{44} \quad \text{(F.4-63)}$$

$$GP_{98} = GP_{62}F_{37} - GP_{63}F_{45} \quad \text{(F.4-64)}$$

$$HP_{11} = GP_{26}L_{11} \quad \text{(F.4-65)}$$

$$HP_{12} = GP_{26}L_{12} + GP_{24}L_{22} \quad \text{(F.4-66)}$$

$$HP_{13} = \frac{GP_{24}L_{22}}{L_{21}} \quad \text{(F.4-67)}$$

$$HP_{21} = HP_{11}F_{31} \quad \text{(F.4-68)}$$

$$HP_{22} = HP_{11}F_{32} + HP_{12}F_{31} \quad \text{(F.4-69)}$$

$$HP_{23} = HP_{11}F_{33} + HP_{12}F_{32} \quad \text{(F.4-70)}$$

$$HP_{24} = HP_{11}F_{34} + HP_{12}F_{33} - HP_{13}F_{41} \quad \text{(F.4-71)}$$

$$HP_{25} = HP_{11}F_{35} + HP_{12}F_{34} - HP_{13}F_{42} \quad \text{(F.4-72)}$$

$$HP_{26} = HP_{11}F_{36} + HP_{12}F_{35} - HP_{13}F_{43} \quad \text{(F.4-73)}$$

$$HP_{27} = HP_{11}F_{37} + HP_{12}F_{36} - HP_{13}F_{44} \quad \text{(F.4-74)}$$

$$HP_{28} = HP_{12}F_{37} - HP_{13}F_{45} \quad \text{(F.4-75)}$$

$$GQ_{41} = GQ_{21}L_{11} \quad \text{(F.4-76)}$$

$$GQ_{42} = GQ_{21}L_{12} + GQ_{22}L_{21} \quad \text{(F.4-77)}$$

$$GQ_{51} = GQ_{41}F_{31} \tag{F.4-78}$$

$$GQ_{52} = GQ_{41}F_{32} + GQ_{42}F_{31} \tag{F.4-79}$$

$$GQ_{53} = GQ_{41}F_{33} + GQ_{42}F_{32} \tag{F.4-80}$$

$$GQ_{54} = GQ_{41}F_{34} + GQ_{42}F_{33} - GQ_{22}F_{41} \tag{F.4-81}$$

$$GQ_{55} = GQ_{41}F_{35} + GQ_{42}F_{34} - GQ_{22}F_{42} \tag{F.4-82}$$

$$GQ_{56} = GQ_{41}F_{36} + GQ_{42}F_{35} - GQ_{22}F_{43} \tag{F.4-83}$$

$$GQ_{57} = GQ_{41}F_{37} + GQ_{42}F_{36} - GQ_{22}F_{44} \tag{F.4-84}$$

$$GQ_{58} = GQ_{42}F_{37} - GQ_{22}F_{45} \tag{F.4-85}$$

$$GQ_{61} = GQ_{25}L_{11} \tag{F.4-86}$$

$$GQ_{62} = GQ_{25}L_{12} + GQ_{24}L_{22} \tag{F.4-87}$$

$$GQ_{81} = GQ_{23}L_{11} \tag{F.4-88}$$

$$GQ_{82} = GQ_{23}L_{12} + GQ_{22}L_{22} \tag{F.4-89}$$

$$GP_{83} = \frac{GQ_{22}L_{22}}{L_{21}} \tag{F.4-90}$$

$$GQ_{71} = GQ_{61}F_{31} \tag{F.4-91}$$

$$GQ_{72} = GQ_{61}F_{32} + GQ_{62}F_{31} \tag{F.4-92}$$

$$GQ_{73} = GQ_{61}F_{33} + GQ_{62}F_{32} \tag{F.4-93}$$

$$GQ_{74} = GQ_{61}F_{34} + GQ_{62}F_{33} - GQ_{24}F_{41} \tag{F.4-94}$$

$$GQ_{75} = GQ_{61}F_{35} + GQ_{62}F_{34} - GQ_{24}F_{42} \tag{F.4-95}$$

$$GQ_{76} = GQ_{61}F_{36} + GQ_{62}F_{35} - GQ_{24}F_{43} \tag{F.4-96}$$

$$GQ_{77} = GQ_{61}F_{37} + GQ_{62}F_{36} - GQ_{24}F_{44} \tag{F.4-97}$$

$$GQ_{78} = GQ_{62}F_{37} - GP_{24}F_{45} \tag{F.4-98}$$

$$GQ_{91} = GQ_{81}F_{31} \tag{F.4-99}$$

$$GQ_{92} = GQ_{81}F_{32} + GQ_{82}F_{31} \tag{F.4-100}$$

$$GQ_{93} = GQ_{81}F_{33} + GQ_{82}F_{32} \quad \text{(F.4-101)}$$

$$GQ_{94} = GQ_{81}F_{34} + GQ_{82}F_{33} - GQ_{83}F_{41} \quad \text{(F.4-102)}$$

$$GQ_{95} = GQ_{81}F_{35} + GQ_{82}F_{34} - GQ_{83}F_{42} \quad \text{(F.4-103)}$$

$$GQ_{96} = GQ_{81}F_{36} + GQ_{82}F_{35} - GQ_{83}F_{43} \quad \text{(F.4-104)}$$

$$GQ_{97} = GQ_{81}F_{37} + GQ_{82}F_{36} - GQ_{83}F_{44} \quad \text{(F.4-105)}$$

$$GQ_{98} = GQ_{82}F_{37} - GQ_{83}F_{45} \quad \text{(F.4-106)}$$

$$HQ_{11} = GQ_{26}L_{11} \quad \text{(F.4-107)}$$

$$HQ_{12} = GQ_{26}L_{12} + GQ_{24}L_{22} \quad \text{(F.4-108)}$$

$$HQ_{13} = \frac{GQ_{24}L_{22}}{L_{21}} \quad \text{(F.4-109)}$$

$$HQ_{21} = HQ_{11}F_{31} \quad \text{(F.4-110)}$$

$$HQ_{22} = HQ_{11}F_{32} + HQ_{12}F_{31} \quad \text{(F.4-111)}$$

$$HQ_{23} = HQ_{11}F_{33} + HQ_{12}F_{32} \quad \text{(F.4-112)}$$

$$HQ_{24} = HQ_{11}F_{34} + HQ_{12}F_{33} - HQ_{13}F_{41} \quad \text{(F.4-113)}$$

$$HQ_{25} = HQ_{11}F_{35} + HQ_{12}F_{34} - HQ_{13}F_{42} \quad \text{(F.4-114)}$$

$$HQ_{26} = HQ_{11}F_{36} + HQ_{12}F_{35} - HQ_{13}F_{43} \quad \text{(F.4-115)}$$

$$HQ_{27} = HQ_{11}F_{37} + HQ_{12}F_{36} - HQ_{13}F_{44} \quad \text{(F.4-116)}$$

$$HQ_{28} = HQ_{12}F_{37} - HQ_{13}F_{45} \quad \text{(F.4-117)}$$

Table F.1 Parameters used in real power and reactive power

$G_{P1\_1} = GP_{51}$	$G_{P2\_1} = GP_{71}$	$G_{P3\_1} = GP_{91}$	$G_{P4\_1} = HP_{21}$
$G_{P1\_2} = GP_{52}$	$G_{P2\_2} = GP_{72}$	$G_{P3\_2} = GP_{92}$	$G_{P4\_2} = HP_{22}$
$G_{P1\_3} = GP_{53}$	$G_{P2\_3} = GP_{73}$	$G_{P3\_3} = GP_{93}$	$G_{P4\_3} = HP_{23}$
$G_{P1\_4} = GP_{54}$	$G_{P2\_4} = GP_{74}$	$G_{P3\_4} = GP_{94}$	$G_{P4\_4} = HP_{24}$
$G_{P1\_5} = GP_{55}$	$G_{P2\_5} = GP_{75}$	$G_{P3\_5} = GP_{95}$	$G_{P4\_5} = HP_{25}$
$G_{P1\_6} = GP_{56}$	$G_{P2\_6} = GP_{76}$	$G_{P3\_6} = GP_{96}$	$G_{P4\_6} = HP_{26}$
$G_{P1\_7} = GP_{57}$	$G_{P2\_7} = GP_{77}$	$G_{P3\_7} = GP_{97}$	$G_{P4\_7} = HP_{27}$
$G_{P1\_8} = GP_{58}$	$G_{P2\_8} = GP_{78}$	$G_{P3\_8} = GP_{98}$	$G_{P4\_8} = HP_{28}$
$G_{Q1\_1} = GQ_{51}$	$G_{Q2\_1} = GQ_{71}$	$G_{Q3\_1} = GQ_{91}$	$G_{Q4\_1} = HQ_{21}$
$G_{Q1\_2} = GQ_{52}$	$G_{Q2\_2} = GQ_{72}$	$G_{Q3\_2} = GQ_{92}$	$G_{Q4\_2} = HQ_{22}$
$G_{Q1\_3} = GQ_{53}$	$G_{Q2\_3} = GQ_{73}$	$G_{Q3\_3} = GQ_{93}$	$G_{Q4\_3} = HQ_{23}$
$G_{Q1\_4} = GQ_{54}$	$G_{Q2\_4} = GQ_{74}$	$G_{Q3\_4} = GQ_{94}$	$G_{Q4\_4} = HQ_{24}$
$G_{Q1\_5} = GQ_{55}$	$G_{Q2\_5} = GQ_{75}$	$G_{Q3\_5} = GQ_{95}$	$G_{Q4\_5} = HQ_{25}$
$G_{Q1\_6} = GQ_{56}$	$G_{Q2\_6} = GQ_{76}$	$G_{Q3\_6} = GQ_{96}$	$G_{Q4\_6} = HQ_{26}$
$G_{Q1\_7} = GQ_{57}$	$G_{Q2\_7} = GQ_{77}$	$G_{Q3\_7} = GQ_{97}$	$G_{Q4\_7} = HQ_{27}$
$G_{Q1\_8} = GQ_{58}$	$G_{Q2\_8} = GQ_{78}$	$G_{Q3\_8} = GQ_{98}$	$G_{Q4\_8} = HQ_{28}$

The coefficient of the real power and reactive power as 7th transfer functions can be rewritten as follows:

$$G_{P1} = \frac{G_{P1\_1}S^7 + G_{P1\_2}S^6 + G_{P1\_3}S^5 + G_{P1\_4}S^4 + G_{P1\_5}S^3 + G_{P1\_6}S^2 + G_{P1\_7}S + G_{P1\_8}}{P_{b1}S^7 + P_{b2}S^6 + P_{b3}S^5 + P_{b4}S^4 + P_{b5}S^3 + P_{b6}S^2 + P_{b7}S + P_{b8}} \tag{F.4-118}$$

$$G_{P2} = \frac{G_{P2\_1}S^7 + G_{P2\_2}S^6 + G_{P2\_3}S^5 + G_{P2\_4}S^4 + G_{P2\_5}S^3 + G_{P2\_6}S^2 + G_{P2\_7}S + G_{P2\_8}}{P_{b1}S^7 + P_{b2}S^6 + P_{b3}S^5 + P_{b4}S^4 + P_{b5}S^3 + P_{b6}S^2 + P_{b7}S + P_{b8}} \tag{F.4-119}$$

$$G_{P3} = \frac{G_{P3\_1}S^7 + G_{P3\_2}S^6 + G_{P3\_3}S^5 + G_{P3\_4}S^4 + G_{P3\_5}S^3 + G_{P3\_6}S^2 + G_{P3\_7}S + G_{P3\_8}}{P_{b1}S^7 + P_{b2}S^6 + P_{b3}S^5 + P_{b4}S^4 + P_{b5}S^3 + P_{b6}S^2 + P_{b7}S + P_{b8}} \tag{F.4-120}$$

$$G_{P4} = \frac{G_{P4\_1}S^7 + G_{P4\_2}S^6 + G_{P4\_3}S^5 + G_{P4\_4}S^4 + G_{P4\_5}S^3 + G_{P4\_6}S^2 + G_{P4\_7}S + G_{P4\_8}}{P_{b1}S^7 + P_{b2}S^6 + P_{b3}S^5 + P_{b4}S^4 + P_{b5}S^3 + P_{b6}S^2 + P_{b7}S + P_{b8}}$$

(F.4-121)

$$G_{Q1} = \frac{G_{Q1\_1}S^7 + G_{Q1\_2}S^6 + G_{Q1\_3}S^5 + G_{Q1\_4}S^4 + G_{Q1\_5}S^3 + G_{Q1\_6}S^2 + G_{Q1\_7}S + G_{Q1\_8}}{P_{b1}S^7 + P_{b2}S^6 + P_{b3}S^5 + P_{b4}S^4 + P_{b5}S^3 + P_{b6}S^2 + P_{b7}S + P_{b8}}$$

(F.4-122)

$$G_{Q2} = \frac{G_{Q2\_1}S^7 + G_{Q2\_2}S^6 + G_{Q2\_3}S^5 + G_{Q2\_4}S^4 + G_{Q2\_5}S^3 + G_{Q2\_6}S^2 + G_{Q2\_7}S + G_{Q2\_8}}{P_{b1}S^7 + P_{b2}S^6 + P_{b3}S^5 + P_{b4}S^4 + P_{b5}S^3 + P_{b6}S^2 + P_{b7}S + P_{b8}}$$

(F.4-123)

$$G_{Q3} = \frac{G_{Q3\_1}S^7 + G_{Q3\_2}S^6 + G_{Q3\_3}S^5 + G_{Q3\_4}S^4 + G_{Q3\_5}S^3 + G_{Q3\_6}S^2 + G_{Q3\_7}S + G_{Q3\_8}}{P_{b1}S^7 + P_{b2}S^6 + P_{b3}S^5 + P_{b4}S^4 + P_{b5}S^3 + P_{b6}S^2 + P_{b7}S + P_{b8}}$$

(F.4-124)

$$G_{Q4} = \frac{G_{Q4\_1}S^7 + G_{Q4\_2}S^6 + G_{Q4\_3}S^5 + G_{Q4\_4}S^4 + G_{Q4\_5}S^3 + G_{Q4\_6}S^2 + G_{Q4\_7}S + G_{Q4\_8}}{P_{b1}S^7 + P_{b2}S^6 + P_{b3}S^5 + P_{b4}S^4 + P_{b5}S^3 + P_{b6}S^2 + P_{b7}S + P_{b8}}$$

(F.4-125)

Note: due to the characteristics of diode rectifier which does not allow the power flowing backward to the power grid, the dynamic response results calculated from the developed dynamic model need to manually assign all negative real power and reactive power values to be 0.

F.5 Initial Values

The initial values used in the formulas are determined in this section. Some parameters are given values, such as

L_{dc}: dc link inductance

r_{dc} : dc link resistance

C_{dc}: dc link capacitance

l_c: commutation inductance

R_s: stator resistance

l_s: stator leakage inductance

R_r: rotor resistance

l_r: rotor leakage inductance

L_m: exciting inductance

H: Motor inertia

p: pole pair

V_{diode}: diode on-state voltage

E_0: power source steady-state rms voltage per phase

ω_g: power source angular frequency

ω_{r0}: rotor steady-state electric angular frequency

ω_{s0}: stator steady-state electric angular frequency

K_{pm}: speed controller proportional gain

K_{im}: speed controller integral gain

V_b: nominal voltage of the motor per phase

ω_b: nominal frequency of the motor

T_{Load}: the load torque

PF: power factor in front of the commutation inductance

P_0: real power

Q_0: reactive power

S_0: apparent power

Some parameters or initial values need to be calculated. The DC link voltage from the diode rectifier at each power module can be calculated as follows:

$$v_{d0} = \frac{3\sqrt{6}}{\pi} E_0 - \frac{3}{\pi} l_c \omega_{g0} i_{d0} - 2V_{diode} \tag{F.5-1}$$

$$v_{d0} = r_{dc} i_{d0} + e_{d0} \tag{F.5-2}$$

Based on Equations (F.5-1) and (F.5-2), the DC link voltage after the capacitor is calculated by

$$e_{d0} = \frac{3\sqrt{6}}{\pi} E_0 - \left(\frac{3}{\pi} l_c \omega_{g0} + r_{dc} \right) i_{d0} - 2V_{diode} \tag{F.5-3}$$

The initial value for the commutation angle, AC input current components of the drive at d- and q-axis, and real and reactive power at the MVD input can be determined as follows:

$$u_0 = \arccos\left(1 - \frac{2 l_c \omega_{g0} i_{d0}}{\sqrt{6} E_0}\right) \tag{F.5-4}$$

$$i_{qgcom0} = \frac{2\sqrt{3}}{\pi} i_{d0} \left[\sin\left(u_0 - \frac{5\pi}{6}\right) - \sin\left(-\frac{5\pi}{6}\right) \right] + \frac{3\sqrt{2}E_0}{\pi l_c \omega_{g0}} (\cos u_0 - 1) + \frac{3\sqrt{2}E_0}{4\pi l_c \omega_{g0}} (1 - \cos 2u_0) \tag{F.5-5}$$

$$i_{dgcom0} = \frac{2\sqrt{3}}{\pi} i_{d0} \left[-\cos\left(u_0 - \frac{5\pi}{6}\right) + \cos\left(-\frac{5\pi}{6}\right) \right] + \frac{3\sqrt{2}E_0}{\pi l_c \omega_{g0}} \sin u_0 - \frac{3\sqrt{2}E_0}{4\pi l_c \omega_{g0}} \sin 2u_0 - \frac{3\sqrt{2}E_0}{2\pi l_c \omega_{g0}} u_0 \tag{F.5-6}$$

$$i_{qgcond0} = \frac{2\sqrt{3}}{\pi} i_{d0} \left[\sin\left(\frac{7\pi}{6}\right) - \sin\left(u_0 + \frac{5\pi}{6}\right) \right] \tag{F.5-7}$$

$$i_{dgcond0} = \frac{2\sqrt{3}}{\pi} i_{d0} \left[-\cos\left(\frac{7\pi}{6}\right) + \cos\left(u_0 + \frac{5\pi}{6}\right) \right] \tag{F.5-8}$$

$$i_{qg0} = i_{qgcom0} + i_{qgcond0} \tag{F.5-9}$$

$$i_{dg0} = i_{dgcom0} + i_{dgcond0} \tag{F.5-10}$$

The total real and reactive power at the input of MVD can be calculated by

$$P_0 = \frac{3 n_{pulse}}{2\sqrt{2}} E_0 i_{qg0} \tag{F.5-11}$$

$$S_0 = \frac{P_0}{PF_0} \tag{F.5-12}$$

where PF_0 is assumed based on the commutation inductance values. If the commutation inductance is 0-1mH, PF_0 = 96-98% (a typical power factor at the ac input of a diode rectifier).

$$Q_0 = \sqrt{S_0^2 - P_0^2} \tag{F.5-13}$$

To determine the parameters in Equations (F.5-3) - (F.5-13), the dc link current i_{d0} must be determined first. Based on induction motors equations and inverter equations, we have:

$$v_{ds0} = R_s i_{ds0} - \omega_{s0}\left(L_s i_{qs0} + L_m i_{qr0}\right) \tag{F.5-14}$$

$$v_{qs0} = R_s i_{qs0} + \omega_{s0}\left(L_s i_{ds0} + L_m i_{dr0}\right) \tag{F.5-15}$$

$$0 = R_r i_{dr0} - \left(\omega_{s0} - \omega_{r0}\right)\left(L_r i_{qr0} + L_m i_{qs0}\right) \tag{F.5-16}$$

$$0 = R_r i_{qr0} + \left(\omega_{s0} - \omega_{r0}\right)\left(L_r i_{dr0} + L_m i_{ds0}\right) \tag{F.5-17}$$

$$v_{ds0} = 0 \tag{F.5-18}$$

$$v_{qs0} = \frac{n_{pulse}}{6} d_0 e_{d0} \tag{F.5-19}$$

From Equation (F.5-16),

$$i_{dr0} = \frac{\left(\omega_{s0} - \omega_{r0}\right)}{R_r}\left(L_r i_{qr0} + L_m i_{qs0}\right) \tag{F.5-20}$$

Substitute Equation (F.5-20) in Equation (F.5-17), after rearrangement, the following equation can be obtained:

$$\left[\frac{R_r^2 + \left(\omega_{s0} - \omega_{r0}\right)^2 L_r^2}{R_r}\right] i_{qr0} + \left[L_m\left(\omega_{s0} - \omega_{r0}\right)\right] i_{ds0} + \left[\frac{\left(\omega_{s0} - \omega_{r0}\right)^2 L_r L_m}{R_r}\right] i_{qs0} = 0 \tag{F.5-21}$$

From Equations (F.5-14) and (F.5-18),

$$i_{qr0} = \left(\frac{R_s}{\omega_{s0} L_m}\right) i_{ds0} - \left(\frac{L_s}{L_m}\right) i_{qs0} \tag{F.5-22}$$

Substitute Equation (F.5-22) in Equation (F.5-21), the following is determined:

$$i_{ds0} = S_{11} i_{qs0} \tag{F.5-23}$$

$$S_{11} = \frac{\left(R_r^2 + (\omega_{s0} - \omega_{r0})^2 L_r^2\right) L_s \omega_{s0} - (\omega_{s0} - \omega_{r0})^2 L_r L_m^2 \omega_{s0}}{\left(R_r^2 + (\omega_{s0} - \omega_{r0})^2 L_r^2\right) R_s + (\omega_{s0} - \omega_{r0}) R_r L_m^2 \omega_{s0}} \tag{F.5-24}$$

Substitute Equation (F.5-23) in Equation (F.5-22),

$$i_{qr0} = S_{12} i_{qs0} \tag{F.5-25}$$

$$S_{12} = \frac{R_s S_{11} - \omega_{s0} L_s}{\omega_{s0} L_m} \tag{F.5-26}$$

Substitute Equation (F.5-25) in Equation (F.5-20),

$$i_{dr0} = S_{13} i_{qs0} \tag{F.5-27}$$

$$S_{13} = \frac{(\omega_{s0} - \omega_{r0})(L_m + L_r S_{12})}{R_r} \tag{F.5-28}$$

Under the steady-state condition, the motor electromagnetic torque should be balanced with the load torque as follows:

$$T_{e0} = 1.5 p L_m \left(i_{dr0} i_{qs0} - i_{qr0} i_{ds0}\right) = T_{Load0} \tag{F.5-29}$$

Substitute Equations (F.5-23), (F.5-25) and (F.5-27) in Equation (F.5-29), i_{qs0} can be calculated as follows:

$$i_{qs0} = \sqrt{\frac{T_{Load0}}{1.5 p L_m (S_{13} - S_{12} S_{11})}} \tag{F.5-30}$$

Substitute Equation (F.5-30) in Equations (F.5-23), (F.5-25) and (F.5-27), i_{ds0}, i_{qr0}, and i_{dr0} can be calculated.

Substitute Equations (F.5-23) and (F.5-27) in Equation (F.5-15), and combining with Equation (F.5-19),

$$v_{qs0} = R_s i_{qs0} + \omega_{s0}\left(L_s S_{11} i_{qs0} + L_m S_{13} i_{qs0}\right) = \frac{n_{pulse}}{6} d_0 e_{d0} \tag{F.5-31}$$

Define a new parameter S_{14} as follows:

$$\begin{aligned} S_{14} = d_0 e_{d0} &= \frac{6}{n_{pulse}} R_s i_{qs0} + \frac{6}{n_{pulse}} \omega_{s0}\left(L_s S_{11} i_{qs0} + L_m S_{13} i_{qs0}\right) \\ &= \left(\frac{6}{n_{pulse}} i_{qs0}\right)\left[R_s + \omega_{s0}\left(L_s S_{11} + L_m S_{13}\right)\right] \end{aligned} \tag{F.5-32}$$

Based on Equation (F.3-8),

$$\left(\frac{n_{pulse}}{4}\right) de_d i_{qs} = \left(\frac{n_{pulse}}{2}\right) e_d i_I \tag{F.5-33}$$

Under steady-state, $i_{I0} = i_{d0}$, Equation (F.5-33) becomes

$$\left(\frac{n_{pulse}}{4}\right) d_0 e_{d0} i_{qs0} = \left(\frac{n_{pulse}}{2}\right) e_{d0} i_{d0} \tag{F.5-34}$$

The dc link steady-state current i_{d0} can be obtained from Equation (F.5-34) as follows:

$$i_{d0} = \frac{1}{2} d_0 i_{qs0} \tag{F.5-35}$$

Multiplying both sides of Equation (F.5-3) by d_0 as follows:

$$S_{14} = e_{d0} d_0 = \frac{3\sqrt{6}}{\pi} E_0 d_0 - \left(\frac{3}{\pi} l_c \omega_g + r_{dc}\right) i_{d0} d_0 - 2V_{diode} d_0 \tag{F.5-36}$$

Substitute Equation (F.5-35) in Equation (F.5-36), we obtain the function of the duty cycle d_0 as follows:

$$\left[\frac{1}{2}\left(\frac{3}{\pi} l_c \omega_g + r_{dc}\right) i_{qs0}\right] d_0^2 - \left(\frac{3\sqrt{6}}{\pi} E_0 - 2V_{diode}\right) d_0 + S_{14} = 0 \tag{F.5-37}$$

Solving Equation (F.5-37), the duty cycle d_0 are determined. All required initial values can be determined accordingly.